

# Land-atmosphere exchange of elemental mercury: New insights using a novel relaxed eddy accumulation system and enclosure techniques

**Inauguraldissertation**

zur

Erlangung der Würde eines Doktors der Philosophie

vorgelegt der

Philosophisch-Naturwissenschaftlichen Fakultät

der Universität Basel

von

Stefan Osterwalder

aus Gaiserwald, St. Gallen

Basel, 2016

Original document stored on the publication server of the University of Basel

[edoc.unibas.ch](http://edoc.unibas.ch)



This work is licensed under the "Creative Commons Attribution-NonCommercial 4.0 International Public License" (CC BY-NC 4.0).

Genehmigt von der Philosophisch-Naturwissenschaftlichen Fakultät  
auf Antrag von

Prof. Dr. Christine Alewell (Fakultätsverantwortliche und Dissertationsleiterin)

Prof. Dr. Mae Sexauer Gustin (Korreferentin)

Basel, den 19. April 2016

Prof. Dr. Jörg Schibler  
(Dekan)

## Summary

Anthropogenic activities, such as mining and burning of fossil fuels, have significantly increased the emissions of mercury (Hg) to the atmosphere, and the subsequent deposition onto global ecosystems. To restrain Hg emissions and reduce its accumulation in biota and human exposure, the UN's legally binding Minamata Convention was signed by 128 countries. To estimate the potential of different ecosystems as sinks or sources for atmospheric Hg, reliable quantification of land-atmosphere exchange of gaseous elemental Hg (GEM) is crucial.

Despite extensive efforts to quantify GEM exchange and to characterize controls, large uncertainty remains due to the complexity of bi-directional GEM flux, model parameterization, and the application of different measurement techniques. The majority of flux studies were temporally biased toward summer and daytime. More than 60% of these measurements have been conducted over Hg-enriched sites and limited to small-scale studies using enclosure techniques.

The main goal of the thesis was to identify the role of boreal peatlands as net sinks or sources of Hg by calculating the first annual Hg budget including continuous measurements of peatland-atmosphere exchange of GEM. Peatlands are major mediators for the high levels of Hg in freshwater fish in Europe and North America, because the peatlands provide favorable conditions for the formation of bioavailable and highly toxic methylmercury. In high latitude regions almost all freshwater fish have Hg concentrations exceeding European limits for good chemical status ( $0.02 \text{ mg Hg kg}^{-1}$  fish muscle, Chalmers et al., 2011, Åkerblom et al., 2014). To test the hypothesis that enough Hg evades from peat to the atmosphere to play a significant role in Hg removal, we developed a relaxed eddy accumulation (REA) system for long-term and large-scale GEM flux monitoring. The first objective was to test the system over an urban site and a boreal peatland at different heights with contrasting surface and turbulence characteristics. In addition, we aimed to inter-compare REA with dynamic flux chambers (DFCs) during a concurrent measurement campaign. DFCs represent the far most common GEM flux measurement technique mainly because they are relatively simple to use and cheaper than micrometeorological methods, while also being suitable for short-term and small-scale flux measurements. As a result they provide an efficient method to resolve confounding influences on GEM flux over a boreal peatland and to test whether GEM emission from contaminated properties constitutes a health risk for residents caused by chronic inhalation of Hg vapor.

The novel REA design features two inlets and two pairs of gold cartridges for continuous sampling of GEM in both updrafts and downdrafts for subsequent measurement on a single Hg detector. We tested the system for two weeks in the center of Basel, Switzerland, and for a period of three weeks during snowmelt above the nutrient poor, minerogenic Degerö Stormyr peatland, located about 50 km NW of Umeå, Sweden. Both environments were identified as net sources of GEM to the atmosphere, with average emission rates of 3 and  $15 \text{ ng m}^{-2} \text{ h}^{-1}$ , respectively. The tests revealed that our REA system reduced major uncertainties caused by the sequential sampling in previous single detector designs. Continuous and autonomous

measurements were facilitated by regular monitoring of detector drift and recovery rates using a GEM reference gas and a Hg zero-air generator. Despite the very low GEM concentration difference between updraft and downdraft ( $0.13 \text{ ng m}^{-3}$ ) at Degerö Stormyr, the results indicate that REA is feasible for measurements that are close to the surface over snow and/or short vegetation.

In a longer deployment we continuously monitored the GEM flux at Degerö Stormyr over a period of one year. The annual Hg mass balance was dominated by net GEM emission ( $10.2 \text{ } \mu\text{g m}^{-2}$ ) due to substantial evasion between May and October. The annual wet bulk deposition was  $3.9 \text{ } \mu\text{g m}^{-2}$ . The annual discharge export of Hg from the peatland area ( $1.9 \text{ km}^2$ ) amounted to  $1.3 \text{ } \mu\text{g m}^{-2}$ .

The GEM evasion rate, a factor of eight higher than runoff Hg export, results most likely from recent declines in atmospheric Hg concentrations (Amos et al., 2015) that have turned the peatland from a net sink into a source of atmospheric Hg. This is consistent with the Hg concentration gradients in the superficial peat which decline from a Hg concentration peak at about 30 cm depth ( $110 \text{ ng g}^{-1}$ , corresponding to Hg emission peaks during the 1950s) towards the surface ( $23 \text{ ng g}^{-1}$ ). Under the assumptions that environmental conditions remain stable and that catchment runoff is dominated by Hg from the uppermost peat layers, it will take around 80 years to deplete the entire pool of legacy Hg in the uppermost 34 cm to a background concentration level of  $20 \text{ ng g}^{-1}$ . We suggest that the strong Hg evasion demonstrated in this study means that open boreal peatlands and thus downstream ecosystems may recover more rapidly from past atmospheric Hg deposition than previously assumed.

The method comparison study investigating differences between a Teflon® PFA DFC (TDFC), a new type DFC (NDFC) and REA was conducted over four days in July 2014. This revealed that the variability in GEM flux increased in the following order: TDFC < NDFC < REA. The average  $\pm$  SD fluxes were  $0.7 \pm 1.3 \text{ ng m}^{-2} \text{ h}^{-1}$ ,  $1.9 \pm 3.8 \text{ ng m}^{-2} \text{ h}^{-1}$  and  $2 \pm 24 \text{ ng m}^{-2} \text{ h}^{-1}$ , respectively. Compared to conventional chamber designs the NDFC is able to account for the effect of wind and yielded cumulative flux values similar to the turbulent fluxes measured by REA (< 2% difference). This result indicates the potential of the NDFC to bridge the gap between turbulent and enclosure-based flux measurements. While the REA flux was rather variable within a day, alternate DFC measurements revealed a distinct diel pattern with highest GEM emission in the early afternoon. Spatial heterogeneity in peatland surface characteristics introduced by total Hg concentrations in the uppermost 34 cm ( $48 - 67 \text{ ng g}^{-1}$ ), vascular plant cover (18 - 60%), water table level (4 - 18 cm) or dissolved gaseous Hg concentrations ( $20 - 82 \text{ } \mu\text{g L}^{-1}$ ) did not appear to significantly influence GEM flux. We conclude that for short-term mechanistic studies DFCs are the preferred tool while the NDFC is suitable for quantitative flux estimations over short vegetation.

The comparison of peatland-atmosphere exchange of GEM from 16 experimental plots determined using a shaded polycarbonate DFC revealed significantly lower flux rates, occasionally indicating Hg uptake, from plots subjected to sulfur additions at rates of  $20 \text{ kg ha}^{-1} \text{ yr}^{-1}$ . These deposition rates were typical during the 1980s in southern Sweden which are approximately seven times faster than contemporary deposition rates in northern Sweden. Enhanced nitrogen deposition and greenhouse treatment had no significant effect on GEM



fluxes. The suppressed GEM evasion from the sulfur-treated plots was most likely related to Hg binding to S in organic matter, making Hg less susceptible to evasion, and more prone to transport in runoff at the start of the S additions 15 years earlier.

The thesis was completed with shaded NDFC flux measurements over industrially polluted properties in Switzerland. Topsoil (0 - 10 cm) THg concentrations from 27 measurement plots at nine properties ranged from 0.2 to 390  $\mu\text{g g}^{-1}$ . We found that atmospheric GEM concentrations at 1 m height over the parcels were up to 14 times higher than northern hemispheric background concentrations ( $\sim 1.5 \text{ ng m}^{-3}$ ), however, they did not appear to reach harmful levels. The parcel averaged fluxes ranged from 38 to 1258  $\text{ng m}^{-2} \text{ h}^{-1}$  and were clearly driven by total Hg concentrations in the soil ( $r^2 = 0.77$ ,  $p < 0.01$ ). GEM emission from the entire area of 8.6  $\text{km}^2$  was estimated to 4.5  $\text{kg yr}^{-1}$ . This accounts for 0.5% of the total Hg emission in Switzerland, as estimated by emission inventories (BAFU, 2015).

It is emphasized that GEM evasion dominates the flux during the growing season over the studied peatland and that elevated sulfur concentrations in the peat also influence flux magnitudes. Spatial heterogeneity in peat characteristics did not explain the variations in flux. The all-season REA measurements identified peatlands as sources of GEM to the atmosphere. Release of Hg that accumulated earlier in the uppermost peat layers may continue for the next half century. This implies that Hg contamination to aquatic ecosystems and food webs will decrease in parts of Europe and North America with substantial areas covered by peatlands. The variation may be even greater between sites located in different climate zones. A combination of long-term GEM flux measurements, Hg tracer and Hg isotope experiments are necessary to further elucidate the complex biogeochemical cycle of Hg in peatlands, especially to detect potential peak flux events, identify mechanisms of Hg reduction in the soils and to pinpoint pathways of GEM transport from soils to the atmosphere.



# Table of Contents

<b>Summary</b> .....	<b>III</b>
<b>Nomenclature</b> .....	<b>XI</b>
<b>1 Introduction</b> .....	<b>13</b>
1.1 Mercury – a heavy metal of global concern .....	13
1.2 Terrestrial mercury cycling: the role of peatlands .....	15
1.3 Elemental mercury flux measurement techniques .....	20
1.4 Objectives and outline of the thesis .....	23
<b>2 A novel relaxed eddy accumulation system for long-term measurement of mercury flux</b> .....	<b>25</b>
Abstract.....	26
2.1 Introduction .....	27
2.2 Methods.....	30
2.2.1 GEM-REA sampling system.....	30
2.2.2 GEM analysis.....	32
2.2.4 Data processing .....	34
2.2.5 Site descriptions .....	35
2.3 Results and Discussion.....	37
2.3.1 REA performance.....	37
2.3.2 Meteorological conditions.....	40
2.3.3 Footprint and turbulence regime .....	41
2.3.4 Atmospheric GEM concentrations .....	43
2.3.5 GEM flux estimation in contrasting environments.....	44
2.4 Conclusion .....	46
Acknowledgements .....	46
<b>3 Mercury emissions from a boreal peatland: Time to rethink timelines for global recovery?</b> .....	<b>47</b>
Abstract.....	48
3.1 Main Section .....	49

3.2 Methods .....	55
3.2.1 Research site .....	55
3.2.2 Peat sampling and Hg analysis .....	55
3.2.3 Hg in wet bulk deposition .....	55
3.2.4 Peatland-atmosphere exchange of GEM .....	55
3.2.5 Hg in catchment discharge .....	56
3.2.6 Dissolved gaseous Hg and other environmental parameters.....	56
Acknowledgements.....	57
<b>4 Comparative study of elemental mercury flux measurement techniques over a boreal peatland .....</b>	<b>59</b>
Abstract.....	60
4.1 Introduction .....	61
4.2 Methods.....	63
4.2.1 Site description .....	63
4.2.2 Relaxed eddy accumulation technique.....	63
4.2.3 Enclosure techniques.....	64
4.2.4 Instrumentation and sampling .....	65
4.2.5 Environmental parameters.....	66
4.3 Results and Discussion .....	68
4.3.1 Environmental conditions.....	68
4.3.2 REA GEM flux characteristics .....	69
4.3.3 DFC GEM flux characteristics .....	70
4.3.4 Comparison of REA and DFC measurement techniques.....	73
4.4 Conclusion.....	76
Acknowledgements.....	76
<b>5 Evasion of elemental mercury from a boreal peatland suppressed by long-term sulfate addition .....</b>	<b>77</b>
Abstract.....	78
5.1 Introduction .....	79
5.2 Methods.....	81
5.3 Results and Discussion .....	83
Acknowledgements.....	85

---

<b>6 Evasion of elemental mercury from contaminated properties in Switzerland</b>	<b>87</b>
Abstract.....	88
6.1 Introduction.....	89
6.2 Methods.....	91
6.2.1 Measurement setup.....	91
6.2.2 Site description and sampling.....	92
6.3 Results and Discussion.....	94
6.4 Conclusion.....	99
Acknowledgements.....	99
<b>7 Overall discussion and outlook.....</b>	<b>101</b>
7.1 Assessing the peatland-atmosphere exchange of GEM.....	101
7.2 GEM evasion and implications for boreal ecosystems.....	104
7.3 Forests, oceans and contaminated sites: the future of REA.....	107
<b>References.....</b>	<b>109</b>
<b>Appendix.....</b>	<b>127</b>
Supporting Information to Chapter 2.....	127
Supporting Information to Chapter 3.....	133
Supporting Information to Chapter 4.....	143
Supporting Information to Chapter 6.....	147
<b>Acknowledgements.....</b>	<b>153</b>
<b>Curriculum Vitae.....</b>	<b>155</b>



# Nomenclature

AGM	Aerodynamic gradient
DFC	Dynamic flux chamber
DGM	Dissolved gaseous mercury
DMHg	Dimethylmercury [(CH <sub>3</sub> ) <sub>2</sub> Hg]
EC	Eddy covariance
ERIC	European Research Infrastructure Consortium
FEP	Fluorinated ethylene propylene
GEM	Gaseous elemental mercury (atmosphere)
GOM	Gaseous oxidized mercury (atmosphere)
Hg <sup>0</sup>	Elemental mercury
Hg <sup>2+</sup>	Divalent mercury
ICOS	Integrated Carbon Observation System
MBR	Modified Bowen ratio
MeHg	Methylmercury [CH <sub>3</sub> Hg <sup>+</sup> ]
MM	Micrometeorological
NDFC	New type dynamic flux chamber
PBM	Particulate bound mercury (atmosphere)
PDFC	Polycarbonate dynamic flux chamber
PFA	Perfluoroalkoxy alkanes
PTFE	Polytetrafluoroethylene
QA/QC	Quality assurance and quality control
REA	Relaxed eddy accumulation
TDFC	Teflon® PFA dynamic flux chamber
THg	Total mercury
VP	Vascular plant cover
WTL	Water table level
Background site <sup>a</sup>	THg ≤ 0.3 µg g <sup>-1</sup> and GEM ≤ 3 ng m <sup>-3</sup>
Hg-enriched site <sup>a</sup>	THg > 0.3 µg g <sup>-1</sup> and/or GEM > 3 ng m <sup>-3</sup>
Atmospherically influenced site <sup>a</sup>	THg ≤ 0.3 µg g <sup>-1</sup> and GEM > 3 ng m <sup>-3</sup>
Naturally enriched site <sup>a</sup>	Hg-enriched site (geologic Hg mineral belt, geothermal areas)
Contaminated site <sup>a</sup>	Hg-enriched site (anthropogenic pollution is indicated)
Mining site <sup>a</sup>	Hg-enriched site (Hg and mainly gold, silver, copper mining)
Uncontaminated <sup>b</sup>	THg < 0.5 µg g <sup>-1</sup>
Slightly contaminated <sup>b</sup>	between THg ≥ 0.5 µg g <sup>-1</sup> and THg < 2 µg g <sup>-1</sup>
Moderately contaminated <sup>b</sup>	between THg ≥ 2 µg g <sup>-1</sup> and THg < 5 µg g <sup>-1</sup>
Heavily contaminated <sup>b</sup>	THg ≥ 5 µg g <sup>-1</sup>

<sup>a</sup> after Agnan et al. (2016)

<sup>b</sup> after VBBo (2016) and valid for residential areas: 0.5 µg THg g<sup>-1</sup> = reference value ("Richtwert"); 2 µg THg g<sup>-1</sup> = test value and remediation value ("Prüf- und Sanierungswert")





# CHAPTER 1

## Introduction

### 1.1 Mercury – a heavy metal of global concern

Mercury (Hg) is toxic to humans and wildlife, and ubiquitous in the environment (Mergler et al., 2007). Due to its unique properties, elemental Hg had a great number of uses historically in paints and cosmetics, and is still commonplace in daily life, e.g. in health care equipment, dental amalgam, electronic devices, light bulbs, batteries or in thermometers (UNEP, 2013a). However, goals have been set to phase out the use of Hg in products and processes, and global demand has fallen annually from about 9000 to about 3500 tons in the last 50 years (UNEP, 2006).

Geogenic Hg is found in concentrated deposits predominantly as cinnabar (HgS) in past and present convergent tectonic margins. Divalent Hg ( $\text{Hg}^{2+}$ ) exists in gaseous, dissolved and solid states and is much more prevalent in waters than in the atmosphere. The elemental form of Hg ( $\text{Hg}^0$ ) is liquid at room temperature, relatively insoluble in water (4.4 ppt at 20°C), and has an anomalously high vapor pressure (0.17 Pa at 20°C) (Schröder and Munthe, 1998). Gaseous elemental mercury (GEM) is therefore the dominant form in the atmosphere and usually constitutes more than 95% of the total airborne Hg (Schröder and Munthe, 1998). The reactivity of GEM is relatively low and it can be distributed globally over short timescales (~1 year) before it is oxidized and deposited on terrestrial or aquatic surfaces far away from emission sources (Fig. 1.1) (Selin et al., 2008, Gustin et al., 2015). Background atmospheric concentrations typically range from 1.3 to 1.7  $\text{ng m}^{-3}$  in the Northern hemisphere and from 1.1 to 1.3  $\text{ng m}^{-3}$  in the Southern hemisphere (Lindberg et al., 2007; Pirrone et al., 2008; Sprovieri et al., 2010). The atmosphere also contains other forms of Hg, i.e. different compounds of gaseous oxidized Hg (GOM) and particulate bound Hg (PBM) (Huang et al., 2013; Gustin et al., 2015). Their atmospheric concentrations are commonly considered low (1 - 100  $\text{pg m}^{-3}$ ) (Bieser et al., 2012). However, recent studies found that GOM may constitute up to 25% of the total Hg in the boundary layer (e.g. Castro et al., 2012; Gustin et al., 2013) and conversion of the total GEM pool to GOM has been observed in the Arctic (Steffen et al., 2014; Steffen et al., 2015). While there is relative confidence in GEM concentration estimates, methods to measure GOM and PBM are sensitive to analytical interferences that vary with changes in relative humidity, ozone, and  $\text{Hg}^{2+}$  present in the air (Gustin et al., 2015).

## 1.1 Mercury – a heavy metal of global concern

Today, between 5 and 13% of all Hg emissions to the atmosphere stem from natural sources such as volcanism or rock weathering (Fig. 1.1). Between 29 and 33% of the global Hg emissions can be attributed to anthropogenic mobilization of Hg, namely artisanal and small-scale gold mining as well as fossil fuel combustion. Other major sectors include cement and metal production, waste incineration and the chlor-alkali industry (Selin et al., 2007; Streets et al., 2011; UNEP, 2013b). It is reported that the dominant Hg emissions shifted from Hg mining and liquid Hg<sup>0</sup> use in gold/silver refining in the 19<sup>th</sup> century to coal combustion and non-ferrous metal production in the 20<sup>th</sup> century (Sun et al., 2016). The GEM fraction in flue gases from coal combustion is 66 - 82% while non-ferrous metal production releases predominantly GOM (29 - 90%). Today, PBM is usually removed simultaneously with other particles in dust collectors (Zhang et al., 2016).

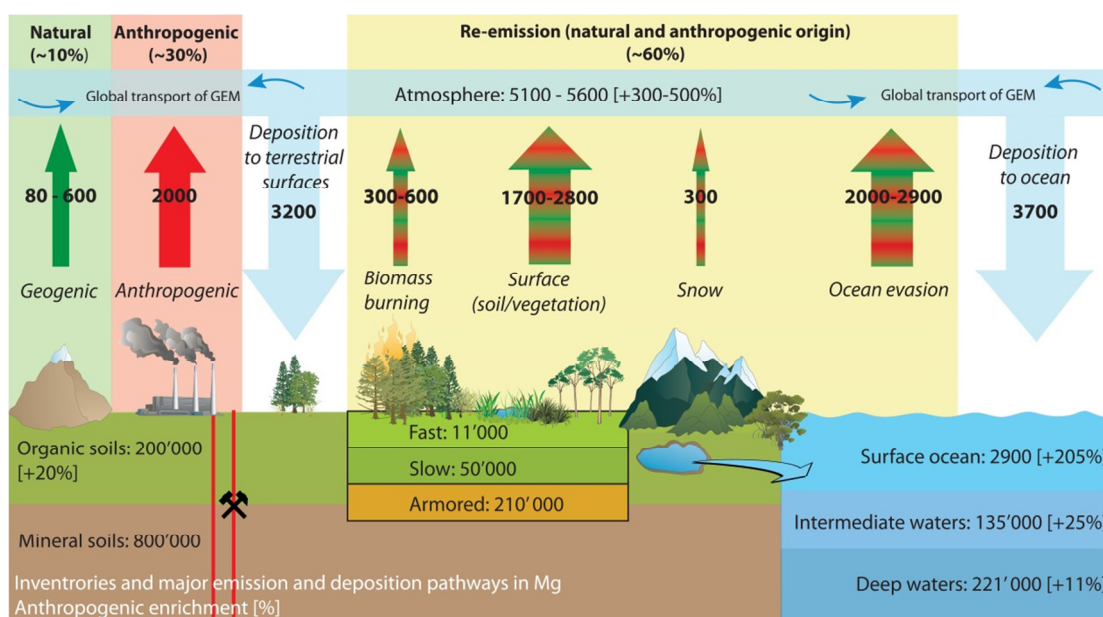


**Figure 1.1:** The most recent estimates of Hg inventories and fluxes at the earth's surface based on previous studies (Selin et al., 2008; Gustin and Jaffe, 2010; Soerensen et al., 2010; Smith-Downey et al., 2010; Corbitt et al., 2011; Mason et al., 2012) Figure adapted from UNEP (2013b), Lubick and Malakoff (2013) and Zhu et al. (2016). Estimates for natural Hg emissions (green), anthropogenic Hg emissions (red) and re-emission (green/red) of Hg deposited previously to terrestrial and aquatic surfaces (blue). The percentage values in brackets indicate the enrichment of Hg in the different pools due to anthropogenic activities in the last century (Mason et al., 2012).

Hg in the atmosphere interacts with ozone, water vapor, hydroxyl and nitrate radicals and undergoes photo-oxidation and reduction processes. All atmospheric Hg species can be deposited on water or land (Fig. 1.1). The global terrestrial mercury model of Smith-Downey et al. (2010) differentiates between (i) an armored soil pool with immobile Hg bound to the mineral fraction occurring predominantly in the soil parent rock (Friedli et al., 2007), (ii) a slow soil pool with Hg incorporated into leaf tissue with very high affinity to reduced sulfur groups in soil organic matter (Skylberg et al., 2000) and (iii) a fast terrestrial pool where newly deposited Hg is loosely bound to soils and leaves. If not sequestered by soils and sediments, oxidized Hg in the slow and fast soil pool can undergo chemical, photolytic, or biological reduction. As a result of this Hg<sup>0</sup> evades. Such re-emissions of historically deposited Hg to

terrestrial surfaces and water bodies (legacy emissions) are responsible for the remaining 56-65% of the total atmospheric Hg emissions (Fig. 1.1).

Globally, anthropogenic Hg releases have increased the atmospheric burden and subsequent cycling of Hg between land, ocean, and atmosphere significantly (Fig. 1.1). This has almost tripled the Hg levels in surface waters (Lamborg et al., 2014) and enriched Hg concentrations in organic topsoil, sediment and peat by a factor of 1.2, 3, and 4.3 since pre-industrial times, respectively (Smith-Downey et al., 2010; Amos et al., 2015). These additional Hg inputs to the environment are of major concern, because of the elevated net production of the more toxic Hg form, methylmercury (MeHg). Most of the MeHg is produced by sulfate-reducing bacteria in anoxic environments (Morel et al., 1998). There are a limited number of other known methylation mechanisms but bacteria appear to be the largest producers in lakes and wetlands (Rudd, 1995; Fitzgerald et al., 2007, Parks et al., 2013). MeHg ingested by zooplankton biomagnifies along the food chain a million-fold by the time it reaches long-lived predatory fish such as pike, tuna, swordfish or shark (Schröder et al., 1998; Hsu-Kim et al., 2013). Therefore, humans that rely on the consumption of fish are most at risk from this neurotoxin. Because developing organ systems are especially sensitive MeHg poses a particular threat to infants, children and pregnant women. This has resulted in regulatory fish consumption guidelines and health advisories worldwide (JECFA, 2014). In order to “protect the human health and the environment from anthropogenic emissions and releases of Hg and Hg compounds”, 128 nations have signed the Minamata Convention on mercury under the framework of the United Nations Environment Programme (UNEP, 2013c). The Minamata Convention also highlights the need for a better understanding of Hg cycling on an ecosystem scale, and in particular, better estimates of Hg remobilization from historic deposition (UNEP, 2013c, article 19).

Under the assumption that worldwide anthropogenic Hg emissions are held constant until 2050, models predict that atmospheric deposition will still increase by 30% (Amos et al., 2013) and re-emission of legacy Hg will delay recovery from both the spatial and temporal extent of Hg pollution via multiple surface-atmosphere exchanges (Agnan et al., 2016). Despite great efforts in determination of GEM re-emission on an annual basis, uncertainty in exchange magnitudes remain large for oceans (2000 - 2950 Mg a<sup>-1</sup>), and for both modeled (1700 - 2800 Mg yr<sup>-1</sup>) and measured (-513 to 1653 Mg yr<sup>-1</sup> [range of 37.5<sup>th</sup> and 62.5<sup>th</sup> %]) terrestrial environments (Mason et al., 2012; Agnan et al., 2016).

## 1.2 Terrestrial mercury cycling: the role of peatlands

Current global Hg models view terrestrial surfaces as net sinks of Hg (Fig. 1.1). However, land-use and different land cover types are critical controllers of GEM re-emission, and can shift the role of terrestrial surfaces from net sinks to net sources of atmospheric GEM (Denkenberger et al., 2012). Agnan et al. (2016) did an upscaling from GEM flux data collected by a total of 132 studies using enclosure and micrometeorological methods. They found that unpolluted terrestrial surfaces (background sites) with low total Hg concentrations (THg) in the soil ( $\leq 0.3 \mu\text{g g}^{-1}$ ) contributed to GEM re-emission in the same order of magnitude as Hg-enriched

sites ( $> 0.3 \mu\text{g THg g}^{-1}$  and/or  $\text{GEM} > 3 \text{ ng m}^{-3}$ ). Zhu et al. (2016) reported that 90% of the measured GEM fluxes from background soils range from  $-5$  to  $10 \text{ ng m}^{-2} \text{ h}^{-1}$ . Similar patterns can also be found for vegetative surfaces (grasslands, forest foliage and canopy level) and mixed vegetated waters (wetlands). However, these are generally lower than those measured over bare soils and open waters, supporting the view that vegetation reduces Hg emission by masking ground floor evasion and plant uptake.

However, quantitative estimates from background sites suffer from considerable uncertainties due to large temporal bias (towards summer and daytime measurements) and spatial bias (towards sites in the US, Europe and East-Asia), together with the large variation introduced by different flux measurement techniques (Agnan et al., 2016). Forests have been identified as net sinks of atmospheric Hg (Ericksen et al., 2003; Obrist, 2007), but estimates introduce large uncertainty in mass balance calculations because foliar exchange of Hg is still poorly understood. Agnan et al. (2016) reported that average GEM flux from background ecosystems such as grasslands and shrub lands ( $\sim 1 \text{ ng m}^{-2} \text{ h}^{-1}$ ) are usually smaller than fluxes from croplands ( $\sim 1.3 \text{ ng m}^{-2} \text{ h}^{-1}$ ) and bare soils ( $\sim 1.6 \text{ ng m}^{-2} \text{ h}^{-1}$ ). GEM flux measurements from snow surfaces were also reviewed and estimated to  $\sim 0.9 \text{ ng m}^{-2} \text{ h}^{-1}$ . The statistical summary of GEM flux observations over all types of wetlands revealed an average flux of  $13 \text{ ng m}^{-2} \text{ h}^{-1}$  ( $n = 23$ ) (Zhu et al., 2016). Agnan et al. (2016) excluded results from Hg-enriched wetland soils and calculated an average GEM flux of  $0.3 \text{ ng m}^{-2} \text{ h}^{-1}$ .

Factors that control GEM exchange at background sites are complex and include meteorological conditions, and atmospheric chemistry, soil characteristics and biological processes in the soil (for detailed discussion see Agnan et al., 2016 and Zhu et al., 2016).

Herein the focus lies on the quantification of land-atmosphere exchange of GEM from a boreal peatland. Hg cycling is illustrated in Figure 1.2 and potential controlling factors and mechanisms of peatland-atmosphere exchange of GEM are discussed below. In the atmosphere GEM can be oxidized to the more water-soluble GOM which may be adsorbed by aerosols to form PBM. The transport of GOM and PBM back to the surface happens directly via wet deposition associated with moisture (i.e. rain, snow, sleet, dew, clouds) or with water leaching from the canopy entering the peatland surface (throughfall). Dry deposition includes foliar uptake of GEM via stomata and through the leaf cuticle (subsequently deposited as litterfall), surface sorption of GEM and GOM to vegetation and soil, dissolution of GEM and GOM in the water body and gravitational deposition of PBM (Demers et al., 2007; Lindberg et al., 2007; Zhang et al., 2009; Gustin et al., 2011). Hg input via litterfall on peatlands is considered lower than in forest ecosystems (Miller et al., 2005), however, atmospheric GEM uptake by vascular plants and moss in northern hemispheric peat bogs is reported to be a factor of 3 to 4 times higher than from wet deposition alone (Biester et al., 2007). In line with these findings Enrico et al. (2016) showed net Hg accumulation in a peat bog in France accounting for  $34 \mu\text{g m}^{-2} \text{ yr}^{-1}$ , whereas Hg wet deposition was only  $9.3 \mu\text{g m}^{-2} \text{ yr}^{-1}$ . The total Hg (THg) concentration in the dominant herbaceous vegetation of a northern Swedish mire was  $17 \text{ ng g}^{-1}$ , with a range from  $5$  to  $48 \text{ ng g}^{-1}$  (Rydberg et al., 2010), whereas Sphagnum species sequestered significantly more THg compared to vascular plants. Strong differences in plant THg sequestration implies that changes in species composition have the potential to affect long-term Hg accumulation in the peat record.

Stamenkovic and Gustin (2009) have shown that both stomatal and non-stomatal processes are viable pathways for bi-directional Hg exchange. However, there is some disagreement regarding the ability of wetland plants to move Hg from the soil to air. Lindberg et al. (2002) suggested that aquatic plants not only uptake Hg but also have the ability to emit Hg into the atmosphere, most likely from pools in the rhizosphere. They showed that substantial amounts of GEM over cattails ( $31 \text{ ng m}^{-2} \text{ h}^{-1}$ ) and sawgrass ( $17 \text{ ng m}^{-2} \text{ h}^{-1}$ ) were “transpired” by plants. GEM evasion from the underlying water surface was comparably low ( $1 - 2 \text{ ng m}^{-2} \text{ h}^{-1}$ ). In contrast, Fay and Gustin (2007) found that cattails were not a source of atmospheric Hg. Disparities in flux measurements are assumed to depend on plant age, growing conditions and on the fact that fluxes are being measured from different surfaces and at different scales. Lindberg et al. (2005) found that transpiration of GEM from emergent macrophytes was associated with  $\text{CH}_4$  showing concurrent emission pulses for both gases. In boreal peatlands translocation of GEM from roots to leaves needs to be investigated but this process may be hindered due to the transport barrier at the root zone (Rutter et al., 2011; Cui et al., 2014), suggesting that the source of Hg in leaves is of atmospheric origin.

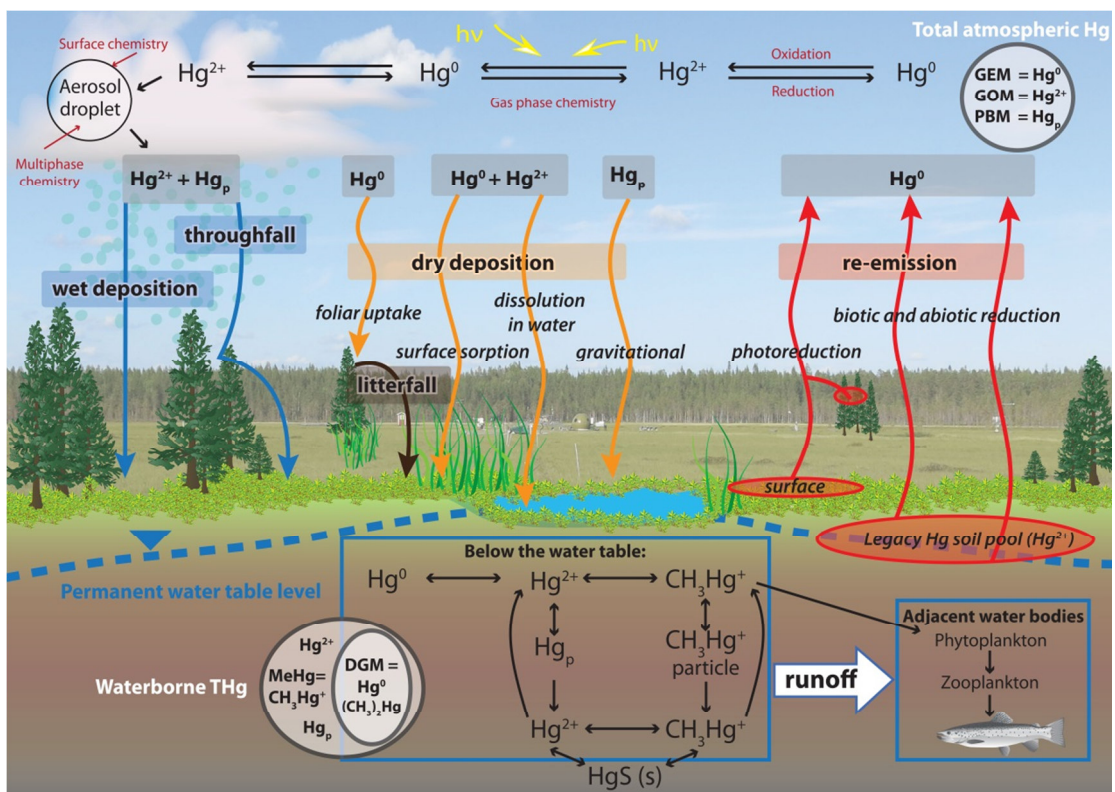


**Figure 1.2:** Conceptual model of the biogeochemical Hg cycle in a boreal peatland. Illustrated are common forms of Hg that are often quantified (adapted from Fritsche, 2008; Lasorsa et al., 2012; Ariya et al., 2015).

At the peatland surface reduction and re-emission of newly deposited Hg (fast soil pool) is reported to be driven by the presence of sunlight (Hintelmann et al., 2002; Poissant et al., 2004b; Selvendiran et al., 2008). The efficiency of photo-reduction depends on the availability of reducible  $\text{Hg}^{2+}$ -complexes, light wave length, and radiation intensity (Zhang et al., 2001; Gustin et al., 2002; Moore et al., 2005; Lin et al., 2010). Poissant et al. (2004b) showed that solar radiation explained almost 60% of the GEM flux variation from a flooded wetland

indicating the formation of dissolved gaseous Hg (DGM) via photochemical reactions and further air-water gas exchange (Amyot et al., 1994; Poissant et al., 2000; Zhang and Lindberg, 2001). Water surface fluxes of GEM in the Florida everglades ranged from  $-0.3$  to  $2.8 \text{ ng m}^{-2} \text{ h}^{-1}$  and showed a strong diel trend with emissions occurring during the day and weak deposition at night. Flux was highly correlated with solar radiation, but poorly correlated with water temperature (Marsik et al., 2005). Air temperature was the dominant controlling factor on GEM flux during dry conditions in the St. Francois wetlands of Canada and the flux was 40% lower compared to wet conditions (Poissant et al., 2004b). Selvendiran et al. (2008) reported both suppressed Hg volatilization from a riparian wetland when the soil surface was saturated and significant GEM emission peaks ( $\sim 12 \text{ ng m}^{-2} \text{ h}^{-1}$ ) in the afternoon from a beaver meadow in July. Average summertime GEM fluxes from a wetland in Finland were very small, ranging from  $-0.3$  to  $0.6 \text{ ng m}^{-2} \text{ h}^{-1}$ , and were lower than GEM emissions from the forest floor (Kyllönen et al., 2012). Enrico et al. (2016) also suggested that little photochemical re-emission takes place from the Sphagnum carpet based on an interpretation of Hg isotopic data.

However, it is not only photochemical processes at the surface that reduce  $\text{Hg}^{2+}$  but also abiotic reduction by natural organic matter associated with the slow soil pool (Alberts et al., 1974; Bergquist and Blum, 2007; Gu et al., 2011; Denkenberger et al., 2012). Nearly identical spatial patterns of THg in the peat and C in topsoil layers suggest that Hg deposition to the peat, i.e. the fraction that accumulates, is associated with organic matter and likely with organic S functional groups (Skjllberg et al., 2003; Selvendiran et al., 2008). Hg in the slow soil pool can reside for months up to centuries (Obrist et al., 2011), before it is eventually reduced and evaded back to the atmosphere. There is evidence that  $\text{Hg}^{2+}$  reduction and subsequent  $\text{Hg}^0$  evasion from soils is mainly related to aerobic organic matter decomposition during periods of elevated soil and air temperatures (Fritsche et al., 2008c; Obrist et al., 2009). A recent study, based on Hg isotope signatures found significant Hg re-emission ( $5 \mu\text{g m}^{-2} \text{ yr}^{-1}$ ) from boreal peat solely driven by non-photochemical abiotic reduction by natural organic matter (Jiskra et al., 2015). This study showed high mobility of Hg in reducing environments, despite high carbon accumulation rates. This indicates that the overall mass transfer of GEM from the saturated peat layers to the surface is less limited by diffusion than anticipated (Kim and Fitzgerald, 1986; Poissant and Casimir, 1998; Kuss et al., 2009). Additionally, ebullition of DGM together with other trace gases such as  $\text{CH}_4$  might play an important role in facilitating  $\text{Hg}^0$  evasion from deeper peat layers (Strack et al., 2005). In the unsaturated peat layers, increased vapor pressure of  $\text{Hg}^0$  and decreased sorption of  $\text{Hg}^{2+}$  to soil due to increasing thermal motion (Lin and Pehkonen, 1999) is suggested to facilitate diffusion and mass transport of  $\text{Hg}^0$  to the surface.

In addition to physically and chemically mediated  $\text{Hg}^0$  emissions, microbes are known to metabolically mediate the reduction of  $\text{Hg}^{2+}$  to  $\text{Hg}^0$  with the Hg reductase enzyme while obtaining energy for growth (Hansen et al., 1984; Schlüter, 2000). Fritsche et al. (2008c) showed that  $\text{Hg}^0$  emission from terrestrial background soils were at least partly controlled by biotic processes. However, low THg concentrations in remote peatlands and high amounts of organic matter are suggested to inhibit biotic reduction (Gabriel and Williamson, 2004).

In any case, some Hg in the peat will be transformed by different strains of bacteria and fungi from its inorganic or elemental form to MeHg (Gabriel and Williamson, 2004). The

abundance of MeHg is the net result of three major processes (i) formation by Hg methylation, (ii) degradation (demethylation), and (iii)  $\text{Hg}^{2+}$  reduction to  $\text{Hg}^0$  followed by evasion to the atmosphere. The methylation process is biotic and mediated by the activity of  $\text{SO}_4^{2-}$  and  $\text{Fe}^{3+}$  reducing bacteria and possibly methanogens. Generally, peatland ecosystems provide enough electron acceptors ( $\text{SO}_4^{2-}$ ,  $\text{Fe}^{3+}$  and  $\text{CO}_2$ ) and electron donors such as low molecular mass organic acids needed for methylation. The major process of MeHg degradation is driven by UV light in surface waters (Fernández-Gómez et al., 2013). Biotic demethylation processes are less well understood, but in several groups of bacteria detoxification processes acting via the merB operon have been identified (Barkay et al., 2003). Experiments have shown that methylation dominates in peatlands, designating them as hotspots for MeHg production and accumulation as well as important sources of MeHg to adjacent water bodies (St. Louis et al., 1994; Krabbenhoft et al., 1995; Driscoll et al., 1998). Availability and distribution of sulfur is probably the most important factor that determines the fate of MeHg in a peatland catchment (Skylberg et al., 2003; Åkerblom et al., 2013), and might also directly influence the quantity of  $\text{Hg}^0$  that evades. In transiently saturated peat layers at redox potentials above which sulfate reduction occurs,  $\text{Hg}^{2+}$  reduction is still possible with the help of electron donors such as  $\text{Fe}^{2+}$ , and humic and fulvic compounds (Gabriel and Williamson, 2004).

The recent era of elevated anthropogenic Hg emissions has increased atmospheric Hg deposition and led to a substantial storage of THg in the peat. Peat cores as archives of atmospheric pollution from Europe and North America indicate the highest THg concentrations in layers dated around 1950 (Jensen and Jensen, 1991; Givelet et al., 2003; Shotyk et al., 2005; Bindler, 2006; Charman, 2009; Farmer et al., 2009; Rydberg et al., 2010). Biester et al. (2012) stated that lower background Hg accumulation rates in peat as compared to lake sediments can be explained by peat diagenesis followed by Hg loss through volatilization or overland flow. Short-term tracer experiments have shown that historically deposited Hg can evade (Southworth et al., 2007). Although it is not known how much of the wet or dry deposited Hg was retained in the past, other trace elements, such as bromine or iodine, which also bind to organic carbon show retention of only 35 - 50% (Biester et al., 2004). Losses of buried Hg are likely to occur when 50 - 80% of the original carbon is lost through decomposition (Biester et al., 2012).

The current understanding is that decreasing Hg deposition will have little immediate impact on the terrestrial loading of Hg and MeHg to the aquatic food chain since there is already so much Hg stored in the peat (Meili et al., 2003). That view, however, is largely based on mass balances, where evasion of  $\text{Hg}^0$  back to the atmosphere is assumed small, but this has been hard to quantify due to the relative short-term data on GEM flux that is both spatially and temporally biased. Therefore, long-term ( $\geq 1$  year), quantitative GEM flux measurements are necessary to determine whether GEM emission from the peat may constitute an important pathway to reduce the pool of Hg available for methylation.



### 1.3 Elemental mercury flux measurement techniques

To reduce uncertainty in ecosystem mass balance calculations, a better mechanistic understanding of Hg reduction and Hg re-emission, together with progress in making continuous, long-term measurements of Hg land-atmosphere exchange are necessary. The theory and application of GEM flux measurement techniques have been documented extensively (Zhang et al., 2009; Gustin et al., 2011; Sommar et al., 2013a). DFCs and micro-meteorological (MM) techniques are the most widely applied approaches accounting for > 95% of all observations to date (Zhu et al., 2016). Bulk methods such as GEM/<sup>222</sup>Rn flux ratio (Obriest et al., 2006) and enriched isotope tracers (<sup>199</sup>Hg) (Mazur et al., 2015) are less abundant. Open-path laser optical spectroscopic (LIDAR) method and GEM/CO ratios have been applied to estimate Hg emissions from local and regional sources (Alden et al., 1982; Edner et al., 1991; Sjöholm et al., 2004; Jaffe et al., 2005; Fu et al., 2015a).

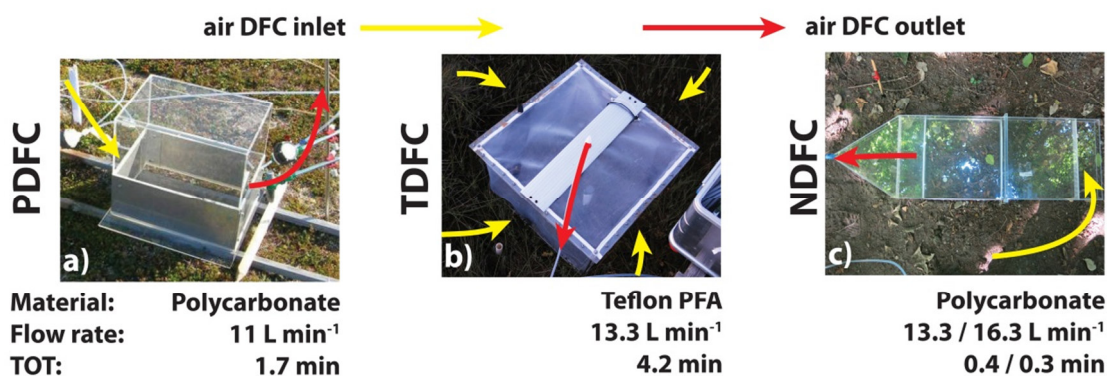


**Figure 1.3:** The herein applied enclosure methods comprise a polycarbonate dynamic flux chamber (PDFC), a Teflon® PFA DFC (TDFC) and a new type DFC (NDFC).

The first stainless steel DFCs were applied in Sweden over background lakes and soils in the 1980s (Schröder et al., 1989; Xiao et al., 1991). DFCs have enjoyed great popularity not only for GEM flux quantification but also in the determination of reactive gaseous compounds (e.g. NO, NO<sub>2</sub>, O<sub>3</sub>, BVOC, CO<sub>2</sub>) due to their relatively low cost, portability, and versatility (Sommar et al., 2013a). They come in many shapes and sizes and have been constructed from several different materials. Teflon® and quartz have been recommended due to their high light transmissivity and low blank values (Kim and Lindberg, 1995; Carpi et al., 2007; Eckley et al., 2010; Edwards and Howard et al., 2013).

The DFC is a mass balance technique with GEM flux calculated as

$$F_{DFC} = \frac{Q(C_i - C_o)}{A}, \quad (1.1)$$

where  $F_{DFC}$  is the flux (ng m<sup>-2</sup> h<sup>-1</sup>),  $Q$  is the DFC internal flushing flow rate (m<sup>3</sup> h<sup>-1</sup>),  $A$  is the DFC footprint (m<sup>2</sup>) and  $C_i - C_o$  is the GEM concentration difference (ng m<sup>-3</sup>) between measurements inside and outside the DFC. The concentrations are typically detected alternately using a cold vapor atomic fluorescence analyzer (e.g. Tekran Model 2537, Toronto, Canada). To derive the DFC mass balance we assume uniform surface shear velocity over the covered area and subsequently a constant flux.



The size of DFCs and applied flushing flow rates range from 1 to 32 L and 1.5 to 20 L min<sup>-1</sup> (Zhu et al., 2016). The continuous flushing of the DFCs resulted in a turnover time of the air volume inside the DFC ranging from 0.1 to 14 min. Eckley et al. (2010) recommended turnover times of 0.3 - 0.8 min.

Recent studies reported that differences in the material, footprint, volumes, sampling port position and, most importantly, the flushing flow rate can effect quantitative GEM flux measurements (Eckley et al., 2010; Lin et al., 2012). In addition to the uncertainties caused by varying flushing flow rates, altered radiation balance, warming of the air and changing moisture regimes inside the DFC resulted in micro-environment modifications that can bias the observed flux (e.g. Zhu et al., 2015a). To overcome the issue of non-uniform airstreams inside the DFC and the resulting unpredictable influence of the flushing flow rate on the measured flux, as well as to account for the effect of atmospheric turbulence, Lin et al. (2012) designed a new type DFC (NDFC). With the NDFC, a representative flux under ambient atmospheric conditions can be inferred from the measured NDFC flux multiplied by the ratio of the overall transfer coefficient under ambient atmospheric conditions and the overall mass transfer coefficient in the NDFC (Eq. 4.4).

Micrometeorological approaches depend on transport processes in the atmosphere and are affected by conditions of atmospheric stability. Compared to DFCs they have the capability of measuring landscape-scale flux under undisturbed conditions and are preferred for GEM flux quantification over vegetated surfaces (Zhu et al., 2015a). Optimal conditions for flux measurements exist if the GEM source area is homogeneous, an atmospheric surface layer develops, horizontal flux variability is low (e.g. no pollution plumes), and the flux above the surface remains constant with height (Wesely and Hicks, 2000). The most straight forward technique without any application of empirical constants would be the eddy covariance method, widely used for the measurement of the CO<sub>2</sub> and water exchange between an ecosystem and the atmosphere (Baldocchi et al., 2001). However, GEM concentrations are ~7 orders of magnitudes lower in the atmosphere compared to CO<sub>2</sub>, and there is no fast response sensor available yet for regular GEM flux measurements. Recently a cavity ring-down spectroscopy eddy covariance system has been deployed over Hg-enriched surfaces (~85 mg kg<sup>-1</sup>), but the detection limit (> 32 ng m<sup>-2</sup> h<sup>-1</sup>) was too high for use over background soils (Pierce et al., 2013; Pierce et al., 2015). The aerodynamic gradient method (AGM), the modified Bowen-ratio method (MBR), and the relaxed eddy accumulation method (REA) are currently the preferred approaches to quantify Hg fluxes. Both, the AGM and MBR rely on the quantification of the vertical concentration gradient of GEM in two or more sampling heights. AGM uses turbulent parameters (eddy diffusivity) while MBR uses scalar eddy covariance fluxes (e.g. CO<sub>2</sub>, sensible and latent heat flux) and a scalar concentration gradient to derive the GEM flux. The main drawbacks of these methods include the potentially different sink source characteristics of the fetch due to the two measurement heights and redox reactions of Hg<sup>0</sup>/Hg<sup>2+</sup> between the sampling inlets.

REA measures the GEM flux at just one height, and does not need a fast response sensor (Fig. 1.4). The technique is based on conditional sampling of GEM in updrafts ( $\overline{C_u}$ ) and downdrafts ( $\overline{C_d}$ ) using the vertical wind velocity signal ( $\sigma_w$ ) from a 3D sonic anemometer to control fast-response valves:

$$F_{REA} = \beta \sigma_w (\overline{C_u} - \overline{C_d}) \quad (1.2)$$

$\beta$  is the relaxation coefficient determined from concurrent eddy covariance measurements of a scalar with similar sink/source characteristics. Most studies use the sensible heat flux to calculate  $\beta$ . Often a zero-centered deadband is introduced. This enlarges the GEM concentration difference but also lowers the amount of air analyzed. Compared to DFCs or gradient methods, REA is expensive and requires specialized staff. REA usually resolves fluxes on a 30 min basis. Particular attention must be paid to potential offsets in updraft and downdraft lines, fast valve switching, flow control and problems associated with lags, length of sampling tubing and deadbands (Sommar et al., 2013b; Osterwalder et al., 2016). Until now GEM-REA systems have only been deployed over agricultural lands (Cobos et al., 2002; Olofsson et al., 2005b; Sommar et al., 2013b; Zhu et al., 2015a) and forest canopies (Bash and Miller, 2009).

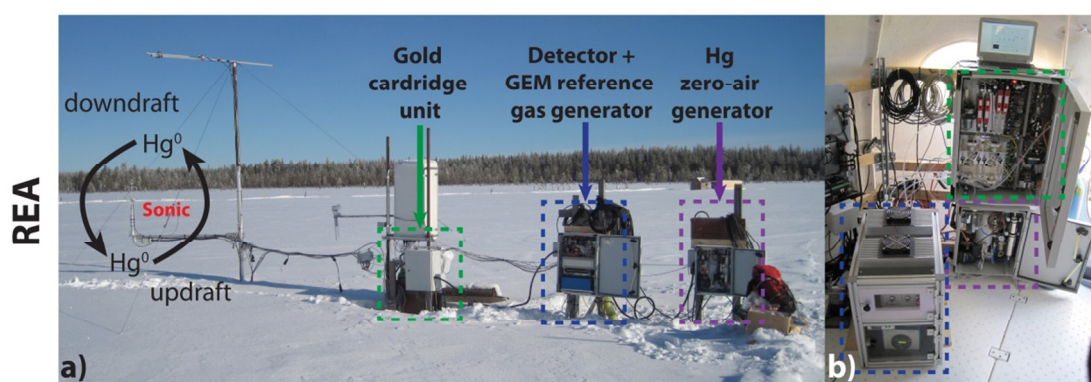


**Figure 1.4:** The REA system was set up at Degerö Stormyr in 2012 (a) and in Basel from 2013 to 2014 (b). It basically consists of a sonic anemometer, a gold cartridge unit, a Hg detector, a GEM reference gas unit and a Hg zero-air generator.

In most studies total gaseous Hg (TGM = GEM + GOM) is measured using a Tekran Model 2537 vapor-phase Hg analyzer. TGM is sampled, pre-concentrated on gold cartridges, thermally desorbed and detected by cold vapor atomic fluorescence spectroscopy (described in Gustin et al., 2015). Ideally the system is extended to a full Tekran 2537/1130/1135 speciation unit able to distinguish between GEM, GOM and PBM (Landis et al., 2002). A comparison of atmospheric Hg concentration measurements at the Dead Sea between a Model 2537 only and a full speciation unit revealed that the Model 2537 primarily measured GEM (Moore et al., 2013). It is likely that GOM and PBM are retained at the inlet filters (usually  $\sim 2\mu\text{m}$ ) (Brunke et al., 2010). For the flux measurements presented herein the term “GEM” was used consistently. This study includes quantitative GEM flux measurements over an urban setting and a boreal peatland using REA (Figs. 1.4a, 1.4b) and short-term campaigns using three different DFC designs at the same peatland as well as at an industrially contaminated site. A polycarbonate DFC (PDFC) and a Teflon® PFA DFC (TDFC) were both applied over the peatland (Figs. 1.3a, 1.3b). The NDFC was applied at the peatland and over the contaminated soils (Fig. 1.3c).

## 1.4 Objectives and outline of the thesis

The main goal of the thesis was to calculate the first annual Hg budget for a boreal peatland based on continuous measurements of the peatland-atmosphere exchange of GEM. It has been previously suggested that significant amounts of Hg return from the peat to the atmosphere and that GEM evasion constitutes an important pathway of Hg removal from the peatland now that global atmospheric GEM concentrations have been reduced compared to the levels several decades ago. Without knowledge of the peatland-atmosphere exchange of GEM we cannot predict how effective efforts to reduce anthropogenic Hg emissions will be in reducing the pool of Hg in peatlands, and ultimately the amount of MeHg in the catchment discharge.

To achieve this goal we developed and tested an advanced dual-inlet, single detector REA system designed to measure continuous, long-term GEM exchange on an ecosystem scale. In order to compare quantitative flux estimates from different methods, concurrent REA and DFC measurements were performed. Another research question was whether warming, changed moisture regimes and atmospheric pollutants influence GEM emission from peatlands. Finally, the NDFC was used to test if Hg vapor evading from industrially contaminated properties pose a risk of chronic poisoning for residents. Figure 1.5 provides an overview of the measurement locations and the time period over which measurements were performed.

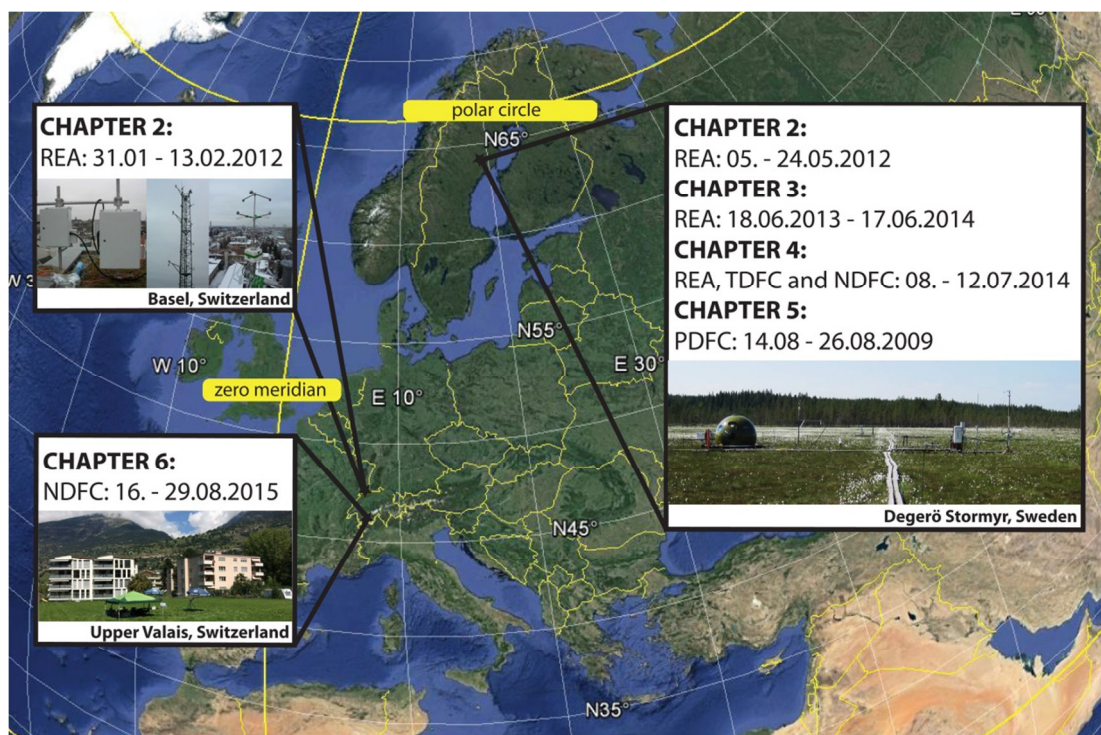


**Figure 1.5:** GEM flux observations were conducted in Switzerland over Basel and contaminated properties in the Upper Valais. The focus of the study lies on Hg cycling in a boreal peatland, located 70 km from the Gulf of Bothnia in the county of Västerbotten, Sweden.

The thesis is divided into five main parts (Fig. 1.5) presenting results and conclusions from field measurement campaigns in Sweden (boreal peatland) and Switzerland (urban canopy and contaminated site):

**Chapter 2** describes the novel functional principle of the dual-inlet, single detector REA system with the objective to reduce the major measurement uncertainty of earlier systems created by sequential sampling. The goals were to achieve (i) continuous simultaneous sampling of GEM in updrafts and downdrafts using two pairs of gold cartridges, (ii) accurate GEM quantification by regular injections of GEM standard concentrations and (iii) fully automated sampling procedures to reduce manpower. For system testing, campaigns were performed over the city of Basel in February 2012 and at Degerö Stormyr in May 2012.

**Chapter 3** presents the first annual (June 2013 - June 2014) Hg mass balance for a peatland based on continuous GEM flux measurements using REA, discharge Hg export, and Hg inputs via wet bulk deposition. The global surface covered by boreal peatlands is relatively small (< 3%). Nevertheless, understanding Hg cycling in peatlands is of particular importance because they are a major source of MeHg that contaminates downstream aquatic food webs and eventually poses serious health risks to humans. In addition, they are considered archives of atmospheric Hg deposition. This chapter aims to identify whether GEM evasion constitutes an important pathway to reduce the Hg pool in the soil available for methylation.

**Chapter 4** focuses on the comparison and evaluation of quantitatively derived GEM fluxes from both REA and two different DFC methods. During four consecutive days in July 2014 two replicate DFC measurements were performed repeatedly in every cardinal direction around the REA tower. The measured fluxes were examined with respect to magnitude, diel trends and correlation with meteorological parameters as well as soil surface characteristics such as THg in the topsoil, vascular plant coverage, water table level and concentration of DGM in the peat pore water.

**Chapter 5** attempts to distinguish how anthropogenic disturbances such as co-deposition of nitrogen and sulfur as well as an increase in temperature affect GEM flux. This was investigated using the PDFC in short-term studies on plots at Degerö that have been manipulated for over a decade to increase temperature, nitrogen and sulfur deposition in a factorial design experiment.

Finally, **Chapter 6** describes the results of measurements performed in order to determine how much the land-atmosphere flux over contaminated properties in the Upper Valais in Switzerland increased the atmospheric Hg concentrations at 1 m above the surface. The motivation behind this study was to estimate potential health risks for residents caused by chronic exposure to Hg vapor. The NDFC was applied to obtain quantitative flux measurements over nine properties with soil THg concentrations exceeding background levels by more than a factor of 1000. The results from the small-scale flux measurements were upscaled to the entire contaminated area to estimate the atmospheric transport of GEM to adjacent landscapes.

## CHAPTER 2

# A novel relaxed eddy accumulation system for long-term measurement of mercury flux

*This chapter is published in Atmospheric Measurement Techniques:*

S. Osterwalder<sup>1\*</sup>, J. Fritsche<sup>1</sup>, C. Alewell<sup>1</sup>, M. Schmutz<sup>1</sup>, M. B. Nilsson<sup>2</sup>, G. Jocher<sup>2</sup>, J. Sommar<sup>3</sup>, J. Rinne<sup>4</sup>, and K. Bishop<sup>5,6</sup>: A dual-inlet, single detector relaxed eddy accumulation system for long-term measurement of mercury flux, *Atmos. Meas. Tech.*, 9, 509-524, 2016.

[1] Department of Environmental Sciences, University of Basel, Basel, Switzerland

[2] Department of Forest Ecology and Management, Swedish University of Agricultural Sciences, Umeå, Sweden

[3] State Key Laboratory of Environmental Geochemistry, Institute of Geochemistry, Chinese Academy of Sciences, Guiyang, China

[4] Department of Physical Geography and Ecosystem Science, Lund University, Lund, Sweden

[5] Department of Aquatic Sciences and Assessment, Swedish University of Agricultural Sciences, Uppsala, Sweden

[6] Department of Earth Sciences, University of Uppsala, Uppsala, Sweden

[\*] Corresponding author

## Abstract

The fate of anthropogenic emissions of mercury (Hg) to the atmosphere is influenced by the exchange of elemental Hg with the earth surface. This exchange holds the key to a better understanding of Hg cycling from local to global scales which has been difficult to quantify. To advance research about land-atmosphere Hg interactions, we developed a dual-inlet, single detector relaxed eddy accumulation (REA) system. REA is an established technique for measuring turbulent fluxes of trace gases and aerosol particles in the atmospheric surface layer. Accurate determination of gaseous elemental mercury (GEM) fluxes has proven difficult due to technical challenges presented by extremely small concentration differences (typically  $< 0.5 \text{ ng m}^{-3}$ ) between updrafts and downdrafts. We present an advanced REA design that uses two inlets and two pairs of gold cartridges for continuous monitoring of GEM fluxes. This setup reduces the major uncertainty created by the sequential sampling in many previous designs. Additionally, the instrument is equipped with a GEM reference gas generator that monitors drift and recovery rates. These innovations facilitate continuous, autonomous measurement of GEM flux. To demonstrate the system performance, we present results from field campaigns in two contrasting environments: An urban setting with a heterogeneous fetch and a boreal peatland during snowmelt. The observed average emission rates were  $15 \text{ ng m}^{-2} \text{ h}^{-1}$  and  $3 \text{ ng m}^{-2} \text{ h}^{-1}$ , respectively. We believe that this dual-inlet, single detector approach is a significant improvement of the REA system for ultra-trace gases and can help to advance our understanding of long-term land-atmosphere exchange of GEM.

## 2.1 Introduction

The UN's legally binding Minamata Convention has been signed by 128 countries since October 2013 and aims to protect human health and welfare by reducing anthropogenic release of mercury (Hg) into the environment (UNEP, 2013c). Current anthropogenic sources, mainly from fossil fuel combustion, mining, waste incineration and industrial processes, are responsible for about 30% of annual Hg emissions to the atmosphere. 10% come from natural geological sources and the remaining 60% from re-emission of previously deposited Hg (UNEP, 2013b). As a result, long-range atmospheric transport of gaseous elemental mercury (GEM or Hg<sup>0</sup>) has led to Hg deposition and accumulation in soils and water bodies well in excess of natural levels even in remote areas, far away from anthropogenic pollution sources (Grigal, 2002; Slemr et al., 2003).

Quantification of Hg emission and deposition is needed to reduce the large gaps that exist in the global Hg mass balance estimates (Mason and Sheu, 2002) and as a basis of legislation targeting the control of Hg emissions (Lindberg et al., 2007). Gustin et al. (2008) suggest that today a substantial amount of Hg deposited on soils with natural background concentrations of Hg ( $< 0.1 \mu\text{g g}^{-1}$ ) is reemitted back to the atmosphere and that over the course of a year deposition is largely compensated for by re-emission, resulting in a net flux close to zero.

The state-of-the-art in field techniques to quantify Hg flux from terrestrial surfaces has been summarized in review papers (Gustin et al., 2005; 2008; 2011; Sommar et al., 2013a; Agnan et al., 2016). They conclude that environmental, physicochemical and meteorological factors as well as surface characteristics determine the accuracy and precision of GEM flux measurements. Fluxes are commonly determined using dynamic flux chambers (DFCs) or micrometeorological techniques (relaxed eddy accumulation [REA], modified Bowen-ratio [MBR] or the aerodynamic gradient [AGM] method). DFCs are the most widely used technique to measure in situ GEM fluxes since they are easy to handle and inexpensive. But DFCs alter the enclosed environment of the volume and surface area being studied by affecting atmospheric turbulence, temperature and humidity (Wallschläger et al., 1999; Gillis and Miller, 2000; Eckley et al., 2010). Also the concern about influencing plant physiology, means that DFCs are restricted to short-term measurements and studies comparing the relative differences between sites only, e.g. control and treatment experiments (Fritsche et al., 2014).

A major advantage of micrometeorological techniques is that they are conducted under conditions with minimal disturbance. As they can be applied continuously, they provide flux data valuable to characterize ecosystems as sinks or sources of atmospheric Hg and to interpret seasonal flux patterns. Micrometeorological techniques are also able to cover a much larger area than DFC techniques, although this larger "footprint" should be relatively flat and homogeneous. Several studies report results from land-atmosphere GEM exchange measurements over a variety of landscapes using MBR and AGM techniques (e.g. Kim et al., 1995; Meyers et al., 1996; Gustin et al., 2000; Lindberg and Meyers, 2001; Fritsche et al., 2008b; Converse et al., 2010). Fritsche et al. (2008a) concluded that micrometeorological techniques are appropriate to estimate Hg exchange rates, but often suffered from large uncertainties due to extremely low concentration gradients over background soils. Eddy covariance (EC) has the potential to detect high frequency atmospheric GEM concentration

fluctuations and might improve flux estimates considerably (Bauer et al., 2002; Fain et al., 2010). Pierce et al. (2015) conducted the first successful EC flux measurements of GEM over Hg-enriched soils measuring atmospheric GEM concentrations at high frequency (25 Hz). However, on background soils measured fluxes were below the detection limit.

To overcome the need for fast-response sensors, Desjardins (1977) has introduced the eddy accumulation method where fast-response sampling valves are combined with slow analysis techniques on the assumption that the turbulent covariance flux can be averaged separately for positive and negative vertical wind velocities. The technical breakthrough for REA was achieved by Businger and Oncley (1990), simulating the method with vertical wind, temperature and humidity time series in the surface layer. The main advantage of REA over other micro-meteorological methods is that REA requires sampling at only one height and therefore flux divergence may be measured directly (Sutton et al., 2001). Reactive substances can be lost by chemical reaction between two sampling heights (Olofsson et al., 2005a; Foken, 2006; Fritsche et al., 2008a), and sensors at two heights also have different footprints. REA eliminates these drawbacks (Bash and Miller, 2008). There are disadvantages to be considered as well though. The technical requirements for REA are very stringent, increasing the demand on the precision of the sampling and chemical analysis. Irregularities in offset measurements and timing of the sampling valves can also not be corrected for later (Sutton et al., 2001).

The REA method has been widely used since 1990 to investigate fluxes of different trace gases and aerosols (e.g. Brut et al., 2004; Gaman et al., 2004; Olofsson et al., 2005a; Haapanala et al., 2006; Arnts et al., 2013). This includes a few applications on land-atmosphere exchange of GEM over soils (Cobos et al., 2002; Olofsson et al., 2005b; Sommar et al., 2013b; Zhu et al., 2015a), and forest canopies (Bash and Miller, 2007; 2008; 2009). Additionally, reactive gaseous Hg fluxes have been measured over snow surfaces in the Arctic (Skov et al., 2006). Besides valuable data of net exchange rates of GEM over different environments, the studies have also identified potential for refinement in the technical implementation of REA. The dual detector system presented by Olofsson et al. (2005b) was criticized since it suffered from inherent variability and drift of sensitivity between the two Hg detectors (Sommar et al., 2013b). Sommar et al. (2013b) modified the systems employed by Cobos et al. (2002) and Bash and Miller (2008) to create a single-inlet REA system. However, their system lacks the capability to accumulate samples from the up- and downdraft channels synchronously. The application of sequential measurement of the channels impairs the accuracy with which fluxes can be gauged when the concentration of atmospheric GEM varies on the scale of the sampling period (Zhu et al., 2015b).

Even though there has been steady improvement in REA systems for measuring GEM fluxes, the financial and technical challenges to accurately measure the extremely low concentration differences (sub-ppt range) in up- and downdrafts have limited the number of studies (Foken, 2006). Thus, there remains a demand for a system especially designed to continuously monitor background GEM fluxes with minimum maintenance requirements. To address these needs we designed a fully automated REA system with two inlet lines for continuous air sampling. The GEM contained in these samples is collected on a pair of gold cartridges: with one for updraft and, the other for downdraft. Two such pairs of gold cartridges are used, with one pair collecting GEM while the other pair is analyzed on a single Hg detector,



one cartridge after the other. To detect any instrument drift, contamination and changes in GEM recovery, the system is equipped with a GEM reference gas generator and a Hg zero-air generator.

Our objective was to develop an advanced REA system that reduces the major measurement uncertainty of earlier systems created by sequential sampling procedures. We achieved this goal by:

- 1) continuous, simultaneous sampling of GEM in up- and downdrafts using two pairs of gold cartridges.
- 2) regular analysis of a GEM reference gas as well as dry, Hg-free air to monitor accurate GEM quantification.
- 3) fully automated air sampling and GEM analysis with an on-line user interface that provides comprehensive information about system performance.

To test the system's performance under field conditions, we deployed it in two contrasting environments during campaigns of two to three weeks each. At the first site in the center of Basel, Switzerland, GEM fluxes were measured 20 m above the roof of a building, 39 m above ground level. Later on the system was installed 1.8 m above a boreal peatland called Degerö Stormyr in northern Sweden during snowmelt.

This paper includes a description of the novelties in the REA design and presents a time series of GEM flux measurements from each of the deployments with contrasting atmospheric conditions and site characteristics. To analyze the system performance we compared source-sink characteristics using footprint models and analyzed turbulence regimes to determine possible flux attenuation. We briefly discuss several instrumental factors which might affect the accuracy of the flux measurements: bias in vertical wind measurements, control and response time of the REA sampling valves, measurement precision of the sample volumes, as well as the performance of analytical schemes and calibration procedures. Furthermore we describe the evaluation of the  $\beta$  constant, the method detection limit and rejection criteria for flux measurements based on the REA validation procedure.

## 2.2 Methods

### 2.2.1 GEM-REA sampling system

The concept of our advanced REA design is based on a GEM sampling unit with two pairs of gold cartridges, a single Hg detector as well as a GEM reference gas generator and a Hg zero-air generator. Figure 2.1 illustrates the setup of the sampling and analysis system. Table S2.1 in the Supporting Information lists the major components. Both study sites are equipped with continuously operating EC systems that have been measuring sensible and latent heat flux and CO<sub>2</sub> exchange at 30 min intervals (Sagerfors et al., 2008; Lietzke and Vogt, 2013) for many years. A suite of meteorological parameters were recorded as well: solar radiation, air and soil temperature, relative humidity, precipitation, snow depth, wind speed and direction, friction velocity, and surface layer stability parameters.

Vertical wind velocity GEM flux quantification was measured with a 3-D sonic anemometer (10 Hz) (A1, A2). The wind signal was transferred to three fast-response switching solenoid valves (B) via LabVIEW (C) enabling sampling and separation of air into updraft, downdraft and deadband channels. The fast-response valves were installed 0.2 m downstream of the sampling inlets. The inlets of the ¼"-Teflon® PTFE sampling lines (D) were mounted near the anemometer head about 15 cm below the midpoint of the ultrasound paths.

GEM carried in the “updrafts” and “downdrafts” was then collected on two pairs of gold cartridges. The flux [ $\text{ng m}^{-2} \text{h}^{-1}$ ] was calculated from the GEM concentration difference [ $\text{ng m}^{-3}$ ] in updraft ( $\overline{C}_u$ ) and downdraft ( $\overline{C}_d$ ) air, multiplied by  $\sigma_w$  [ $\text{m s}^{-1}$ ], the standard deviation of vertical wind velocity.

$$F_{GEM} = \beta \sigma_w (\overline{C}_u - \overline{C}_d) \quad (2.1)$$

$\beta$  is the unitless flux proportionality coefficient and depends on the wind velocity deadband (see Sect. 2.3.1) that is implemented to increase the concentration difference.  $\beta$ -values typically range between 0.4 and 0.6. Deadband widths [ $\text{m s}^{-1}$ ] used in recent REA measurement studies ranged from 0.33 to 0.6 times  $\sigma_w$  (Grönholm et al., 2008).

During the campaign in Basel larger eddies resulted in lower valve switching frequencies relative to the situation at Degerö. The atmospheric GEM concentration differences between updraft and downdraft were also larger in Basel. This made the fixed deadband appropriate for Basel, while a dynamic deadband was more favorable for Degerö. A fixed deadband makes  $\beta$  dependent on atmospheric conditions (Milne et al., 1999, 2001), with increased deadband widths leading to lower  $\beta$ -values (Ammann, 1999). The application of a dynamic deadband at Degerö, with its smaller eddies, aimed to reduce the switching frequency of the fast-response valves. Using a dynamic deadband also ensured that large enough air volumes for the GEM analysis were measured that would not have been guaranteed by measuring with a fixed deadband. A dynamic deadband is applied more often (cf. Gaman et al., 2004; Olofsson et al., 2005b; Haapanala et al., 2006; Ren et al., 2011) and enables the use of a constant  $\beta$  (Grönholm et al., 2008).

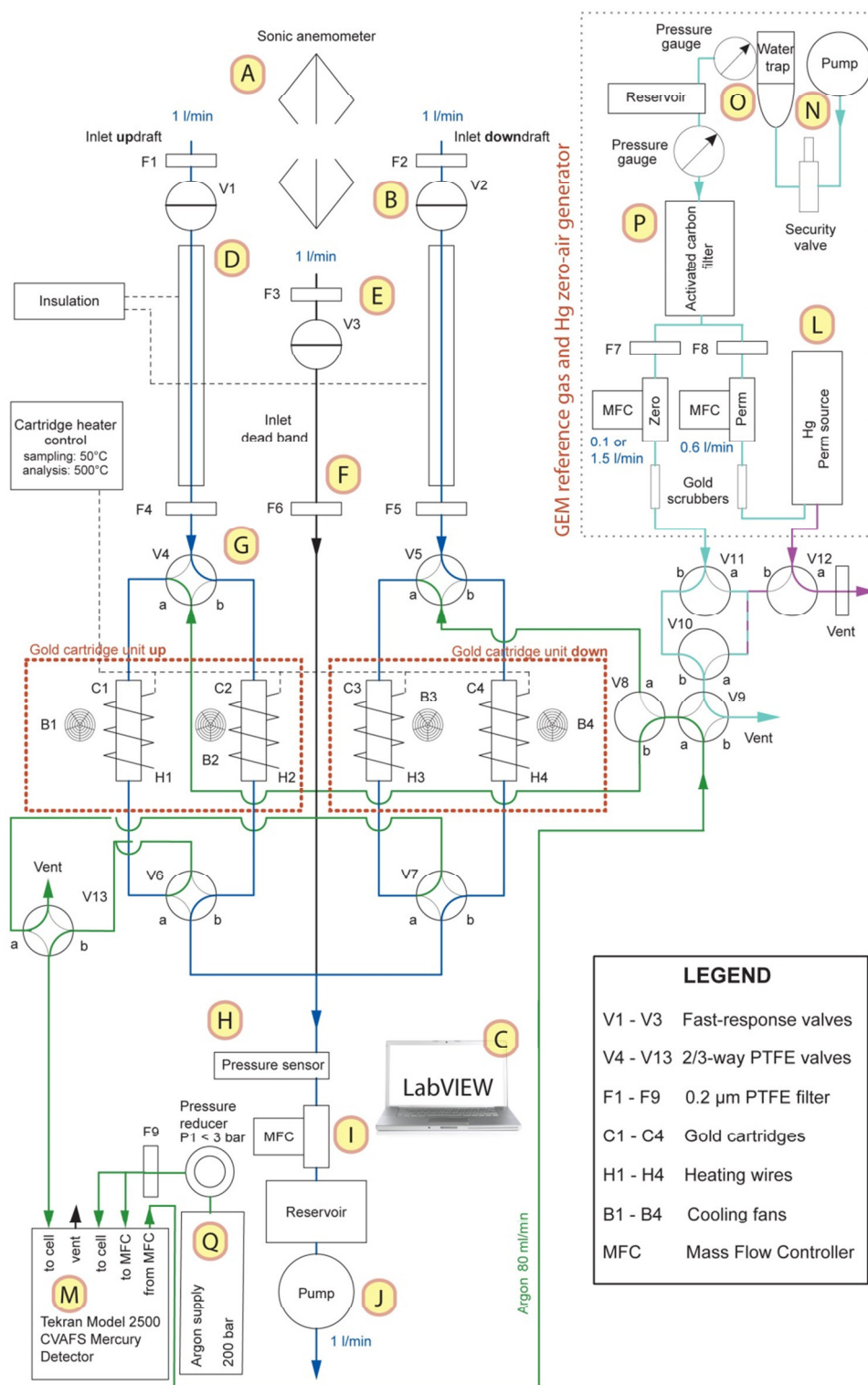


**Figure 2.1:** Schematic of the REA system hardware. It consists of a GEM sampling unit, a GEM reference gas generator and a Hg zero-air generator (upper right). Capital letters refer to REA components mentioned in the text and described in Table S2.1 in the Supporting Information. The air volume drawn over the gold cartridges equaled  $1 \text{ L min}^{-1}$  in Basel and  $1.5 \text{ L min}^{-1}$  at Degerö.

$\beta$  was calculated from the sonic temperature for each 30 min period at the same intervals used for the “up” and “down” GEM sampling system:

$$\beta = \frac{\overline{w'T'}}{\sigma_w(\overline{T_u} - \overline{T_d})}, \quad (2.2)$$

where  $\overline{T_u}$  and  $\overline{T_d}$  are the “up” and “down” averages of temperature,  $\overline{w'T'}$ , is the EC sensible heat flux. In our application a recursive high-pass filter was implemented to reduce low-frequency bias in turbulent time series of the vertical wind velocity (McMillen, 1988; Richardson et al., 2012):

$$\chi_i = \alpha\chi_{i-1} + (1 - \alpha)\chi, \quad (2.3)$$

where  $\chi_i$  is the filtered value,  $\chi_{i-1}$  was the running mean from the previous time step, and  $\chi$  the current, instantaneous value (Meyers et al., 2006).

$$\alpha = e^{-\frac{\Delta t}{\tau}} \quad (2.4)$$

The constant  $\alpha$  results from the sampling interval of 10 Hz ( $\Delta t$ ) and the time constant ( $\tau$ ) which was set to 1000 s.

The sampling lines were 20 m long, and insulated to avoid condensation. 0.2  $\mu\text{m}$  Teflon® PTFE filters (E, F) were installed after the inlets and before the Teflon® PTFE valves, V4 and V5 (G). The resistance through the sampling lines was checked to be equal using thermal mass flow meters (Vögtlin Instruments AG, Switzerland). Conditionally sampled GEM is subsequently accumulated on two matched pairs of gold cartridges (Tekran, Canada, difference between cartridge sensitivity < 5% according to manufacturing tests by the supplier). Heating wires around the cartridges were kept at 50°C during the sampling phase and heated to 500°C during the desorption process (see Sect. 2.2.2). Downstream, a pressure sensor (H) operating at 10 Hz was installed to monitor pressure fluctuations. A high-precision thermal mass flow controller (MFC) (I) with a response time of 50 ms was used to regulate the air volume drawn over the gold cartridges. To dampen sampling flow disturbances a reservoir of 200 mL was installed between the pump and the MFC. Air was drawn through the three lines by a rotary vane pump (J) at a rate of 1 L min<sup>-1</sup> (Basel) and 1.5 L min<sup>-1</sup> (Degerö), respectively. Three temperature-controlled, weatherproof boxes (K) contained the GEM reference gas generator (L) and Hg detector (M), the gold cartridge unit and the control system as well as a Hg zero-air generator to produce dry, Hg-free air. Remote control of the system allowed online checks of the data and detection of instrumental failures.

### 2.2.2 GEM analysis

Air sampling and GEM analysis was performed in parallel in 30 min intervals (Fig. 2.2). GEM in air samples and injections from the GEM reference gas and Hg zero-air generator were quantified using cold vapor atomic fluorescence spectroscopy (CVAFS) (M). The temperature controlled GEM reference gas generator provided precise GEM concentrations in a constant stream of dry, Hg-free air. The average recovery of the GEM standard was determined by back calculation from the manual calibration of the Hg detector. The average loading on gold cartridge pair 2-4 corresponded to 27.2  $\pm$  1.1 and 22.2  $\pm$  1.3 pg in Basel and 32.1  $\pm$  2.1 and 32.1  $\pm$  2.3 pg at Degerö. Dry, Hg-free air was generated using an air compressor (N) with air

dryer (O) and an activated carbon filter (P). Additional gold mercury scrubbers were installed at the outlet of the Hg zero-air generator.

Figure 2.2 illustrates the sampling and analysis sequence. Upon startup cartridges C2 and C4 are in the air sampling mode, while GEM previously collected on C1 and C3 is analyzed. During the first 5 min GEM of the idle cartridges is desorbed by heating the cartridges to 500°C in a stream (80 mL min<sup>-1</sup>) of high purity Argon (Ar) carrier gas (Q). The cartridge analysis procedure for individual samples included five steps: Ar-flushing (20 s), recording baseline (10 s), cartridge heating (28 s), peak delay (30 s) and cooling of the cartridges (60 s). After up- and downdraft air samples had been analyzed (Aa), the cartridges were loaded for 5 min each with either GEM reference gas (ref) or dry, Hg-free air (clean). The flow rate of dry, Hg-free air (carrier gas) through the GEM reference gas generator was set to 600 mL min<sup>-1</sup> using a MFC. The GEM reference gas was pre-mixed with 100 mL min<sup>-1</sup> dry, Hg-free air before being supplied to the cartridges. Dry, Hg-free air was delivered at a flow rate of 1500 mL min<sup>-1</sup> regulated by another MFC. The cartridges loaded with ref/clean air were analyzed (Ab phase in Fig. 2.2) following the same procedure as the air samples.

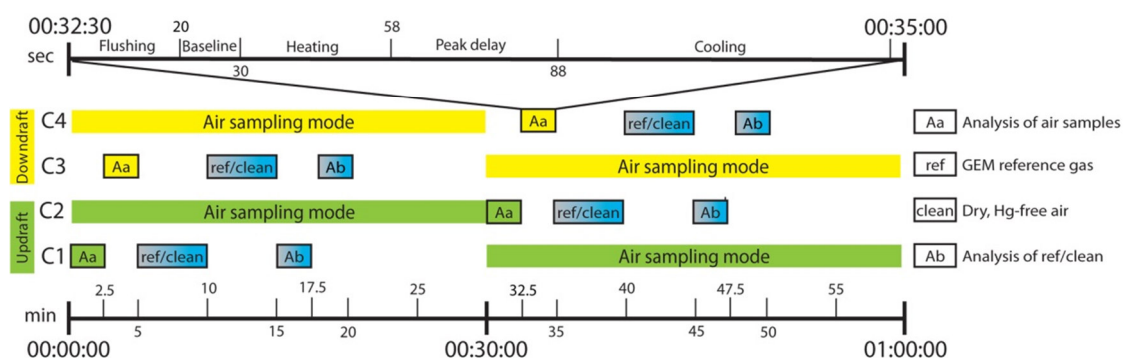


**Figure 2.2:** The hourly measuring cycle of the REA system subdivided into the air sampling and GEM analysis procedures (Aa, ref/clean, Ab). At the start of a sequence, gold cartridge pair C2 and C4 adsorb GEM in the up- and downdraft simultaneously while previously adsorbed GEM from gold cartridges C1 and C3 is analyzed. During each cycle, eight analysis procedures which last for 2.5 min were conducted.

The average and standard deviation of the Hg detector baseline were calculated for periods of three seconds before and after the Hg peak. The baseline below the peak was interpolated and subtracted from the peak. The peak areas were logged together with 30 min averages of the sampled air volume, opening times and number of switching operations of the fast-response valves. Air temperatures within the weatherproof boxes, Hg detector lamp- and UV sensor voltages as well as pressure sensor data were also recorded.

### 2.2.3 QA/QC

#### Calibration of Hg detector

The REA system was calibrated after the field campaigns using a temperature-controlled Hg vapor calibration unit (R) together with a digital syringe (S). Different concentrations of saturated GEM vapor were injected into the Hg-free air stream provided by a Hg zero-air

generator (T). During calibration a simulated wind signal was used to supply both lines with an equal amount of air. Calibration factors were gained by linear regression between the injected quantity of GEM and observed peak areas (Fig. S2.1).

### Monitoring of GEM recovery

Repeated injections from the GEM reference gas and Hg zero-air generator (Fig. 2.2) were performed to observe possible contamination, passivation or drift of the gold cartridges, as well as to check for temperature sensitivity in the Hg detector. Before and after a measurement campaign the system was checked for leaks by measuring dry, Hg-free air from the Hg zero-air generator and by constricting the sampling lines temporarily to check for pressure decrease within the lines. Teflon® PTFE parts and tubing were cleaned with 5% nitric acid according to a standard operating procedure (adapted from Keeler and Landis, 1994).

### Bias of sampling lines

To assess potential systematic bias between up- and downdraft sampling lines, GEM reference gas was supplied to both lines. During five days in Basel and 28h at Degerö, the REA-system dynamically sampled reference gas using 2s-simulated wind signal to acquire identical up- and downdraft samples with respect to volume and GEM concentration. Accordingly, concentration bias between the REA sampling lines was corrected for in the GEM flux calculation.

#### 2.2.4 Data processing

The analyzed air samples ( $Aa$ ) for each gold cartridge were corrected for temperature sensitivity of the Hg detector by dividing the average GEM reference gas concentration over the entire campaign ( $\overline{Ab_r}$ ) through single GEM reference gas measurements ( $Ab_r$ ) according to:

$$A_{corr} = Aa \cdot \frac{\overline{Ab_r}}{Ab_r}. \quad (2.5)$$

GEM concentrations ( $\overline{C_{GEM}}$ ) in up- and downdraft were computed by applying intercept ( $b$ ) and slopes ( $s$ ) calculated from the manual calibration procedure (Sect. 2.2.3) and the air volumes ( $V$ ) drawn over the gold cartridges:

$$\overline{C_{GEM}} = \frac{A_{corr} - b}{s} \cdot \frac{1}{V}. \quad (2.6)$$

GEM concentration differences were corrected for the bias between the two sampling lines (Sect. 2.3.3). Finally, the GEM flux was derived following Equation 2.1. As the sampled air was not dried before being measured with a MFC calibrated for dry air, GEM fluxes were corrected for variations in the water vapor content of the air following Lee (2000):

$$F_{GEMcorr} = (1 + 1.85\zeta)F_{GEM} + 1.85 \frac{\overline{D_{GEM}}}{\overline{p_a}} LE_m, \quad (2.7)$$

where  $F_{GEMcorr}$  is the corrected and  $F_{GEM}$  the uncorrected GEM flux [ $\text{ng m}^{-2} \text{h}^{-1}$ ].  $\zeta$  is the water vapor mixing ratio [ $\text{kg kg}^{-1}$ ].  $LE_m$  is the water vapor flux [ $\text{ng m}^{-2} \text{h}^{-1}$ ], and the ratio of mean GEM

density ( $\bar{\rho}_{GEM}$ ) to mean air density ( $\bar{\rho}_a$ ) were determined from the data for each measurement interval.

Criteria to identify conditions under which REA is not valid will be presented in Sect. 2.3.1. Among them an integral turbulence characteristics test was applied to identify the development of turbulent conditions:

$$\frac{\sigma_w}{u_*} = 1.3 \cdot \left(1 - 2 \cdot \frac{z}{L}\right)^{\frac{1}{3}}, \quad (2.8)$$

including  $\sigma_w$ , friction velocity ( $u^*$ ), measuring height ( $z$ ) and Obukhov length ( $L$ ). Therein, the dependent integral turbulence characteristic for vertical wind velocity ( $\sigma_w/u^*$ ) equates with a model dependent on stability ( $z/L$ ) (Panofsky and Dutton, 1984; Foken and Wichura, 1996; Foken, 2006). A deviation by more than a factor of 2 from the model was used as the threshold to reject periods of insufficient turbulence as well as periods of larger than expected turbulence (Fig. S2.2).

The effect of a potentially dampened GEM flux due to high- and low-frequency losses of the turbulent eddies has been derived by interpretation of turbulence spectra for both sites dependent on instrumental properties (lateral sensor separation), measuring height, wind speed and stability conditions (Sect. 2.3.3). The applied high-pass filter (Eqs. 2.3, 2.4) amplifies the attenuation by reducing random or systematic noise in the flux estimates caused by low-frequency bias in the turbulent time series. High frequency attenuation might be caused by an electronic delay of the valve switching and sensor separation (Foken et al., 2012).

To predict the size of REA flux source areas during the campaigns the footprint model of Kormann and Meixner (2001) was applied in Basel and a Lagrangian stochastic forward model following Rannik et al. (2000) at Degerö. The footprint models were chosen in order to fit the specific requirements as defined by the source areas at each site. The actual source area was estimated for each half-hour period based on wind direction, wind speed, stability, surface roughness and sensor height.

### 2.2.5 Site descriptions

The climate in the city of Basel, Switzerland (47.56 N, 7.58 E; 264 m a.s.l.) is temperate with a mean annual temperature of +9.8 °C and 776 mm precipitation (MeteoSchweiz, 2014). The REA system was deployed on the flat roof of the University of Basel's Meteorology, Climatology and Remote Sensing Laboratory (MCR) 20 m above the ground. The REA sampling inlets were mounted on the top of the permanently installed tower at 39 m above ground level. The average building height around the tower is 17 m and the 90% cumulative footprint mirrors dominant wind directions, which are W to NW (240° - 340°) and ESE (100° - 140°). Results from this site reflect the situation within the urban inertial sublayer (Lietzke and Vogt, 2013).

The second campaign was conducted at an Integrated Carbon Observation System (ICOS) site in the center of a boreal peatland in Sweden (64.18 N, 19.55 E; 270 m.a.s.l.) during snowmelt. The mixed acid mire system covers 6.5 km<sup>2</sup> and is located in the Kulbäcksliden Research Park of the Svartberget Long-Term Experimental Research (LTER) facility near the town of Vindelön, county of Västerbotten, Sweden. The site is part of the Swedish research infra-structure (funded by the Swedish Research Council). The snow cover normally reaches a

depth up to 0.6 m and lasts for 6 months on average (Sagerfors et al., 2008). The average  $\pm$  SD total Hg concentrations (THg) in the upper 40 cm of the peatland soil are  $57 \pm 6$  ng g<sup>-1</sup> dry matter, which is a typical value for soils in northern Sweden (Shanley and Bishop, 2012; Åkerblom et al., 2013). The climate of the site is defined as humid cold temperate with mean annual precipitation and temperature of 523 mm and +1.2°C, respectively (Alexandersson et al., 1991). A measurement height of 1.8 m above the surface was maintained by gradually decreasing of the instrumentation boom to account for snowmelt. Dominant wind direction during summer is NE and SE during winter. For a more detailed site description see Granberg et al. (2001) or Peichl et al. (2013).



## 2.3 Results and Discussion

### 2.3.1 REA performance

#### Sampling accuracy

Compared to single-inlet REA designs, systems with separate inlets for up- and downdraft are less prone to measurement uncertainty due to unsynchronized conditional sampling (Baker et al., 1992) and high frequency concentration fluctuations in the tube flow (Moravek et al., 2013). Zhu et al. (2015b) found that the calculation of concentration differences based on temporally intermittent GEM measurements (non-stationarity of atmospheric GEM concentrations) introduced the largest source of uncertainty in their single-inlet Hg<sup>0</sup>-REA system. Accurate simultaneous sampling of GEM concentration using a two-inlet design is thus the major technical improvement of our system compared to most Hg-REA systems used to date, as summarized in Sommar et al. (2013a). But even though the dual-inlet avoids a major source of error, there are a number of other aspects of a REA-Hg system that need to work as well as possible to measure land-atmosphere GEM fluxes. One of these is the determination of the  $\beta$ -value, which includes sonic temperature and sensible heat flux measurements (Sect. 2.3.1). It is estimated to introduce an uncertainty similar to Zhu et al. (2015b) of approximately 10%. Uncertainty due to flux dampening of sampled low and high frequency concentration fluctuations is small and just relevant during specific stability and wind speed conditions depending on measurement height and quality of turbulence (Sect. 2.3.3). There are several other sources of error in the measurements such as (I) the possible bias in vertical wind velocity measurements, (II) the precision of the switching of the fast-response valves, (III) the sampled air volume, (IV) the peak integration and (V) the field calibration procedure (cf. Zhu et al., 2015b).

(I) Vertical wind velocity is used for instantaneous valve control. Ammann (1999) ascribed the main error here to be the possibility for misalignment between the wind field and the sensor head due to a tilted sensor setup or wind distortion around the sensor. However, the application of a high-pass filter combined with a deadband was able to alleviate averaged vertical wind velocity bias from the wind signal.

(II) It is important to limit the electronic delay to switch the fast-response valves caused by the digital measurements system and signal processing. The effective response time to actuate the fast-response valves was determined to be 18 ms for the opening and 8 ms for the closing.

(III) A major challenge in applying a system with two inlet tubes and no dry Hg-free air addition at the inlets (as applied by Sommar et al., 2013b) is to control flow pressure that builds up within the sampling lines. Flow surges are dependent on the time the fast-response valves remain closed. Pressure variations were dampened by a reservoir of 200 mL volume between the pump and mass flow controller (Fig. 2.1). The resistance within the lines was initially checked to be equal to minimize pressure anomalies between the three flow paths. A simulated wind signal with fast-response valve opening times of 2 s for the up- and downdraft and 1 s for the deadband was applied and revealed maximal

pressure fluctuations of 35 mbar. The vast majority of the 30 min measurements in Basel and Degerö showed higher switching rates which are generally associated with lower pressure fluctuations. The total volumes drawn over updraft, downdraft and deadband lines averaged  $30 \pm 0.09$  in Basel and  $45 \pm 0.01$  l ( $\pm$ SD) at Degerö. The proportion of the air not analyzed accounted for 10.5 l in Basel and 20.3 l at Degerö. Measurements were discarded if the volume deviated more than 2.5% from the flow setting value of the mass flow controller (cf. Sect. 2.3.1).

(IV) An analysis of the detector peaks indicated that the signal for atmospheric and GEM reference gas samples were statistically different from blank measurements (99% confidence) (Fig. 2.3).

(V) The manual calibration procedure revealed a strong linear relationship between peak areas and syringe-injected GEM reference gas for the gold cartridge pairs (Fig. S2.1). The automated injection of GEM reference gas provided a 2-hourly quality control measure to monitor any bias caused by the temperature sensitivity of the Hg detector. The air temperature surrounding the Hg detector showed a strong linear relationship with the GEM reference gas measurements for up- and downdraft in Basel and a less pronounced dependence at Degerö (Fig. 2.4). The uncertainty of concentration measurements for our REA system is basically introduced by sampling-line bias, wherefrom the method detection limit is derived (Sects. 2.2.3 and 2.3.1).

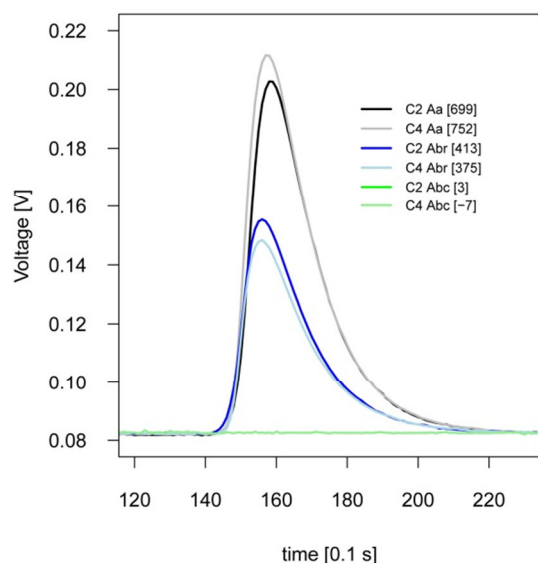


**Figure 2.3:** Representative peak recovery for gold cartridge pair C2-C4 during ambient air (Aa), GEM reference gas (Abr) and dry, Hg-free air measurements (Abc) on 11 February 2012, between 14:00 and 15:30 in Basel. The values in squared brackets equal the areas between the curves and the baseline. The plots show an extract of 10 s from the peak delay sequence which takes 30 seconds in total. Y axis indicates the Hg detector baseline voltage (V).

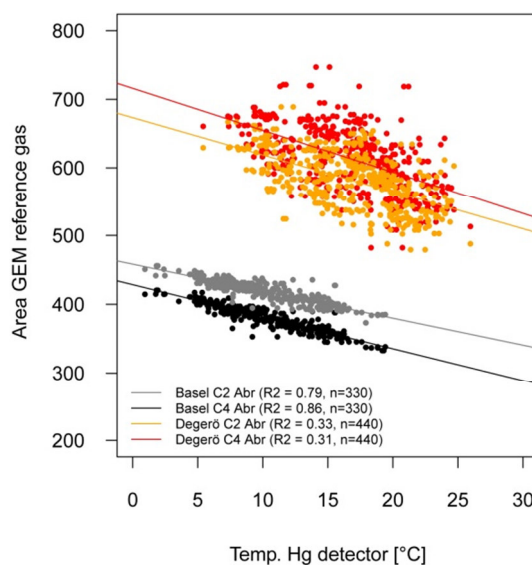


**Figure 2.4:** Linear relationship between GEM reference gas (Abr) measured with gold cartridge pair C2-C4 in Basel (grey, black) and Degerö (orange, red), respectively and air temperatures within the Hg detector box.

### **$\beta$ -factor evaluation**

In this study,  $\beta$  is derived from EC time series of temperature and vertical wind speed at both sites (Eq. 2.2) during methodologically favorable conditions (cf. Sect. 3.1.4) with respect to turbulence for every 30 min GEM flux measurement averaging period. Due to considerable scatter in  $\beta$  especially during periods when sensible heat flux diminished to near zero, data were omitted for kinematic heat flux within the range of  $\pm 0.01 \text{ K m s}^{-1}$  (Ammann and Meixner, 2002; Sommar et al., 2013b). In accordance with Hensen et al. (2009) only  $\beta$  factors in the range of 0.1 - 1 were used. During the first study in Basel a fixed deadband of  $|w'| = 0.2 \text{ m s}^{-1}$  was applied. This was done to restrict the analysis to periods when the discrimination between updraft and downdraft was large enough to allow for accurate estimation and to prolong the opening times of the fast-response valves. At Degerö a dynamic deadband approach with a sampling threshold  $\pm 0.5\sigma_w$  was used. Data analysis revealed that the effect of surface layer stability or  $u^*$  on  $\beta$ -calculation was negligible. The median  $\pm$  mad (median absolute deviation) of observed  $\beta$ -values in Basel and Degerö was  $0.49 \pm 0.21$  ( $n = 391$ ) and  $0.45 \pm 0.20$  ( $n = 342$ ), respectively. Median  $\beta$ -values observed at Basel and Degerö concurred with literature in the range of 0.4 - 0.6 as listed in Grönholm et al. (2008), Bash and Miller (2009), Arnts et al. (2013), Sommar et al. (2013a).

The Basel measurements resulted in broad non-Gaussian frequency distributions for the fraction of time when air was sampled into up- and down reservoirs. The average cumulated opening times for the 30 min sampling periods for the up- and downdrafts were 9.6 and 9.8 min respectively, which results in maxima in up/down/deadband sampling fractions of about 32%/33%/35%. Periods of less developed turbulence caused the fast-response valves to switch less often and increased the opening times of the deadband. The corresponding confined frequency distributions observed at Degerö were 28%/27%/45% and showed significantly lower variation than for the Basel measurements.

### **Detection limit**

The Hg instrument detection limit was  $< 0.1 \text{ ng m}^{-3}$ , and allowed discernment of GEM peaks from the baseline noise for all measurements. The gold cartridge pair offset criteria, and the method detection limit, were derived in the field from sampling the same air through updraft and downdraft lines. For this study, we defined two strict rejection criteria: 1) maximum standard deviation of the offset of 0.05, and 2) maximum difference in gold cartridge response of 10%. The assessment of the offset between the sampling lines during the Basel measurements was  $0.009 \pm 0.06$  ( $\pm$ SD) and  $0.016 \pm 0.01 \text{ ng m}^{-3}$  for gold cartridge pairs 1-3 and 2-4 respectively. At Degerö the offset was  $0.17 \pm 0.06$  and  $-0.004 \pm 0.02 \text{ ng m}^{-3}$  for 1-3 and 2-4. If up- and downdraft lines sample the same air, the offset between these should be constant, independent of air Hg content. Scaling the GEM area difference detected in the up- and downdraft air by GEM area of the updraft air revealed an erroneous behavior of gold cartridge pair 1-3. Further inspection showed that the Teflon® PTFE valves (V4 - V7) seemed to restrict the air flow when energized, thus leading to erroneous air volume readings. In contrast, when air flows through gold cartridge pair 2-4, the valves are in the idle mode with free flow. Therefore, measurements with gold cartridge pair 1-3 were discarded for both campaigns due to the above threshold variability in Basel and the large gold cartridge pair offset at Degerö.

Although data availability was reduced by 50% this technical shortcoming may be solved by use of different valves, e.g. 3-way flipper valves. Detailed results from the sampling line bias tests are presented in Figures S2.3 and S2.4 of the Supporting Information.

From these individual sampling lines bias measurements for Basel and Degerö, a minimum detectable GEM concentration difference based on  $1\sigma$  was derived. Thus, 98% of the available 30 min data in Basel and 83% at Degerö were above that limit. Zhu et al. (2015b) reported that 55% of their Hg-REA flux data were significantly different from zero. Data from bias determination for gold cartridge pair 2-4 did not reveal any significant diel pattern or trend over time for both sites.

### Data coverage

Based on the systematic bias when using gold cartridge pair 1-3, 50% of the data from both sites, Basel and Degerö were discarded (Table 2.1). Some of the remaining flux measurements were rejected due to logging failures including power breakdowns. 6% of the data at Basel and 4% at Degerö were rejected due to poorly developed turbulence, determined by applying an integral turbulent characteristics test (Sect. 2.3.3). GEM flux measurements during extremely stable conditions were omitted ( $z/L > 2$ ). The data were also screened for irregularities in the measured sampling air flow (deviation from the flow setting value  $> 2.5\%$ ). Dry Hg-free air was used to determine possible gold cartridge or sampling line contamination and to discard periods of a noisy Hg detector baseline, due to rapid temperature changes within the detector box. GEM flux measurements were discarded if the signal of the blank measurements exceeded 10% of the integration peak area that is detected for atmospheric GEM. In other Hg-REA studies, 44% (Sommar et al., 2013b) and 28% (Zhu et al., 2015b) of the data were flagged as moderate and low data quality due to turbulence characteristics (cf. Mauder and Foken, 2004). In our study the overall half-hourly data loss was 62% at Basel and 66% at Degerö.

**Table 2.1:** Overview of rejection criteria for the evaluation of REA field measurements. Rejected amount of data and remaining numbers of observations are given.

Criterion	Basel	Degerö
	Rejection percentage	
Gold cartridge pair offset	50%	50%
Logging failure	4%	7%
Insufficient turbulence ( $\sigma_w/u^*$ )	6%	4%
Extreme stability ( $ z/L  > 2$ )	0%	0%
Sampling air flow and blank irregularities	1%	4%
Total rejection (excl. cartridge pair offset)	12%	16%
Remaining observations	n=292	n=380

### 2.3.2 Meteorological conditions

During the measurements in Basel air temperatures averaged  $-7.9 \pm 3.3$  °C ( $\pm$ SD). Precipitation occurred in the first two days and caused substantial loss of EC data, while GEM flux determination was not affected (Table 2.1). From 3 - 12 February 2012, measurements were done during predominantly cloudless conditions with daily solar radiation ( $R_g$ ) peaks between 300 - 500 W m<sup>-2</sup>. Relative humidity ranged between 20 and 91% and was on average significantly lower in Basel than at Degerö. Wind speed in Basel averaged 2.6 m s<sup>-1</sup> and did not differ

significantly between day ( $R_g > 5 \text{ W m}^{-2}$ ) and night ( $R_g < 5 \text{ W m}^{-2}$ ). Wind direction was predominantly from the northwest during the day and the southeast during the night. Polar histograms of 30 min averaged wind speed and atmospheric GEM concentration measurements at both sites are presented in Figure S2.5. Unstable atmospheric stratification ( $z/L < -0.05$ ) was predominant (92% of time) during the Basel campaign while less than 3% of the measurements were conducted during stable conditions ( $z/L > 0.05$ ).

The campaign on the boreal peatland commenced on 5 May 2012. The surface was covered by maximum of 33 cm snow which melted away towards the end of the campaign on 24 May 2012. A total precipitation amount of 19.6 mm was recorded during the campaign including a heavy snowfall during the morning of May 6. Air temperatures averaged  $5.4 \pm 3.5 \text{ }^\circ\text{C}$ , whereas daily averages increased from 0 to  $9.1^\circ\text{C}$  over the period. Soil temperatures at 2 cm depth likewise increased from 3.2 to  $8.0 \text{ }^\circ\text{C}$  (daily averages). The prevailing wind direction at Degerö was from the northeast to south with an average wind speed at  $2.9 \text{ m s}^{-1}$  (daytime mean:  $3.1 \text{ m s}^{-1}$ , nighttime mean:  $2.1 \text{ m s}^{-1}$ ). Conditions were stable ( $z/L > 0.02$ ) 22% of the time (daytime: 15%, nighttime: 43%), unstable for another 38% (daytime: 42%, nighttime: 22%) ( $z/L < -0.02$ ) and neutral during the remaining 40% (daytime: 43%, nighttime: 34%).

### 2.3.3 Footprint and turbulence regime

In Basel, GEM flux measurements were conducted over a rough surface showing strongly modified vertical turbulent exchange processes. Measurements were conducted within the inertial sublayer 39 m above ground, which overlays the urban roughness sublayer assuming that the upper level of the roughness sublayer is about two times the average building height of 17 m (Feigenwinter et al., 2012). 90% of the GEM fluxes measured in Basel originated from a source area that covered 78 ha and reflected a blended, spatially averaged signal (Fig. 2.5a). Within that footprint the water fraction accounts for 7%, the vegetation fraction for 19%, the building fraction for 36% and impervious ground surface for 38%. Main wind directions during the campaign mimicked the dominant seasonal wind direction from NNW and ESE.

An inspection of the normalized co-spectra for sensible heat, latent heat and  $\text{CO}_2$  flux revealed the occurrence of large eddies leading to comparably low switching intervals of  $1.4 \pm 0.3 \text{ Hz}$  (mean  $\pm$  SD). The co-spectral estimates were derived from 20 Hz data over the entire campaign during unstable conditions and demonstrate that high-frequency losses for sensible heat, latent heat and  $\text{CO}_2$  fluxes were minimal. Low-frequency losses resulted due to the applied high-pass filter which attenuated fluctuations at periods larger than the time constant of 16.6 min (RF in Fig. 2.6). Frequency distributions (ogive curves) were calculated after Foken et al. (2012) and converged at approximately 90% of all cases within the 30 min averaging period (Fig. 2.6a). Simulated damping factors for REA fluxes revealed that at a mean wind speed of  $2.6 \text{ m s}^{-1}$  less than 10% of the flux was dampened. We conclude that applying a 30 min averaging interval, a high-pass filter and valve switching at 10 Hz was adequate for REA flux calculations since considerable flux damping occurred just at low frequency ranges, unstable conditions and low wind velocities.

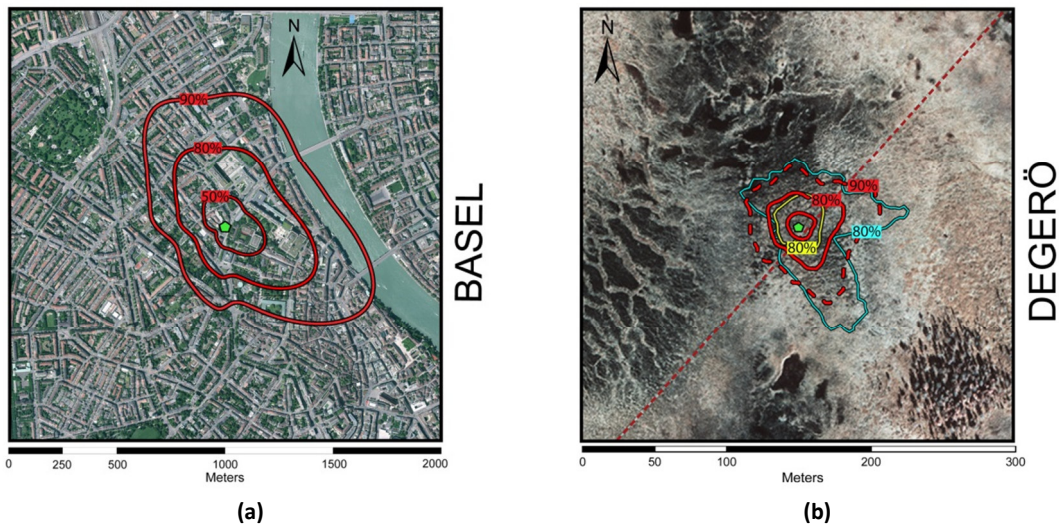


**Figure 2.5:** Aerial RGB and IR photographs with red contours containing 50, 80 and 90% of the flux during the campaign in Basel (a) and Degerö (b). The yellow and blue 80% contours at Degerö stand for instable and stable conditions, respectively. The green pentagons indicate the location of the flux towers.

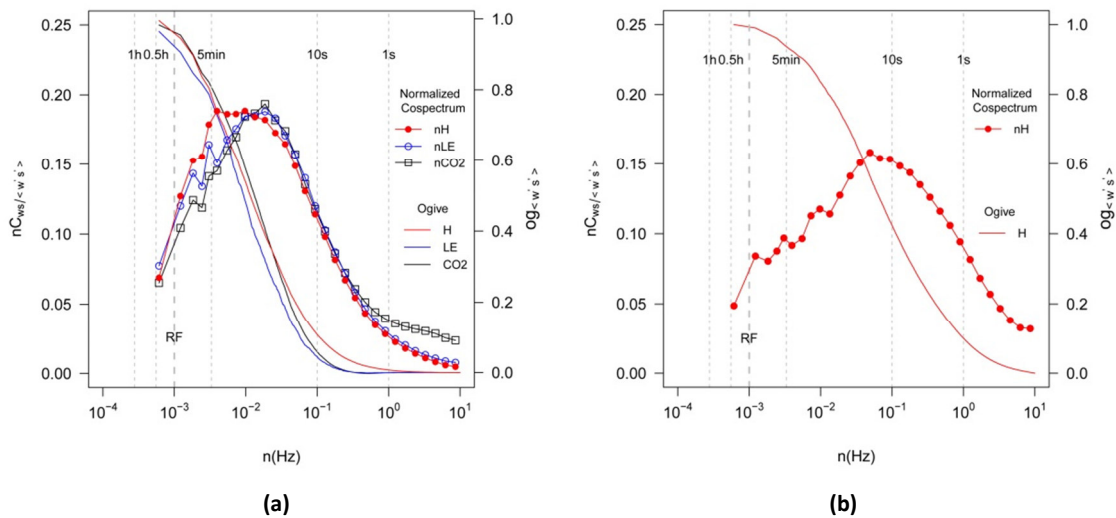


**Figure 2.6:** Normalized turbulence co-spectra (y axis, lines + symbols) and converging ogives (secondary y axis, lines) of sensible heat (red), latent heat (blue) and CO<sub>2</sub> flux (black) during unstable conditions for Basel (a) and Degerö (b). The vertical line labeled as RF indicates the time constant of the applied high-pass filter. At Degerö only high-resolution air temperature data were used.

90% of the footprint at Degerö comprised 0.6 ha (Fig. 2.5b). For all contour lines calculated, the surface was physically homogenous. The roughness length  $z_0$  present during the campaign was only a few millimeters due to the short vegetation (Sagerfors et al., 2008) and negligible when there was snow-cover. During the Degerö campaign, the normalized turbulence spectra and ogives were derived for sensible heat flux during unstable conditions (Fig. 2.6b). Due to technical problems regarding the LI-6262 closed-path infrared gas analyzer, CO<sub>2</sub> and latent heat flux data were not used for spectral analysis. In comparison to Basel the co-spectrum of the sensible heat flux was shifted significantly towards higher frequencies. The occurrence of more smaller eddies increased the fast-response valve switching interval ( $2.9 \pm 0.7$  Hz; mean  $\pm$  SD) which increased with increasing  $u^*$  (Fig. S2.6). High frequency losses at 10 Hz accounted for less than 5% of the sensible heat flux. The ogive converged a constant value at

RF and indicates that large eddies were sampled completely over the averaging period (Fig. 2.6b). At Degerö the integral damping factor for the REA flux was more than 20% at high frequencies especially during stable and strong wind conditions. Simulated integral REA flux damping factors dependent on wind speed and stability conditions and cospectral density plots for site-averaged wind speeds are illustrated for Basel and Degerö in Figures S2.7 and S2.8.

### 2.3.4 Atmospheric GEM concentrations

Mean  $\pm$  SD atmospheric GEM concentration in Basel was  $4.1 \pm 1.0 \text{ ng m}^{-3}$ . The average concentration difference between up and downdraft was  $0.26 \pm 0.3 \text{ ng m}^{-3}$  (median:  $0.19 \text{ ng m}^{-3}$ ) (Fig. 2.7). It might be possible that during the exceptionally cold period in Basel gas and oil-fired thermal power stations within the dense urban source area contributed to enhanced atmospheric GEM concentrations. In urban areas total gaseous Hg concentrations were highest during heating season (Fang et al., 2004). Highest GEM levels in Basel were observed during periods of low wind velocities ( $u^* < 0.3 \text{ m s}^{-1}$ ) and southern wind directions. Most likely additional GEM emissions from vehicular traffic along a highly frequented road contributed to elevated Hg concentrations during southerlies. GEM concentrations in the exhaust of motor vehicles in driving mode are elevated and range from 2.8 to  $26.9 \text{ ng m}^{-3}$  depending on fuel types (Won et al., 2007). The road runs in a north/south direction and is the major source of  $\text{CO}_2$  (Lietzke and Vogt, 2013).

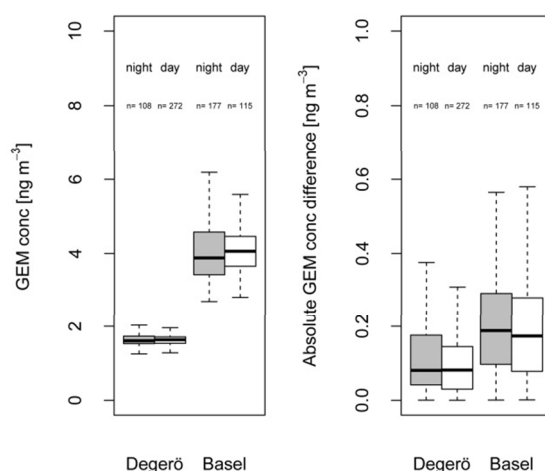


**Figure 2.7:** Box plots display atmospheric GEM concentration (a) and the absolute GEM concentration difference between updraft and downdraft (b) during day and night at Degerö and Basel. Number of observations is indicated. The bold line in the box represents the median GEM concentration. The horizontal border lines indicate the 25<sup>th</sup> (Q1) and 75<sup>th</sup> (Q3) percentiles, from bottom to top. The lower whisker marks Q1 minus 1.5 times the interquartile range (IQR). The upper whisker marks Q3 plus 1.5 IQR. Outliers are not displayed.

The average air concentration during snowmelt at Degerö was  $1.6 \pm 0.2 \text{ ng m}^{-3}$ , comparable to observations made in 2009 (Fritsche et al., 2014). Concentration difference in REA conditional samples collected at Degerö averaged  $0.13 \pm 0.2 \text{ ng m}^{-3}$  (median:  $0.09 \text{ ng m}^{-2}$ ) that is about a factor of two lower than the magnitude observed in Basel (Fig. 2.7). No significant concentration relationships were found with either wind direction or atmospheric stability.

## 2.3 Results and Discussion

**Table 2.2:** Summary of averaged, median and distribution of GEM fluxes, atmospheric GEM concentrations and environmental conditions during the measurement campaigns. Pearson correlation coefficients (*r*) between GEM flux and environmental parameters are given if statistically significant ( $p < 0.05$ ).

Variable	unit	Basel				Degerö			
		mean	median	10 <sup>th</sup> /90 <sup>th</sup> %ile	<i>r</i>	mean	median	10 <sup>th</sup> /90 <sup>th</sup> %ile	<i>r</i>
GEM flux	ng m <sup>-2</sup> h <sup>-1</sup>	15.4	34.9	-262/270	[-]	3.0	2.6	-71/67	[-]
GEM concentration	ng m <sup>-3</sup>	4.1	3.9	3.3/5.6	-0.23	1.6	1.6	1.4/1.8	-0.14
Sensible heat flux (EC)	Wm <sup>-2</sup>	74	65	20/134	[-]	11.8	2.4	-17/58	0.23
Latent heat flux (EC)	Wm <sup>-2</sup>	12.3	10.6	1.8/24.5	0.26	[-]	[-]	[-]	[-]
CO <sub>2</sub> flux (EC)	μmol m <sup>-2</sup> s <sup>-1</sup>	0.02	0.01	0/0.04	0.36	[-]	[-]	[-]	[-]
Friction velocity	m s <sup>-1</sup>	0.41	0.39	0.2/0.7	0.2	0.19	0.18	0.07/0.34	-0.23
Wind speed	m s <sup>-1</sup>	2.6	2.5	1.3/3.9	0.13	2.9	2.7	1.0/4.8	-0.26
Solar radiation	Wm <sup>-2</sup>	78	[-]	0/312	-0.22	159	[-]	0/455	0.14
Air temperature	°C	-7.9	-8	-12/3.4	0.23	5.3	5.4	0.1/10.2	0.26
Soil temperature	°C	[-]	[-]	[-]	[-]	6.7	7	4.4/8.2	0.2
Relative humidity	%	62	60	40/85	-0.23	76	80	47/98	-0.3

### 2.3.5 GEM flux estimation in contrasting environments

Urban areas are of particular concern with respect to the global Hg cycle. Industrial sectors and anthropogenic combustion processes emit large quantities of Hg to the atmosphere (Walcek et al., 2003) and gaseous oxidized Hg and particulate bound Hg will be deposited locally. Highly variable Hg air concentrations, the physically and chemically diverse nature of urban surface covers and urban meteorology (e.g. heat island effect) are suggested to create complex Hg flux patterns above cities (Gabriel et al., 2005). Up to now, just a handful of studies have described GEM emissions from urban environments (Kim and Kim, 1999; Feng et al., 2005; Gabriel et al., 2006; Obrist et al., 2006; Eckley and Branfireun, 2008). GEM fluxes measured in Basel showed a diel trend with a maximum deposition around noon and highest emissions around 7 PM (Fig. 2.8a). The mean flux  $\pm$  SE of  $15.4 \pm 13.3$  ng m<sup>-2</sup> h<sup>-1</sup> indicated that this urban area was a net source of atmospheric Hg during the study period. Similarly, for the same site in spring and fall, Obrist et al. (2006) observed average  $\pm$  SD GEM emissions of  $6.5 \pm 0.9$  ng m<sup>-2</sup> h<sup>-1</sup> in the stable nocturnal boundary layer using the <sup>222</sup>Rn/Hg<sup>0</sup> method. Environmental conditions such as solar radiation, air and soil temperature are known to be major drivers of natural GEM emission (e.g. Steffen et al., 2002; Choi and Holsen, 2009). North westerly wind directions were associated with GEM deposition between 2 AM and 1 PM. In contrast, emission events were linked to wind directions from the south east.

Determination of GEM snow-air exchange has been a subject of interest since the first atmospheric mercury depletion events (AMDEs) were observed (Schröder et al., 1998). Non-arctic GEM flux studies from snowpack report deposition, as well as emission events, with near zero net fluxes (Faïn et al., 2007; mean: 0.4 ng m<sup>-2</sup> h<sup>-1</sup>; Fritsche et al., 2008a; mean: 0.3 ng m<sup>-2</sup> h<sup>-1</sup>).

Mean  $\pm$  SE GEM snow-air transfer observed at Degerö was  $3.0 \pm 3.8$  ng m<sup>-2</sup> h<sup>-1</sup>. It is the result of a balance between deposition prevailing from midnight to noon and vice versa during the rest of the day when emission predominates (Fig. 2.8b). REA fluxes varied strongly during both the day and night, but revealed a significant difference between GEM fluxes during unstable (median: 8.7 ng m<sup>-2</sup> h<sup>-1</sup>), stable (median: -0.1 ng m<sup>-2</sup> h<sup>-1</sup>), and neutral conditions



(median:  $-4 \text{ ng m}^{-2} \text{ h}^{-1}$ ) (Mann-Whitney U test,  $p < 0.05$ ). GEM concentrations in the surface snow layers were not determined in this study, but in accordance with Faïn et al. (2013), GEM is likely enhanced during the course of daytime compared to ambient air due to sunlight-mediated processes. An impact of fresh snowfall and possible wet Hg deposition on GEM fluxes could not be observed with REA, but precipitation events occurred regularly in the afternoon and might have contributed to GEM volatilized in the evenings together with GEM produced during dusk and night (Faïn et al., 2013).

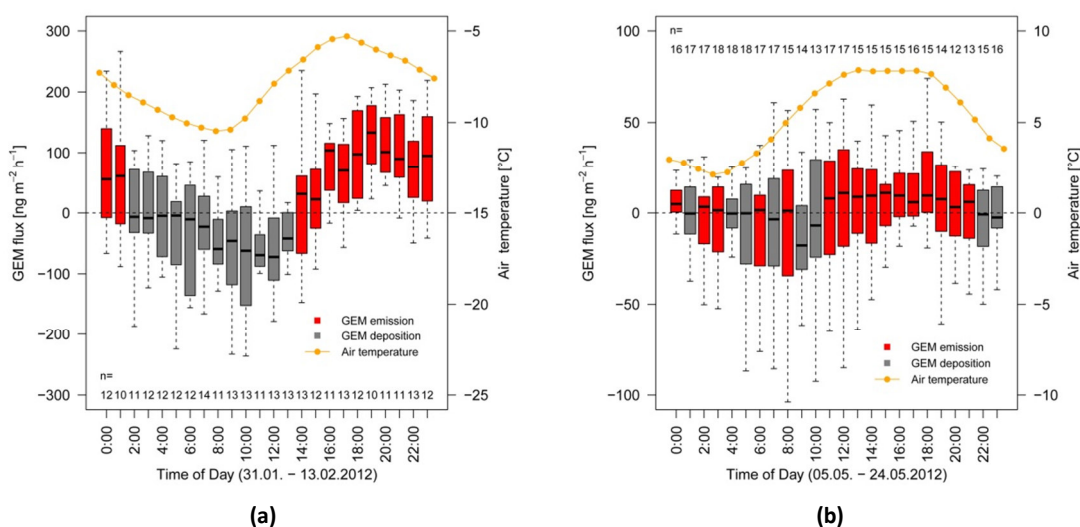


**Figure 2.8:** Diel patterns of GEM flux during the campaign in Basel (a) and Degerö (b) using the 6-hourly smoothed GEM flux time series. Red and gray colored boxplots indicate median Hg emission and Hg deposition at different times of the day, respectively. Hourly average of air temperatures are given (orange). Horizontal dashed line indicates the zero line of GEM flux and/or air temperature. Boxplot description in caption of Figure 2.7.

GEM flux quantification is improved, compared to previous systems, by the synchronous sampling, as well the regular monitoring of GEM reference gas concentration and dry, Hg-free air. As demonstrated here, these improvements make REA feasible for measurements over tall buildings, but also short vegetation and snow-cover. At Degerö, however, higher abundance of smaller eddies increased the GEM flux variability. However, the REA technique remains better suited to assessing magnitudes and variability of fluxes rather determining the effects of short-term variability in environmental parameters on GEM fluxes (cf. Gustin et al., 1999).

For future long-term REA applications we have three suggestions: (I) a more regular determination of the bias between both sampling lines. Either by a weekly check of the bias or by implementing an additional valve to switch up- and downdraft lines every hour (each gold cartridge would measure up- and downdraft). (II) Hg detector sensitivity due to rapid air temperature changes are corrected for but could be avoided to a large extent by using a more effective temperature control unit. (III) To improve the accuracy in the air volumes sampled by installing mass flow meters for up- and downdraft lines.

## 2.4 Conclusion

The need to precisely determine land-atmosphere exchange of GEM over long continuous periods is widely recognized. REA has the potential to do this more effectively than other methods. Therefore, several REA systems have been deployed, but their accuracy has been impaired by several design features such as the use of multiple detectors and non-synchronous sample collection. We developed a dual-inlet, single analyzer system that overcomes these shortcomings, and included new features, such as the integrated GEM reference gas and Hg zero-air generator for continuous monitoring of GEM recovery, as well as blank measurements. The data acquisition and control system is fully automated and could be remotely controlled which reduces the workload compared to other REA systems. We have demonstrated the system in contrasting environments to measure turbulent transport of GEM 39 m above ground level in Basel, Switzerland and 1.8 m above a snow covered boreal peatland in Sweden. While the demonstration identified room for further improvements, we believe this novel design has the potential to facilitate the use of REA for measuring land-atmosphere exchange of Hg for sustained periods in a variety of environments.

## Acknowledgements

This research was funded by the Swedish Research Council (#2009-15586-68819-37), the Department of Earth Sciences, Uppsala University, and the Department of Environmental Geosciences, University of Basel. We thank William Larsson and the late Lars Lundmark from Umeå University for technical assistance and engineering, Roland Vogt from the University of Basel's MCR lab for using their EC setup. The study at Degerö also received technical and maintenance support from the Svartberget Experimental Forest, Vindeln, Sweden. The study was also supported by the Swedish research infrastructures, ICOS Sweden (Integrated Carbon Observation System) and SITES (Swedish Infrastructure for Ecosystem Science) at Degerö, both partly financed by the Swedish Research Council.

## CHAPTER 3

### **Mercury emissions from a boreal peatland: Time to rethink timelines for global recovery?**

*In preparation*

S. Osterwalder<sup>1</sup>, K. Bishop<sup>2,3</sup>, C. Alewell<sup>1</sup>, J. Fritsche<sup>1</sup>, H. Laudon<sup>4</sup>, S. Åkerblom<sup>2</sup> and M. B. Nilsson<sup>4</sup>: Mercury emissions from a boreal peatland: Time to rethink timelines for global recovery?

[1] Department of Environmental Sciences, University of Basel, Basel, Switzerland

[2] Department of Aquatic Sciences and Assessment, Swedish University of Agricultural Sciences, Uppsala, Sweden

[3] Department of Earth Sciences, University of Uppsala, Uppsala, Sweden

[4] Department of Forest Ecology and Management, Swedish University of Agricultural Sciences, Umeå, Sweden

## **Abstract**

Peatlands are a major source of methylmercury that contaminates downstream aquatic food webs (St. Louis et al., 1994, Mitchell et al., 2008). The large store of mercury (Hg) in peatlands suggests that peatlands will continue to be a source of Hg for more than a century even if deposition is dramatically reduced (Grigal, 2003). However the reliability of Hg mass-balances can be questioned due to the inability to reliably quantify the long-term land-atmosphere exchange of Hg. We used a novel micrometeorological system to derive the first annual Hg budget for a peatland, based on continuous measurements of the peatland-atmosphere exchange of gaseous elemental Hg. Here we show that evasion of Hg was eight times greater than stream Hg export, and more than twofold higher than Hg in wet bulk deposition. The net efflux results most likely from recent declines in atmospheric Hg concentrations (Amos et al., 2015) that have turned the peatland from a net sink into a source of atmospheric Hg. The strong Hg evasion suggests that open boreal peatlands and downstream ecosystems will recover more rapidly from past atmospheric Hg deposition than previously assumed. This has important implications for future human consumption of fresh water fish, as well as the value of the 2013 UN Minamata Convention on Mercury that seeks to further reduce Hg emissions.

### 3.1 Main Section

Global anthropogenic mercury (Hg) emissions have increased the amount of Hg cycling between vegetation, surface soil, ocean, and the atmosphere by about a factor of three compared to pre-industrial levels (Selin et al., 2008; Driscoll et al., 2013). Gaseous elemental mercury (GEM) has an atmospheric lifetime of 0.8 - 1.7 years after emission, resulting in long range transport before deposition on the earth surface (Ariya et al., 2015). This poses a threat to humans and wildlife even in remote areas (Lindberg et al., 2007). Current global models assume that Hg deposition to non-contaminated terrestrial surfaces and subsequent re-emission are similar in magnitude. However, large uncertainty remains mostly due to a strong spatial and temporal bias in direct flux measurements towards Hg-enriched sites, short-term, daytime and summertime measurements (Amos et al., 2013; Agnan et al., 2016).

Peatlands play an important role in Hg cycling because they constitute a major source of methylmercury (MeHg), the Hg species most prone to biomagnification, to fresh water ecosystems (UNEP, 2013). The large amount of Hg in peatlands relative to wet bulk deposition and export in surface water runoff indicates that they have accumulated Hg deposited from the atmosphere (Grigal, 2003). In high latitude regions almost all freshwater fish have Hg concentrations exceeding European limits for good ecological status ( $0.02 \text{ mg Hg kg}^{-1}$  fish muscle, Chalmers et al., 2011, Åkerblom et al., 2014). To predict future MeHg levels in fish of these regions, the annual net ecosystem Hg flux from peatlands needs to be quantified.

Since the store of Hg in peat is so large compared to runoff fluxes, it is generally assumed that it will take several decades, if not centuries, before a reduction in atmospheric deposition could lead to any reduction in the Hg pools in peatlands, thus putting the prospect of significant recovery far into the future (Meili et al., 2003; Grigal, 2003). Such calculations, however, neglect GEM emission to the atmosphere which preliminary measurements indicate to be substantial (Marsik et al., 2005; Selvendiran et al., 2008; Osterwalder et al., 2016).

Earlier research indicates that at a certain threshold of atmospheric GEM concentration terrestrial surfaces switch from net sinks to net sources of Hg (Gustin et al., 2011; Wright and Zhang, 2015). For terrestrial background sites this so called 'compensation point' is estimated to be  $2.8 \text{ ng m}^{-3}$  (Agnan et al., 2016). We hypothesize that declines in atmospheric GEM concentrations have passed this "compensation point", increasing Hg emission from peatlands to the point where peatlands may no longer be a net sink of atmospheric Hg. As a result, the loading of Hg from peatlands to aquatic food webs would be reduced substantially faster than previously anticipated.

To investigate this assumption, we conducted the first full year, catchment scale, measurements of land-atmosphere exchange of GEM. Together with continuous data on export of total mercury (THg) in stream runoff, wet bulk deposition, and peat Hg storage, these measurements allowed us to estimate the major components of the annual Hg mass balance of a boreal peatland.

The most challenging component of a catchment scale Hg mass balance is the long-term continuous measurement of land-atmosphere exchange of GEM. We used a novel, dual-inlet, single detector relaxed eddy accumulation (REA) system to quantify this (Osterwalder et al., 2016). REA is a direct measurement approach that overcomes uncertainties associated with

other micrometeorological techniques (aerodynamic gradient and modified Bowen ratio) that rely on concentration measurements at different heights. Compared to other GEM-REA systems, the advanced REA design used in this study is fully automated and simultaneously collects GEM in air that moves down to, and away from, the ground surface (Osterwalder et al., 2016).

The system was deployed in the center of an open area of the nutrient poor, minerogenic Degerö Stormyr peatland [64°11'N, 19°33'E]. The sampling inlets were mounted 3.5 m above the peatland surface, with a ca. 2.5 ha footprint. Continuous measurements integrating exchange over such a large area overcome much of the measurement uncertainty that would otherwise be introduced with small scale dynamic flux chambers. Chambers cover only small fractions of the peatland surface and are normally only deployed during short time periods, thus introducing large uncertainties with respect to both area and time (Gustin et al., 1999; Agnan et al., 2016)

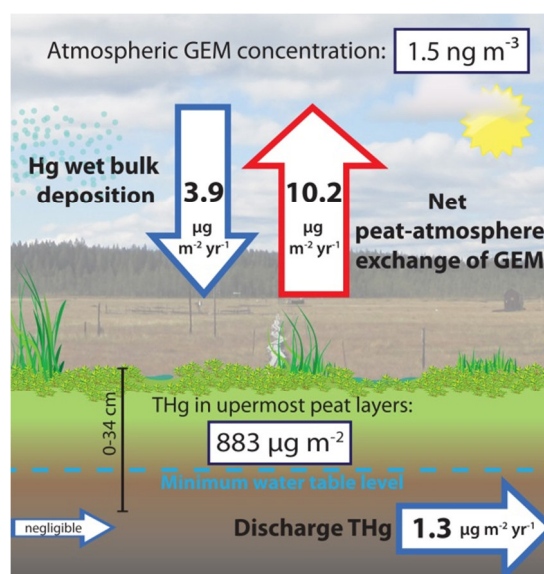


**Figure 3.1:** Simplified schematic of the annual Hg mass balance at Degerö Stormyr. Net peatland-atmosphere exchange of gaseous elemental Hg (GEM) and total Hg (THg) in discharge are the major Hg output pathways. Wet bulk deposition is considered as the only Hg input pathway. The atmospheric GEM concentration and the pool of THg in the uppermost peat layers (0 - 34 cm) are indicated.

We found that the annual Hg mass balance at the Degerö Stormyr peatland was clearly dominated by net GEM evasion (Fig. 3.1) due to substantial net emission between May and October (Fig. 3.2). The annual GEM emission was  $10.2 \text{ } \mu\text{g m}^{-2}$  and the wet bulk deposition was  $3.9 \text{ } \mu\text{g m}^{-2}$ . Annual discharge export of Hg from the peatland area (70% of total catchment area) amounted to  $1.3 \text{ } \mu\text{g m}^{-2}$  (Fig. 3.1). The THg export in discharge has commonly been thought of as the dominant output pathway for most catchments (Meili et al., 2003; Shanley and Bishop, 2012). But at the study peatland the land-atmosphere evasion was eight times larger than stream discharge of Hg.

Observed GEM emission during the growing season was  $11 \text{ } \mu\text{g m}^{-2}$  and substantially exceeded Hg wet bulk deposition during the same time period ( $2.5 \text{ } \mu\text{g m}^{-2}$ ) (Fig. 3.3). During the growing season the peatland emitted GEM to the atmosphere at an average  $\pm$  SE rate of  $3 \pm 0.5 \text{ ng m}^{-2} \text{ h}^{-1}$ . Outside the growing season (October, November and April) the average GEM

flux was  $0.4 \pm 0.7 \text{ ng m}^{-2} \text{ h}^{-1}$  with emission from 9 AM to 8 PM and GEM deposition during the night (Fig. 3.4). Measurements during March revealed a net GEM flux of  $-0.4 \pm 1.5 \text{ ng m}^{-2} \text{ h}^{-1}$  between air and the snow covered surface (see Table 3.1). Winter time GEM exchange also showed a diel pattern indicating photochemical GEM production at the snow surface and subsequent emission of previously deposited GEM in the afternoon (Fig. 3.5). These data clearly demonstrate the importance of continuous, long-term measurements to derive complete, unbiased annual budgets of the land-atmosphere exchange of GEM.

**Table 3.1:** Summary of monthly means  $\pm$  SE of the gaseous elemental mercury flux ( $F_{\text{GEM}}$ ) and monthly means of the atmospheric GEM concentration, dissolved gaseous mercury (DGM) concentration ( $\pm$ SE), saturation of DGM with respect to atmospheric GEM ( $\text{DGM}_{\text{SAT}}$ ), water table level (WTL), precipitation (Precip), air temperature ( $T_{\text{air}}$ ) and solar radiation (Rg). The italic numbers indicate estimated GEM flux and atmospheric concentrations during winter derived from measurements in March over snowpack.

Month	n	$F_{\text{GEM}}$ ( $\text{ng m}^{-2} \text{ h}^{-1}$ )	GEM ( $\text{ng m}^{-3}$ )	DGM ( $\text{ng L}^{-1}$ )	$\text{DGM}_{\text{SAT}}$ (-)	WTL (cm)	Precip (mm)	$T_{\text{air}}$ ( $^{\circ}\text{C}$ )	Rg ( $\text{W m}^{-2}$ )
Jan 14	[-]	<i>-0.4</i>	1.65	[-]	[-]	[-]	25.7	-9.4	5.1
Feb 14	[-]	<i>-0.4</i>	1.65	[-]	[-]	[-]	66.7	-1.4	14.3
Mar 14	466	$-0.4 \pm 1.5$	1.65	[-]	[-]	[-]	20	-0.3	84.7
Apr 14	439	$0.8 \pm 0.9$	1.50	[-]	[-]	-2.9	1	2.8	138.3
May 14	358	$2.6 \pm 1.6$	1.41	$14.7 \pm 1.9$	1.1	-6.7	50.9	12.1	173.9
June 13/14	603	$3.7 \pm 1.2$	1.54	$30.3 \pm 3.2$	3.4	-10.2	52.8	14.7	173.2
Jul 13	655	$2.5 \pm 0.8$	1.45	$41.9 \pm 3.0$	5.5	-13.3	93.4	14.8	181.5
Aug 13	420	$3.5 \pm 1.2$	1.49	$40.7 \pm 3.7$	5.5	-11.8	54.3	14.6	194.9
Sep 13	435	$2.9 \pm 1.2$	1.42	$24.8 \pm 3.3$	2.9	-12.2	95.4	13.1	134.7
Oct 13	415	$2.4 \pm 1.2$	1.59	$16.7 \pm 2.1$	1.5	-10.0	47.7	2.6	42.1
Nov 13	284	$-2.9 \pm 1.6$	1.50	[-]	[-]	[-]	39.9	-3.0	9.7
Dec 13	[-]	<i>-0.4</i>	1.65	[-]	[-]	[-]	72.4	-1.7	2.1

There are several factors which corroborate the overall rates of evasion and temporal variation. The largest evasion rates during the summer correspond to peak pore water concentrations of dissolved gaseous mercury (DGM, see Fig. 3.7). This suggests the importance of peat pore water DGM concentrations as a driving factor for the net annual land-atmosphere exchange of GEM. The mire surface water was supersaturated in DGM relative to atmospheric GEM concentrations on 86% of the measurement occasions between May and October, peaking in July and August. Summertime evasion also corresponds to the highest levels of incident radiation that can drive photoreduction of  $\text{Hg}^{2+}$  to  $\text{Hg}^0$  at the peat surface. The largest gross ecosystem production of vascular plants (Peichl et al., 2015) and concurrent high uptake of GEM in July is reflected by about 30% lower GEM net emission rates as compared to June and August (Obrist et al., 2007; Enrico et al., 2016).

The unexpectedly high annual net evasion is also consistent with the pattern of superficial peat Hg concentration-depth profiles. The average  $\pm$  SE concentration of Hg within the top 34 cm was  $57 \pm 8 \text{ ng g}^{-1}$  dry matter (DM). That is within the range of 10 - 115  $\text{ng g}^{-1}$  DM representing typical soil THg concentrations from boreal forest catchments (Skjellberg et al., 2003). Peat THg concentrations increased with depth to a peak of about 110  $\text{ng g}^{-1}$  dated to ca. 1950 (Figs. 3.6, S3.2). This pattern is similar to that of other Hg concentration profiles from open peatlands in Canada (Givelet et al., 2003), Scotland (Farmer et al., 2009) and Sweden (Rydberg et al., 2010). This might indicate that the decrease in THg concentration towards the surface (24  $\text{ng THg g}^{-1}$  in the top 10 cm) not only represents lower Hg deposition rates but also

evasion of Hg that began at some point after 1985 if atmospheric GEM concentrations fell below the compensation point (Slemr et al., 2003, Agnan et al., 2016).

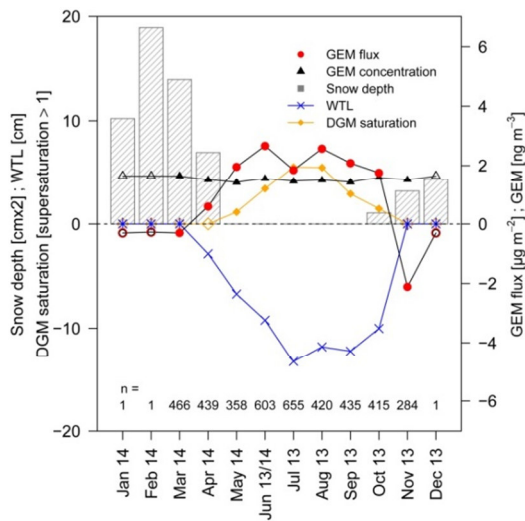


**Figure 3.2:** Monthly average of the net gaseous elemental Hg (GEM) flux, atmospheric GEM concentration, snow depth, water table level (WTL) and saturation index of dissolved gaseous Hg (DGM) in the peat pore water. Negative GEM exchange represents GEM deposition, while positive fluxes represent GEM emission. Empty symbols indicate that no measurements were conducted during the months in question. The figures at the bottom of the panel represent numbers of 60-min averages of both GEM flux and atmospheric GEM concentration.

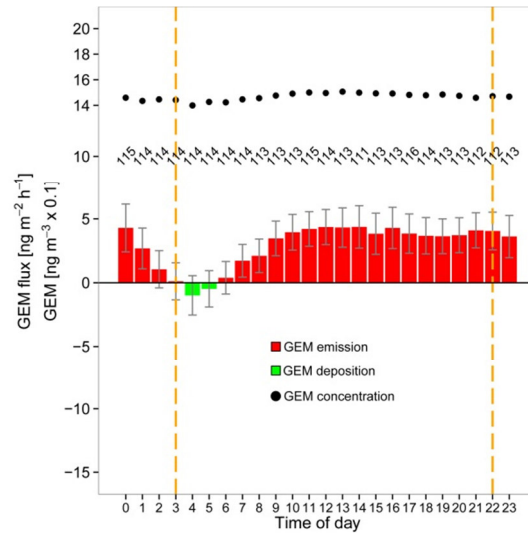


**Figure 3.3:** 12-hourly smoothed average  $\pm$  SE diel pattern of gaseous elemental Hg (GEM) exchange between the peatland surface and the atmosphere during the growing season (May - September). The black dots show the atmospheric GEM concentration. Vertical orange dashed lines separate between day ( $R_g \geq 5 \text{ Wm}^{-2}$ ) and night ( $R_g < 5 \text{ Wm}^{-2}$ ).  $R_g$  is the hourly average global radiation. The number of observations of GEM flux and atmospheric GEM concentration are given.

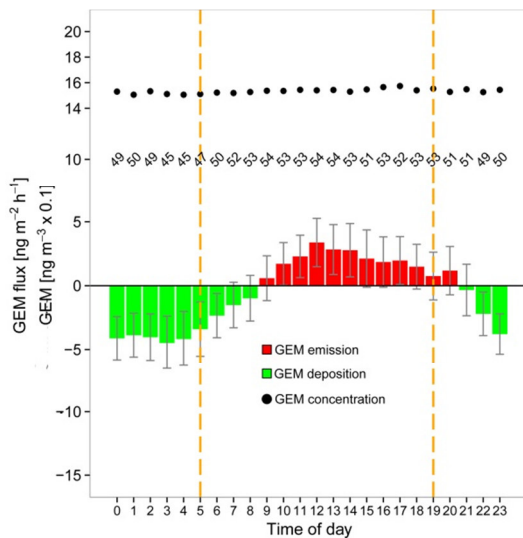


**Figure 3.4:** Diel pattern of GEM flux and GEM concentration during non-growing season (October, November, and April). See Figure 3.3 for details.

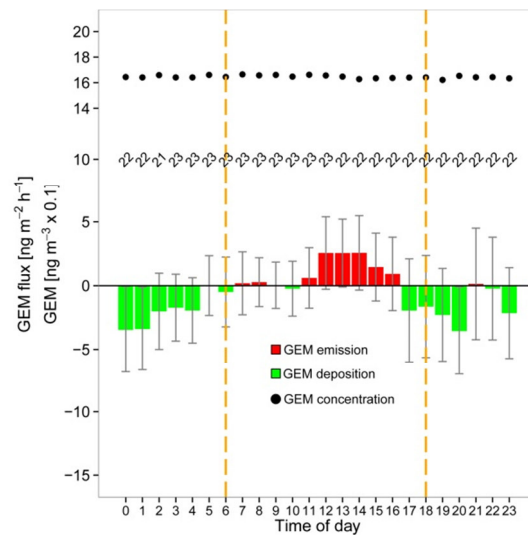


**Figure 3.5:** Diel pattern of GEM flux and GEM concentration during snow covered winter time period (represented by data from March). See Figure 3.3 for details.



Recent advances in the interpretation of Hg isotope signatures have also revealed high mobility of Hg in peat soils. Jiskra et al. (2015) deduced significant re-emission upon non-photochemical reduction by natural organic matter and estimated that 30% of the historically deposited Hg on their study site has already been re-emitted to the atmosphere. They calculated a peat Hg re-emission flux of  $5 \mu\text{g m}^{-2} \text{yr}^{-1}$  which is about 50% of the net GEM flux measured with REA in this study.

The vertical distribution of Hg in surface peat at Degerö Stormyr corresponds to the period of maximum anthropogenic emissions to the atmosphere with peak atmospheric concentrations during the second half of the 20<sup>th</sup> century followed by declines in more recent decades (Beal et al., 2015; Amos et al., 2015). Accumulation rates of Hg in peat during the industrial period until ca. 1990 are estimated to have been up to 15 times greater than those during the pre-industrial era for northern Europe (Steinnes and Sjøbakk, 2004). Between 1990 and 2011, Hg emissions from European sources decreased by ~60 % due to both abatement strategies and the closing of many coal-fired power plants, chlor-alkali plants, etc. (UNECE, 2010; EMEP, 2013). This was associated with roughly a halving of global atmospheric GEM concentrations (Slemr et al., 2003). In Sweden atmospheric GEM went down from more than  $3 \text{ ng m}^{-3}$  in the 1980s to northern hemispheric background concentrations of  $1.3 - 1.9 \text{ ng m}^{-3}$  after 1995 (Iverfeldt et al., 1995; Wängberg et al., 2007).

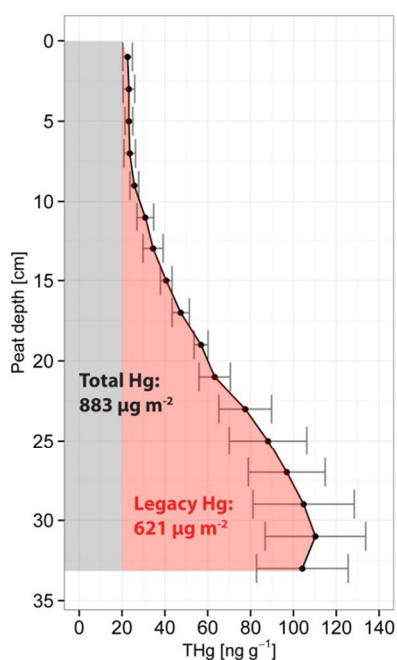


**Figure 3.6:** Depth profile of THg concentrations from eight peat cores with average and 95% confidence interval. The zero level denotes the surface of living Sphagnum moss. The red area indicates the amount of legacy Hg stored in the uppermost peat without accounting for a “background” concentration of  $20 \text{ ng g}^{-1}$ .

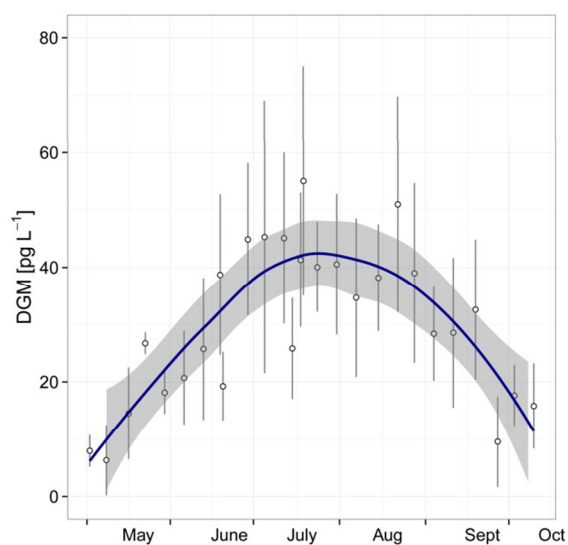


**Figure 3.7:** Seasonal pattern of DGM concentrations from July to October 2013 and May to July 2014. Error bars indicate standard deviation of every daily mean ( $n = 4$ ). Local polynomial regression fit (blue) with 95% confidence level (shaded grey).

We hypothesize that this reduction in deposition of atmospheric Hg to terrestrial ecosystems has impacted the bi-directional exchange of GEM in remote areas. More specifically at Degerö Stormyr, where the current levels of wet bulk Hg deposition are low relative to our observed evasion, the emission of legacy Hg suggests that the peat soil pool is the dominant source for Hg loss from open boreal peatlands. If this situation with high re-emissions of GEM is sustained, it will lead to a much faster than anticipated reduction in the pool of Hg from the Degerö peatland, and eventually a reduction in the supply of Hg to downstream aquatic food webs.

To make an initial estimate of the time this would take, we assumed that the observed levels of evasion will remain constant while no significant change occurs in either the wet bulk deposition, discharge or the growing season water balance (Teutschbein et al., 2015). With a further assumption that catchment runoff is dominated by Hg from the uppermost peat, then it will take around 80 years to deplete the entire pool of legacy Hg in the uppermost 34 cm to a background concentration level of 20 ng THg g<sup>-1</sup> (DM) in the peat.

We conclude that GEM emission to the atmosphere may constitute a major loss term in the Hg balance of boreal peatlands. This will lead to decreased Hg contamination of downstream aquatic ecosystems in the coming decades, provided that atmospheric Hg levels do not increase. Evasion from peatlands would thereby attenuate the negative effects of past Hg deposition on ecosystems and human health.

The proven reliability of the novel REA system for long-term measurements of land atmosphere exchange of GEM (Osterwalder et al., 2016) creates possibilities for similar long-term measurements at other peatlands as well as over other ecosystems, including forests and oceans. If the reversal of the net flux of Hg from the atmosphere into peatlands is occurring at a global scale, and possibly even for other ecosystems, then it will increase the societal value of the ambitious goals set by the UN Minamata Convention for reducing anthropogenic Hg emissions to the atmosphere.

## 3.2 Methods

### 3.2.1 Research site

The annual Hg mass balance was estimated for the period 18.06.2013 - 17.06.2014, for the nutrient-poor, boreal mire, Degerö Stormyr (64°11'N, 19°33'E, altitude 270 m above sea level), Västerbotten, Sweden. The study focused on an open peatland area of 1.9 km<sup>2</sup> with an average peat depth of 3 - 4 m (max. 8 m). The GEM flux source area is characterized by uniform microtopography and vegetation, dominated by lawn and carpet plant communities (Fig. S3.1). The climate is generally cold and humid with persistent snow cover during ~6 months (Fig. 3.2). The 30-year (1981 - 2010) mean annual temperature is 1.8 °C and the mean precipitation is 614 mm, of which about 35% falls as snow (Laudon et al., 2013). A detailed description of the site can be found in Section S3.1 and in Granberg et al. (2001).

### 3.2.2 Peat sampling and Hg analysis

In autumn 2015 two replicate peat profiles were taken in every cardinal direction from the REA tower (n = 8; Fig. S3.2). The 34 cm long profiles (100 cm<sup>2</sup> cross section) were cut in 2 cm increments freeze-dried for 5 days and then weighed for the determination of their dry mass and bulk density. The THg in peat samples was analyzed using a SMS100 (Perkin Elmer, Waltham, USA) through thermal decomposition atomic absorption spectrometry according to EPA method 7473. Certified reference lake sediment (IAEA SL1 [130 ng g<sup>-1</sup>]) and pine needle material (PINE1575a [40 ng g<sup>-1</sup>]) were used for calibration. Replicate samples and the reference material were analyzed regularly (10% of the sampling sequence). The precision was ≤ 5% relative standard deviation. See Section S3.2 for further details.

### 3.2.3 Hg in wet bulk deposition

Atmospheric wet bulk deposition was sampled continuously at the EMEP station Bredkälen (63°51'N, 15°20'E; 210 km west of Degerö Stormyr) using IVL wet bulk samplers. Cumulative wet bulk deposition was derived from THg concentrations. Precipitation was obtained from the reference climate station Kulbäcksliden, located 1 km east of Degerö Stormyr (Tab. S3.2). Precipitations was measured manually on a daily basis, using a standard collector with a wind-screen following WMO-recommendations.

### 3.2.4 Peatland-atmosphere exchange of GEM

The dual-inlet, single detector REA system was set up in the center of the peatland (Fig. S3.2), 15 m south of a fully equipped EC tower (Sagerfors et al., 2008). Sampling inlets were mounted at 3.5 m above the ground. A short description of the REA design and operating parameters are given in Section S3.4. For details see Osterwalder et al. (2016). Monthly averages of GEM flux were computed based on an annual total of 4075 60-min values. Between December 2013 and February 2014 no measurements were performed. System maintenance was done monthly. The REA sampling interval was 30 min. The overall data coverage was 32%. The GEM flux source area covered 2.5 ha of homogenous wet lawns and carpet plant communities during snow-free conditions. The Hg detector and the two gold cartridge pairs were calibrated

every second month by injection of different volumes of Hg saturated air from a temperature controlled Hg vapor calibration unit (Tekran Model 2505, Toronto, Canada). GEM recovery was monitored automatically using the GEM reference gas and Hg zero-air generator (see Fig. S3.4). The system was regularly set into a reference mode (2s-simulated wind signal) to check for sampling line bias and to investigate the precision of concentration difference measurements. The detection limits were derived from the absolute standard deviation of the residuals from orthogonal linear regression fitting (cf. Zhu et al., 2015b). Residuals ( $n = 960$ ) did not show any trend with time or GEM concentration. The detection limit ( $1\sigma$ ) was 0.05 and 0.04  $\text{ng m}^{-3}$  for gold cartridge pair 1 and pair 2, respectively. In total 53% and 52% of the measured GEM differences were above these limits. Please note that the average flux values reported in the main text include data below the detection limit (average exchange rates would otherwise be overestimated).

### **3.2.5 Hg in catchment discharge**

Continuous discharge was measured in a heated flume at the catchment outlet averaged to hourly values. Stream water was sampled twelve times for Hg during the measurement period. The THg analyses were performed at Stockholm University Department of Applied Environmental Science following the US EPA standard method 1631 (US EPA, 2002) using a 10.035 Millennium Merlin 1631 CV-AFS (PSA, Orpington, UK). Annual THg export in discharge was calculated by multiplying the interpolated THg concentration with discharge quantity (see Sect. S3.5).

### **3.2.6 Dissolved gaseous Hg and other environmental parameters**

Dissolved gaseous elemental Hg concentration in the pore water was measured weekly during June - October 2013 and May - June 2014 using a Tekran Automated Purging System developed and described by Lindberg (2000) (see Sect. S3.6). Instruments to determine meteorological parameters were mounted at 2 m height above the peatland surface on the same tower as the eddy covariance system. Air temperature and humidity were determined by an MP100 temperature and moisture sensor (Rotronic AG, Bassersdorf, Switzerland) equipped with a ventilated shield. Global radiation was measured using a Li200sz sensor (LI-COR, Lincoln, USA). Water table levels were measured in a lawn plant community using a float and counterweight system attached to a potentiometer (Roulet et al., 1991). The snow depth was measured by a Sr-50 ultrasonic sensor (Campbell Scientific Logan, USA) mounted on the REA tower.

## Acknowledgements

We thank Markus Meili at Stockholm University for the discharge THg analysis and Ingvar Wängberg from IVL for providing wet bulk deposition data. The crew of the Field-based Forest Research Unit in Vindeln, Sweden is acknowledged for technical and maintenance support. The study was supported by the Swedish research infrastructures, ICOS and SITES, both partly financed by the Swedish Research Council. The research was financed by the Swiss National Foundation (Doc.Mobility fellowship #P1BSP2\_148458) and the Swedish Research Council (#2009-15586-68819-37).



## CHAPTER 4

# Comparative study of elemental mercury flux measurement techniques over a boreal peatland

*In preparation*

S. Osterwalder<sup>1</sup>, J. Sommar<sup>2</sup>, S. Åkerblom<sup>3</sup>, G. Jocher<sup>4</sup>, J. Fritsche<sup>1</sup>, M. B. Nilsson<sup>4</sup>, K. Bishop<sup>3,5</sup> and C. Alewell<sup>1</sup>: Comparative study of elemental mercury flux measurement techniques over a Fennoscandian boreal peatland.

[1] Department of Environmental Sciences, University of Basel, Basel, Switzerland

[2] State Key Laboratory of Environmental Geochemistry, Institute of Geochemistry, Chinese Academy of Sciences, Guiyang, China

[3] Department of Aquatic Sciences and Assessment, Swedish University of Agricultural Sciences, Uppsala, Sweden

[4] Department of Forest Ecology and Management, Swedish University of Agricultural Sciences, Umeå, Sweden

[5] Department of Earth Sciences, University of Uppsala, Uppsala, Sweden

## Abstract

Quantitative estimates of the land-atmosphere exchange of gaseous elemental mercury (GEM) are largely biased by the employed measurement technique, because no standard method and operating protocols exist. Here we present concurrent measurements of a novel relaxed eddy accumulation (REA) system, a rectangular Teflon® PFA and a new type dynamic flux chamber (DFC) over a boreal peatland. During four consecutive days the DFCs were placed alternately on two measurement plots in every cardinal direction around the REA tower. Spatial heterogeneity in peat surface characteristics was identified by measuring total mercury in the soil (49 - 62 ng g<sup>-1</sup>), vascular plant coverage (32 - 52%), water table level (4.5 - 13.9 cm) and dissolved gaseous elemental mercury concentrations (28 - 51 pg L<sup>-1</sup>) in the peat water. The GEM fluxes measured by the DFCs showed a distinct diel pattern, but no spatial difference in the average fluxes was detected (ANOVA,  $\alpha = 0.05$ ). Even though the correlation between the Teflon® PFA DFC and the new type DFC was significant ( $\rho = 0.76$ ,  $p < 0.05$ ) the cumulative flux of the NDFC was a factor 3 higher and close to the REA cumulative flux (< 2% difference). The average flux of the NDFC (1.9 ng m<sup>-2</sup> h<sup>-1</sup>) and REA (2 ng m<sup>-2</sup> h<sup>-1</sup>) were in good agreement with the averaged REA flux measured during a previous study in July 2013 (2.5 ng m<sup>-2</sup> h<sup>-1</sup>) at the same site. As typical for micrometeorological methods, REA showed higher temporal variability and the correlation of GEM fluxes between REA and the DFCs was insignificant ( $\rho < 0.1$ ,  $p < 0.05$ ). This was primarily due to the different underlying methodological assumptions and different impacts of meteorological parameters. The results indicate that the novel REA design is not subject to significant flux overestimation and that the new type DFC, which includes the effect of atmospheric turbulence, has the potential to bridge the gap between flux estimates derived from micrometeorological and enclosure techniques.



## 4.1 Introduction

Globally, anthropogenic mercury (Hg) emissions to the atmosphere and its subsequent deposition have increased the storage of this neurotoxic element in organic soils by 20% (Smith-Downey et al., 2010). The semi-volatile elemental form is produced in organic soils by a suite of reductive (photochemical, microbial, and dark abiotic) processes from the Hg<sup>2+</sup> pool and can be re-emitted to the atmosphere. The quantification of GEM fluxes from terrestrial environments is important, because the re-emission of GEM to the atmosphere converts the soil bound and rather immobile Hg into a mobile form with potential long-range transport, (Selin et al., 2008) subsequent deposition, and accumulation in food chains.

Two main methodologies exist to measure land-atmosphere exchange of GEM: First, dynamic flux chambers (DFCs) representing small-scale spatial measurements which are ideal for comparison studies to understand the influence of individual controlling factors on GEM flux (Gustin et al., 1999). The method is based on GEM concentration measurements between the inlet and outlet of the DFC. Up to now DFCs have been used for 85% of GEM flux measurements (Agnan et al., 2016). However, DFC measurements have been criticized since the enclosure disturbs the microclimate by influencing aerodynamics, temperature and the radiation balance (Wallschläger et al., 1999; Gustin et al., 1999). Furthermore, among DFC studies a high variability was observed due to differences in designs, operating procedures, and application protocols (Eckley et al., 2010), as well as a limited spatial representativeness (as reviewed by Agnan et al., 2016).

To overcome the limitation of the DFC measurements, micrometeorological methods (MM) have been developed which allow larger-scale measurements and only marginally modify environmental conditions. They include the relaxed eddy accumulation (REA) method (Cobos et al., 2002; Olofsson et al., 2005b; Bash and Miller, 2008; Sommar et al., 2013b; Osterwalder et al., 2016), the aerodynamic gradient (AGM) methods (e.g. Lindberg et al., 1995; Fritsche et al., 2008b; Baya and Van Heyst, 2010), and the modified Bowen ration (MBR) method (e.g. Obrist et al., 2006; Fritsche et al., 2008b; Converse et al., 2010). Field trials of Hg eddy covariance (EC) measurements over background sites revealed no manifest GEM-vertical wind covariance, indicating fluxes were below the method detection limit (Pierce et al., 2015). Comparison studies over Hg-enriched soils have shown that fluxes determined with DFCs were nearly 3 times lower compared to fluxes derived from AGM and MBR method fluxes (Wallschläger et al., 1999; Gustin et al., 1999; Zhu et al., 2015a). Carpi and Lindberg (1997) found that MM-derived fluxes were generally up to 20% higher than DFC fluxes for sludge-amended soils and Pierce et al. (2015) reported 16% lower fluxes measured with a DFC compared to MBR fluxes. A new type of dynamic flux chamber (NDFC) designed by Lin et al., (2012) accounts for atmospheric surface-layer shear properties by a scaling procedure. Field examination indicated that NDFC may bridge the gap in magnitude between DFC- and MM-derived flux. NDFC differed less than 10% from AGM and MBR, while the flux derived from a traditional DFC was 42% and 31% lower compared to AGM and MBR (Zhu et al., 2015a)

In the study we present the first method comparison between a Teflon<sup>®</sup> PFA DFC (TDFC), a NDFC and a dual-inlet, single detector REA system deployed at a pristine peatland catchment site in northern Sweden. Peatlands were identified as hot spots in the landscape for

production of highly toxic methylmercury (MeHg) species that in-turn biomagnifies in aquatic food webs (Watras and Bloom, 1992). This makes investigations of Hg cycling in such environments of high interest (St. Louis et al., 1994; Mitchell et al., 2008). GEM land-atmosphere exchange studies conducted over northern peatlands are scarce, but indicated that wetland GEM evasion may seasonally rival the input flux of Hg wet deposition (e.g. Kyllönen et al., 2012; Osterwalder et al., 2016).

The choice of methods to capture GEM fluxes highly depends on availability of resources as well as expert knowledge. While DFC measurements are relatively low-cost and require only medium expert knowledge, MM methods and especially the REA method are highly cost intensive and require long-term availability of highly specialized staff. The question remains if DFC measurements still deliver valuable quantitative GEM flux estimates, where MM methods are not feasible. Due to the different scales associated, a comparison of DFC (surface area of typically  $< 0.1 \text{ m}^2$ ) to MM methods (in our case 80% of the flux originates from a footprint of  $11500 \text{ m}^2$ ) has to consider the site heterogeneity. The peatland surface within the EC footprint has previously been defined as homogeneous and is made up of wet lawns and carpet plant communities (Nilsson et al., 2008). Nevertheless, the GEM source strength could be altered by spatial changes in total Hg concentrations in the peat (THg), abundance of vascular plants (VP), water table level (WTL), or dissolved gaseous Hg (DGM) concentration in peatland pore water. Correlations between THg in the soil and GEM fluxes have been found across individual background sites (Nacht et al., 2004; Sigler et al., 2006). Higher abundance of vascular plants is expected to contribute more to GEM re-emission due to less Hg sequestration compared to bryophytes (Selvendiran et al., 2008) and the capacity of DGM transport by transpiration flow and release of GEM through stomata and cuticles (Lindberg et al., 2002). Water bodies are defined as net sources of GEM to the atmosphere (Wang et al., 2014). Thus, high water table levels and elevated concentrations of volatilizable DGM especially during periods of high surface wind speeds may promote GEM emissions.

The objective of this study was to investigate whether DFC and REA measurements are comparable if small-scale variation in the GEM flux was accounted for with spatial repetitions of DFC measurements. As such, the integrated GEM flux over a larger spatial extension upwind of the REA sampling tower was compared with simultaneous GEM fluxes determined over spatially repeated small footprints using a pair of co-located TDFC and NDFC. For the first time we compared and evaluated quantitatively derived GEM fluxes from REA and the set of DFCs, and contribute to evaluation of standardized methods.

## 4.2 Methods

### 4.2.1 Site description

Measurements were performed continuously between July 8 and 12, 2014 in the center of Degerö Stormyr (2.7 km<sup>2</sup>), a mixed acid mire system (64°11'N, 19°33'E; 270 m a.s.l.) situated in the Kulbäcksliden domain of the Svartberget long-term experimental research (LTER) facility near Vindeln in the county of Västerbotten, Sweden. The surrounding forest is a mixed coniferous forest (*Pinus sylvestris* L and *Picea abies* L. H. Karst) with minor contribution by birch (*Betula pubescens* Ehrh.). The average peat depth is generally between 3 and 4 m. The deepest layers correspond to an age of ~8000 years. THg concentrations between 0 - 34 cm measured in autumn 2015 averaged  $57 \pm 8$  ( $\pm$ SE) ng g<sup>-1</sup> and designating the area as typical background site (see peat profile in Fig. S3.3). Vegetation cover within the REA fetch mainly consists of vascular plants (dominated by *Eriophorum vaginatum* L., *Trichophorum cespitosum* L. Hartm., *Vaccinium oxycoccos* L., *Andromeda polifolia* L., *Rubus chamaemorus* L. and sparsely interspersed by *Carex limosa* L., and *Schezeria palustris* L.) and Sphagnum species (*Sphagnum majus* Russ. C. Jens, *S. lindbergii* Schimp., *S. balticum* Russ. C. Jens, *S. fuscum* Schimp. Klinggr. and *S. rubellum* Wils) (Nilsson et al., 2008; Laine et al., 2012). The 30 year (1981 - 2010) mean annual precipitation and temperature are 614 mm and +1.8°C while the mean temperatures in July are +14.7°C (Ottosson-Löfvenius et al., 2013; Laudon et al., 2013). The dominant wind-direction in summer is northeast (Sagerfors et al., 2008).

### 4.2.2 Relaxed eddy accumulation technique

The dual-inlet, single detector REA system consists of a USA-1 ultrasonic anemometer (METEK GmbH, Elmshorn, Germany) to measure standard deviation of the vertical wind velocity, two sets of fast-response valves (Model 6128, Bürkert, Ingelfingen, Germany) to sample and separate vertically upward and downward moving air parcels, GEM adsorption cartridges, an atomic fluorescence analytical unit as well as a GEM reference gas and Hg zero-air generator unit. The REA design and operation parameters are described in detail by Osterwalder et al. (2016). A schematic of the applied system is presented in Figure S3.4. The vertical GEM-flux is calculated over 30 min intervals using:

$$F_{REA} = \beta \sigma_w (\overline{C_u} - \overline{C_d}), \quad (4.1)$$

where  $\sigma_w$  is the standard deviation of the vertical wind velocity,  $\overline{C_u} - \overline{C_d}$  is the difference between the average GEM concentration in updrafts and downdrafts, respectively and  $\beta$  is the relaxation coefficient determined by assuming the EC sensible heat flux (see Sect. 2.2) equal to corresponding REA flux derived analogous to Equation 4.1:

$$\beta = \frac{\overline{w'T'}}{\sigma_w (\overline{T_u} - \overline{T_d})}, \quad (4.2)$$

where  $\overline{T_u} - \overline{T_d}$  is the difference between averaged air temperatures measured in updrafts and downdrafts, respectively. A zero centered dynamic deadband ( $0.5\sigma_w$ ) was introduced. A recursive high-pass filter removed bias in measurements of vertical wind velocity (McMillen,

1988; Richardson et al., 2012). GEM recovery was monitored by automated and alternate injections (every 30 min) of a GEM reference gas and dry Hg-free air.

REA raw flux data were post-processed by implementing a series of standard corrections and were screened for low quality data by applying rejection criteria following Osterwalder et al. (2016). 8% of the data were discarded. The gaps were filled for better comparability with DFC fluxes using a look-up table where 6 fixed intervals for air temperatures between 5 and 35°C were defined. Air temperature showed a light but significant correlation with the REA flux ( $\rho = 0.26$ ,  $p < 0.05$ ) and was recorded completely during the campaign. Before and after the measurement campaign the system was set to operate in a reference mode to check for up- and downdraft sampling line bias. Based on the performance in reference mode, the detection limit was derived in two steps by (i) calculating the GEM concentration difference between the two gold cartridge pairs and by (ii) resolving the absolute standard deviation of the residuals from orthogonal regression fitting (cf. Zhu et al., 2015b).

### 4.2.3 Enclosure techniques

Two types of DFC were deployed in side-by-side measurements (the set-up is visualized in Fig. S4.2). The TDFC with a square footprint (0.44 m x 0.44 m) was made of 0.25 mm Teflon® PFA film supported by a rectangular frame (height: 0.29 m). The TDFC has five 1 cm diameter holes in regular distance along each sidewall located 6 cm above the surface. The sample port ( $\varnothing$  0.5 cm) was located in the top and center of the DFC. The characteristics and performance of the polycarbonate NDFC has been previously been documented in Lin et al. (2012) and Zhu et al. (2015a, b). The aerodynamic design of the NDFC covering a surface of 0.09 m<sup>2</sup> produces a uniform surface friction velocity that can be controlled by the sampling flow rate. Therefore, the flux under atmospheric conditions can be derived from measured flux normalized by the ratio of the overall mass transfer coefficient in ambient air to that in the NDFC (Eq. 4.4). Both DFCs were operated at a flow rate of 13.3 L min<sup>-1</sup> corresponding to turnover times of 4.2 min and 0.4 min for TDFC and NDFC, respectively. The TDFC flux was calculated according to Equation 4.3 (Xiao et al., 1991) and the NDFC flux determined with Equation 4.4, incorporating surface shear properties (Lin et al., 2012):

$$F_{TDFC} = \frac{Q(C_i - C_o)}{A_{TDFC}}, \quad (4.3)$$

$$F_{NDFC} = \frac{Q(C_i - C_o)}{A_{NDFC}} \cdot \frac{k_{atm}}{k_{NDFC}} = \frac{Q(C_i - C_o)}{A_{NDFC}} \cdot \frac{\left(4.86 + \frac{0.03h^2 u_* D_H / (6kz_0 D l)}{1 + 0.016 \sqrt{\{(h^2 u_* D_H) / (6z_0 D l)\}^2}}\right)}{\left(4.86 + \frac{0.03h Q D_H / (A_c D l)}{1 + 0.016 \sqrt{\{(h Q D_H) / (A_c D l)\}^2}}\right)}, \quad (4.4)$$

where  $F_{TDFC}$  and  $F_{NDFC}$  are the GEM fluxes derived from the TDFC and NDFC method, respectively,  $Q$  is the applied flow rate (13.3 L min<sup>-1</sup>),  $C_i$  and  $C_o$  are the inlet and outlet GEM concentrations, respectively and  $A$  is the surface enclosed by the DFCs.  $h$  is the NDFC height (0.03 m),  $l$  is the distance measured from the starting point of the measurement zone (0.15 m),  $u_*$  is the friction velocity,  $k$  is the Kármán constant (0.41) (Seinfeld and Pandis, 1998),  $z_0$  is surface roughness height,  $A_c$  is the flow cross-sectional area (0.009 m<sup>2</sup>) and  $D_H$  and  $D$  are the hydraulic radius (0.0545 m) and diffusivity of GEM (1.194·10<sup>-5</sup> m<sup>2</sup> s<sup>-1</sup>), respectively.

Prior to application in the field, the DFCs were cleaned in a 5% nitric acid bath for 24h and rinsed with ultrapure water (Milli-Q, 18.2 M $\Omega$ -cm, Millipore Corp.). Blank measurements were performed on site over an acid-cleaned Teflon<sup>®</sup> PTFE film before and after the campaign. The blanks calculated for TDFC ( $0.1 \pm 0.2 \text{ ng m}^{-2} \text{ h}^{-1}$ ,  $n = 51$ ) and NDFC ( $0.3 \pm 0.3 \text{ ng m}^{-2} \text{ h}^{-1}$ ,  $n = 115$ ) were interpolated and subtracted from the calculated GEM fluxes. Typical sources of uncertainty for REA and DFC measurements can be reviewed in Zhu et al. (2015b).

#### 4.2.4 Instrumentation and sampling

The anemometer and intake lines of the REA system were installed at 3.5 m above the surface. The former measured turbulent fluctuations of the horizontal and vertical wind at a resolution of 20 Hz. 30 min averages of horizontal wind speed, wind direction, friction velocity ( $u^*$ ) and stability ( $z/L$ ) were derived. EC systems with sensors installed 15 m north of the REA tower have been measuring exchange of greenhouse gases, water vapor and energy at 1.8 m height a.g.l. since 2001 (Sagerfors et al., 2008) and since 2013 within the Pan-European Integrated Carbon Observation System (ICOS) infrastructure. From these measurements 30 min averages of the sensible heat flux were derived for  $\beta$ -calculations (Eq. 4.2). Sensors to measure additional climate variables were placed on the same tower (see details below). 8.5 m long Teflon<sup>®</sup> PFA sampling tubes connected the fast-response valves with the GEM-accumulation and analysis system. The system was installed in a temperature controlled dome shaped plexiglass container (Igloo Satellite Cabin, Icewall One, Australia), which also houses the main part of ICOS instrumentation.

The REA footprint was estimated for each half-hour period during the campaign and beyond (July 2 - 17, 2014) using a Lagrangian stochastic forward model (Rannik et al., 2000) based on atmospheric conditions, measurement height and surface roughness (0.02 m). Footprint modeling is crucial to pin-point overlap between the source area of REA flux and the DFC measurement plots. These plots are located within 65 m of the REA tower in E, S and W direction. The N plots are more distant ( $\sim 120$  m) from the REA tower (Fig. 4.1a).

The ground based, mobile DFC sampling setup basically consisted of a flushing unit, a two port sampling valve system and an automated Hg vapor analyzer (further details can be reviewed in Figure S4.2). Alternately, in one hour intervals the DFCs were deployed over two plots at every cardinal direction. In clockwise direction, the DFC measurements started at the plots in the north and were rotated for four full laps during the campaign. At the inlet and outlet of the DFCs, a sub-stream of air ( $1.3 \text{ L min}^{-1}$ ) was sequentially sampled twice at 5 min intervals using a Synchronized Two-Port Sampler (Tekran Model 1110, Toronto, Canada). Plot specific one hour GEM fluxes were calculated using Equations 4.3 and 4.4 for TDFC ( $n = 32$ ) and NDFC ( $n = 32$ ), respectively. The measurements were evenly distributed over the 4 days in order to be comparable with the 30 min REA fluxes ( $n = 192$ ). Boardwalks gave access the all measurement plots and guaranteed an undisturbed investigation of the peatland surface. After every measurement, the DFCs were cleaned with ultrapure water and air dried. 15 min prior to sampling the DFCs were put on the plots again. The DFC and REA Hg analyzers (Tekran Model 2537A and 2500, respectively) were calibrated in-situ before and after the field campaign using a temperature-controlled Hg vapor calibration unit (Tekran Model 2505). Multiple volumes (3 - 8  $\mu\text{l}$ ) of saturated GEM vapor were manually injected into a Hg-free air

stream obtained from a zero-air generator (Tekran Model 1100) using a 10  $\mu\text{l}$  digital gas-tight syringe (Hamilton, Reno, USA).

Dry deposition velocities were calculated for the REA and DFC method by dividing the GEM flux by the atmospheric GEM concentration measurements at the same height (Poissant et al., 2004a). Statistical calculations were performed using R version 3.1.2 (R Core Team, 2011).

### 4.2.5 Environmental parameters

Eight peat cores (0 - 34 cm) were taken in autumn 2015 close to the plots where GEM flux measurements were performed. The cores were cut in 2 cm increments, air-dried and sieved (< 2 mm). THg analysis was performed by thermal decomposition (750°C) followed by amalgamation on gold-traps, thermal desorption, and analysis of vapor Hg by Atomic Absorption Spectroscopy according to EPA method 7473. Certified reference lake sediment material (IAEA SL-1) was used for calibrations. Replicate samples and the reference material were analyzed regularly (10% of the sampling sequence) with an established precision of  $\leq 10\%$  (relative SD). For further details on peat core analysis see section “Supporting Information to Chapter 3”.

On the eight measurement plots, vegetation composition was investigated using percent cover estimates following Wiedermann et al. (2007). The flat area within the plots was representative for the REA footprint and was fully covered by Sphagnum. Vascular plants growing within the plots were dominated by sedges and dwarf-shrubs. The partial vascular plant coverage was calculated for each plot.

Water table levels were determined after every GEM flux measurement ( $n = 64$ ) using basic plumbing well-tubes ( $\varnothing$  16 mm) drilled into the peat next to the plots. A standard procedure was applied by inserting a scaled PVC-tube into the wells and blowing into it until a bubbling was heard.

The DGM sampling setup that was applied during two days after the campaign is illustrated in the “Supporting Information to Chapter 3” (Fig. S3.6). Surface water samples (collected at WTL-10 cm) were collected in a 1 L PFA vessel and analyzed immediately in the field using an automated purging system following Lindberg et al. (2000). The samples were purged with Hg-free air (Tekran Model 1100) for a total of 60 min (40 min sample, 20-min whole-blank) at a flow rate of 1.2 L  $\text{min}^{-1}$ . The DGM concentration was then calculated from the difference between the sample and blank ( $1.3 \pm 0.8$  pg) purges and was expressed on a water volume basis. Between the single measurements the vessel was purged with ultrapure water for 20 min. DGM in ultrapure water was always below the detection limit of  $\sim 0.5$  pg. Diurnal cycles for DGM in the peat water were not pronounced during the entire growing season (Fig. S3.6b).

Meteorological parameters were measured by sensors mounted on the EC tower. Global radiation ( $R_g$ ) was measured on 4 m height using a Li200sz sensor (LICOR, Lincoln, Nebraska, USA). Air temperature ( $T_a$ ) and humidity (Rh) were determined by a MP100 temperature and moisture sensor (Rotronic AG, Bassersdorf, Switzerland) inside a ventilated radiation shield mounted 1.8 m above the peatland surface. Mean water levels and soil temperatures representative for the REA footprint were measured 100 m northeast of the EC tower. The WTL was measured using a float and counterweight system attached to a potentiometer (Roulet et al., 1991). Soil temperature ( $T_s$ ) at 2 cm depth was measured by TO3R thermistors

mounted in sealed, waterproof, stainless steel tubes (TOJO Skogsteknik, Djäkneboda, Sweden). Due to an instrument failure,  $T_s$  data for only 65% of the campaign period were logged. All environmental data were stored as 30 min averages on a data logger (CR10X, Campbell Scientific, Logan, Utah). Air temperature and relative humidity inside and outside (10 cm above surface) the DFC were measured every 5 min by a ELUSB-2 Humidity, Temperature and Dew Point Data Logger on a 5 min base (DATAQ Instruments, Akron, USA).

## 4.3 Results and Discussion

### 4.3.1 Environmental conditions

Meteorological conditions during the campaign were persistently very fair and unusually warm ( $19.7 \pm 6.1^\circ\text{C}$ ) (see time series in Fig. S4.3). No precipitation was recorded during the measurements. Nighttime conditions with global radiation below  $5 \text{ Wm}^{-2}$  accounted for 19% of the time. Fog formed during the nights when relative humidity was close to 100%. Wind speed was considerably higher during the day ( $2.0 \pm 1.0 \text{ m s}^{-1}$ ) than at night ( $0.9 \pm 0.9 \text{ m s}^{-1}$ ). Prevailing winds were from north (39%) and east (46%) (Fig. 4.1b).

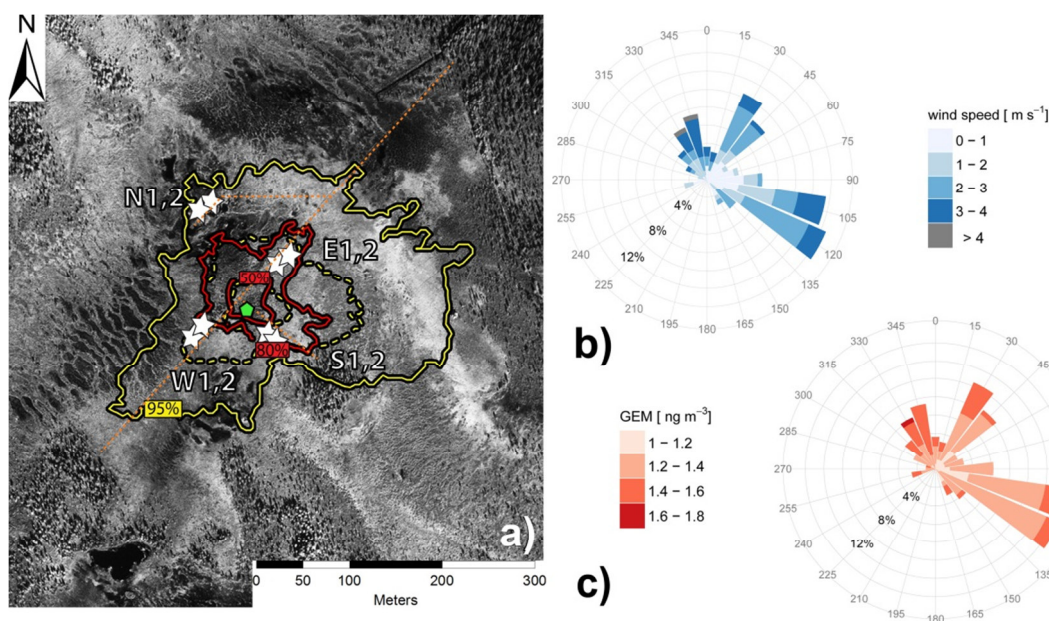


**Figure 4.1:** Aerial photograph of Degerö Stormyr with contour lines indicating the predicted source area of GEM flux measured by the relaxed eddy accumulation (REA) system (a). The green polygon marks the location of the REA tower. The footprint of the innermost red circle corresponds to 50% of the measurements performed during the 4-day campaign. The second red circle includes 80% of the measurements. The yellow contours (50% and 80% dashed line, 95% continuous line) indicate the source area of the measurements for the period from 02.07 - 17.07.2014). Locations of the 8 plots for the DFC measurements are shown as white stars arranged in all four cardinal directions. The polar histogram for wind speed (b) and atmospheric GEM concentration (c) describe the conditions during the campaign.

Atmospheric conditions were stable ( $z/L > 0.2$ ; where  $z$  is the measuring height and  $L$  the Monin-Obukhov stability length), neutral ( $-0.2 < z/L < 0.2$ ) and unstable ( $z/L < 0.2$ ) during 23%, 8% and 69% of the time, respectively. At nighttime, stable conditions were dominant (64%). 77% of the measurement time featured windy conditions ( $u^* > 0.1 \text{ m s}^{-1}$ ), during which turbulent transport of GEM is assumed to dominate convectively driven transport.

The mean water table within the REA fetch (Fig. 4.1a) decreased from 14.2 to 16.6 cm below the surface during the course of the measurements. The atmospheric GEM concentration measured at 3.5 m a.g.l. ranged between 0.9 and  $1.7 \text{ ng m}^{-3}$  and showed no discernible dependence on wind direction (Fig. 4.1c). The corresponding mean of  $1.3 \pm 0.1 \text{ ng m}^{-3}$  during the 4-day campaign compares with observations made in boreal Fennoscandia (Nerentorp et al., 2013). Thus, to summarize, due to the heatwave present in July 2014,



meteorological conditions were very stable during the campaign and ideal for a field inter-comparison of flux measurement methods operating over differing spatio-temporal scales.

#### 4.3.2 REA GEM flux characteristics

The average  $\pm$  SD GEM flux measured with REA was  $2 \pm 24$  ng m<sup>-2</sup> h<sup>-1</sup> and ranged from -83 to 72 ng m<sup>-2</sup> h<sup>-1</sup> (Tab. 4.1). The median  $\pm$  MAD (median absolute deviation) was  $1.6 \pm 17$  ng m<sup>-2</sup> h<sup>-1</sup>. Both, average atmospheric GEM concentration and turbulent flux were independent of wind direction (Fig. 4.1c and Fig. 4.3c). The mean concentration difference between up- and downdrafts measured with the gold cartridge pairs C1-C3 and C2-C4 were 0.05 and 0.04 ng m<sup>-3</sup>, respectively. Even though 36% and 59% of the GEM fluxes were below the detection limit of 0.03 ng m<sup>-3</sup> for respective gold cartridge pairs, smaller concentration gradients were included in the results, as average fluxes would otherwise be overestimated (Fritsche et al., 2008b).

**Table 4.1:** Summary of mean, median and 10<sup>th</sup> and 90<sup>th</sup> percentiles of the GEM flux determined with a Teflon® PFA and new type dynamic flux chamber (TDFC and NDFC) and the relaxed eddy accumulation (REA) technique. Simultaneously determined atmospheric GEM concentrations (measured with the DFC and REA setup) and environmental parameters are listed. Pearson correlation coefficients ( $\rho$ ) between GEM flux and factors controlling GEM flux are given in bold if statistically significant ( $p < 0.05$ )

Variable	08.07 - 12.07.2014									
	unit	Mean	Median	10 <sup>th</sup> /90 <sup>th</sup> %	$\rho_{\text{TDFC}}$	n	$\rho_{\text{NDFC}}$	n	$\rho_{\text{REA}}$	n
TDFC flux	ng m <sup>-2</sup> h <sup>-1</sup>	0.66	0.4	-0.77/2.6	[-]	[-]	[-]	[-]	[-]	[-]
NDFC flux	ng m <sup>-2</sup> h <sup>-1</sup>	1.93	0.63	-1.78/7.73	<b>0.76</b>	32	[-]	[-]	[-]	[-]
REA flux	ng m <sup>-2</sup> h <sup>-1</sup>	2	1.6	-27/34	0.06	96	0.03	96	[-]	96
<b>REA Footprint parameters</b>										
GEM concentration REA	ng m <sup>-3</sup> [3.5 m]	1.3	1.3	1.15/1.46	[-]	[-]	[-]	[-]	-0.02	192
GEM concentration DFCs	ng m <sup>-3</sup> [20 cm]	1.5	1.57	1.17/1.46	<b>0.87</b>	32	<b>0.75</b>	32	[-]	[-]
Solar radiation	W m <sup>-2</sup>	253	208	1.7/559	<b>0.8</b>	32	<b>0.79</b>	32	-0.01	192
Temperature [2m]	°C	19.7	20.9	11.1/27.5	<b>0.81</b>	32	<b>0.74</b>	32	<b>0.26</b>	192
Temperature inside TDFC	°C	25.8	31	9/39.1	<b>0.81</b>	32	[-]	[-]	[-]	[-]
Temperature inside NDFC	°C	22.3	18	7.5/39.2	[-]	[-]	<b>0.82</b>	32	[-]	[-]
Temperature outside DFCs	°C [10 cm]	20.2	21.5	8.8/30.1	<b>0.81</b>	32	<b>0.8</b>	32	[-]	[-]
Soil temperature	°C [-2 cm]	18.5	18.7	14.9/21.7	[-]	[-]	[-]	[-]	<b>0.51</b>	127
Relative humidity	%	66.8	64.5	40.7/97.1	<b>-0.79</b>	32	<b>-0.68</b>	32	<b>-0.31</b>	192
Wind speed	m s <sup>-1</sup>	1.6	1.7	0.3/2.9	<b>0.42</b>	32	<b>0.49</b>	32	<b>0.16</b>	192
Friction velocity	m s <sup>-1</sup>	0.2	0.2	0.07/0.32	[-]	[-]	[-]	[-]	0.16	192
Mean water level	cm	-15.5	-15.4	-16.6/-14.6	[-]	[-]	[-]	[-]	0.12	127
Substrate Hg [0-10 cm]	ng g <sup>-1</sup>	23.7	24	20/28	[-]	8	[-]	8	[-]	[-]

Based on the REA footprint calculations after Rannik et al. (2000), 80% of the REA GEM flux during the campaign originated from an area of 11500 m<sup>2</sup> (Fig 4.1). The measurement plots in the north (N 1,2), east (E 1,2) and south (S 1,2), were situated within the main wind directions which were from northwest to southeast. The area southwest of the tower contributed only 5% of the GEM source area and was represented by plot (W 1,2). We conclude that GEM exchange from the western part of the peatland was rather underrepresented in the REA signal, while northwestern, northeastern and southeastern areas contributing 23%, 31% and 41% to the GEM source area, respectively (Fig. 4.3c).

### 4.3.3 DFC GEM flux characteristics

The average  $\pm$  SD of the GEM flux was  $0.7 \pm 1.3$  for the TDFC ( $n = 32$ ) and  $1.9 \pm 3.8$  for the NDFC ( $n = 32$ ) (Tab. 4.1). Median  $\pm$  MAD were  $0.4 \pm 1.3$   $\text{ng m}^{-2} \text{h}^{-1}$  and  $0.6 \pm 3.2$   $\text{ng m}^{-2} \text{h}^{-1}$ , respectively. The two averages were not significantly different (Mann-Whitney U test,  $\alpha = 0.05$ ) but the NDFC flux displayed a higher variance (Fig. 4.4b). The higher variability in the NDFC flux is not just associated with the correction for atmospheric boundary shear conditions (Eq. 4.4) but already exhibited larger median absolute deviation ( $\pm 2.6$   $\text{ng m}^{-2} \text{h}^{-1}$ ) prior to correction (see Fig. S4.1).

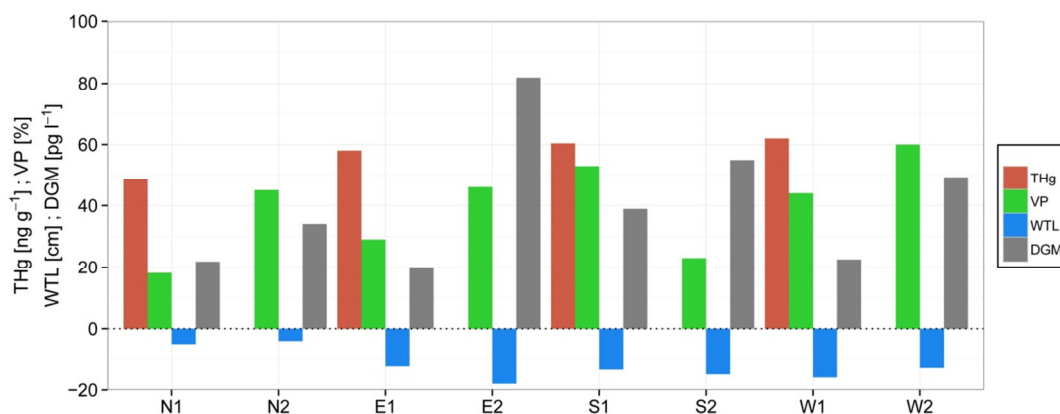


**Figure 4.2:** The bar chart indicates plot characteristics dependent on total Hg in the peat (THg, 0 - 34 cm, averaged for each cardinal direction), abundance of vascular plants (VP), water table level (WTL) and dissolved gaseous Hg (DGM).

Besides methodological bias, spatial heterogeneity of the DFC footprints has been shown to influence the magnitude of the parallel flux measurements (Wallschläger et al., 1999 and Gustin and Lindberg, 2000). Within the REA footprint, divergences in peat THg, abundance of vascular plants, water table level and DGM were investigated for every cardinal direction (Fig. 4.2). In the peatland area north of the flux tower THg in the top 34 cm was  $48.7$   $\text{ng g}^{-1}$  and lower compared to the E ( $58.0$   $\text{ng g}^{-1}$ ), S ( $60.4$   $\text{ng g}^{-1}$ ) and W ( $62.0$   $\text{ng g}^{-1}$ ) plots. In the same area vascular plants were less abundant (32%), water table level in the plots was highest (4.5 cm below the surface), and the pore water DGM concentrations were lowest ( $28$   $\text{ng L}^{-1}$ ). The THg pool in the soil (0 - 34 cm) differed considerably in the following order: N ( $718$   $\mu\text{g m}^{-2}$ ) < W ( $801$   $\mu\text{g m}^{-2}$ ) < S ( $880$   $\mu\text{g m}^{-2}$ ) < E ( $1131$   $\mu\text{g m}^{-2}$ ). Water table level in the other areas of the peatland was in a similar range (12.5 - 14.1 cm below the surface), whereas vascular plant coverage was highest (52%) within the plots located in the west. Overall, DGM was supersaturated with respect to Henry's law equilibrium with atmospheric GEM and showed highest concentrations south ( $46.2$   $\text{pg L}^{-1}$ ) and east ( $50.9$   $\text{pg L}^{-1}$ ) of the REA tower. GEM fluxes measured over a total of eight plots were averaged and inter-compared by analysis of variance (ANOVA,  $p < 0.05$ ). Prior to analysis the response variables were log-normalized to achieve normal distribution. Variability in GEM flux was neither displayed between plots nor directions (Fig. 4.3a and 4.3b). Thus, we conclude that the REA footprint is spatially homogenous with respect to GEM source strength.

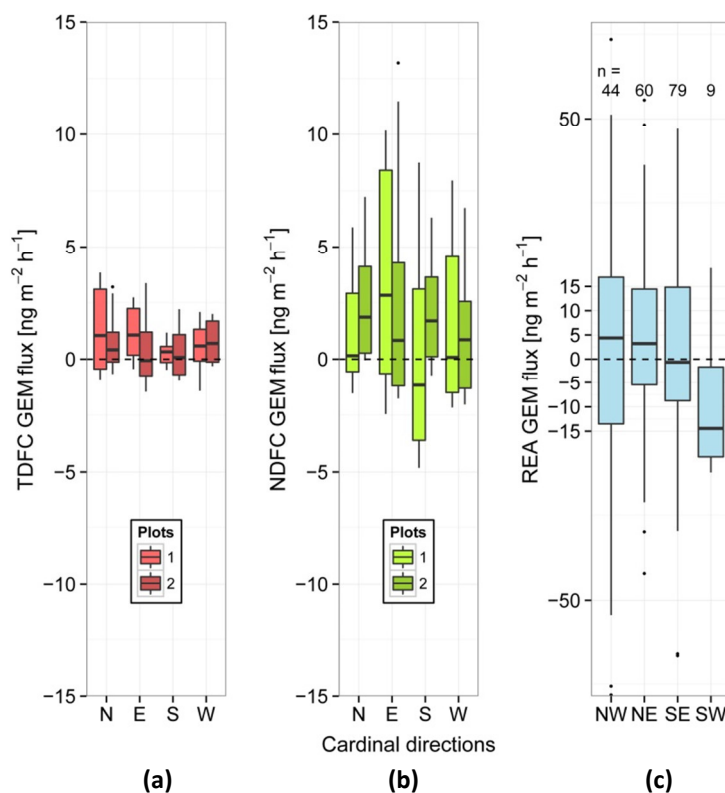


**Figure 4.3:** GEM fluxes measured with the Teflon® PFA DFC (TDFC) (a) and new type DFC (NDFC) (b) over two plots at each cardinal direction surrounding the relaxed eddy accumulation (REA) system (c) ( $n = 8$  per boxplot). The REA GEM flux is separated in four sectors of wind direction (blue). The N, E, S and W plots were located within the NW, NE, SE, SW wind sectors, respectively. The black bar indicates the median, the top and bottom edges of the boxes indicate the 75<sup>th</sup> and the 25<sup>th</sup> percentiles, respectively. The whiskers indicate 1.5 times the interquartile range.

The higher total variance in the NDFC flux was largely driven by a more pronounced diel pattern (Fig 4.4a). Reasons for amplification of the rather well-defined temporal pattern with discernible sharp maximum (emission) and shallow minimum (deposition) include:

- 1) DFC geometry and aerodynamics: The flat, rectangular design of the NDFC ensured a more uniform airflow over the surface and increased airstream velocity. This resulted in thinner surface boundary layer with diminished soil/air exchange resistance advancing GEM emission from the soil. Non-horizontal flow in the TDFC reduced the exchange surface area (Zhang et al., 2002; Eckley et al., 2010; Agnan et al., 2016).
- 2) DFC air exchange rate: The volume and turnover time for the TDFC was 10 times higher compared to the NDFC. Less voluminous DFCs and shorter turnover times were reported to positively influence GEM emission (Eckley et al., 2010). Though, the DFC turnover time and the flushing flow rate which was set to  $13.3 \text{ L min}^{-1}$  for both DFCs must have an identifiable influence on GEM fluxes (Eckley et al., 2016). The flushing flow rate was considered as ideal for the NDFC (Lin et al., 2012). This also holds for the TDFC since lower flushing flow rates are recommended for much smaller traditional DFCs at background sites (Eckley et al., 2010; Engle et al., 2006). However, the slower turnover time may have created an artificial boundary layer with elevated Hg concentrations at the air-surface interface resulting in a suppression of emissions (Gustin et al., 1999).

3) Fabrication material: The NDFC displayed a slightly higher and more variable blank in comparison to the consistently low TDFC blank. Teflon® PFA film is in addition considered an ideal material for Hg research DFCs due to its full transmission of actinic light (Eckley et al., 2010). Polycarbonate DFCs in contrast block wavelengths below 320 nm and therefore tend to underestimate GEM fluxes (Eckley et al., 2010). A recent synthesis of GEM flux measurements in Western North America found that fluxes from Teflon® DFCs were 150% higher than fluxes measured using polycarbonate DFCs (Eckley et al., 2016). Nevertheless, DFCs seem not able to preserve ambient air temperature due to altered long-wave radiation balance. On an average, we found a substantially positive difference between inside and outside temperature that is more pronounced for the TDFC ( $5.3 \pm 4.9$  °C) compared to the NDFC ( $2.6 \pm 5.7$  °C). We presume that the effect is substantially less in terms of surface soil temperature difference and plausibly less grave in perturbing the GEM exchange process at the soil interface.

Bi-directional exchange of GEM was evident with daytime (02:30 - 21:30) emission and shallow nighttime (22:00 - 02:00) deposition (Fig. 4.4a). Both the TDFC and NDFC flux data sets showed positive skewness (0.43 and 0.59) due to a sharper daytime peak than the features of nocturnal levelling-off.

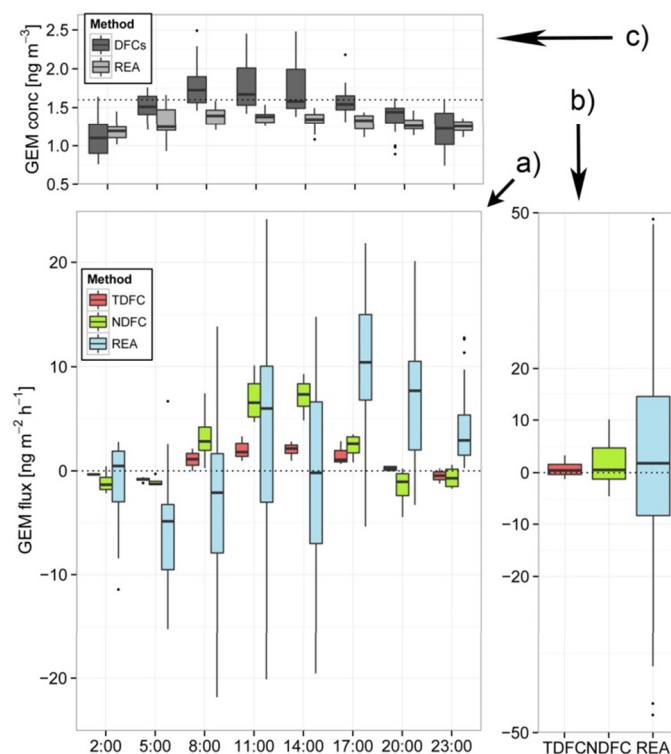


**Figure 4.4:** Diel plot of 3-hourly mean GEM fluxes measured during 4 days (July 08, 06:00 - July 12, 06:00) with a Teflon® PFA (red) and new type (green) dynamic flux chamber (TDFC and NDFC) and the relaxed eddy accumulation (REA) technique (blue). TDFC and NDFC measurements were plot averaged ( $n = 4$  per boxplot). For better comparison a 6-hourly smoothed REA GEM flux ( $n = 24$  per boxplot) time series is illustrated (a). Values beyond  $\pm 50$  ng m<sup>-2</sup> h<sup>-1</sup> are not shown (b). Diel pattern of atmospheric GEM concentration measured with DFCs 20 cm above the surface ( $n = 16$  per boxplot) and with REA at 3.5 m ( $n = 24$  per boxplot) are given (c). Details of the boxplot data presentation are provided in the caption of Figure 4.2.

#### 4.3.4 Comparison of REA and DFC measurement techniques

Our results suggest that site heterogeneity was minimal and that a direct method comparison was possible. The means of GEM fluxes derived from the REA and the NDFC method were not statistically different (Mann-Whitney U test,  $\alpha = 0.05$ ) albeit the REA flux had a considerably higher variation (Fig. 4.4b). The highly variable 30 min turbulent fluxes are subject to constant changes of atmospheric turbulence within the surface layer and are typical for MM measurements. The REA flux is considered as net ecosystem Hg flux including GEM emission from the soils, water and vegetation surfaces and dry deposition i.e. GEM uptake by vegetation. The estimated strong influence by atmospheric conditions on the REA flux seems to smear distinct diel patterns gauged by the DFC systems. Surface soil temperature was the only environmental variable strongly positively correlated with REA GEM flux (generally:  $\rho \leq 0.3$ ,  $p < 0.05$ ). Weak correlations with environmental parameters are most common within MM-flux studies (e.g. Fritsche et al., 2008a; Fritsche et al., 2008b; Bash and Miller, 2009; Converse et al., 2010).

Nevertheless, the REA flux indicated net GEM deposition in the early morning hours and predominant GEM emission from midday until after midnight. The drop in GEM emission in the early afternoon probably indicates compensation of elevated GEM volatilization due to solar radiation, air and soil temperature by uptake of GEM by plants (Fig. 4.4a). GEM dry deposition to the peat surface by foliar uptake has been shown to be the dominant deposition pathway in a peat bog in the French Pyrenees (Enrico et al., 2016). THg content in sedges ( $11 \pm 4.4 \text{ ng g}^{-1}$ ) and moss ( $77 \pm 30 \text{ ng g}^{-1}$ ) vary considerably and the mechanism of atmospheric GEM uptake is still unclear especially for moss due to the absence of stomata. However, an inconsiderable diel pattern of GEM concentrations at 3.5 m was found (Fig. 4.4c). Atmospheric GEM concentrations measured with the DFC setup were  $1.5 \pm 0.3 \text{ ng m}^{-3}$ , and 15% higher compared to REA derived concentrations. This implies the development of a concentration gradient between 0.2 m (DFC measurement) and 3.5 m (REA) a.g.l during sun-light hours (Fig. 4.4c). Atmospheric GEM concentrations at 0.2 m above the surface showed a distinct diel pattern with highest median concentrations between 8 AM and 2 PM. During the DFC measurements a significant positive correlation between atmospheric GEM concentrations and GEM exchange was found ( $\rho = 0.87$  and  $\rho = 0.75$ ,  $p < 0.05$ ), while most studies report negative correlations (reviewed by Agnan et al., 2016).

Estimated current Hg accumulation rates based on THg in the peat profiles and peat growth rates account for  $\sim 4 \mu\text{g m}^{-2} \text{ yr}^{-1}$  and is much lower than average Hg accumulation rates from Pinet bog ( $34 \pm 8 \text{ m}^{-2} \text{ yr}^{-1}$ ) and from other wetlands worldwide ( $25 \mu\text{g m}^{-2} \text{ yr}^{-1}$ ) (Enrico et al., 2016; Amos et al., 2015). In concert with low Hg accumulation rates the flux measurements revealed low GEM dry deposition velocities measured with the TDFC, NDFC and REA of 0.008, 0.012 and  $0.043 \text{ cm s}^{-1}$ , respectively. Median GEM dry deposition velocities were generally lower than in other DFC studies ( $< 0.05 \text{ cm s}^{-1}$ ; Zhang et al., 2009;  $0.1 \text{ cm s}^{-1}$ ; Enrico et al., 2016) and REA studies ( $< 0.2 \text{ cm s}^{-1}$ ; Zhu et al., 2015a). Deposition velocities  $< 0.03 \text{ cm s}^{-1}$  indicates hindered GEM deposition and probably low uptake of GEM by plants (Lee et al., 2000). At Degerö, net dry deposition occurred in 41% (TDFC), 38% (NDFC) and 37% (REA) of the measurement period.

In this perspective, the REA diel flux patterns may reflect coupling with variations in larger scale atmospheric GEM concentrations over the landscape indicated by a maximum rate of change in GEM concentrations of  $0.22 \text{ ng m}^{-3} \text{ h}^{-1}$ . Larger, low-frequency flow patterns, i.e. coherent structures, may cause (opposite flux) differences between DFCs and MM measurement results (Riederer et al., 2014).

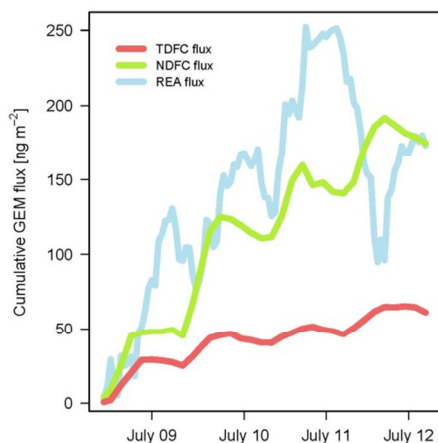


**Figure 4.5:** Time series of the cumulative TDFC, NDFC and REA GEM flux.

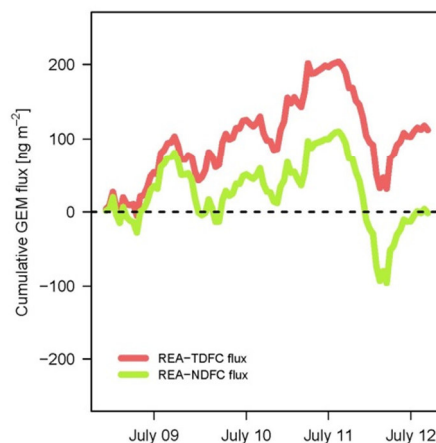


**Figure 4.6:** Time series of the cumulative flux difference between REA and the TDFC and NDFC.

Long-term measurements conducted at the same site in July 2013 designate the short-term REA measurements presented herein representative for summer time GEM emission rates (cf. Chapter 3). There were no other MM-flux studies performed over peatlands with background THg concentrations in the peat of  $< 0.3 \mu\text{g g}^{-1}$ . Globally GEM flux measurements performed over background wetlands ( $n = 23$ ) ranged between  $-4.8$  and  $6.6 \text{ ng m}^{-2} \text{ h}^{-1}$  (Agnan et al., 2016).

DFC fluxes followed a distinct diel pattern during the campaign with the change from GEM emission to net deposition between 17 and 23 PM (Fig. 4.4a). DFC emission peaked between 11:00 and 14:00 and was in concert with daytime peaks of global radiation, air and soil temperature. Besides these main controlling factors on land-atmosphere exchange of GEM other meteorological variables, such as relative humidity, wind speed/turbulence and air Hg and oxidant concentrations, can also affect GEM exchange (Carpi and Lindberg, 1997; Engle et al., 2005; Poissant et al., 1999; Xin and Gustin, 2007). Pearson correlation coefficients showed a significant positive relationship for both DFCs between GEM flux ( $\rho = 0.76$ ,  $p < 0.05$ ) and global radiation, air and soil temperature (correlation coefficients are listed in Tab. 4.1). A strong negative correlation was found with relative humidity.

Even though DFCs operate decoupled from atmospheric conditions and are subject to measurement artifacts due to the perturbed microenvironment enclosed the cumulative fluxes indicated similar source strength from small NDFC ( $0.09 \text{ m}^2$ ) and larger REA footprints ( $11500 \text{ m}^2$ ). The cumulative flux gauged by the TDFC was just 37% of the NDFC and REA fluxes, which summed up to 175 and 173  $\text{ng m}^{-2}$ , respectively (Fig. 4.5). However, the temporal feature of the REA flux reveals different flux pattern, occasionally in reverse directions, reflecting the inherent variability in the turbulent fluxes (Fig. 4.6). Despite this observed flux variability, the mean and magnitude of the REA flux is comparable with the fluxes derived from the NDFC.

This indicates that in contrast to the TDFC, the NDFC flux correction with synchronized surface shear properties seem to bridge discrepancies in the magnitude of fluxes gauged between DFCs and the REA method. However, DFC measurements remain biased by altering temperature and moisture regimes over the footprint and are insensitive to changes in atmospheric conditions that can control the flux (Lai et al., 2012). The application of DFCs is impeded over tall vegetation and limited during precipitation or snow events (Hg wet deposition). Prolonged DFC measurements are also supposed to modify GEM uptake by foliage influencing plant physiology. To assess net annual Hg exchange on an ecosystem scale, heterogeneity in soil surface characteristics has to be addressed with spatially and temporally repeated measurements. In a boreal peatland with a pronounced seasonal climate many DFC measurement campaigns under different meteorological conditions and subsequently high demand for manpower would be necessary to upscale a quantitative flux based on field measurements. To rule out the possibility that means and magnitudes of the REA and NDFC flux were similar by coincidence we suggest prolonged method inter-comparison campaigns. Concurrent measurements with DFCs, REA and other MM-methods under changing environmental conditions are required to define methodological bias and to derive a standard protocol for flux measurements.

## 4.4 Conclusion

In this study we compared quantitative summertime GEM flux exchange over a boreal peatland using a TDFC, NDFC and the novel dual-inlet, single detector REA system during four consecutive days. A method inter-comparison was propitious, because alternate DFC measurements identified the REA footprint as a homogeneous GEM source area independent of small-scale changes in topsoil THg concentration, abundance of vascular plants, water table levels or dissolved gaseous mercury concentrations in the peat pore water. There was good agreement among timely averages of GEM flux derived from the three methods even though variation in the measured fluxes increased (TDFC < NDFC < REA) when taking atmospheric conditions into account. DFC time series showed distinct diel patterns indicating that repetitive 24h measurements are necessary for quantitative flux estimates on an ecosystem scale. The NDFC technique measured cumulative fluxes similar to the turbulent fluxes obtained by REA. This indicates that the NDFC has the potential to bridge the gap in GEM flux magnitude frequently reported between turbulent and enclosure-based measurements and that the novel REA design has improved measurement precision and is not subject to significant flux overestimation any longer (as was concluded by Zhu et al., 2015a). However, to identify landscape-specific GEM sink-source characteristics REA should be favorably applied in long-term measurement campaigns that allow flux time averaging. Caution must be taken in the interpretation of short-term REA fluxes especially during periods when GEM difference in updrafts and downdrafts are small and turbulence is insufficient. For short-term, mechanistic studies DFCs are the favorable tool with the NDFC suitable for quantitative flux estimations over low vegetation.

## Acknowledgements

We thank the Swiss National Foundation (Doc.Mobility fellowship #P1BSP2\_148458) and the Swedish Research Council (SMAREF Multi-project grant #2013-15586-107068-84) for financing this project. We would like to acknowledge the crew of the field-based forest research station in Vindeln for using their research infrastructure and to make meteorological and soil data available. The study was also supported by ICOS Sweden (Integrated Carbon Observatory System) and SITES (Swedish Infrastructure for Ecosystem Science) at Degerö Stormyr, both partly financed by the Swedish Research Council.



## CHAPTER 5

# Evasion of elemental mercury from a boreal peatland suppressed by long-term sulfate addition

*This chapter is published in Environmental Science and Technology Letters:*

J. Fritsche<sup>1</sup>, S. Osterwalder<sup>1\*</sup>, M. B. Nilsson<sup>2</sup>, J. Sagerfors<sup>3</sup>, S. Åkerblom<sup>4</sup>, K. Bishop<sup>4,5</sup> and C. Alewell<sup>1</sup>: Evasion of elemental mercury from a boreal peatland suppressed by long-term sulfate addition.

[1] Department of Environmental Sciences, University of Basel, Basel, Switzerland

[2] Department of Forest Ecology and Management, Swedish University of Agricultural Sciences, Umeå, Sweden

[3] Unit for field-based forest research, Swedish University of Agricultural Sciences, Svartberget Forest Research Station, SE-922 91 Vindeln, Sweden

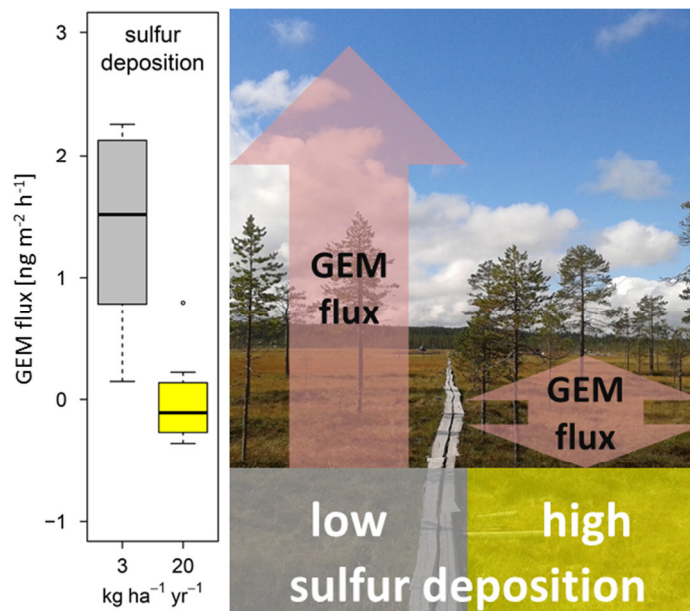
[4] Department of Aquatic Sciences and Assessment, Swedish University of Agricultural Sciences, Uppsala, Sweden

[5] Department of Earth Sciences, University of Uppsala, Uppsala, Sweden

[\*] Corresponding author

## Abstract

We investigated the evasion of gaseous elemental mercury from experimental plots on a boreal peatland that had been exposed for 15 years to different combinations of atmospheric sulfur and nitrogen deposition as well as greenhouse treatments simulating climate change. Shaded dynamic flux chamber measurements during the summer 2009 showed emissions of GEM to the atmosphere from most of the treated plots ( $0.7 \pm 0.9 \text{ ng m}^{-2} \text{ h}^{-1}$ ). However, GEM exchange rates were significantly lower, occasionally indicating Hg uptake, on plots subjected to sulfur addition at rates of  $20 \text{ kg ha}^{-1} \text{ yr}^{-1}$ . Enhanced nitrogen deposition and greenhouse treatment had no significant effect on GEM fluxes. We hypothesize that the lower Hg evasion from the sulfur-treated plots is related to either earlier Hg evasion or Hg binding to sulfur in organic matter, making Hg less susceptible to volatilization and more prone to transport in runoff.



## 5.1 Introduction

Mercury (Hg) pollution is a major concern, with Hg concentrations in freshwater fish often exceeding acceptable levels, especially in high-latitude regions where peatlands are a common landscape element. Peatlands, with their low redox status and high carbon content provide favorable conditions for formation of the more bioavailable methylmercury (MeHg) (St. Louis et al., 1994; Selvendiran et al., 2008) and are thus considered to be a major mediator for the increased levels of Hg in freshwater fish.

Methylation of inorganic Hg to MeHg is strongly enhanced under anaerobic conditions and conducted by Hg-methylating bacteria from several microbial genera but mainly sulfate-reducing bacteria (SRB) when sulfate is in surplus compared to other electron acceptors (Shao et al., 2012; Yu et al., 2012; Gilmour et al., 2013). The reduction of sulfate ( $\text{SO}_4$ ) to  $\text{H}_2\text{S}$  provides an important binding ligand for inorganic Hg (Skylberg et al., 2003; Gabriel and Williamson, 2004; Harmon et al., 2004) and as a byproduct, most likely through co-metabolism, MeHg is formed in quantities dependent on the prevailing level of sulfide (Benoit et al., 1999; Pedrero et al., 2012; Truong et al., 2013). Application of sulfate to wetlands in field and laboratory experiments has verified the linkage between enhanced sulfate deposition and MeHg production (Gilmour et al., 1992; Branfireun et al., 2001; King et al., 2002; Galloway and Branfireun, 2004; Jeremiason et al., 2006; Bergman et al., 2012; Åkerblom et al., 2013).

However, sulfur also affects other processes within the Hg cycle. The reduction of  $\text{Hg}^{2+}$  to  $\text{Hg}^0$ , which evades to the atmosphere, is connected to relatively high redox potentials (redox equilibria at +659 mV [Bisogni, 1989]). This suggests that  $\text{Hg}^{2+}$  reduction is not rivaled by sulfate reducers that are bound to much lower redox potentials ( $\text{Eh} < -221$  mV at pH 7 and 25°C). However, reduced sulfur species, and especially sulfides, effectively bind  $\text{Hg}^{2+}$  by forming stable  $\text{HgS}$  complexes, thus decreasing the size of the  $\text{Hg}^{2+}$  pool available for reduction. Following this line of reasoning, we would expect more Hg complexation in soils that have been exposed to elevated levels of S deposition. In contrast, Åkerblom et al. (2013) have shown that the total Hg stored in the peat layer of experimental plots from the surface down to 40 cm significantly declined in response to elevated levels of sulfur deposition compared to that in neighboring control plots after 12 years (Tab. 5.1).

A variety of factors have been found to influence the emission of Hg from soils such as soil and atmospheric Hg concentrations (Kuiken et al., 2008a; Miller et al., 2011), soil and air temperature (Kim et al., 2012; Moore and Castro, 2012) soil moisture (Xin et al., 2007; Rinklebe et al., 2010) and incident solar radiation (Moore and Carpi, 2005). Several recent studies have determined TGM (total gaseous mercury, which predominantly consists of gaseous elemental mercury, [GEM]) fluxes from wetlands (Munthe et al., 2001). Most of these studies have employed dynamic flux chambers (DFCs) with a focus on key factors influencing Hg emission (During et al., 2009; Kyllönen et al., 2012; and others listed in Sommar et al., 2013a). However, the comparison of fluxes from different studies is often challenging due to the different designs and varying operating procedures (Eckley et al., 2010)

To investigate the hypothesis that GEM evasion is affected by sulfate deposition, we measured GEM flux with a shaded polycarbonate DFC (PDFC) on experimental plots exposed to increased sulfur separately and in combination with two other simulated anthropogenic

influences, increased nitrogen deposition rates and a greenhouse treatment to increase soil and air temperatures.

## 5.2 Methods

The mixed acid peatland of Degerö Stormyr, which covers an area of  $\sim 6.5 \text{ km}^2$  and is located  $\sim 60 \text{ km}$  north of Umeå, Sweden, was our study site. The evasion of GEM was measured on  $2 \times 2 \text{ m}$  plots, arranged in a random, duplicate  $2^3$ -factorial design with ambient and elevated levels of sulfur (S) and nitrogen (N) as well as ambient and elevated temperature simulated using a greenhouse cover (GH). This has been in operation since 1995 to study the effects of S and N deposition as well as temperature on the emission of methane (see Granberg et al., 2001 for a detailed description of the experimental setup). The lower levels of S and N correspond to ambient deposition rates at the site ( $3$  and  $2 \text{ kg ha}^{-1} \text{ yr}^{-1}$ , respectively) while the high levels of  $20 \text{ kg ha}^{-1} \text{ yr}^{-1}$  S and  $30 \text{ kg ha}^{-1} \text{ yr}^{-1}$  N correspond to maximal deposition levels in southern Sweden during the 1980's. N as ammonium nitrate ( $\text{NH}_4\text{NO}_3$ ) and S as sodium sulfate ( $\text{Na}_2\text{SO}_4$ ) are dissolved in  $10 \text{ L}$  of surface water and evenly distributed over the plots with a watering can. Each year one-third is directly applied after snowmelt and the rest is divided into four doses applied at the beginning of every month from June to September. The temperature was increased by covering the plots with perforated plastic sheets during the snow-free period, resulting in a mean increase of daily air temperatures  $25 \text{ cm}$  above the vegetation surface of  $3.6^\circ\text{C}$  and significant soil heating ( $\sim 2^\circ\text{C}$ ) over ambient conditions between May and September (Granberg et al., 2001).

Differences in GEM fluxes between the three main treatments and their two-way and three-way interactions were evaluated by analysis of variance (ANOVA) using R version 2.15.1 (R Core Team, 2011) The level of significance was taken as  $p < 0.05$ .

Between August 14 and 26, 2009, the emission of GEM was measured two times on each plot with a PDFC [ $0.367 \text{ m}$  (length)  $\times$   $0.267 \text{ m}$  (width)  $\times$   $0.195 \text{ m}$  (height)]. The PDFC was shaded to exclude the effect of direct sunlight on GEM emissions. Although sunlight is a major driver of evasion of GEM from soils (Carpi et al., 2007) we minimized the effect of this factor to reveal the influences and interactions of S, N and GH on the exchange of GEM. Ambient air was circulated through the PDFC at a flow rate of  $11 \text{ L min}^{-1}$ . At the inlet and outlet a sub-stream of air was diverted and drawn over a pair of gold cartridges at  $0.5 \text{ L min}^{-1}$  for  $30 \text{ min}$ . The Hg on the gold cartridges was then thermally desorbed and analyzed with a Tekran 2537A mercury vapor analyzer. Fluxes were then derived from Equation 5.1:

$$F_{GEM} = \frac{Q(C_i - C_o)}{A}, \quad (5.1)$$

where  $C_i$  and  $C_o$  designate the inlet and outlet concentrations of GEM,  $Q$  the air flow rate and  $A$  the surface area covered by the PDFC. The sampling lines to the gold cartridges were heated to avoid water condensation and loss of Hg. Passivation of the gold cartridges was checked repeatedly by adding GEM saturated air from a temperature controlled permeation source (Tekran Model 2505, Toronto, Canada) to the sampled air stream. The recovery rate of these standard additions reached  $98.3\%$  and  $99.7\%$ . Thus it was assured that instrumental artifacts did not affect our measurements. PDFC blanks were performed in the field with the PDFC placed on an acid-cleaned Teflon® PTFE film and measured three times for  $1.5 \text{ h}$  before and after, and two times in the middle of the campaign ( $n = 8$ ). The blanks averaged zero and were not subtracted upon calculating of soil fluxes. The air temperature and relative humidity inside

and outside the PDFC were determined simultaneously with the flux measurements using EL-USB-2 Humidity, Temperature and Dew Point Data Loggers (DataQ Instruments, Akron, OH, USA).

## 5.3 Results and Discussion

The emission of GEM from the peatland surface was generally low at all plots [mean =  $0.7 \text{ ng m}^{-2} \text{ h}^{-1}$ , standard deviation (SD) =  $0.9$ ,  $n = 16$ ] compared to earlier published results, most likely because we minimized photoreduction processes by shading the PDFC. Other published GEM flux rates measured over nonpolluted wetland sites remote from major Hg pollution sources (soils with  $< 0.1 \text{ mg Hg kg}^{-1}$ ) using enclosure methods without shading range between  $-1.5$  to  $7.1 \text{ ng m}^{-2} \text{ h}^{-1}$  (Lindberg et al., 2000; Poissant et al., 2004b; Marsik et al., 2005; Kyllönen et al., 2012).

Just a few DFC studies are published using shaded DFCs (Carpi and Lindberg, 1998) or comparing day and night fluxes (Kuiken et al., 2008b; Magarelli and Fostier, 2005; Ericksen et al., 2006). Ericksen et al. (2006) measured GEM fluxes over 46 background soils, including agricultural, grassland, desert and mixed and pine forest ecosystems, across the United States and report significantly elevated GEM emissions in the light compared to dark for all except grassland sites. Most of the dark fluxes ranged from  $-0.1$  to  $2.7 \text{ ng m}^{-2} \text{ h}^{-1}$  and are thus similar in magnitude to the GEM exchange rates at Degerö Stormyr.

A significant ( $p < 0.001$ , ANOVA) reduction in the rate of evasion of GEM from the HighS plots was observed (Fig. 5.1). While the average flux from the LowS plots was  $1.40 \pm 0.78 \text{ ng m}^{-2} \text{ h}^{-1}$ , it was  $-0.01 \pm 0.38 \text{ ng m}^{-2} \text{ h}^{-1}$  from the HighS plots.

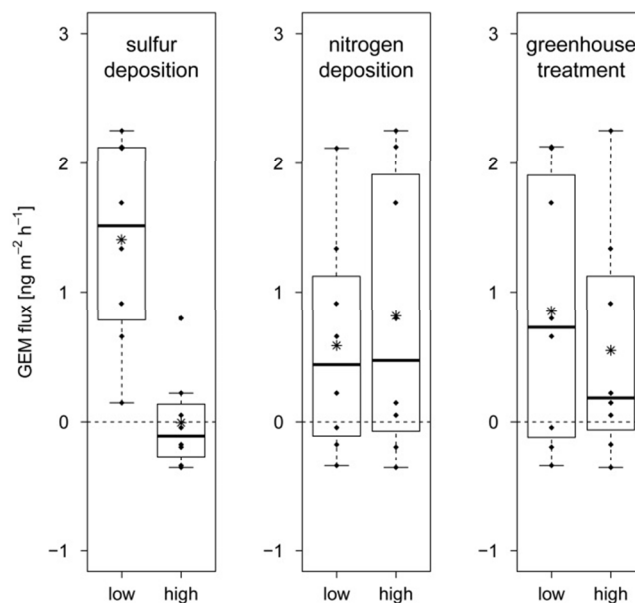


**Figure 5.1:** Effect of S, N and GH treatments on GEM flux at Degerö Stormyr. Low level of sulfur and nitrogen deposition =  $3 \text{ kg S}$  and  $2 \text{ kg N ha}^{-1} \text{ yr}^{-1}$ , respectively. High level of sulfur and nitrogen deposition =  $20 \text{ kg ha}^{-1} \text{ yr}^{-1}$  and  $30 \text{ kg ha}^{-1} \text{ yr}^{-1}$ , respectively.  $n = 8$  for each boxplot, data averaged for each of the runs (one run includes 16 measurements). The upper edge of the box indicates the 75<sup>th</sup> percentile, the lower indicates the 25<sup>th</sup> percentile. Whiskers indicate the 90<sup>th</sup> and 10<sup>th</sup> percentiles, while the line within the box marks the median. Asterisks denote means.

Using a conventionally calculated method detection limit (e.g.  $3 \times \text{SD}$ ; see Eckley et al., 2010), the flux values reported here are technically below detection limit. However, a clear and highly significant HighS treatment effect is revealed by the factorial design. Regardless, absolute flux values presented here should be viewed with caution.

No main treatment effects of N and GH and no two-way or three-way interactions of all three factors were observed. The redox status of the peatland was not monitored during this study. However, at pH 4 the odor of H<sub>2</sub>S being emitted from the HighS plots was clearly perceptible, confirming the presence of reduced S species.

It is tempting to suggest that the observed suppression of the GEM evasion may be entirely attributed to elevated levels of S in the peatland and its ability to form stable Hg complexes that reduce the bioavailability of Hg and prevent evasion of GEM to the atmosphere. However, Åkerblom et al. (2013) reported that the total Hg content in the soil (THg and Hg<sub>inorg</sub> as the mass of Hg per unit dry mass of peat) decreased significantly by 34 % in the S-only plots compared to the control plots and by 14 % in the HighS plots compared to the LowS plots after enhanced S deposition for 12 years (Tab. 5.1). GEM flux and THg in the peat correlate weakly for all plots ( $r_{\text{Spearman}} = 0.24$ ). The amount of S is also larger in the peat of the HighS plots, and highest in the S-only plots.

This indicates that since the experiment began, more THg was lost from the HighS plots, while more S accumulated in these plots. One possibility is that the loss of THg resulted from higher rates of evasion of GEM from the HighS compared to the LowS plots earlier in the experiment when evasion measurements were not being made. This could have lowered the amount of Hg in the peat and contributed to the lower rate of evasion observed in the experiment over a decade after the addition of S began.

A second possible pathway through which Hg could leave the plots is lateral loss via overland flow bound to the S in organic material. We suggest that elevated rates of S deposition increased the number of available Hg-binding sites in peat organic matter because of the increased availability of thiols and polysulfides as has been shown by Skyllberg (2008). This favored the export of complexed Hg species via runoff while also hindering GEM evasion. Additionally, changes in methylation rates of inorganic Hg within the experimental plots could have fundamentally altered its mobility and bioavailability, thereby influencing GEM evasion rates (Boening et al., 2000; Frohne et al., 2012).

Besides solar radiation, air temperature is important and also positively correlated to Hg evasion (Kim et al., 2012), whereas relative humidity is usually negatively correlated to GEM fluxes (Poissant et al., 1998). Fluxes from the HighS and LowS plots showed weak ( $r_{\text{Spearman}}$  range from -0.38 to 0.21) and insignificant correlations with meteorological parameters and inlet air Hg concentrations (Tab. 5.1). Compared to ambient values, relative humidity inside the PDFC was elevated by 11% on average, but no condensation was observed. We conclude that our comparison study was not biased because of changes in weather conditions and that the shading minimized warming of the air inside the PDFC.

This study demonstrates that the long-term addition of S to the peatland surface has significantly reduced the evasion of GEM. This result, together with those of Åkerblom et al. (2013) who showed a reduced store of Hg in the upper 40 cm of the peat (and an increase in S), suggests that the reducing HighS peatland environment not only favors the formation of MeHg, but also alters the long-term balance of Hg inputs and outputs.



**Table 5.1:** Means and standard deviation of GEM flux and inlet air GEM concentrations (GEM inlet) detected on the HighS and LowS plots. Data for the S-only treatment and control plot (without combinations) are given separately. Air temperatures inside the flux polycarbonate dynamic flux chamber ( $T_{PDFC}$ ) and ambient air temperatures ( $T_{air}$ ) and relative humidity (Rh) were measured simultaneously. Total Hg (THg), inorganic Hg ( $Hg_{inorg}$ ) and total sulfur ( $S_{tot}$ ) concentrations in the soil (0 - 40 cm depth) were determined by Åkerblom et al. (2013) in 2007. The pore water pH was published in Bergman et al. (2012) and determined in August 1999.

Sites	GEM flux [ng m <sup>-2</sup> h <sup>-1</sup> ]	GEM inlet [ng m <sup>-3</sup> ]	THg [ng g <sup>-1</sup> ]	$Hg_{inorg}$ [ng g <sup>-1</sup> ]	$S_{tot}$ [μg dm <sup>-3</sup> ]	$T_{PDFC}$ [°C]	$T_{air}$ [°C]	Rh [%]	pH
HighS (n = 16)	-0.01 ± 0.4	1.48 ± 0.16	45.9 ± 12	43.5 ± 11.5	10.3 ± 2.7	20.3 ± 4	20 ± 4.1	65.4 ± 11	4
LowS (n = 16)	1.40 ± 0.8	1.63 ± 0.14	53.1 ± 11	51 ± 11.2	8.3 ± 2.1	22.3 ± 4	20.2 ± 4.5	52.6 ± 8.5	4
S-only (n = 4)	-0.19 ± 0.8	1.51 ± 0.12	38.1 ± 4.1	34.8 ± 3.1	11.7 ± 0.9	16.7 ± 0.8	17.2 ± 1	50.3 ± 3.4	4
control (n = 4)	1.39 ± 2.3	1.7 ± 0.11	57.3 ± 6	56.3 ± 6.1	7.2 ± 2.7	21.6 ± 1.4	18.7 ± 2.5	79.2 ± 6.4	3.9

Until now, two mechanisms that link the S and Hg cycles had been identified in previous studies: first, increased bioavailability of HgS-species enhances the uptake of  $Hg^{2+}$  by sulfate-reducing bacteria (Gilmour et al., 1992) and, second, increased sulfate reduction promotes methylation of  $Hg^{2+}$  (Ranchou-Peyruse et al., 2009). Our study revealed that after 15 years of enhanced S deposition, the rate of GEM evasion is significantly lower likely due to a combination of direct (suppressed evasion) and indirect (loss of Hg from peat) effects, although this experiment cannot offer a definitive mechanistic explanation. To fully understand the net effects of changes in anthropogenic S deposition on the Hg exchange between the atmosphere and peatlands, this single measurement campaign should be complemented by longer-term observations of exchange dynamics from daily to decadal scales. Such observations will be a useful basis for developing a better process understanding of the specific mechanisms that drive these dynamics of which our study has provided a glimpse of.

## Acknowledgements

This work was funded by the Swedish Research Council (#2009-15586-68819-37).



## **CHAPTER 6**

### **Evasion of elemental mercury from contaminated properties in Switzerland**

*In preparation*

S. Osterwalder<sup>1</sup> and C. Alewell<sup>1</sup>: Industrial mercury pollution in the Upper Valais, Switzerland: Evasion of elemental mercury from contaminated properties

[1] Department of Environmental Sciences, University of Basel, Basel, Switzerland

## Abstract

Between 1930 and 1970 a chemical factory located in Visp, Switzerland, discharged waste water polluted with dozens of tons of mercury (Hg) to a nearby canal. The Hg-enriched sediments from the canal contaminated adjacent playgrounds, gardens, and agricultural land. Out of 1277 investigated properties 12% have been found to contain more than 2 mg Hg kg<sup>-1</sup> in the upper 20 cm of the soil and require remediation actions. Gaseous elemental mercury (GEM) can evade from these soils, elevate atmospheric GEM concentrations close to the surface and pose a potential health risk to residents. In order to quantify the amount of Hg mobilized by GEM emission and to estimate the emission potential a new type dynamic flux chamber was used to determine the all-day GEM flux over nine properties with total soil Hg concentrations ranging between < 0.1 and 210 mg kg<sup>-1</sup>. The property averaged GEM flux was between 38 and 1258 ng m<sup>-2</sup> h<sup>-1</sup> and showed a significant relationship with total Hg in the soil ( $r^2 = 77\%$ ,  $p < 0.01$ ). GEM emission was found to enhance average GEM concentrations at a height of 1 m above the properties by a factor ranging from 1.4 to 4.6 compared with background concentrations. To allow better comparability between the sites the dynamic flux chamber was shaded. No distinct diel patterns in GEM flux were found. Annual GEM emissions projected from all properties (8.6 km<sup>2</sup>) amount for 4.5 kg and constitute about 0.5% of the total Hg emissions in Switzerland. The Hg pollution potential in the top 20 cm of the area is ~4900 kg and represents a long-term source of atmospheric Hg. As a result it is recommended to take remediation measures in order to decrease Hg mobilization by GEM emission and subsequent deposition elsewhere. The present atmospheric GEM concentrations are not expected to lead to any medical conditions as a result of chronic inhalation of Hg vapor.

## 6.1 Introduction

Global emissions of gaseous elemental mercury (GEM) from contaminated surfaces are estimated to be approximately 82000 kg. This figure was obtained via modeling of fluxes from more than 3000 point sources including Hg mines and various industrial locations e.g. non-ferrous metal production and precious metal processing facilities (Kocman et al., 2013). Elevated GEM concentrations in the air, in the range of 2 - 4 orders of magnitude, have been reported from mining areas in China (Li et al., 2009). Besides dental fillings, inhalation of GEM in ambient air is perhaps one of the most important sources for human exposure to metallic mercury (Hg) vapor. Acute inhalation of GEM might also occur in laboratories, work places as well as in homes (e.g. broken thermometers and fluorescent lamps). Chronic exposure to lower GEM concentrations induces symptoms from the central nervous system including tremors, delusions, memory loss and neurocognitive disorders (Clarkson and Magos, 2006). Industrially contaminated sites usually emit GEM from small areas, but can pose a strong environmental impact on the surrounding habitats. Industrial locations represent a long-term source of Hg to the air (40% of the total emissions), soil and water if not managed properly (Kocman et al., 2013).

Between 1930 and 1973 a chemical factory owned by Lonza AG in Visp, Switzerland, was regularly releasing Hg as a waste product to the environment. Mercury(II) sulfate was used as a catalyst for the production of acetaldehyde from acetylene and water. The company admitted that during that period about 50 tons of Hg were emitted to the air and another 50 tons were discharged with waste water into the nearby canal, called "Grossgrundkanal". The sediments in the "Grossgrundkanal" have since been dredged regularly to guarantee unhindered water drainage into the river Rhône. Through maintenance work, these contaminated sediments were spread on surrounding lands as well as on sites further away (backfills). As a result, there are more than 100 properties with Hg concentrations above  $2 \text{ mg kg}^{-1}$  which is the threshold above which soil remediation is required (Verordnung über Belastung des Bodens, VBBo, 2016).

These Hg contaminated soils have a high potential to pollute surrounding landscapes via GEM emission and subsequent atmospheric deposition. Based on 3501 soil samples analyzed for THg we aim to derive the total surface-atmosphere GEM exchange over a populated area of  $8.6 \text{ km}^2$  between Visp and Niedergesteln and relate it to contemporary emission rates in Switzerland. This zone makes up 0.02% of the country's land surface area. In order to achieve this, we established levels of GEM emission from nine sites contaminated with a wide range of THg ( $< 0.1 - 210 \text{ mg kg}^{-1}$ ) in the topsoil. In addition, we determined soil characteristics (pH, moisture and temperature) as well as meteorological variables during 24h-GEM flux measurements to define potential controls on GEM flux in addition to the topsoil THg content.

The measurements were implemented to contribute to a more comprehensive series of studies collectively aiming to assess the chronic exposure of the local residents to Hg vapor as a result of the elevated Hg content in the contaminated soil. In addition to our current study, Prof. Pascal Boivin (hepia, Geneva, Switzerland), Prof. Ruben Kretzschmar (ETH Zurich, Switzerland) and Prof. Laurent Charlet (University of Grenoble, France) were investigating the representativeness of the sampling and analysis done by the engineering office Arcadis

Schweiz AG. Their focus was to investigate (i) speciation and mobility of Hg in the soil, (ii) methylation potential in saturated zones, (iii) isolation of Hg hotspots and (iv) spatial and depth heterogeneity of Hg concentrations. The linkage of in-depth investigations of Hg in the atmosphere, soil and water is expected to not only influence remediation strategies but also provide new insights into Hg cycling between soil, water and air at contaminated sites.

## 6.2 Methods

### 6.2.1 Measurement setup

Dynamic flux chambers (DFCs) are suitable for small-scale measurements (Cobos et al., 2002) and site comparison studies (Fritsche et al., 2014), and therefore ideal for the application described herein. Our setup consisted of a flushing unit (Fig. 6.1a) and a detector valve unit (Fig. 6.1b) which could be easily deployed in the field. The measurement setup was very similar to that used in Chapter 4 (Fig. S4.2) with the only difference being that only one DFC was used in this work. The flushing unit (metal box) was placed close to the new type DFC (NDFC) and connected to the detector valve unit with 30 m of Teflon® PFA tubing. Pumps generated a continuous airflow of  $15 \text{ L min}^{-1}$  through the NDFC that is regulated by a mass flow controller.  $1.3 \text{ L air min}^{-1}$  was analyzed for GEM using a Hg detector (Tekran Model 2537A, Toronto, Canada). High-purity Argon was used as a carrier gas. Alternately, GEM concentrations inside and outside the NDFC were determined to calculate the GEM flux (see Eq. 4.4).

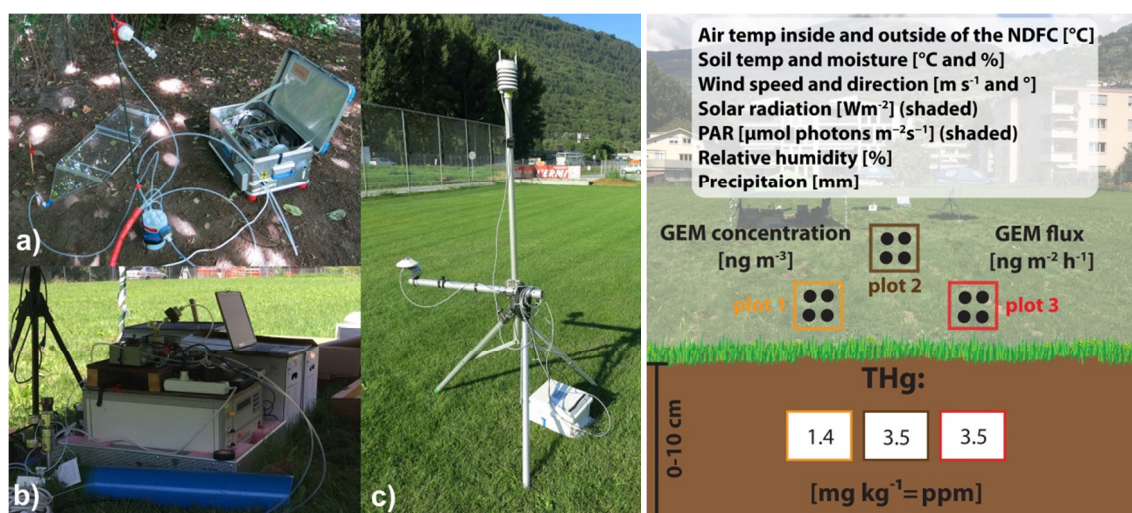


**Figure 6.1:** Flushing unit (metal box), new type DFC and ambient air inlet during measurements on site VS009 (a). Detector valve unit, Ar bottle, laptop, and Teflon® PFA tubing are displayed during measurements on site HK045. A tent protects the equipment from rain and heating by direct solar irradiation (b). The mobile tower equipped with meteorological measuring instruments and logger cabinet at site XX32 (c).

**Figure 6.2:** Illustration of all meteorological and soil parameters measured on every site (example of site HK045). Atmospheric GEM concentration and GEM flux, soil and meteorological parameters were determined simultaneously. THg concentrations within the top 10 cm at plots 1-3 accounted for 1.4, 3.5 and 3.5  $\text{mg kg}^{-1}$ , respectively.

The NDFC is described in Lin et al. (2012) and has been applied by Zhu et al. (2015a) over bare soils in China in 2013 and successfully operated to conduct the study presented in Chapter 4 at Degerö Stormyr in summer 2014. The NDFC is made of polycarbonate and encloses a soil surface of  $0.09 \text{ m}^2$ . The total flowrate through the chamber was  $16.3 \text{ L min}^{-1}$ . The detection limit of the method was derived from NDFC blank measurements ( $n = 204$ ) and averaged  $2.8 \pm 2.4 \text{ ng m}^{-2} \text{ h}^{-1}$ . Blanks were measured before, during and after the campaign over an acid-cleaned Teflon® PTFE film. The instrument detection limit of the Hg detector is  $0.1 \text{ ng m}^{-3}$  which is sufficient to resolve GEM fluxes from background sites.

### 6.2.2 Site description and sampling

GEM fluxes were measured over nine sites, five of which are located in Visp and the remaining four in Raron, Canton Valais, Switzerland. Figure 6.3 shows a map (1:25000) displaying the location of the parcels. Sites VS009 and VS015 were located in the center of Visp (not on the map). The uncontaminated property VS015 ( $< 0.1 \text{ mg THg kg}^{-1}$ ) was chosen as control site.

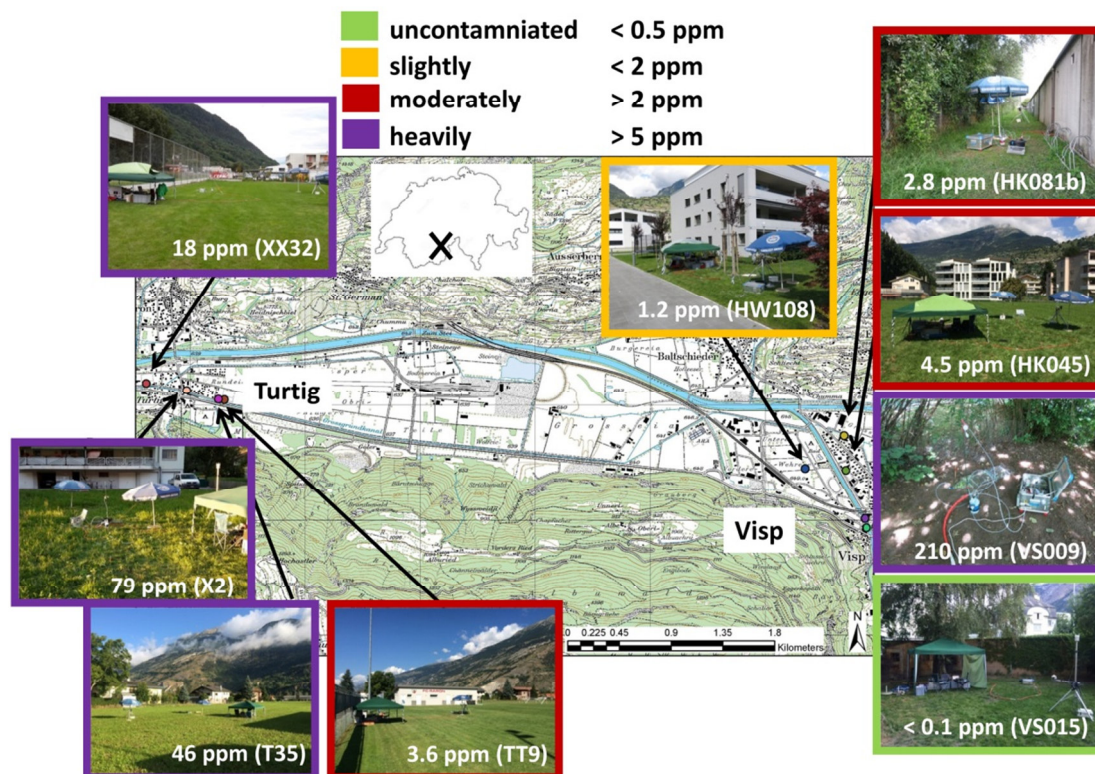


**Figure 6.3:** Selected sites with different THg concentrations in ppm (mixed soil samples from 0 - 20 cm) in Visp and Raron. The pictures of the sites were taken during the GEM flux measurements.

The mixed THg concentration at each site was previously determined by Arcadis Schweiz AG and derived from 16 soil samples (0 - 20 cm). These samples were taken within an area of 10 x 10 m or along a line-transect and analyzed following the protocol defined by the “Verordnung über Belastung des Bodens” (VBBo) using 2M HNO<sub>3</sub> extraction (sieved < 2mm and dried at 40°C for 48h). THg concentrations were below 0.5 ppm (green), between 0.5 and 2 ppm (orange), between 2 - 5 ppm (red) and > 5 ppm (purple). The slightly contaminated property HW108 is registered in the “Kataster der belasten Standorte (KbS)” of the Canton Valais and no remediation action is scheduled. According to the VBBo 0.5 ppm is defined as the reference value (“Richtwert”). For the sites with > 2 ppm THg remediation actions will be enforced because the test value (“Prüfwert”) and remediation value (“Sanierungswert”) were set to 2 ppm in March 2015 (AltIV, Art. 12 Abs. 1).

The study sites were chosen according to THg concentrations in the soil, homogeneous vegetation cover, access permits granted to private properties, line power supply and accessibility (see photo documentation in the Supporting Information to Chapter 6).

The field-campaign lasted for 10 days between August 16 and 29, 2015. Atmospheric GEM concentrations (inlet at 1 m height) and GEM fluxes were measured over three different plots



alternately during a 24h period at each site (Fig. 6.2). Where possible, the plots were located within a 10 m radius. During one day the NDFC was placed 8 times on the same plot for 40 min. Between the measurements, the NDFC was cleaned with ultrapure water (Milli-Q, 18.2 M $\Omega$ -cm, Millipore Corp.) and dried. Simultaneously, air temperature outside the NDFC, relative humidity, wind speed and direction and precipitation were measured with a weather transmitter (Vaisala WXT520, Vantaa, Finland) mounted onto a tower two meters above the surface (Fig. 6.1c). 1 m above the NDFC, in the shade, solar radiation and photosynthetically active radiation (PAR) were measured using a CM11 (Kipp&Zonen, Delft, Netherlands) and a QS5 Quantum Sensor (Delta-T Devices, Cambridge, UK), respectively. Soil temperatures were measured at 2 cm depth with a Campbell Scientific 107 temperature probe and logged every 10 min, in addition to all the other parameters, using a CR1000 (Campbell Scientific, Logan, USA). Soil moisture was determined manually using a ML3 Theta Probe (Delta-T Devices, Cambridge, UK). Air temperature inside the NDFC was logged with two DS1923 iButtons (Maxim Integrated, San Jose, USA). Four soil cores (0 - 10 cm) were taken from each plot after the measurements using a Pürckhauer. The soil was dried at 40°C and sieved (< 2 mm). Analysis of THg in soil samples was done by thermal decomposition (750°C) followed by amalgamation on a gold-trap, thermal desorption, and analysis of vapor Hg by Atomic Absorption Spectroscopy according to EPA method 7473. Certified reference lake sediment material (IAEA SL-1) was used for calibration. Replicate samples and the reference material were analyzed regularly (10% of the sampling sequence) and the precision was under 10% relative standard deviation (SD).

## 6.3 Results and Discussion

Air temperatures during the measurements averaged at 18.9°C and ranged from 8.7 to 33°C. There were only few incidents of precipitation (1.3 L m<sup>-2</sup>) (Fig. 6.5b) and mostly cloudless conditions prevailed. Daily averaged atmospheric GEM concentrations at the sites ranged from 2.2 to 7.3 ng m<sup>-3</sup>. The minimum and maximum recorded values were 1.6 and 20.3 ng m<sup>-3</sup>, respectively. The property averaged GEM fluxes ranged from 38 to 1258 ng m<sup>-2</sup>h<sup>-1</sup> (Tab. 6.1).

**Table 6.1:** Site information and measured GEM fluxes and atmospheric GEM concentrations. Soil THg concentrations (0-10 cm) and mixed samples analyzed by Arcadis AG from 0-20 and 20-40 cm depth are given. The color code is associated to Figure 6.3 and indicates the uncontaminated property (green) and the slightly (yellow), moderately (red) and heavily (purple) contaminated properties.

site	location	zone	land-use	coord x	coord y	GEM [ng m <sup>-3</sup> ]	GEM flux [ng m <sup>-2</sup> h <sup>-1</sup> ]	THg 0-10 [mg kg <sup>-1</sup> ]	THg 0-20 [mg kg <sup>-1</sup> ]	THg 20-40 [mg kg <sup>-1</sup> ]
VS015	Visp South	residential	grassland	634358	126871	2.2	45	0.5	< 0.1	< 0.1
HW108	Visp West	residential	lawn	633348	127450	2.6	38	1	1.2	0.3
HK081b	Visp Kleeg.	residential	lawn	633686	127734	3.5	113	2.7	2.8	14
TT9	Turtig East	sport	soccer field	628300	128045	3.6	100	2.6	3.6	2.6
HK045	Visp Kleeg.	sport	lawn	633703	127435	3.3	237	2.8	4.5	4.8
XX32	Turtig West	public	soccer field	627620	128192	3.3	207	7.5	18	19
T35	Turtig East	residential	grassland	628247	128049	5.2	675	38	46	23
X2	Turtig East	residential	grassland	627977	128141	4.1	174	17	79	8.9
VS009	Visp South	residential	bare soil	634297	126890	7.3	1258	310	210	250

At all of the investigated locations the atmospheric GEM concentrations were found to be directly proportional to the THg concentrations in soil. Generally no significant difference was found for the atmospheric GEM concentrations measured over the 3 different plots at each site (Fig. 6.4a). In the heavily contaminated plots (> 5 mg kg<sup>-1</sup>) the GEM fluxes were found to be two-to-three orders of magnitude higher than at background sites (Fig. 6.4b). Small-scale heterogeneity of soil contamination was reflected at sites TT9 and X2 by substantial variability of GEM flux measured over the 3 plots. Depth and spatial heterogeneity in THg concentrations is primarily due to uneven spreading of the filling material or sediments used as soil improver in gardens (Tab. S6.1). Our THg measurements (0 - 10 cm) from 3 plots at each site allowed the parcels to be classified as slightly (0.5 - 2 mg kg<sup>-1</sup>), moderately (2 - 5 mg kg<sup>-1</sup>) and heavily contaminated (> 5 mg kg<sup>-1</sup>) sites. However, the uncontaminated property (VS015) showed higher THg concentrations and had to be categorized as slightly contaminated and also be listed in the Kataster der belasteten Standorte (KbS).

Diel patterns of the GEM concentration were identified for open sites such as XX32, TT9, T35 and X2. At sites surrounded by buildings and protected from wind no diel variation was recorded (Fig. 6.5a). The highest atmospheric GEM concentrations were found to coincide with stable stratification in the nocturnal boundary layer when wind speeds were low and turbulence and vertical mixing suppressed (Fig. S6.5). Buildup of a convective mixed layer after sunrise (ca. 06:45) and rising wind speeds in the afternoon were responsible for efficient mixing of accumulated GEM in the atmospheric surface layer (Fig. 6.5a).

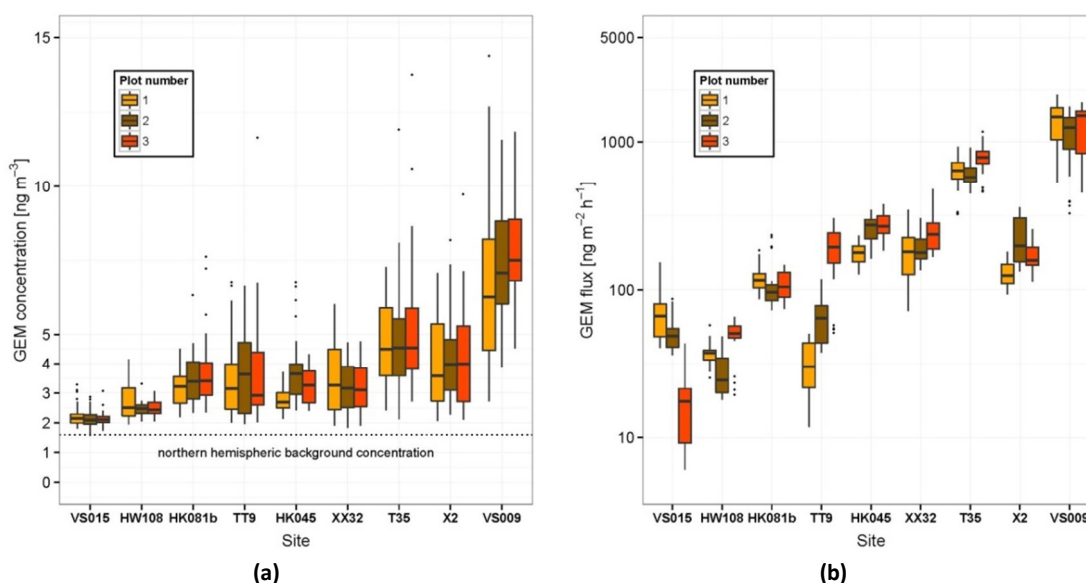


**Figure 6.4:** Atmospheric GEM concentrations (a) and GEM fluxes (b) measured over the plots 1, 2 and 3 (orange, brown, red) at the nine different sites. Boxes contain the middle 50% of the data. The edges of the boxes show the 25<sup>th</sup> and the 75<sup>th</sup> percentiles, respectively. The whiskers indicate 1.5 times the interquartile range. Outliers are given as black dots.

Diel patterns of the GEM flux were not pronounced (Fig. 6.5b), because shading of the NDFC suppressed the photochemical reduction of  $\text{Hg}^{2+}$  to GEM at the soil and vegetation, a process that was reported to be the major drive for GEM evasion (e.g. Moore and Carpi, 2005). However, GEM fluxes during the day increased at some sites (e.g. X2, VS009) (Fig. 6.5b). This is largely due to elevated air and soil temperatures (Engle et al., 2001, Poissant et al., 1999) and increased atmospheric turbulence (Lindberg et al., 1999, Wallschläger et al., 1999) (Figs S6.2, S6.3). At 6 out of 9 sites the plots were temporally shadowed by nearby houses. Therefore, the quantitative GEM flux measurements presented here must be interpreted with caution because blocked solar radiation could lead to reduced flux.

Almost 77% of the variability in observed GEM fluxes ( $\text{ng m}^{-2} \text{h}^{-1}$ ) was explained by soil THg concentration ( $\text{mg kg}^{-1}$ ) (Fig. 6.6). The relationship can be explained by the following linear regression:

$$\log_{GEMflux} = 0.51 \log_{THg} + 1.84 \quad (R^2 = 0.77, p < 0.01) \quad (6.1)$$

Thus, overall soil THg exerted the dominant control on GEM flux and maintained higher GEM emissions even during colder periods of the year. The slope is in the same order of magnitude compared to slopes (0.51 - 0.68) from naturally Hg-enriched sites in the United States (Gustin et al., 2000; Coolbaugh et al., 2002; Zehner et al., 2002) and the slope of 0.43 derived from 381 flux measurements from industrially contaminated, mining, naturally enriched and atmospherically influenced sites worldwide (Agnan et al., 2016). Strong enhancement of GEM emission was repeatedly reported in many other studies from Hg-enriched sites (e.g. Wang et al., 2005). GEM emission rates from contaminated sites worldwide are estimated to be  $8.5 \text{ ng m}^{-2} \text{ h}^{-1}$  (cp. Agnan et al., 2016). These are areas where anthropogenic pollution is indicated and soil THg concentration is larger than  $0.3 \text{ mg kg}^{-1}$ . The GEM fluxes in Visp and

Raron were notably higher and rather comparable to average GEM fluxes from mining sites ( $686 \text{ ng m}^{-2} \text{ h}^{-1}$ ; Agnan et al., 2016).

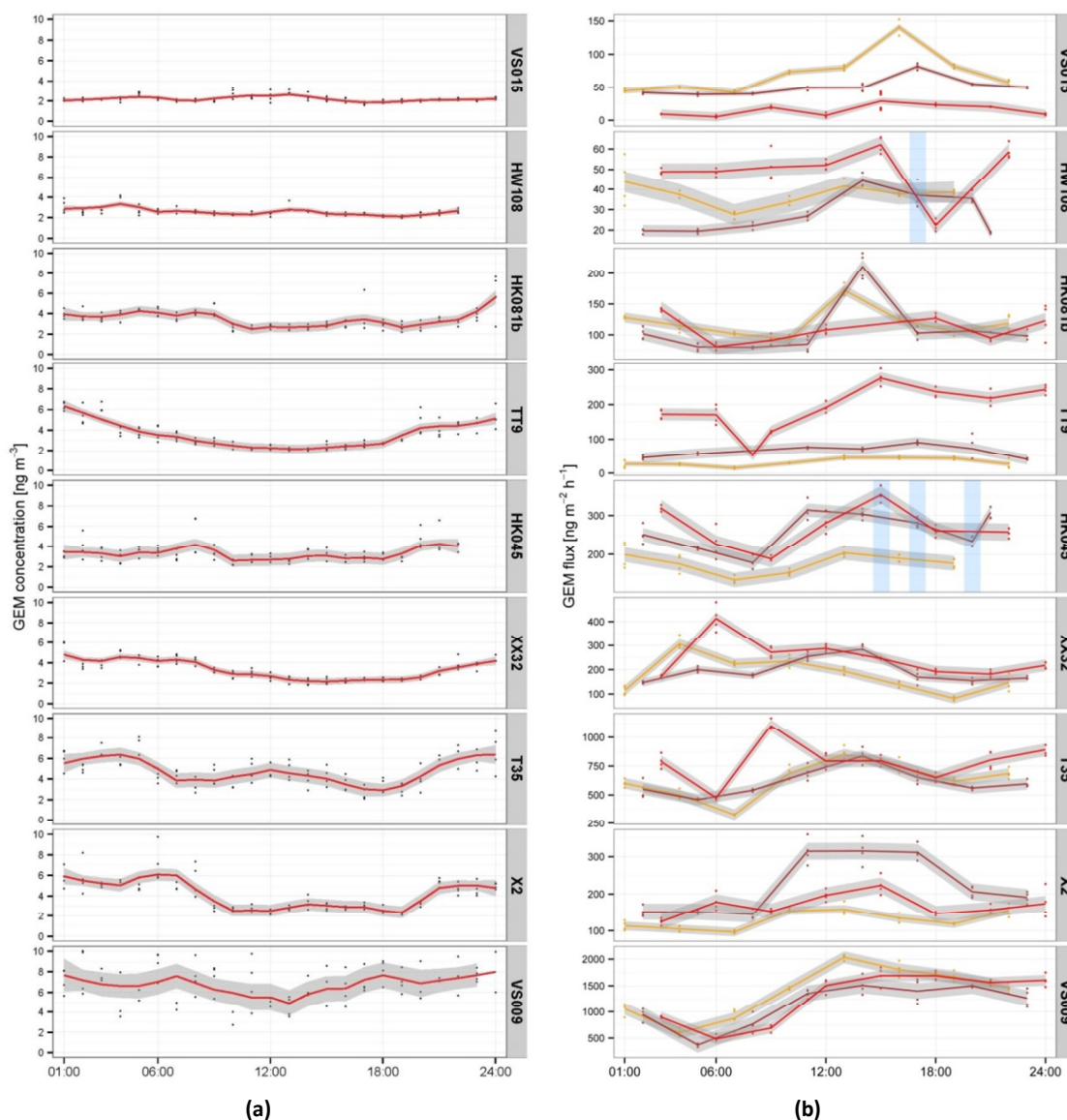


**Figure 6.5:** Diel patterns of atmospheric GEM concentration (a) and GEM flux separated by plots (plot 1 = orange, plot 2 = brown, plot 3 = red) at each site (b). Atmospheric GEM concentrations are not displayed if higher than  $10 \text{ ng m}^{-3}$ . Precipitation events during flux measurements are indicated by blue vertical bars. The smoothing curve shows local polynomial regression fitting (R v3.1.2, loess {stats}, span = 0.3) with a confidence interval of 95% (grey).

Despite attempts to keep the solar radiation constant during the measurements, GEM flux at the site VS015 was significantly higher over plot 1 ( $0.2 \text{ mg THg kg}^{-1}$ ) than over plot 3 ( $0.7 \text{ mg THg kg}^{-1}$ ) (Tab. S6.1). This was also true for site VS009 where GEM evasion over plot 3 was expected to be higher compared to plot 1 due to higher THg concentration. This variability indicates that there are other controlling factors than THg concentration (e.g. pH, soil moisture, soil texture, vegetation cover) influencing the GEM flux on a small scale. For example, soil moisture showed a negative influence on GEM emissions across Hg-enriched sites (Agnan et al., 2016). However, in this study diel patterns were not pronounced enough to

observe any significant correlation (Fig. S6.4). Atmospheric GEM concentrations were also positively correlated to the GEM flux:

$$\log_{GEMflux} = 2.96 \log_{GEMconc} + 0.54 \quad (R^2 = 0.76, p < 0.01) \quad (6.2)$$

This relationship is in contrast to that from background sites where low atmospheric GEM concentrations were found to favor evasion of GEM to the atmosphere (see the discussion on compensation points in Chapter 3). Over the study sites described herein high surface GEM emission lead to the high atmospheric GEM concentrations. A similar relationship between GEM flux and atmospheric GEM concentrations (slope = 0.82, intercept = 0.70) has been found for 262 measurements over Hg-enriched sites (Agnan et al., 2016).

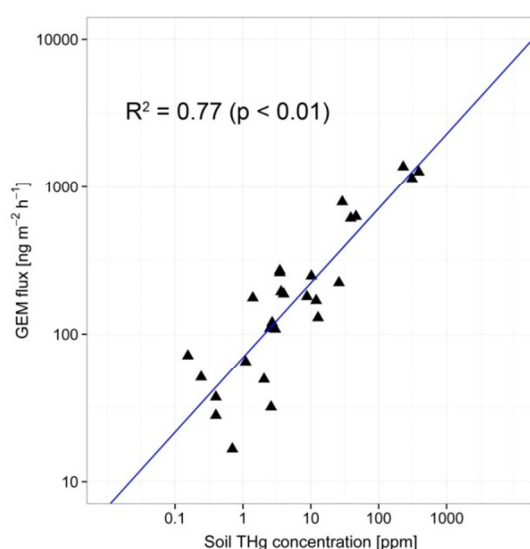


**Figure 6.6:** Log-log-relationship (blue trendline) between daily averaged GEM flux over each plot and soil THg concentrations in the top 10 cm analyzed for each plot (filled triangles black, n = 27).

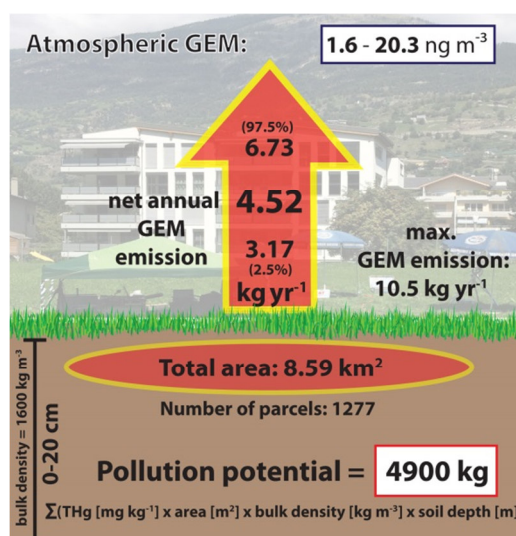


**Figure 6.7:** Upscaling of GEM flux to 1277 parcels located in the canton Valais which cover an area of 8.6 km<sup>2</sup>. The maximal GEM emission is based on the maximum THg found in the soils in every parcel (0 - 20 cm). The 95% confidence level for the annually averaged GEM flux is given within the red emission arrow.

Average atmospheric GEM concentrations over the contaminated parcels were 1.4 to 4.6 times elevated compared to northern hemispheric background concentrations (ca. 1.6 ng m<sup>-3</sup>). These levels are within the range of acceptable outdoor GEM concentrations of 5 - 10 ng m<sup>-3</sup> (WHO, 2000). The daily amount absorbed into the bloodstream of adults as a result of respiratory exposure to 10 ng GEM m<sup>-3</sup> is about 160 ng. The daily Hg intake from dental fillings is about 2000 ng (Olsson and Bergman, 1992). This indicates that the exposure to GEM from outdoor air in Visp and Raron probably have no direct adverse effects on the health of the local residents. However, such conclusions are not based on any substantive information since there is a lack of studies investigating chronic Hg vapor exposure and no clear threshold has been defined. The WHO recommends a guideline value for ambient GEM concentrations of 1000 ng m<sup>-3</sup> (WHO, 2000).

The THg concentrations from 3501 mixed soil samples (0 - 20 cm) taken at 1277 different parcels located in the municipalities Baltschieder, Niedergesteln, Raron, Unterbäch and Visp

were previously analyzed by Arcadis Schweiz AG. Based on Equation 6.1 the net annual GEM emission from the total surface area of 8.59 km<sup>2</sup> was 4.52 kg yr<sup>-1</sup> (Fig. 6.7). The maximum GEM emission of 10.5 kg yr<sup>-1</sup> only reflects evasion from parcels with the highest measured THg concentrations. Around 72.5% of the parcels were categorized as uncontaminated (< 0.5 mg kg<sup>-1</sup>), 15.5% as slightly contaminated (0.5 - 0.2 mg kg<sup>-1</sup>), 5.5 % as moderately contaminated (< 2 - 5 mg kg<sup>-1</sup>) and 6.5% were heavily contaminated (> 5 mg kg<sup>-1</sup>). On average the parcels contained 1.8 mg THg kg<sup>-1</sup> with a maximum THg concentration of 295 mg kg<sup>-1</sup> found in Raron. We found even higher THg values (310 mg kg<sup>-1</sup>) at a parcel in the southern parts of Visp. The Hg pollution potential within the top 20 cm of all the investigated parcels amounted to 4900 kg. At the current GEM emission rates it would take more than 1000 years to deplete the entire soil Hg pool.

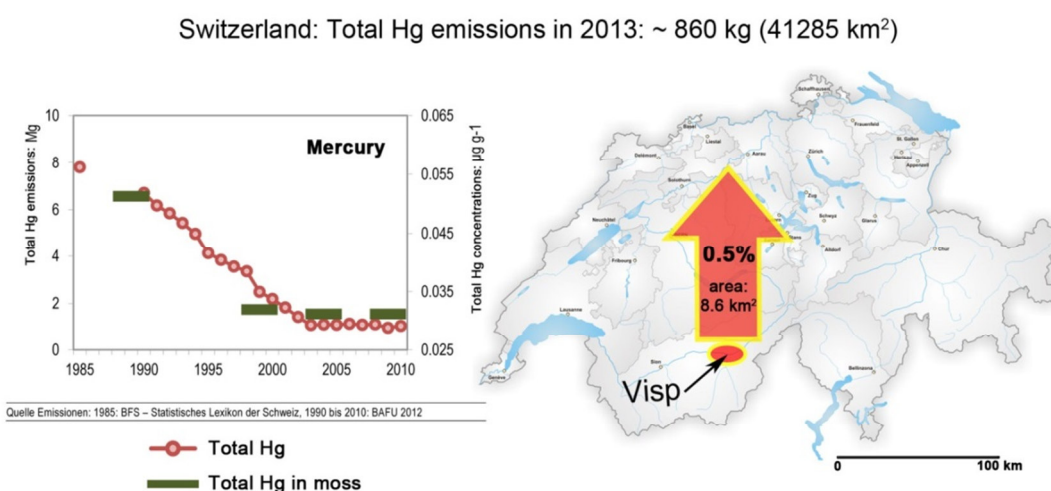


**Figure 6.8:** Median total Hg concentrations in moss (green) compared with modelled Hg emission rates (red) in Switzerland (BAFU, 2013). The map indicates GEM emission from the partially contaminated sites in Visp and surroundings, in the canton of Valais, Switzerland. Map adapted from: [www.weltkarte.com/europa/schweiz.htm](http://www.weltkarte.com/europa/schweiz.htm)

Total Hg emissions in Switzerland decreased significantly from 6570 kg in 1990 to 860 kg in 2013 (Tab. S2). This drop in emissions can be explained by retrofitting the steelworks in the years 1999 and optimization and maintenance of waste incineration plants and crematoria before 2003 (BAFU, 2013; BAFU, 2015). THg concentrations measured in moss have also indicated stable GEM emission rates since 2003 (Fig. 6.8). According to our data GEM emissions from the partly contaminated area (8.6 km<sup>2</sup>) in the Upper Valais account for about 0.5% of the total Hg emissions in Switzerland as estimated by emission inventories (BAFU, 2015). No estimates are available for land-atmosphere emissions of GEM from uncontaminated or contaminated sites in Switzerland, i.e. it is unclear to what degree natural landscapes add to atmospheric GEM emissions.

## 6.4 Conclusion

This study clearly demonstrated that the THg content in the soil was the main factor that drove GEM emission from topsoil ( $r^2 = 0.77$ ). Therefore, flux scaling over the entire partly contaminated area along the Grossgrundkanal, between Visp and Niedergesteln, was possible. The total annual GEM emission rate amounted to  $4.5 \text{ kg yr}^{-1}$  indicating that the studied area is a potential long-term source of Hg to the atmosphere. The GEM fluxes from the highly contaminated properties ( $7.5 - 310 \text{ mg kg}^{-1}$ ) were comparable to the fluxes measured at Hg mining sites worldwide. Accordingly, remediation actions are strongly recommended in order to prevent further GEM emissions to the atmosphere and long-range transboundary air pollution. However, substantial amounts of GEM could be released to the atmosphere during remediation actions. In this context atmospheric GEM concentrations should be monitored before, during and after remediation actions to possibly alert the residents against high Hg vapor exposure. The measured atmospheric GEM concentrations ( $\leq 20.3 \text{ ng m}^{-3}$ ) were clearly below the guidelines given by the World Health Organization ( $1000 \text{ ng m}^{-3}$ ) (WHO, 2000). However, the assessment of chronic toxic effects on local residents remains ambiguous.

## Acknowledgements

This study was financed by the Freiwillige Akademische Gesellschaft (FAG) Basel, the Dienststelle für Umweltschutz (DUS) of the Canton Valais and the Department of Environmental Geosciences, University of Basel. Special thanks go to Prof. Christine Alewell for supporting the project and Jaqueline Riedi for excellent assistance during system preparation and fieldwork. Many thanks go to Dr. Staffan Åkerblom and Prof. Kevin Bishop from the Swedish University of Agricultural Sciences in Uppsala for the THg analysis and Michael Schmutz and Dr. Roland Vogt from the University of Basel's MCR lab for the use of their mobile weather station. I also acknowledge Dr. David Trudel from Arcadis Schweiz AG, and Prof. Daniel Obrist and Dr. Stéphane Westermann from DUS for administrative and scientific support.





# CHAPTER 7

## Overall discussion and outlook

Exchange of gaseous elemental mercury (GEM) between the land and atmosphere is challenging to quantify. As a result flux magnitudes and their confounding factors remain somewhat uncertain. Fluxes from Hg-enriched sites have been the focus of much work. GEM fluxes from weak diffuse sources (i.e. background soils) need to be better quantified to allow global analysis and modelling of the atmospheric Hg budget using data from extensive whole-ecosystem flux studies (Agnan et al., 2016).

The main objective of this study was to provide and assess the first seasonal-scale measurements of GEM exchange from a boreal peatland. In order to achieve this goal we developed a dual-inlet, single detector relaxed eddy accumulation (REA) system. In this chapter we address advantages and disadvantages of the novel REA design in comparison with dynamic flux chamber (DFC) methods, and briefly discuss potential REA applications over forests, oceans as well as a contaminated site. The year-long application of REA revealed that boreal peatlands release significant amounts of Hg to the atmosphere. That has major implications on the future MeHg levels in Nordic freshwater fish and the interpretation of peat Hg records. Furthermore, we suggest that high sulfur deposition during the 1980s suppressed GEM evasion from boreal peatlands and corroborate that even though GEM emission from an industrially polluted site increased the local ambient GEM concentration it did not pose a risk for residents (judged by WHO criteria, 2000).

### 7.1 Assessing the peatland-atmosphere exchange of GEM

The novel dual-inlet single analyzer design of the REA system improved precision compared to the single-inlet, serially open systems (Sommar et al., 2013b; Zhu et al., 2015b). This was achievable due to the synchronous sampling (intermittent conditional sampling introduced flux uncertainty of  $14 \pm 17\%$ ), combined with the regular monitoring of GEM reference gas concentrations and dry Hg-free air (Chapter 2). The basic idea was to separate the updraft and downdraft sampling unit (two pairs of gold cartridges) from the Hg detector. The system was designed to run fully automated with an online user interface that provides comprehensive information about the system performance. Although the REA construction, deployment in the field and maintenance were time consuming, cost intensive and needed specialized expertise, autonomous operation in the field could reduce the required presence of specialized staff in

the future. REA proved suitable not only to measure fluxes over tall canopy sites (e.g. urban areas) where other micrometeorological techniques have frequently been found impracticable (Zhu et al., 2015a), but also for measurements over the open peatland closer to the surface. However, due to the smaller eddies, higher switching frequencies of the fast-response valves applied above the peatland (in 1.8 and 3.5 m height) resulted in small GEM concentration gradients in updrafts and downdrafts (usually about  $0.1 \text{ ng m}^{-3}$ ) that were challenging to resolve. Therefore, flux calculations required strict data rejection criteria (Chapter 2).

Compared to DFCs, the REA method does not disturb the investigated environment and provides an integrated flux over a larger source area. Analysis of turbulence regimes over the urban canopy and the peatland identified a 30 min flux averaging interval as adequate. However, short-term variability in the GEM flux induced by environmental parameters might be overlooked by REA. Only weak correlations between REA and environmental parameters were found during a four-day comparison study with concurrent measurements of two types of dynamic flux chambers (DFCs) (Chapter 4). Direct comparison between REA and DFCs was possible because spatially different peatland surface characteristics within the REA footprint did not significantly influence the flux magnitudes measured by DFCs. The GEM flux derived with the new type DFC (NDFC) was in good agreement with the average (< 5% difference) and cumulative (< 2% difference) REA flux. The NDFC produces a steady and uniform airstream over the enclosed surface and makes the effect of the flushing flow rate on the GEM flux predictable (Lin et al., 2012). In the past the large variability in DFC designs was reported to cause a flux difference by changing flushing flow rates by an order of magnitude (Eckley et al., 2010). With the new design we were not only able to account for the effect of the flushing flow rate, but also to relate the shear parameters over the measured area with the corresponding friction velocity in the atmospheric boundary layer. Therefore measurements using conventional DFCs likely tend to result in an underestimation of the GEM flux (Gustin et al., 1999; Schröder et al., 2005; Zhu et al., 2015a). This seems also to hold for our Teflon® PFA DFC which measured a cumulative flux that was a factor of 3 lower compared to the NDFC. Even though Teflon® is the preferred material due to its full transmission of actinic light, we suggest that the non-uniform airstream over the peat and the comparably high turnover time (an order of magnitude larger compared to the NDFC) led to an underestimation of the quantitative flux. In line with Zhu et al., (2015a) who performed an inter-comparison study using traditional DFCs, NDFC and micrometeorological methods over agricultural fields in China, we conclude that the NDFC has the potential to bridge the gap between flux estimates derived from micrometeorological and enclosure techniques.

Our measurements highlight that efforts to standardize Hg flux measurement techniques, and establish data comparison strategies must be made in order to allow direct comparison of data collected by different research groups, and to properly evaluate ecosystem sink-source characteristics, as a basis for Hg flux scaling. Future applications of DFCs over peatlands with low-standing vegetation are desirable not only in summer, but during the entire snow-free season. Compared to micrometeorological measurements DFC setups are less elaborate, cost-intensive, relatively simple to use, and show better diel variability in the flux measurements. Therefore we agree that DFCs are often the preferred method especially to

determine both small scale heterogeneity in fluxes within land-use types, and confounding factors of soil and soil-surface characteristics.

Our REA system is a valuable step towards the ideal of continuous, long-term applications to derive seasonal patterns and annual totals of GEM exchange from any arbitrary environment. It can also be utilized to fill substantial data gaps in the current GEM flux database in terms of geographical regions and ecosystem type. To achieve better data coverage and subsequently reduce the uncertainty in flux averaging for future applications we suggest the following:

- 1) The REA system should be deployed at sites where concurrent eddy covariance measurements provide CO<sub>2</sub>, sensible or latent heat flux data ideal to derive the REA  $\beta$ -factor.  $\beta$  was typically stable during the campaigns (Basel = 0.49; Degerö = 0.45), but can be highly variable when the corresponding scalar flux is close to zero. Accurate measurements of meteorological parameters such as wind velocity and direction, stability parameters, solar radiation, temperature, humidity, precipitation, and eventually snow depth are indispensable to measure and interpret the GEM flux. The new European Research Infrastructure Consortium, Integrated Carbon Observation System (ICOS ERIC) was established to understand source and sink characteristics of greenhouse gases on an ecosystem scale. These sites would be ideal to apply REA and to answer questions related to the determination of the whole ecosystem GEM flux.
- 2) A combined application of REA together with DFCs, Modified Bowen ration or aerodynamic gradient methods is desirable for creating confidence in flux measurements and for supporting their interpretation. We also recommend a system extension to occasionally measure CO<sub>2</sub> concentrations in updrafts and downdrafts using REA which can then be compared to the flux measured concurrently with an eddy covariance system.
- 3) The regularly performed reference mode measurements to assess potential systematic bias between up-and downdraft sampling lines introduced a reduction in data coverage by about 15%. This could be avoided by implementing an additional valve and changing the software in order to measure GEM in updrafts and downdrafts on every gold cartridge alternately.
- 4) The GEM concentration bias between the REA sampling lines can be corrected for if the maximum standard deviation of the offset is below 0.05 ng m<sup>-3</sup> (Chapter 2). To avoid significant bias of sampling lines the replacement of the Teflon® PTFE valves is necessary to ensure equal airflows through both sampling lines.
- 5) For the application at ICOS sites and eventually on high flux towers, a potential influence of long sampling tubes (30 - 50 m) on the GEM concentration measurements must be tested. A climate controlled environment for the permeation source and the Hg detector are necessary to provide a stable measurement baseline and injections of constant concentration of GEM reference gas.

## 7.2 GEM evasion and implications for boreal ecosystems

Emission of GEM from the peat was more than twofold higher than Hg in wet bulk deposition and indicated that substantial amounts of historically deposited Hg evade to the atmosphere (Chapter 3). Hg loss in catchment discharge, often identified as the major output pathway, was only about 13% of the peatland-atmosphere emission (Fig. 7.2). Generally, forested/vegetated ecosystems are considered as net Hg sinks when accounting for input via wet deposition (Zhu et al., 2016; Eckley et al., 2016). However, Eckley et al. (2016) reported that net Hg emission from sparsely vegetated background ecoregions such as deserts or the Mediterranean California were about 2 and 8 times higher compared to wet deposition, respectively. Changes in climate (e.g. temperature, precipitation), atmospheric chemistry and deposition (e.g. GEM, O<sub>3</sub>, N, S), soil properties (e.g. total Hg (THg), soil moisture), and vegetation cover (e.g. deforestation, farming) are generally regarded as the major factors that collectively determine the Hg sink-source characteristics of soils.

Our measured annual GEM emission rates of 10.2  $\mu\text{g m}^{-2}$  also corroborate the hypothesis that declining atmospheric GEM concentrations in northern Europe crossed a compensation point sometime after 1985, which turned the peat into a source of atmospheric Hg, following its accumulation during the period when the atmospheric GEM concentration was above the compensation point ( $\sim 2.8 \text{ ng m}^{-3}$ , Agnan et al., 2016). This is consistent with Hg depth profiles from Degerö Stormyr that indicate a six-fold decrease in Hg stored in the peat between the 1950s and today. Enrico et al. (2016) suggested that ombrotrophic peatlands record predominantly atmospheric GEM dry deposition ( $\sim 80\%$  of total deposition) and that Hg accumulation rates represent local atmospheric GEM concentrations. It is striking that the modern peat accumulation rates at Degerö Stormyr ( $\sim 4 \mu\text{g m}^{-2} \text{ yr}^{-1}$ ) were more than 8 times lower compared to Pinet peat bog in France ( $34 \mu\text{g m}^{-2} \text{ yr}^{-1}$ ), which was identified as a clear sink for GEM. During the contemporary growing season GEM uptake by plants at Degerö Stormyr was estimated to 4.3  $\mu\text{g m}^{-2}$ , and was in accordance with the Hg accumulation rates derived from the peat cores. GEM plant uptake was calculated assuming THg concentrations in vegetation of 20  $\mu\text{g Hg kg}^{-1}$  (Obrist et al., 2007; Selvendiran et al., 2008; Rydberg et al., 2010), and by using the growing season mean carbon net ecosystem exchange ( $-85 \text{ g C m}^{-2}$ ) measured with eddy covariance from 2001 to 2012 (Peichl et al., 2014). Hence, it is concluded that wet bulk and dry deposition of GEM were of similar magnitude at Degerö Stormyr.

DFC measurements identified solar radiation as well as soil and air temperature ( $\rho > 0.7$ ,  $\rho < 0.05$ ) as the main controlling factors on GEM flux from the peat. This has also been reported by many individual GEM exchange studies from a wide range of terrestrial surfaces (Chapter 1 and reviewed by Agnan et al., 2016). However, lower emission and deposition of GEM has been frequently observed from foliage, possibly facilitated by uptake of GEM through stomata (Zhu et al., 2016). Interestingly, atmospheric GEM concentrations (20 cm height) also revealed a diel pattern during sunny and warm days in the summer indicating GEM accumulation in the air masses close to the surface. Short-term REA flux was only moderately correlated with soil temperature during the method inter-comparison study ( $\rho > 0.5$ ). All the other parameters had little correlation with REA GEM flux ( $\rho < 0.3$ ). The annual REA time series showed little if any linear correlation between environmental parameters and the GEM flux

( $\rho < 0.3$ ). Such low correlations with environmental parameters are common within MM-flux studies (e.g. Fritsche et al., 2008a; Fritsche et al., 2008b; Bash and Miller, 2009), because they show high temporal dynamic variability due to different underlying methodological assumptions and different impacts of meteorological parameters. Zhu et al. (2015a) for instance reported that Pearson correlations between fluxes derived from micrometeorological methods and environmental variables were below 0.5.

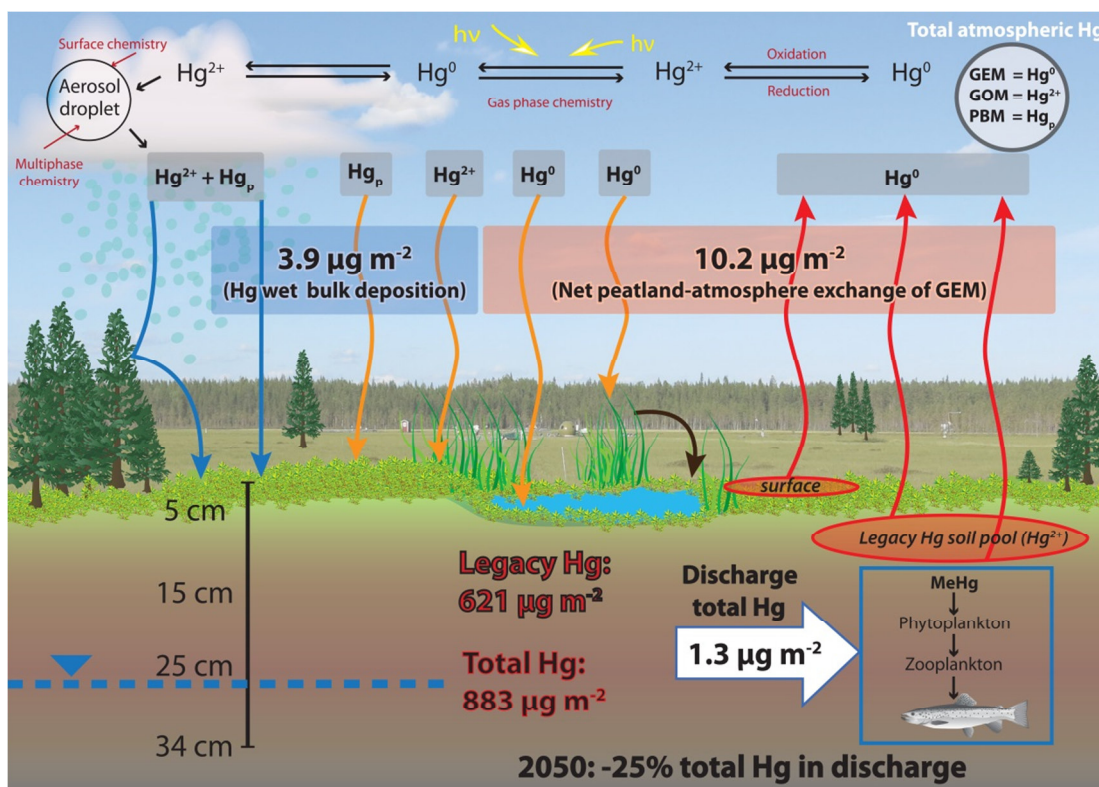


**Figure 7.1:** Synthesis of annual Hg fluxes at Degerö Stormyr a nutrient poor, minerogenic peatland located in northern Sweden. The net GEM peat atmosphere exchange was determined using the relaxed eddy accumulation technique. Total Hg in catchment discharge was measured and wet bulk deposition was derived from close by precipitation samples. Total Hg analysis from eight peat cores allowed the calculation of the Hg pool within the uppermost peat layers (0 - 34 cm). The groundwater level varies between the peat surface and ca. 25 cm depth.

While photochemical mediated reduction of  $\text{Hg}^{2+}$  at the peat surface is hypothesized to be an important driver of GEM evasion at Degerö Stormyr (diel patterns observed in DFC measurements with peaks in the early afternoon) we can only speculate about biotic and abiotic processes that also contribute to  $\text{Hg}^{2+}$  reduction and subsequent  $\text{Hg}^0$  evasion. Recent advances in Hg isotopic fractionation techniques are yielding mechanistic insights into Hg sorption and redox processes. The pioneering study by Jiskra et al. (2015) at a site ca. 10 kilometers from Degerö Stormyr indicated higher mobility of Hg in peat soils than previously anticipated. They reported significant re-emission upon non-photochemical reduction by natural organic matter, accounting for about 50% of the net GEM emission measured with REA at Degerö Stormyr. In addition, they concluded that 30% of the historically deposited Hg was re-emitted to the atmosphere. We stated that oversaturation of the peat pore water with dissolved gaseous elemental Hg relative to atmospheric GEM concentrations creates the

potential for GEM loss during the growing season. The absence of a forest canopy increases photo-reduction processes at the peat surface as well as facilitating diffusion and mass transport across the soil-boundary layer during periods of elevated soil and air temperature, which results in elevated GEM re-emission during summertime.

A significant decrease in atmospheric sulfur deposition of about 85% since the 1980s has potentially also been identified as a factor influencing GEM exchange from peatlands (Chapter 5). Today, such elevated sulfur deposition rates ( $20 \text{ kg ha yr}^{-1}$ ) would suppress GEM emission due to elevated Hg binding to sulfur associated with organic matter making Hg less susceptible to volatilization and more prone to transport in catchment run-off.

Under the assumption that the observed levels of GEM emission remain constant such that no significant change occurs in the wet bulk deposition, discharge, and growing season water balance, it would take about 80 years to deplete the Hg pool down to 34 cm (dated to ca. 1945), leaving background concentration in the peat of  $20 \text{ ng THg g}^{-1}$ . Since THg in runoff from boreal forest soils is suggested to be dominated by Hg from the organic topsoil (60 - 85%) (Jiskra, 2014; Eklöf et al., 2015), this could also hold for the top peat layers at Degerö Stormyr, where the major part of the historically deposited Hg is stored. Bergman et al. (2012) also found that peat pore water concentrations just below the groundwater surface (often 5 - 15 cm depth) were similar to runoff concentrations during the snow free months of 2000.

Our findings about the substantial GEM emission from a boreal peatland to the atmosphere have several important implications particularly for the future levels of MeHg in Nordic freshwater fish and interpretation of peat Hg records for estimating historical Hg accumulation rates: In Sweden the median Hg concentration of fish from all species and sizes was  $0.7 \text{ mg kg}^{-1}$  wet weight and exceeded the EU Environmental Quality Standard of  $0.02 \text{ mg kg}^{-1}$  in all waters. The FAO/WHO guideline for Hg levels in fish used for human consumption is  $0.5 - 1 \text{ mg kg}^{-1}$  was exceeded in fish from half of the Swedish waters after 2000 (Åkerblom et al., 2014). Decreasing trends in fish Hg concentrations (-20%) during recent decades could result from both reduced Hg wet bulk deposition inputs of about 16% since 1990 (EMEP, 2013) and/or decreasing inputs of MeHg to freshwater lakes from peatlands. We speculate that until 2050 THg concentrations in peatland discharge will decline by about 25% assuming that current peatland-atmosphere exchange of GEM remains the same and that 80% of the THg in discharge originates from the uppermost peat layers (Jiskra, 2014). We hypothesize that this decline also holds for MeHg which usually accounts for < 5% of the THg in wetland discharge (Shanley and Bishop, 2012), even though THg and MeHg concentration dynamics in stream flow are not always correlated (Porvari and Verta, 2003; Eklöf et al., 2012). Reduced sulfur deposition to the peat has not only increased GEM emission, but has also been demonstrated to decrease methylation rates and subsequently the loading of MeHg to surface waters (Drevnick et al., 2007)

However, there is a complex interplay of many other factors that may influence GEM surface-air exchange, and THg and MeHg outputs from peatland catchments in the near future. Climate change can influence both ground water levels and changes in carbon pools in the soil. Factors that reduce the C pool will increase the output of legacy Hg via GEM emission and reduce the ability to retain new inputs (Shanley and Bishop, 2012). Predictions of future

Hg cycling in peatlands, namely GEM emission and MeHg export, depend on both process-based assessments in the soil and measurements of GEM exchange at the surface.

Since peatlands are neither static environments nor similar from one location to another, GEM exchange patterns might be expected to vary from year-to-year at the same location and between nearby sites if the example of net carbon balance is a guide. Many environmental parameters (e.g. climate, soil properties, land-use change) influence vegetation type, plant composition and plant growth, all of which can influence net deposition and sequestration of Hg. For instance, Rydberg et al. (2010) found that at the same study site peat and sphagnum mosses had higher (100% and 71% higher for peat and plants, respectively) Hg content in the pine-covered area compared to the open area. Peat decomposition, changes in carbon accumulation and carbon loss can differ considerably at the same peatland from year to year (Peichl et al., 2014, Leach et al., 2016) and between peatlands in the boreal zone (Turunen et al., 2002, Loisel et al., 2014). Net carbon ecosystem exchange and loss of carbon in catchment discharge at Degerö Stormyr was measured from 2003 to 2012. The stream carbon export accounted for 25 to 90% of the annual net ecosystem exchange that varied between -18 and -105 g C m<sup>-2</sup> yr<sup>-1</sup> for the respective period (Peichl et al., 2014, Leach et al., 2016). These changing conditions in time and space indicate that annual GEM flux estimates could also differ considerably among years.

Changes in peat Hg sequestration and losses over time may have the potential to alter the signal from atmospheric Hg deposition. The peat archive may also be susceptible to overprinting by Hg<sup>2+</sup> reduction and subsequent GEM emissions to the atmosphere (Jiskra et al., 2015). Potential losses must be carefully considered for Hg and other elements that can evade (Pb, Sb, As and Se) when interpreting historical and present accumulation rates (cf. Vriens et al., 2014). As for example stated by Biester et al. (2007) and Jiskra et al. (2015), GEM emission provides an alternative explanation for discrepancies between peat and lake sediment archives in the ratio of Hg accumulation rates from preindustrial to modern times (Amos et al., 2015). In line with Jiskra et al. (2015) our results indicate limitations in the coupling of Hg to C as used in global Hg models.

## 7.3 Forests, oceans and contaminated sites: the future of REA

Forests introduce the largest uncertainty in global terrestrial GEM flux estimations (-727 - 703 Mg yr<sup>-1</sup>; range of 37.5<sup>th</sup> and 62.5<sup>th</sup> %, Agnan et al., 2016). Mainly because the contribution from leaf-atmosphere exchanges is largely undefined and whole-ecosystem forest flux measurements over the canopy soils are very scarce. The main advantage of REA over the other micrometeorological methods used for GEM flux estimations is that it requires sampling at only one height resulting in a clearly defined source area, thus substantially reducing some sources of uncertainty. Therefore REA is appropriate for measurements over the forest canopy, even though processes within the forest canopy create the possibility for GEM storage and advection events (Zhu et al., 2016). To account for these in getting a forest-atmosphere GEM exchange value may require larger footprints above the canopy than are feasible.

ICOS ERIC offer excellent conditions for long-term REA GEM measurements. Two potential forest sites for such measurements are a mixed boreal forest (60% *Pinus sylvestris* and 40% *Picea abies*) at the Svartberget experimental forest in Vindeln, Sweden or over a subalpine coniferous forest dominated by *Picea abies* at Davos-Seehornwald, Switzerland. GEM gradient measurements within the canopy would be useful complement to REA in trying to define the true forest-atmosphere exchange, though no feasible path to a complete solution is yet clear.

GEM emission from ocean surface waters are estimated to be in the same order of magnitude as wet deposition input (Fig. 1.1). The annual water-atmosphere exchange of Hg in the Baltic Sea was  $9.5 \mu\text{g m}^{-2}$ , and balanced the input by wet deposition (Wängberg et al., 2001). These estimates are largely based on flux calculations derived from dissolved gaseous Hg and atmospheric GEM data based on Henry's law. We plan to compare these measurements with the first REA derived GEM ocean-atmosphere fluxes. The study could be performed at the ICOS station Östergarnsholm, which is situated 4 km east of Herrvik on the east coast of Gotland, Sweden.

Industrially contaminated properties in the canton Valais, Switzerland, have been shown to increase atmospheric GEM concentrations up to 14 times compared to background concentrations (Chapter 5). The annual GEM emission rate from an area of  $8.6 \text{ km}^2$  (0.02% of the country's land surface) is estimated to increase total Hg emissions in Switzerland by 0.5% and designates the area as a potential long-term source of Hg to adjacent landscapes and beyond. The REA system might also be deployed on a tower high up over the entire valley to record the spatial GEM flux signal, downwind of the contaminated area. Measurement campaigns during remediation actions would be particularly useful to estimate the amount of Hg mobilized by GEM emission.



## References

- Agnan, Y., Le Dantec, T., Moore, C. W., Edwards, G. C. and Obrist, D.: New constraints on terrestrial surface-atmosphere fluxes of gaseous elemental mercury using a global database, *Environ. Sci. Technol.*, 50, 507-524, 2016.
- Åkerblom, S., Bishop, K., Björn, E., Lambertsson, L., Eriksson, T. and Nilsson, M. B.: Significant interaction effects from sulfate deposition and climate on sulfur concentrations constitute major controls on methylmercury production in peatlands, *Geochim. Cosmochim. Ac.*, 102, 1-11, 2013.
- Åkerblom, S., Bignert, A., Meili, M., Sonesten, L. and Sundbom, M.: Half a century of changing mercury levels in Swedish freshwater fish, *Ambio*, 43, 91-103, 2014.
- Alberts, J. J., Schindler, J. E., Miller, R. W. and Nutter, D. E.: Elemental mercury evolution mediated by humic acid, *Science*, 184, 895-897, 1974.
- Aldén, M., Edner, H., and Svanberg, S.: Remote measurement of atmospheric mercury using differential absorption lidar, *Optics Letters*, 7, 221-223, 1982.
- Alexandersson, H., Karlström, C. and Larsson-McCann, S.: Temperaturen och nederbörden i Sverige 1961-1990, The Swedish Meteorological and Hydrological Institute, Norrköping, Sweden, 1991.
- Ammann, C.: On the applicability of Relaxed Eddy Accumulation and Common Methods for Measuring Trace Gas Fluxes, Ph.D. thesis, ETH Zürich, Switzerland, 229 pp., 1999.
- Ammann, C. and Meixner, F. X.: Stability dependence of the relaxed eddy accumulation coefficient for various scalar quantities, *J. Geophys. Res.*, 107, ACL7-1, 2002.
- Amos, H. M., Jacob, D. J., Streets, D. G. and Sunderland, E. M.: Legacy impacts of all-time anthropogenic emissions on the global mercury cycle, *Glob. Biogeochem. Cycles*, 27, 410-421, 2013.
- Amos, H. M., Sonke, J. E., Obrist, D., Robins, N., Hagan, N., Horowitz, H. M., Mason, R. P., Witt, M., Hedgecock, I. M., Corbitt, E. S. and Sunderland, E. M.: Observational and Modeling Constraints on Global Anthropogenic Enrichment of Mercury, *Environ. Sci. Technol.*, 49, 4036-4047, 2015.
- Amyot, M., McQueen, D. J., Mierle, G. and Lean, D. R. S.: Sunlight-induced formation of dissolved gaseous mercury in lake waters, *Environ. Sci. Technol.*, 28, 2366-2371, 1994.
- Ariya, P. A., Amyot, M., Dastoor, A., Deeds, D., Feinberg, A., Kos, G., Poulain, A., Ryjkov, A., Semeniuk, K., Subir, M. and Toyota, K.: Mercury Physicochemical and Biogeochemical Transformation in the Atmosphere and at Atmospheric Interfaces: A Review and Future Directions. *Chem. Rev.*, doi:10.1021/cr500667e, 2015.
- Arnts, R. R., Mowry, F. L. and Hampton, G. A.: A high-frequency response relaxed eddy accumulation flux measurement system for sampling short-lived biogenic volatile organic compounds, *J. Geophys. Res.-Atmos.*, 118, 4860-4873, 2013.
- BAFU: Deposition von Luftschadstoffen in der Schweiz. Moosanalysen 1990-2010, available at: <http://www.bafu.admin.ch/uz-1328-d> [last access: 31 March 2016], 2013.
- BAFU: Switzerland's Informative Inventory Report 2015. Submission under the UNECE Convention on Long-range Transboundary Air Pollution to the UNECE Secretariat, available at: <http://www.bafu.admin.ch/luft/11017/11024/11592/index.html?lang=de> [last access: 31 March 2016], 2015.
- Baker, J. M., Norman, J. M. and Bland, W. L.: Field-scale application of flux measurement by conditional sampling, *Agric. Forest Meteorol.*, 62, 31-52, 1992.

## References

---

- Baldocchi, D., Falge, E., Gu, L. H., Olson, R., Hollinger, D., Running, S., Anthoni, P., Bernhofer, C., Davis, K., Evans, R., Fuentes, J., Goldstein, A., Katul, G., Law, B., Lee, X. H., Malhi, Y., Meyers, T., Munger, W., Oechel, W., U, K., Pilegaard, K., Schmid, H. P., Valentini, R., Verma, S., Vesala, T., Wilson, K. and Wofsy, S.: FLUXNET: A new tool to study the temporal and spatial variability of ecosystem-scale carbon dioxide, water vapor, and energy flux densities, *Bull. Amer. Meteorol. Soc.*, **82**, 2415-2434, 2001.
- Barkay, T., Miller, S. M. and Summers, A. O.: Bacterial mercury resistance from atoms to ecosystems. *FEMS, Microbiology Reviews*, **27**, 355-384, 2003.
- Bash, J. O. and Miller, D. R.: A note on elevated total gaseous mercury concentrations downwind from an agriculture field during tilling, *Sci. Total Environ.*, **388**, 379-388, 2007.
- Bash, J. O. and Miller, D. R.: A relaxed eddy accumulation system for measuring surface fluxes of total gaseous mercury, *J. Atmos. Ocean. Tech.*, **25**, 244-257, 2008.
- Bash, J. O. and Miller, D. R.: Growing season total gaseous mercury (TGM) flux measurements over an *Acer rubrum* L. stand, *Atmos. Environ.*, **43**, 5953-5961, 2009.
- Bauer, D., Campuzano-Jost, P. and Hynes, A. J.: Rapid, ultrasensitive detection of gas phase elemental mercury under atmospheric conditions using sequential two-photon laser induced fluorescence, *J. Environ. Monitor.*, **4**, 339-343, 2002.
- Baya, A. P. and Van Heyst, B.: Assessing the trends and effects of environmental parameters on the behaviour of mercury in the lower atmosphere over cropped land over four seasons, *Atmos. Chem. Phys.*, **10**, 8617-8628, 2010.
- Benoit, J. M., Gilmour, C. C., Mason, R. P. and Heyes, A.: Sulfide controls on mercury speciation and bioavailability to methylating bacteria in sediment pore waters, *Environ. Sci. Technol.*, **33**, 951-957, 1999.
- Bergman, I., Bishop, K., Tu, Q., Frech, W., Åkerblom, S. and Nilsson, M.: The Influence of Sulfate Deposition on the Seasonal Variation of Peat Pore Water Methyl Hg in a Boreal Mire, *PLoS One*, **7**, e45547, 2012.
- Bergquist, B. A. and Blum, J.D.: Mass-dependent and -independent fractionation of Hg isotopes by photoreduction in aquatic systems, *Science*, **318**, 417-420, 2007.
- Bieser, J., Volker, M., Aulinger, A., Greyer, B., Hedgecock, I., De Simone, F., Gencarelli, C. and Travníkov, O.: Impact of Mercury Chemistry on Regional Concentration and Deposition Patterns, in: *Air Pollution Modeling and its Application*, edited by: Steyn, D., Mathur, R., Springer, 189-195, 2012.
- Biester, H., Keppler, F., Putschew, A., Martínez-Cortizas, A. and Petri, M.: Halogen Retention, Organohalogens and the Role of Organic Matter Decomposition on Halogen Enrichment in Two Chilean Peat bogs, *Environ. Sci. Technol.*, **38**, 1984 - 1991, 2004.
- Biester, H., Bindler, R., Martínez-Cortizas, A. and Engstrom, D.R.: Modeling the past atmospheric deposition of mercury using natural archives, *Environ. Sci. Technol.*, **41**, 4851-4860, 2007.
- Biester, H., Hermanns, Y.-M. and Martínez-Cortizas, A.: The influence of organic matter decay on the distribution of major and trace elements in ombrotrophic mires – a case study from the Harz Mountains, *Geochim. Cosmochim. Acta*, doi:10.1016/j.gca.2012.01.003, 2012.
- Bindler, R.: Mired in the past - looking to the future: Geochemistry of peat and the analysis of past environmental changes, *Glob. Planet. Change*, **53**, 209-221, 2006.
- Bisogni, J. J.: Using mercury volatility to measure redox potential in oxic aqueous systems, *Environ. Sci. Technol.*, **23**, 828-831, 1989.
- Boening, D. W.: Ecological effects, transport, and fate of mercury: a general review, *Chemosphere*, **40**, 1335-1351, 2000.

- Branfireun, B. A., Bishop, K., Roulet, N. T., Granberg, G. and Nilsson, M.: Mercury cycling in boreal ecosystems: The long-term effect of acid rain constituents on peatland pore water methylmercury concentrations, *Geophys. Res. Lett.*, 28, 1227-1230, 2001.
- Brunke, E.-G., Labuschagne, C., Ebinghaus, R., Kock, H. H. and Slemr, F.: Gaseous elemental mercury depletion events observed at Cape Point during 2007-2008, *Atmos. Chem. Phys.* 10, 1121-1131, 2010.
- Brut, A., Legain, D., Durand, P. and Laville, P.: A relaxed eddy accumulator for surface flux measurements on ground-based platforms and aboard research vessels, *J. Atmos. Ocean. Tech.*, 21, 411-427, 2004.
- Businger, J. and Oncley, S.: Flux Measurement with Conditional Sampling, *J. Atmos. Ocean. Tech.* 7, 349-352, 1990.
- Carpi, A. and Lindberg, S.E.: Sunlight-mediated emission of elemental mercury from soil amended with municipal sewage sludge, *Environ. Sci. Technol.*, 31, 2085-2091, 1997.
- Carpi, A. and Lindberg, S. E.: Application of a Teflon (TM) dynamic flux chamber for quantifying soil mercury flux: Tests and results over background soil, *Atmos. Environ.*, 32, 873-882, 1998.
- Carpi, A., Frei, A., Cocris, D., McCloskey, R., Contreras, E. and Ferguson, K.: Analytical artifacts produced by a polycarbonate chamber compared to a Teflon chamber for measuring surface mercury fluxes, *Anal. Bioanal. Chem.*, 388, 361-365, 2007.
- Castro, M. S., Moore, C., Sherwell, J., and Brooks, S. B.: Dry deposition of gaseous oxidized mercury in Western Maryland, *Sci. Total Environ.*, 417, 232-240, 2012.
- Chalmers, A. T., Argue, D. M., Gay, D. A., Brigham, M. E., Schmitt, C. J. and Lorenz, D. L.: Mercury trends in fish from rivers and lakes in the United States, 1969-2005, *Environ. Monit. Assess.*, 175, 175-191, 2011.
- Charman, D. J.: Peat and Peatlands, in *Encyclopedia of Inland Waters*, edited by: Likens G. E., Academic Press, 541-548, 2009.
- Choi, H.-D. and Holsen, T. M.: Gaseous mercury fluxes from the forest floor of the Adirondacks, *Environ. Pollut.*, 157, 592-600, 2009.
- Clarkson T. W. and Magos, L.: The toxicology of mercury and its chemical compounds, *Crit. Rev. Toxicol.*, 36, 609-62, 2006.
- Cobos, D. R., Baker, J. M., and Nater, E. A.: Conditional sampling for measuring mercury vapor fluxes, *Atmos. Environ.*, 36, 4309-4321, 2002.
- Converse, A. D., Riscassi, A. L., and Scanlon, T. M.: Seasonal variability in gaseous mercury fluxes measured in a high-elevation meadow, *Atmos. Environ.*, 44, 2176-2185, 2010.
- Coolbaugh, M., Gustin, M. S. and Rytuba, J.: Annual emissions of mercury to the atmosphere from natural sources in Nevada and California, *Environ. Geol.*, 42, 338-349, 2002.
- Corbitt, E. S., Jacob, D. J., Holmes, C. D., Streets, D. G. and Sunderland, E. M.: Global source-receptor relationships for mercury deposition under present-day and 2050 emissions scenarios, *Environ. Sci. Technol.*, 45, 10477-10484, 2011.
- Cui, L., Feng, X., Lin, C.-J., Wang, X., Meng, B., Wang, X., Wang, H.: Accumulation and Translocation of (198) Hg in Four Crop Species. *Environ. Toxicol. Chem.* 33, 334-340, 2014.
- Demers, J. D., Driscoll, C. T., Fahey, T. J. and Yavitt, J. B.: Mercury cycling in litter and soil in different forest types in the Adirondack region, New York, USA, *Ecol. Appl.*, 17, 1341-1351, 2007.

## References

---

- Denkenberger, J. S., Driscoll, C. T., Branfireun, B. A., Eckley, C. S., Cohen, M. and Selvendiran, P.: A synthesis of rates and controls on elemental mercury evasion in the Great Lakes Basin, *Environ. Pollut.*, 161, 291-298, 2012.
- Desjardins, R. L.: Energy budget by an eddy correlation method, *J. Appl. Meteorol.*, 16, 248-250, 1977.
- Drevnick, P. E., Canfield, D. E., Gorski, P. R., Shinneman, A. L. C., Engstrom, D. R., Muir, D. C. G., Smith, G. R., Garrison, P. J., Cleckner, L. B., Hurley, J. P., Noble, R. B., Otter, R. R. and Oris, J. T.: Deposition and cycling of sulfur controls mercury accumulation in isle Royale fish, *Environ. Sci. Technol.*, 41, 7266-7272, 2007.
- Driscoll, C. T., Holsapple, J., Schofield, C. L. and Munson, R.: The chemistry and transport of mercury in a small wetland in the Adirondack region of New York, USA, *Biogeochemistry* 40, 137-146, 1998.
- Driscoll, C. T., Mason, R. P., Chan, H. M., Jacob, D. J. and Pirrone, N.: Mercury as a Global Pollutant: Sources, Pathways, and Effects, *Environ. Sci. Technol.*, 47, 4967-4983, 2013.
- During, A., Rinklebe, J., Boehme, F., Wennrich, R., Staerk, H.-J., Mothes, S., Du Laing, G., Schulz, E. and Neue, H.-U.: Mercury Volatilization from Three Floodplain Soils at the Central Elbe River, Germany, *Soil. Sediment. Contam.*, 18, 429-444, 2009.
- Eckley, C. S. and Branfireun, B.: Gaseous mercury emissions from urban surfaces: controls and spatiotemporal trends, *Appl. Geochem.*, 23, 369-383, 2008.
- Eckley, C. S., Gustin, M., Lin, C. J., Li, X. and Miller, M. B.: The influence of dynamic chamber design and operating parameters on calculated surface-to-air mercury fluxes, *Atmos. Environ.*, 44, 194-203, 2010.
- Eckley, C. S., Tate, M. T., Lin, C.-J., Gustin, M., Dent, S., Eagles-Smith, C., Lutz, M. A., Wickland, K. P., Wang, B., Gray, J. E., Edwards, G. C., Krabbenhoft, D. P. and Smith, D. B.: Surface-air mercury fluxes across Western North America: A synthesis of spatial trends and controlling variables, *Sci. Total Environ.*, 2016.
- Edner, H., Faris, G., Sunesson, A., Svanberg, S., Bjarnason, J. Ö., Kristmannsdottir, H., and Sigurdsson, K.: Lidar 1026 search for atmospheric atomic mercury in Icelandic geothermal fields, *Journal of Geophysical Research*, 96, 2977-2986, 1991.
- Edwards, G. C. and Howard, D. A.: Air-surface exchange measurements of gaseous elemental mercury over naturally enriched and background terrestrial landscapes in Australia, *Atmos. Chem. Phys.*, 13, 5325-5336, 2013.
- Eklöf, K., Kraus, A., Weyhenmeyer, G. A., Meili, M. and Bishop, K.: Forestry Influence by Stump Harvest and Site Preparation on Methylmercury, Total Mercury and Other Stream Water Chemistry Parameters Across a Boreal Landscape, *Ecosystems*, 15, 1308-1320, 2012.
- Eklöf, K., Kraus, A., Futter, M., Schelker, J., Meili, M., Boyer, E. W. and Bishop, K.: Parsimonious Model for Simulating Total Mercury and Methylmercury in Boreal Streams Based on Riparian Flow Paths and Seasonality, *Environ. Sci. Technol.*, 49, 7851-7859, 2015.
- EMEP: Heavy Metals: Transboundary Pollution of the Environment. EMEP Status Report 2/2013, available at: [http://www.emep.int/publ/common\\_publications.html](http://www.emep.int/publ/common_publications.html) [last access: 31 March 2016], 2013.
- Engle, M. A., Gustin, M. S. and Zhang, H.: Quantifying natural source mercury emissions from the Ivanhoe Mining District, northcentral Nevada, USA, *Atmos. Environ.*, 35, 3987-3997, 2001.
- Engle, M. A., Gustin, M. S., Goff, F., Counce, D. A., Janik, C. J., Bergfeld, D. and Rytuba, J. J.: Atmospheric mercury emissions from substrates and fumaroles associated with three hydrothermal systems in the western United States, *J. Geophys. Res.-Atmos.*, 111, D17304, 2006.
- Engle, M. A., Gustin, M. S., Lindberg, S. E., Gertler, A. W. and Ariya, P. A.: The influence of ozone on atmospheric emissions of gaseous elemental mercury and reactive gaseous mercury from substrates, *Atmos. Environ.*, 39, 7506-7517, 2005.

- Enrico, M., Le Roux, G., Maruszczak, N., Heimbürger, L.-E., Claustres, A., Fu, X., Sun, R. and Sonke, J. E.: Atmospheric mercury transfer to peat bogs dominated by gaseous elemental mercury dry deposition, *Environ. Sci. Technol.*, doi:10.1021/acs.est.5b06058, 2016.
- Ericksen, J. A., Gustin, M. S., Schorran, D. E., Johnson, D. W., Lindberg, S. E., Coleman, J. S.: Accumulation of atmospheric mercury in forest foliage, *Atmospheric Environment* 37, 1613-1622, 2003.
- Ericksen, J. A., Gustin, M. S., Xin, M., Weisberg, P. J. and Fernandez, G. C. J.: Air-soil exchange of mercury from background soils in the United States, *Sci. Total Environ.*, 366, 851-863, 2006.
- Faïn, X., Grangeon, S., Bahlmann, E., Fritsche, J., Obrist, D., Dommergue, A., Ferrari, C. P., Cairns, W., Ebinghaus, R., Barbante, C., Cescon, P. and Boutron, C.: Diurnal production of gaseous mercury in the alpine snowpack before snowmelt, *J. Geophys. Res.*, 112, D21311, 2007.
- Faïn, X., Helmig, D., Hueber, J., Obrist, D. and Williams, M. W.: Mercury dynamics in the Rocky Mountain, Colorado, snowpack, *Biogeosciences*, 10, 3793-3807, 2013.
- Faïn, X., Moosmueller, H., and Obrist, D.: Toward real-time measurement of atmospheric mercury concentrations using cavity ring-down spectroscopy, *Atmos. Chem. Phys.* 10, 2879-2892, 2010.
- Fang, F., Wang, Q. and Li, J.: Urban environmental mercury in Changchun, a metropolitan city in Northeastern China: source, cycle, and fate, *Sci. Total Environ.*, 330, 159-170, 2004.
- Farmer, J. G., Anderson, P., Cloy, J. M., Graham, M. C., MacKenzie, A. B. and Cook, G. T.: Historical accumulation rates of mercury in four Scottish ombrotrophic peat bogs over the past 2000 years, *Sci. Total Environ.*, 407, 5578-5588, 2009.
- Fay, L. and Gustin, M. S.: Investigation of mercury accumulation in cattails growing in constructed wetland mesocosms, *Wetlands*, 27, 1056-1065, 2007.
- Feigenwinter, C., Vogt, R. and Christen, A.: Eddy covariance measurements over urban areas, in: *Eddy Covariance – a Practical Guide to Measurement and Data Analysis*, edited by: Aubinet, M., Vesala, T., and Papale, D., Springer Science+Business Media B.V., Dordrecht, the Netherlands, 377-397, 2012.
- Feng, X. B., Wang, S. F., Qiu, G. A., Hou, Y. M. and Tang, S. L.: Total gaseous mercury emissions from soil in Guiyang, Guizhou, China, *J. Geophys. Res.-Atmos.*, 110, D14306, 2005.
- Fernández-Gómez, C., Drott, A., Björn, E., Díez, S., Bayona, J. M., Tesfalidet, S., Lindfors, A. and Skjllberg, U.: Towards Universal Wavelength-Specific Photodegradation Rate Constants for Methyl Mercury in Humic Waters, Exemplified by a Boreal Lake-Wetland Gradient, *Environ. Sci. Technol.* 47, 6279-6287, 2013.
- Fitzgerald, W.F., Lamborg, C.H. and Hammerschmidt, C.R.: Marine biogeochemical cycling of mercury, *Chem. Rev.* 107, 641-662, 2007.
- Foken, T.: *Angewandte Meteorologie, Mikrometeorologische Methoden*, 2nd edition, Springer, Berlin, Germany, 2006.
- Foken, T., and Wichura, B.: Tools for quality assessment of surface-based flux measurements, *Agr. Forest. Meteorol.*, 78, 83-105, 1996.
- Foken, T., Leuning, R., Oncley, S. R., Mauder, M. and Aubinet, M.: Corrections and data quality control, in: *Eddy Covariance – a Practical Guide to Measurement and Data Analysis*, edited by: Aubinet, M., Vesala, T., and Papale, D., Springer Science+Business Media B.V., Dordrecht, the Netherlands, 85-131, 2012.
- Friedli, H. R., Radke, L. F., Payne, N. J., McRae, D. J., Lynham, T. J. and Blake, T. W.: Mercury in vegetation and organic soil at an upland boreal forest site in Prince Albert National Park, Saskatchewan, Canada. *J. Geophys. Res.-Biogeosci.* 112, G01004, 2007.

## References

---

- Fritsche, J.: Air-Surface exchange of elemental mercury in uncontaminated grasslands. Determination of fluxes and identification of forcing factors with micrometeorological methods and controlled laboratory studies, Ph.D. thesis, University of Basel, Switzerland, 95 pp., 2008.
- Fritsche, J., Obrist, D., Zeeman, M. J., Conen, F., Eugster, W. and Alewell, C.: Elemental mercury fluxes over a sub-alpine grassland determined with two micrometeorological methods, *Atmos. Environ.*, 42, 2922-2933, 2008a.
- Fritsche, J., Obrist, D., Zeeman, M. J., Conen, F., Eugster, W. and Alewell, C.: Elemental mercury fluxes over a sub-alpine grassland determined with two micrometeorological methods, *Atmos. Environ.*, 42, 2922-2933, 2008b.
- Fritsche, J., Obrist, D. and Alewell, C.: Evidence of microbial control of  $\text{Hg}^0$  emissions from uncontaminated terrestrial soils, *J. Plant Nutr. Soil Sci.*, 171, 200-209, 2008c.
- Fritsche, J., Osterwalder, S., Nilsson, M. B., Sagerfors, J., Åkerblom, S., Bishop, K. and Alewell, C.: Evasion of elemental mercury from a boreal peatland suppressed by long-term sulfate addition, *Environ. Sci. Technol.*, 1, 421-425, 2014.
- Frohne, T., Rinklebe, J., Langer, U., Du Laing, G., Mothes, S. and Wennrich, R.: Biogeochemical factors affecting mercury methylation rate in two contaminated floodplain soils, *Biogeosciences*, 9, 493-507, 2012.
- Fu, X. W., Zhang, H., Lin, C. J., Feng, X. B., Zhou, L. X., and Fang, S. X.: Correlation slopes of GEM/CO, GEM/CO<sub>2</sub>, and GEM/CH<sub>4</sub> and estimated mercury emissions in China, South Asia, the Indochinese Peninsula, and 1146 Central Asia derived from observations in northwestern and southwestern China, *Atmos. Chem. Phys.*, 15, 1013-1028, 2015a.
- Gabriel, M. C. and Williamson, D. G.: Principal biogeochemical factors affecting the speciation and transport of mercury through the terrestrial environment, *Environ. Geochem. Hlth.*, 26, 421-434, 2004.
- Gabriel, M. C., Williamson, D., Lindberg, S., Zhang, H. and Brooks, S.: Spatial variability of total gaseous mercury emission from soils in a southeastern US urban environment, *Environ. Geol.*, 48, 955-964, 2005.
- Gabriel, M. C., Williamson, D. G., Zhang, H., Brooks, S. and Lindberg, S.: Diurnal and seasonal trends in total gaseous mercury flux from three urban ground surfaces, *Atmos. Environ.*, 40, 4269-4284, 2006.
- Galloway, M. and Branfireun, B.: Mercury dynamics of a temperate forested wetland, *Sci. Total Environ.*, 325, 239-254, 2004.
- Gaman, A., Rannik, Ü., Aalto, P., Pohja, T., Siivola, E., Kulmala, M. and Vesala, T.: Relaxed eddy accumulation system for size-resolved aerosol particle flux measurements, *J. Atmos. Ocean. Tech.*, 21, 933-943, 2004.
- Gårdfeldt, K., Feng, X. B., Sommar, J. and Lindqvist, O.: Total gaseous mercury exchange between air and water at river and sea surfaces in Swedish coastal regions, *Atmos. Environ.*, 35, 3027-3038, 2001.
- Gillis, A. and Miller, D. R.: Some potential errors in the measurement of mercury gas exchange at the soil surface using a dynamic flux chamber, *Sci. Total Environ.*, 260, 181-189, 2000.
- Gilmour, C. C., Henry, E. A. and Mitchell, R.: Sulfate stimulation of mercury methylation in freshwater sediments, *Environ. Sci. Technol.*, 26, 2281-2287, 1992.
- Gilmour, C., Podar, M., Bullock, A. L., Graham, A. M., Brown, S. D., Somenahally, A. C., Johs, A., Hurt, R. A., Bailey, K. L. and Elias, D. A.: Mercury methylation by novel microorganisms from new environments, *Environ. Sci. Technol.*, 47, 11810-11820, 2013.

- Givelet, N., Roos-Barracough, F. and Shotyk, W.: Predominant anthropogenic sources and rates of atmospheric mercury accumulation in southern Ontario recorded by peat cores from three bogs: comparison with natural "background" values (past 8000 years), *J. Environ. Monit.*, 5, 935-949, 2003.
- Granberg, G., Sundh, I., Svensson, B. H. and Nilsson, M.: Effects of temperature, and nitrogen and sulfur deposition, on methane emission from a boreal mire, *Ecology*, 82, 1982-1998, 2001.
- Grigal, D. F.: Inputs and outputs of mercury from terrestrial watersheds: a review, *Environ. Rev.*, 10, 1-39, 2002.
- Grigal, D. F.: Mercury sequestration in forests and peatlands: A review, *J. Environ. Qual.*, 32, 393-405, 2003.
- Grönholm, T., Haapanala, S., Launiainen, S., Rinne, J., Vesala, T. and Rannik, Ü.: The dependence of the coefficient of REA system with dynamic deadband on atmospheric conditions, *Environ. Pollut.*, 152, 597-603, 2008.
- Gu, B., Bian, Y., Miller, C. L., Dong, W., Jiang, X. and Liang, L.: Mercury reduction and complexation by natural organic matter in anoxic environments, *Proc. Natl. Acad. Sci. U. S. A.*, 108, 1479-1483, 2011.
- Gustin, M. S.: Exchange of mercury between the atmosphere and terrestrial ecosystems, in: *Advances in Environmental Chemistry, and Toxicology of Mercury*, edited by: Cai, Y., Liu, G., and O'Driscoll, N. J., John Wiley & Sons, Hoboken, NJ, USA, 423-452, 2011.
- Gustin, M. S. and Lindberg, S.E.: Assessing the contribution of natural sources to the global mercury cycle: The importance of intercomparing dynamic flux measurements, *Fresenius J. Anal. Chem.* 366, 417-422, 2000.
- Gustin, M. S. and Lindberg, S. E.: Terrestrial mercury fluxes: is the next exchange up, down, or neither?, in: *Dynamics of Mercury Pollution on Regional and Global Scales*, edited by: Pirrone, N. and Mahaffey, K. R., Springer, New York, 241-259, 2005.
- Gustin, M. S., Lindberg, S., Marsik, F., Casimir, A., Ebinghaus, R., Edwards, G., Hubble-Fitzgerald, C., Kemp, R., Kock, H., Leonard, T., London, J., Majewski, M., Montecinos, C., Owens, J., Pilote, M., Poissant, L., Rasmussen, P., Schaedlich, F., Schneeberger, D., Schröder, W., Sommar, J., Turner, R., Vette, A., Wallschlaeger, D., Xiao, Z. and Zhang, H.: Nevada STORMS project: Measurement of mercury emissions from naturally enriched surfaces, *J. Geophys. Res.-Atmos.*, 104, 21831-21844, 1999.
- Gustin, M. S., Lindberg, S. E., Austin, K., Coolbaugh, M., Vette, A. and Zhang, H.: Assessing the contribution of natural sources to regional atmospheric mercury budgets, *Sci. Total Environ.*, 259, 61-71, 2000.
- Gustin, M. S., Biester, H. and Kim, C. S.: Investigation of lightenhanced emission of mercury from enriched substrates, *Atmos. Environ.*, 36, 3241-3254, 2002.
- Gustin, M. S., Lindberg, S. E. and Weisberg, P. J.: An update on the natural sources and sinks of atmospheric mercury, *Appl. Geochem.*, 23, 482-493, 2008.
- Gustin, M. S., Huang, J., Miller, M. B., Peterson, C., Jaffe, D. A., Ambrose, J., Finley, B. D., Lyman, S. N., Call, K., Talbot, R., Feddersen, D., Mao, H., and Lindberg, S. E.: Do We Understand What the Mercury Speciation Instruments Are Actually Measuring? Results of RAMIX, *Environ. Sci. Technol.*, 47, 7295-7306, 2013.
- Gustin, M. S., Amos, H. M., Huang, J., Miller, M. B. and Heidecorn, K.: Measuring and modeling mercury in the atmosphere: a critical review, *Atmos. Chem. Phys.*, 15, 5697-5713, 2015.
- Hsu-Kim, H., Kucharzyk, K. H., Zhang, T. and Deshusses, M. A.: Mechanisms regulating mercury bioavailability for methylating microorganisms in the aquatic environment: a critical review. *Environ. Sci. Technol.*, 47, 2441-2456, 2013.

## References

---

- Haapanala, S., Rinne, J., Pystynen, K.-H., Hellén, H., Hakola, H. and Riutta, T.: Measurements of hydrocarbon emissions from a boreal fen using REA technique, *Biogeosciences*, 3, 103-112, 2006.
- Hansen, C., Zwolinski, G., Martin, D. and Williams, J.: Bacterial Removal of Mercury from Sewage. *Biotechnol. Bioeng.* 26, 1330-1333, 1984.
- Harmon, R., King J., Gladden, J. B., Chandler, G. and Newman, L.: Methylmercury formation in a wetland mesocosm amended with sulfate, *Environ. Sci. Technol.*, 38, 650-356, 2004.
- Hensen, A., Nemitz, E., Flynn, M. J., Blatter, A., Jones, S. K., Sorensen, L. L., Hensen, B., Pryor, S. C., Jensen, B., Otjes, R. P., Cobussen, J., Loubet, B., Erisman, J. W., Gallagher, M. W., Neftel, A. and Sutton, M.A.: Inter-comparison of ammonia fluxes obtained using the Relaxed Eddy Accumulation technique, *Biogeosciences*, 6, 2575-2588, 2009.
- Hintelmann, H., Harris, R., Heyes, A., Hurley, J. P., Kelly, C. A., Krabbenhoft, D. P., Lindberg, S., Rudd, J. W. M., Scott, K.J. and St. Louis, V.L. Reactivity and mobility of new and old mercury deposition in a Boreal forest ecosystem during the first year of the METAALICUS study, *Environ. Sci. Technol.*, 36, 5034-5040, 2002.
- Huang, J. Y., Miller, M. B., Weiss-Penzias, P., and Gustin, M. S.: Comparison of Gaseous Oxidized Hg Measured by KCl-Coated Denuders, and Nylon and Cation Exchange Membranes, *Environ. Sci. Technol.*, 47, 7307-7316, 2013.
- Iverfeldt, Å., Munthe, J., Brosset, C., and Pacyna, P.: Long-term changes in concentration and deposition of atmospheric mercury over Scandinavia, *Water Air Soil Pollut.*, 80, 227-233, 1995.
- Jaffe, D., Prestbo, E., Swartzendruber, P., Weiss-Penzias, P., Kato, S., Takami, A., Hatakeyama, S., and Kajii, Y.: 1236 Export of atmospheric mercury from Asia, *Atmospheric Environment*, 39, 3029-3038, 2005.
- JECFA.: Methylmercury, in: Safety evaluation of certain food additives and contaminants. Report of the 61<sup>st</sup> Joint FAO/WHO Expert Committee on Food Additives. International Programme on Chemical Safety. WHO Technical Report Series, Geneva, 132-139, 2004.
- Jensen, A. and Jensen, A.: Historical Deposition Rates of Mercury in Scandinavia Estimated by Dating and Measurement of Mercury in Cores of Peat Bogs, *Water Air Soil Pollut.*, 56, 769-777, 1991.
- Jeremiason, J. D., Engström, D. R., Swain, E. B., Nater, E. A., Johnson, B. M., Almendinger, J. E., Monson, B. A. and Kolka, R. K.: Sulfate addition increases methylmercury production in an experimental wetland, *Environ. Sci. Technol.*, 40, 3800-3806, 2006.
- Jiskra, M., Wiederhold, J. G., Skjellberg, U., Kronberg, R.-M., Hajdas, I. and Kretzschmar, R.: Mercury Deposition and Re-emission Pathways in Boreal Forest Soils Investigated with Hg Isotope Signatures, *Environ. Sci. Technol.*, 49, 7188-7196, 2015.
- Jiskra, M.: Terrestrial mercury cycling investigated with stable mercury isotopes, Ph.D. thesis, ETH Zürich, Switzerland, 227 pp., 2014.
- Keeler, G. J. and Landis, M. S.: Standard operating procedure for sampling vapor phase mercury, *EPA Laboratory methods*, 2, 405-419, 1994.
- Kim, J. and Fitzgerald, W.: Sea-Air Partitioning of Mercury in the Equatorial Pacific-Ocean, *Science* 231, 1131-1133, 1986.
- Kim, K. H., and Lindberg, S. E.: Design and initial tests of a dynamic enclosure chamber for measurements of 1248 vapor-phase mercury fluxes over soils, *Water Air Soil Poll.*, 80, 1059-1068, 1995.
- Kim, K. H. and Kim, M. Y.: The exchange of gaseous mercury across soil-air interface in a residential area of Seoul, Korea, *Atmos. Environ.*, 33, 3153-3165, 1999.



- Kim, K.-H., Lindberg, S. E. and Meyers T. P.: Micrometeorological measurements of mercury vapor fluxes over background forest soils in eastern Tennessee, *Atmos. Environ.*, 29, 267-282, 1995.
- Kim, K.-H., Yoon, H.-O., Jung, M.-C., Oh, J.-M. and Brown, R. J. C.: A Simple Approach for Measuring Emission Patterns of Vapor Phase Mercury under Temperature-Controlled Conditions, *Soil. Sci. World J.*, 940413, 2012.
- King, J. K., Harmon, S. M., Fu, T. T. and Gladden, J. B.: Mercury removal, methylmercury formation, and sulfate-reducing bacteria profiles in wetland mesocosms, *Chemosphere*, 46, 859-870, 2002.
- Kocman, D., Horvat, M., Pirrone, N. and Cinnirella, S.: Contribution of contaminated sites to the global mercury budget, *Environ. Res.*, 125, 160-170, 2013.
- Kormann, R. and Meixner, F. X.: An analytical footprint model for non-neutral stratification, *Bound.-Lay. Meteorol.*, 99, 207-224, 2001.
- Krabbenhoft, D., Benoit, J., Babiarz, C., Hurley, J. and Andren, A.: Mercury Cycling in the Allequash Creek Watershed, Northern Wisconsin, *Water Air Soil Pollut.*, 80, 425-433, 1995.
- Kuiken, T., Zhang, H., Gustin, M. and Lindberg, S.: Mercury emission from terrestrial background surfaces in the eastern USA. Part I: Air/surface exchange of mercury within a southeastern deciduous forest (Tennessee) over one year, *Appl. Geochem.*, 23, 345-355, 2008a.
- Kuiken, T., Gustin, M., Zhang, H., Lindberg, S. and Sedinger, B.: Mercury emission from terrestrial background surfaces in the eastern USA. II: Air/surface exchange of mercury within forests from South Carolina to New England, *Appl. Geochem.*, 23, 356-368, 2008b.
- Kuss, J., Holzmann, J. and Ludwig, R.: An Elemental Mercury Diffusion Coefficient for Natural Waters Determined by Molecular Dynamics Simulation., *Environ. Sci. Technol.*, 43, 3183-3186, 2009.
- Kyllönen, K., Hakola, H., Hellen, H., Korhonen, M. and Verta, M.: Atmospheric Mercury Fluxes in a Southern Boreal Forest and Wetland, *Water Air Soil Pollut.*, 223, 1171-1182, 2012.
- Lai, D. Y. F., Roulet, N. T., Humphreys, E. R., Moore, T. R. and Dalva, M.: The effect of atmospheric turbulence and chamber deployment period on autochamber CO<sub>2</sub> and CH<sub>4</sub> flux measurements in an ombrotrophic peatland, *Biogeosciences*, 9, 3305-3322, 2012.
- Laine, A. M., Bubier, J., Riutta, T., Nilsson, M. B., Moore, T. R., Vasander, H. and Tuittila, E. S.: Abundance and composition of plant biomass as potential controls for mire net ecosystem CO<sub>2</sub> exchange, *Botany*, 90, 63-74, 2012.
- Lamborg, C.H., Hammerschmidt, C. R., Bowman, K. L., Swarr, G. J., Munson, K. M., Ohnemus, D. C., Lam, P. J., Heimburger, L.-E., Rijkenberg, M. J. A., Saito, M. A.: A global ocean inventory of anthropogenic mercury based on water column measurements, *Nature*, 512, 65-68, 2014.
- Landis, M. S., Stevens, R. K., Schaedlich, F., and Prestbo, E. M.: Development and characterization of an annular denuder methodology for the measurement of divalent inorganic reactive gaseous mercury in ambient air, *Environ. Sci. Technol.*, 36, 3000-3009, 2002.
- Lasorsa, B.K., Gill, G.-A. and Horvat, M.: Analytical Methods for Measuring Mercury in Water, Sediment, and Biota, in: *Mercury in the Environment: pattern and process.*, 1st edn., edited by Bank, M. S., University of California Press, Berkeley, CA. 27-54, 2012.
- Laudon, H., Taberman, I., Agren, A., Futter, M., Ottosson-Löfvenius, M. and Bishop, K.: The Krycklan Catchment Study – A flagship infrastructure for hydrology, biogeochemistry, and climate research in the boreal landscape, *Water Resources Research*, 49, 7154-7158, 2013.
- Leach, J. A., Larsson, A., Wallin, M. B., Nilsson, M. B. and Laudon, H.: Twelve year interannual and seasonal variability of stream carbon export from a boreal peatland catchment, *J. Geophys. Res. Biogeosci.*, 121, doi:10.1002/2016JG003357, 2016.

## References

---

- Lee, D. S., Nemitz, E., Fowler, D., Hill, P., Clegg, S. and Kingdon, R. D.: Sources, sinks and levels of atmospheric mercury in the UK, Rep. DERA/AS/PTD/CR000114, Farnborough, UK, available at: [http://uk-air.defra.gov.uk/library/reports?report\\_id=102](http://uk-air.defra.gov.uk/library/reports?report_id=102) [last access: 31 March 2016], 2000.
- Lee, X. H.: Water vapor density effect on measurements of trace gas mixing ratio and flux with a massflow controller, *J. Geophys. Res.-Atmos.*, 105, 17807-17810, 2000.
- Li, P., Feng, X.B., Qiu, G.L., Shang, L.H. and Li, Z.G.: Mercury pollution in Asia: A review of the contaminated sites, *J. Hazard. Mater.*, 168, 591-601, 2009.
- Lidman, F., Köhler, S. J., Mörtz, C.-M. and Laudon, H.: Metal Transport in the Boreal Landscape - The Role of Wetlands and the Affinity for Organic Matter, *Environ. Sci. Technol.* 48, 3783-3790, 2014.
- Lietzke, B. and Vogt, R.: Variability of CO<sub>2</sub> concentrations and fluxes in and above an urban street canyon, *Atmos. Environ.*, 74, 60-72, 2013.
- Lin, C. J. and Pehkonen, S. O.: Aqueous free radical chemistry of mercury in the presence of iron oxides and ambient aerosol. *Atmos. Environ.*, 31, 4125-4137, 1997.
- Lin, C. J. and Pehkonen, S. O.: The chemistry of atmospheric mercury: a review. *Atmos. Environ.* 33, 2067-2079, 1999.
- Lin, C. J., Gustin, M. S., Singhasuk, P., Eckley, C. and Miller, M. Empirical models for estimating mercury flux from soils, *Environ. Sci. Technol.*, 44, 8522-8528, 2010.
- Lin, C.-J., Zhu, W., Li, X., Feng, X., Sommar, J., and Shang, L.: Novel dynamic flux chamber for measuring air-surface exchange of Hg<sub>0</sub> from soils, *Environ. Sci. Technol.*, 46, 8910-8920, 2012.
- Lindberg, S. E. and Price, J. L.: Airborne Emissions of Mercury from Municipal Landfill Operations: A Short-Term Measurement Study in Florida, *J Air Waste Management*, 49, 520-532, 1999.
- Lindberg, S. E. and Zhang, H.: Air/water exchange of mercury in the Everglades II: measuring and modeling evasion of mercury from surface waters in the Everglades Nutrient Removal Project, *Sci. Total Environ.*, 259, 135-143, 2000.
- Lindberg, S. and Meyers, T.: Development of an automated micrometeorological method for measuring the emission of mercury vapor from wetland vegetation, *Wetl. Ecol. Manag.*, 9, 333-347, 2001.
- Lindberg, S. E., Kim, K.-H., Meyers, T. P. and Owens, J. G.: Micrometeorological gradient approach for quantifying air/surface exchange of mercury vapor: tests over contaminated soils, *Environ. Sci. Technol.*, 29, 126-135, 1995.
- Lindberg, S. E., Vette, A. F., Miles, C. and Schaedlich, F.: Mercury speciation in natural waters: Measurement of dissolved gaseous mercury with a field analyzer, *Biogeochemistry*, 48, 237-259, 2000.
- Lindberg, S. E., Dong, W. J. and Meyers, T.: Transpiration of gaseous elemental mercury through vegetation in a subtropical wetland in Florida, *Atmos. Environ.*, 36, 5207-5219, 2002.
- Lindberg, S. E., Dong, W. J., Chanton, J., Qualls, R. G. and Meyers, T.: A mechanism for bimodal emission of gaseous mercury from aquatic macrophytes, *Atmos. Environ.*, 39, 1289-1301, 2005.
- Lindberg, S., Bullock, R., Ebinghaus, R., Engstrom, D., Feng, X. B., Fitzgerald, W., Pirrone, N., Prestbo, E., and Seigneur, C.: A synthesis of progress and uncertainties in attributing the sources of mercury in deposition, *Ambio*, 36, 19-32, 2007.
- Loisel, J., Yu, Z., Beilman, D.W. et al.: A database and synthesis of northern peatland soil properties and Holocene carbon and nitrogen accumulation. *Holocene*, 24, 1028-1042, 2014.
- Magarelli, G. and Fostier, A. H.: Influence of deforestation on the mercury air/soil exchange in the Negro River Basin, Amazon, *Atmos. Environ.*, 39, 7518-7528, 2005.

- Marsik, F. J., Keeler, G. J., Lindberg, S. E. and Zhang, H.: Air-surface exchange of gaseous mercury over a mixed sawgrass-cattail stand within the Florida Everglades, *Environ. Sci. Technol.*, 39, 4739-4746, 2005.
- Mason, R. P. and Sheu, G.-R.: Role of the ocean in the global mercury cycle. *Global Biogeochem. Cy.*, 16, doi:10.1029/2001GB001440, 2002.
- Mason, R. P., Choi, A. L., Fitzgerald, W. F., Hammerschmidt, C. R., Lamborg, C. H., Soerensen, A. L and E. M. Sunderland.: Mercury biogeochemical cycling in the ocean and policy implications, *Environ. Res.*, 119, 101-117, 2012.
- Mauder, M. and Foken, T.: Documentation and instruction manual of the eddy covariance software package TK2, vol 26, Arbeitsergebnisse, Abteilung Mikrometeorologie. Universität Bayreuth, Bayreuth, Germany, 42 pp., ISSN 1614-8916, 2004.
- Mazur, M. E. E., Eckley, C. S. and Mitchell C. P. J.: Susceptibility of Soil Bound Mercury to Gaseous Emission As a Function of Source Depth: An Enriched Isotope Tracer Investigation, *Environ. Sci. Technol.*, 49, 9143-9149, 2015.
- Mcmillen, R.: An Eddy-Correlation Technique with Extended Applicability to Non-Simple Terrain. *Bound.-Layer Meteor.*, 43, 231-245, 1988.
- Meili, M., Bishop, K., Bringmark, L., Johansson, K., Munthe, J., Sverdrup, H. and de Vries, W.: Critical levels of atmospheric pollution: criteria and concepts for operational modelling of mercury in forest and lake ecosystems, *Sci. Total Environ.*, 304, 83-106, 2003.
- Mergler, D., Anderson, H. A., Chan, L. H. M., Mahaffey, K. R., Murray, M., Sakamoto, M. and Stern, A. H.: Methylmercury Exposure and Health Effects in Humans: A Worldwide Concern. *AMBIO: A Journal of the Human Environment*, 36, 3-11, 2007.
- MeteoSchweiz: Klimanormwerte Basel/Binningen, Normperiode 1961-1990, available at: <http://www.meteoschweiz.admin.ch> [last access: 31 March 2016]
- Meyers, T. P., Hall, M. E., Lindberg, S. E. and Kim, K.: Use of the modified Bowen-ratio technique to measure fluxes of trace gases, *Atmos. Environ.*, 30, 3321-3329, 1996.
- Meyers, T. P., Luke, W. T. and Meisinger, J. J.: Fluxes of ammonia and sulfate over maize using relaxed eddy accumulation, *Agric. Forest Meteorol.*, 136, 203-213, 2006.
- Miller, E. K., Vanarsdale, A., Keeler, G. J., Chalmers, A., Poissant, L., Kamman, N. C. and Brulotte, R.: Estimation and mapping of wet and dry mercury deposition across northeastern North America, *Ecotoxicology*, 14, 53-70, 2005.
- Miller, M. B., Gustin, M. S. and Eckley, C. S.: Measurement and scaling of air-surface mercury exchange from substrates in the vicinity of two Nevada gold mines, *Sci. Total Environ.*, 409, 3879-3886, 2011.
- Milne, R., Beverland, I. J., Hargreaves, K. and Moncrieff, J. B.: Variation of the  $\beta$  coefficient in the relaxed eddy accumulation method, *Bound.-Lay. Meteorol.*, 93, 211-225, 1999.
- Milne, R., Mennim, A., and Hargreaves, K.: The value of the beta coefficient in the relaxed eddy accumulation method in terms of fourth-order moments, *Bound.-Lay. Meteorol.*, 101, 359-373, 2001.
- Mitchell C. P. J., Branfireun B. A. and Kolka R. K.: Spatial characteristics of met methylmercury production hot spots in peatlands, *Environ. Sci. Technol.*, 42, 1010-1016, 2008.
- Moore, C. and Carpi, A.: Mechanisms of the emission of mercury from soil: Role of UV radiation, *J. Geophys. Res.-Atmos.*, 110, D24302, 2005.
- Moore, C. W. and Castro, M. S.: Investigation of factors affecting gaseous mercury concentrations in soils, *Sci. Total Environ.*, 419, 136-143, 2012.

## References

---

- Moore, C. W., Obrist, D. and Luria, M.: Atmospheric mercury depletion events at the Dead Sea: Spatial and temporal aspects, *Atmos. Environ.*, 69, 231-239, 2013.
- Moravek, A., Trebs, I. and Foken, T.: Effect of imprecise lag time and high-frequency attenuation on surface-atmosphere exchange fluxes determined with the relaxed eddy accumulation method, *J. Geophys. Res.-Atmos.*, 118, 10210-10224, 2013.
- Morel, F. M. M., Kraepiel, A. M. L. and Amyot, M.: The chemical cycle and bioaccumulation of mercury, *Annu. Rev. Ecol. Syst.* 29, 543-566, 1998.
- Munthe, J., Wangberg, I., Pirrone, N., Iverfeldt, A., Ferrara, R., Ebinghaus, R., Feng, X., Gardfeldt, K., Keeler, G., Lanzillotta, E., Lindberg, S. E., Lu, J., Mamane, Y., Prestbo, E., Schmolke, S., Schröder, W. H., Sommar, J., Sprovieri, F., Stevens, R. K., Stratton, W., Tuncel, G. and Urba, A.: Intercomparison of methods for sampling and analysis of atmospheric mercury species, *Atmos. Environ.*, 35, 3007-3017, 2001.
- Nacht, D. M. and Gustin, M. S.: Mercury emissions from background and altered geologic units throughout Nevada, *Water, Air, Soil Pollut.*, 151, 179-193, 2004.
- Nerentorp, M., Kyllönen, K., Wängberg, I. and Kuronen, P.: Speciation measurements of airborne mercury species in northern Finland; Evidence for long range transport of air masses depleted in mercury, *E3s Web Conf* 1, 27003, 2013.
- Nilsson, M., Sagerfors, J., Buffam, I., Laudon, H., Eriksson, T., Grelle, A., Klemetsson, L., Weslien, P. and Lindroth, A.: Contemporary carbon accumulation in a boreal oligotrophic minerogenic mire - a significant sink after accounting for all C-fluxes, *Glob. Change Biol.*, 14, 2317-32, 2008.
- Obrist, D.: Atmospheric mercury pollution due to losses of terrestrial carbon pools?, *Biogeochemistry*, 85, 119-123, 2007.
- Obrist, D., Conen, F., Vogt, R., Siegwolf, R. and Alewell, C.: Estimation of  $Hg^0$  exchange between ecosystems and the atmosphere using  $^{222}Rn$  and  $Hg^0$  concentration changes in the stable nocturnal boundary layer, *Atmos. Environ.*, 40, 856-866, 2006.
- Obrist, D., Johnson, D.W., Lindberg, S.E.: Mercury concentrations and pools in four Sierra Nevada forest sites, and relationships to organic carbon and nitrogen. *Biogeosciences*, 6, 765-777, 2009.
- Obrist, D., Johnson, D. W., Lindberg, S. E., Luo, Y., Hararuk, O., Bracho, R., Battles, J. J., Dail, D. B., Edmonds, R. L., Monson, R. K., Ollinger, S. V., Pallardy, S. G., Pregitzer, K. S. and Todd, D. E.: Mercury Distribution Across 14 US Forests. Part I: Spatial Patterns of Concentrations in Biomass, Litter, and Soils, *Environ. Sci. Technol.*, 45, 3974-3981, 2011.
- Olid, C., Nilsson, M. B., Eriksson, T. and Klaminder, J.: The effects of temperature and nitrogen and sulfur additions on carbon accumulation in a nutrient-poor boreal mire: Decadal effects assessed using  $^{210}Pb$  peat chronologies, *J. Geophys. Res.-Biogeosci.*, 119, 392-402, 2014.
- Olofsson M., Ek-Olausson B., Jensen N.O., Langer S. and Ljungström E.: The flux of isoprene from a willow plantation and the effect on local air quality, *Atmos. Environ.*, 39, 2061-2070, 2005a.
- Olofsson, M., Sommar, J., Ljungstrom, E., Andersson, M. and Wängberg, I.: Application of relaxed eddy accumulation technique to quantify  $Hg^0$  fluxes over modified soil surfaces, *Water Air Soil Pollut.*, 167, 331-352, 2005b.
- Olsson, S. and Bergman, M.: Daily dose calculations from measurements of intra-oral mercury vapor, *Journal of dental research*, 71, 414-423, 1992.
- Osterwalder, S., Fritsche, J., Alewell, C., Schmutz, M., Nilsson, M. B., Jocher, G., Sommar, J., Rinne, J., and Bishop, K.: A dual-inlet, single detector relaxed eddy accumulation system for long-term measurement of mercury flux, *Atmos. Meas. Tech.*, 9, 509-524, 2016.
- Ottosson-Löfvenius, M., Kluge, M. and Lundmark, T.: Snow and soil frost depth in two types of shelterwood and a clear-cut area, *Scandinavian Journal of Forest Research*, 18, 54-63, 2003.

- Panofsky, H. A. and Dutton, J. A.: Atmospheric Turbulence – models and methods for engineering applications, Wiley, New York, USA, 397 pp., 1984.
- Parks, J.M., Johs, A., Podar, M., Bridou, R., Hurt, R.A., Smith, S.D., Tomanicek, S.J., Qian, Y., Brown, S.D., Brandt, C.C., Palumbo, A.V., Smith, J.C., Wall, J.D., Elias, D.A. and Liang, L.: The genetic basis for bacterial mercury methylation, *Science*, 339, 1332-1335, 2013.
- Pedrero, Z., Bridou, R., Mounicou, S., Guyoneaud, R., Monperrus, M. and Amouroux, D.: Transformation, localization, and biomolecular binding of Hg species at subcellular level in methylating and nonmethylating sulfate-reducing bacteria, *Environ. Sci. Technol.*, 46, 11744-11751, 2012.
- Peichl, M., Sagerfors, J., Lindroth, A., Buffam, I., Grelle, A., Klemedtsson, L., Laudon, H. and Nilsson, M. B.: Energy exchange and water budget partitioning in a boreal minerogenic mire, *J. Geophys. Res.-Biogeo.*, 118, 1-13, 2013.
- Peichl, M., Sonnentag, O. and Nilsson, M.B.: Bringing Color into the Picture: Using Digital Repeat Photography to Investigate Phenology Controls of the Carbon Dioxide Exchange in a Boreal Mire, *Ecosystems*, 18, 115-131, 2015.
- Peichl, M., Oquist, M., Lofvenius, M. O., Ilstedt, U., Sagerfors, J., Grelle, A., Lindroth, A. and Nilsson, M.B.: A 12-year record reveals pre-growing season temperature and water table level threshold effects on the net carbon dioxide exchange in a boreal fen, *Environ. Res. Lett.*, 9, doi:10.1088/1748-9326/9/5/055006, 2014.
- Pierce, A., Obrist, D., Moosmüller, H., Fain, X., and Moore, C.: Cavity ring-down spectroscopy sensor development for high-time-resolution measurements of gaseous elemental mercury in ambient air, *Atmos. Meas. 1470 Tech.*, 6, 1477-1489, 2013.
- Pierce, A. M., Moore, C. W., Wohlfahrt, G., Hörtnagl, L., Kljun, N., and Obrist, D.: Eddy Covariance Flux Measurements of Gaseous Elemental Mercury Using Cavity Ring-Down Spectroscopy, *Environ. Sci. Technol.*, 49, 1559-1568, 2015.
- Pirrone, N., Hedgecock, I. M. and Sprovieri, F. New Directions: Atmospheric mercury, easy to spot and hard to pin down: Impasse?, *Atmos. Environ.*, 42, 8549-8551, 2008.
- Poissant, L. and Casimir, A.: Water-air and soil-air exchange rate of total gaseous mercury measured at background sites, *Atmos. Environ.*, 32, 883-893, 1998.
- Poissant, L., Pilote, M. and Casimir, A.: Mercury flux measurements in a naturally enriched area: Correlation with environmental conditions during the Nevada Study and Tests of the Release of Mercury From Soils (STORMS), *J. Geophys. Res.-Atmos.*, 104, 21845-21857, 1999.
- Poissant, L., Amyot, M., Pilote, M. and Lean, D.: Mercury water-air exchange over the Upper St. Lawrence River and Lake Ontario, *Environ. Sci. Technol.*, 34, 3069-3078, 2000.
- Poissant, L., Pilote, M., Xu, X.H., Zhang, H. and Beauvais, C.: Atmospheric mercury speciation and deposition in the Bay St. Francois wetlands, *J. Geophys. Res.-Atmos.*, 109, D11301, 2004a.
- Poissant, L., Pilote, M., Constant, P., Beauvais, C., Zhang, H.H. and Xu, X.H.: Mercury gas exchanges over selected bare soil and flooded sites in the bay St. Francois wetlands (Quebec, Canada), *Atmos. Environ.*, 38, 4205-4214, 2004b.
- Porvari, P. and Verta, M.: Total and methyl mercury concentrations and fluxes from small boreal forest catchments in Finland, *Environ. Pollut.*, 123, 181-191, 2003.
- R Development Core Team.: R: A Language and Environment for Statistical Computing. Vienna, Austria : the R Foundation for Statistical Computing. ISBN: 3-900051-07-0, available at: <http://www.R-project.org/> [last access: 31 March 2016], 2011.
- Ranchou-Peyruse, M., Monperrus, M., Bridou, R., Duran, R., Amouroux, D., Salvado, J. C. and Guyoneaud, R.: Overview of mercury methylation capacities among anaerobic bacteria including representatives of the sulphate-reducers: Implications for environmental studies, *Geomicrobiol. J.*, 26, 1-8, 2009.

## References

---

- Rannik, U., Aubinet, M., Kurbanmuradov, O., Sabelfeld, K.K., Markkanen, T. and Vesala, T.: Footprint analysis for measurements over a heterogeneous forest, *Bound.-Lay. Meteorol.*, 97, 137-166, 2000.
- Ren, X., Sanders, J. E., Rajendran, A., Weber, R. J., Goldstein, A. H., Pusede, S. E., Browne, E. C., Min, K.-E. and Cohen, R. C.: A relaxed eddy accumulation system for measuring vertical fluxes of nitrous acid, *Atmos. Meas. Tech.* 4, 2093-2103, 2011.
- Richardson, A. D., Aubinet, M., Barr, A. G., Hollinger, D. Y., Ibrom, A., Lasslop, G. and Reichstein, M.: Uncertainty quantification, in: *Eddy Covariance – a Practical Guide to Measurement and Data Analysis*, edited by: Aubinet, M., Vesala, T., and Papale, D., Springer Science+Business Media B.V., Dordrecht, the Netherlands, 173-209, 2012.
- Riederer, M., Serafimovich, A. and Foken, T.: Net ecosystem CO<sub>2</sub> exchange measurements by the closed chamber method and the eddy covariance technique and their dependence on atmospheric conditions, *Atmos. Meas. Tech.*, 7, 1057-1064, 2014.
- Rinklebe, J., During, A., Overesch, M., Du Laing, G., Wennrich, R., Staerk, H.-J. and Mothes, S.: Dynamics of mercury fluxes and their controlling factors in large Hg-polluted floodplain areas, *Environ. Pollut.*, 158, 308-318, 2010.
- Roulet, N., Hardill, S. and Comer, N.: Continuous measurement of the depth of water table (inundation) in wetlands with fluctuating surfaces, *Hydrological Processes*, 5, 399-403, 1991.
- Rudd, J.: Sources of Methyl Mercury to Fresh-Water Ecosystems - a Review, *Water Air Soil Pollut.* 80, 697-713, 1995.
- Rutter, A. P., Schauer, J. J., Shafer, M. M., Creswell, J. E., Olson, M. R., Robinson, M., Collins, R. M., Parman, A. M., Katzman, T. L. and Mallek, J. L.: Dry deposition of gaseous elemental mercury to plants and soils using mercury stable isotopes in a controlled environment, *Atmos. Environ.* 45, 848-855, 2011.
- Rydberg, J., Karlsson, J., Nyman, R., Wanhatalo, I., Naethe, K. and Bindler, R.: Importance of vegetation type for mercury sequestration in the northern Swedish mire, Rodmossamyran, *Geochim. Cosmochim. Acta*, 74, 7116-7126, 2010.
- Sagerfors, J., Lindroth, A., Grelle, A., Klemetsson, L., Weslien, P. and Nilsson, M. B.: Annual CO<sub>2</sub> exchange between a nutrient-poor, minerotrophic, boreal mire and the atmosphere, *J. Geophys. Res.-Biogeosci.*, 113, G01001, 2008.
- Schlüter, K.: Review: evaporation of mercury from soils. An integration and synthesis of current knowledge, *Environ. Geol.*, 39, 249-271, 2000.
- Schröder, W. H., Munthe, J., and Lindqvist, O.: Cycling of mercury between water, air, and soil compartments of the environment, *Water, Air, and Soil Pollution*, 48, 337-347, 1989.
- Schröder, W.H. and Munthe, J.: Atmospheric mercury - An overview, *Atmos. Environ.* 32, 809-822, 1998.
- Schröder, W. H., Anlauf, K. G., Barrie, L. A., Lu, J. Y., Steffen, A., Schneeberger, D. R. and Berg, T.: Arctic springtime depletion of mercury, *Nature*, 394, 331-332, 1998.
- Schröder, W. H., Beauchamp, S., Edwards, G., Poissant, L., Rasmussen, P., Tordon, R., Dias, G., Kemp, J., Van Heyst, B. and Banic, C. M.: Gaseous mercury emissions from natural sources in Canadian landscapes, *J. Geophys. Res.-Atmos.*, 110, doi:10.1029/2004JD005699, 2005.
- Seinfeld, J. H. and Pandis, S. N.: *Meteorology of the Local Scale. Atmospheric Chemistry and Physics: From Air Pollution to Climate Change*, 2nd Ed., 1998.
- Selin, N. E., Javob, D. J., Park, R. J., Yantosca, R. M., Strode, S., Jaeglé, L. and Jaffe, D.: Chemical cycling and deposition of atmospheric mercury: Global constraints from observations, *Journal of Geophysical Research Atmospheres*, 112, doi:10.1029/2006JD007450, 2007.

- Selin, N. E., Jacob, D. J., Park, R. J., Yantosca, R. M., Strode, S., Jaeglé, L. and Sunderland, E.: Global 3-D land-ocean-atmosphere model for mercury: Present-day versus preindustrial cycles and anthropogenic enrichment factors for deposition, *Global Biogeochem. Cycles*, 22, GB2011, 2008.
- Selvendiran, P., Driscoll, C. T., Montesdeoca, M. R. and Bushey, J. T.: Inputs, storage, and transport of total and methyl mercury in two temperate forest wetlands, *J. Geophys. Res.*, 113, G00C01, 2008.
- Shanley, J. B. and Bishop, K.: Mercury cycling in terrestrial watersheds, in: *Mercury in the Environment: Pattern and Process*, edited by: Bank, M. S., University of California Press, Berkely, CA, 119-141, 2012.
- Shao, D., Kang, Y., Wu, S. and Wong, M. H.: Effects of sulfate reducing bacteria and sulfate concentrations on mercury methylation in freshwater sediments, *Sci. Total Environ.*, 1, 331-336, 2012.
- Shotyk, W., Goodsite, M. E., Roos-Barraclough, F., Givélet, N., Le Roux, G., Weiss, D., Cheburkin, A. K., Knudsen, K., Heinemeier, J., Van der Knaap, W. O., Norton, S.A. and Lohse, C.: Accumulation rates and predominant atmospheric sources of natural and anthropogenic Hg and Ph on the Faroe Islands, *Geochim. Cosmochim. Acta*, 69, 1-17, 2005.
- Sigler, J. M. and Lee, X.: Gaseous mercury in background forest soil in the northeastern United States, *J. Geophys. Res.*, 111, G02007, 2006.
- Sjöholm, M., Weibring, P., Edner, H., and Svanberg, S.: Atomic mercury flux monitoring using an optical 1554 parametric oscillator based lidar system, *Optics Express*, 12, 551-556, 2004.
- Skov, H., Brooks, S. B., Goodsite, M. E., Lindberg, S. E., Meyers, T. P., Landis, M. S., Larsen, M. R. B., Jensen, B., McConville, G. and Christensen, J.: Fluxes of reactive gaseous mercury measured with a newly developed method using relaxed eddy accumulation, *Atmos. Environ.*, 40, 5452-5463, 2006.
- Skylberg, U.: Competition among thiols and inorganic sulfides and polysulfides for Hg and MeHg in wetland soils and sediments under suboxic conditions: Illumination of controversies and implications for MeHg net production, *J. Geophys. Res. -Biogeosci.*, 113, G00C03, 2008.
- Skylberg, U., Qian, J., Frech, W., Xia, K. and Bleam, W.F.: Distribution of Mercury, Methyl Mercury and Organic Sulphur Species in Soil, Soil Solution and Stream of a Boreal Forest Catchment, *Biogeochemistry*, 64, 53-76, 2003.
- Skylberg, U., Xia, K., Bloom, P.R., Nater, E.A., Bleam, W.F., 2000. Binding of mercury(II) to reduced sulfur in soil organic matter along upland-peat soil transects. *J. Environ. Qual.* 29, 855-865.
- Slemr, F., Brunke, E., Ebinghaus, R., Temme, C., Munthe, J. Wängberg, I., Schröder, W., Steffen, A. and Berg, T.: Worldwide trend of atmospheric mercury since 1977, *Geophys. Res. Lett.*, 30, 1516, doi:10.1029/2003GL016954, 2003.
- Smith-Downey, N. V., Sunderland, E. M. and Jacob, D. J.: Anthropogenic impacts on global storage and emissions of mercury from terrestrial soils: Insights from a new global model. *J. Geophys. Res.-Biogeosci.* 115, G03008, 2010.
- Sommar, J., Zhu, W., Lin, C.-J. and Feng, X.: Field approaches to measure Hg exchange between natural surfaces and the atmosphere – a review, *Critical Reviews in Environ. Sci. Technol.*, 43, 1657-1739, 2013a.
- Sommar, J., Zhu, W., Shang, L., Feng, X. and Lin, C.-J.: A whole-air relaxed eddy accumulation measurement system for sampling vertical vapor exchange of elemental mercury, *Tellus B*, 65, 19940, 2013b.

## References

---

- Southworth, G., Lindberg, S., Hintelmann, H., Amyot, M., Poulain, A., Bogle, M., Peterson, M., Rudd, J., Harris, R., Sandilands, K., Krabbenhoft D. and Olsen, M.: Evasion of added isotopic mercury from a northern temperate lake, *Environ. Toxicol. Chem.*, 26, 53-60, 2007.
- Sprovieri, F., Pirrone, N., Ebinghaus, R., Kock, H. and Dommergue, A.: A review of worldwide atmospheric mercury measurements, *Atmos. Chem. Phys.* 10, 8245-8265, 2010.
- St. Louis, V. L., Rudd, J. W. M., Kelly, C. A., Beaty, K. G., Bloom, N. S. and Flett, R. J.: Importance of wetlands as sources of methylmercury to boreal forest ecosystems, *Can. J. Fish Aquat. Sci.*, 51, 1065-1076, 1994.
- Stamenkovic, J. and Gustin, M.S.: Nonstomatal versus Stomatal Uptake of Atmospheric Mercury, *Environ. Sci. Technol.*, 43, 1367-1372, 2009.
- Steffen, A., Schröder, W. H., Bottenheim, J., Narayan, J. and Fuentes, J. D.: Atmospheric mercury concentrations: measurements and profiles near snow and ice surfaces in the Canadian Arctic during Alert 2000, *Atmos. Environ.*, 36, 2653-2661, 2002.
- Steffen, A., Bottenheim, J., Cole, A., Ebinghaus, R., Lawson, G., and Leitch, W. R.: Atmospheric mercury speciation and mercury in snow over time at Alert, Canada, *Atmos. Chem. Phys.*, 14, 2219-2231, 2014.
- Steffen, A., Lehnerr, I., Cole, A., Ariya, P., Dastoor, A., Durnford, D., Kirk, J., and Pilote, M.: Atmospheric mercury measurements in the Canadian Arctic Part 1: A review of recent field measurements, *Sci. Total Environ.*, 509-510, 3-15, 2015.
- Steinnes, E. and Sjøbakk, T. E.: Order-of-magnitude increase of Hg in Norwegian peat profiles since the outset of industrial activity in Europe, *Environmental Pollution*, 137, 365-370, 2004.
- Strack, M., Kellner, E. and Waddington, J.M.: Dynamics of biogenic gas bubbles in peat and their effects on peatland biogeochemistry, *Global Biogeochem. Cycles*, 19, GB1003, 2005.
- Streets, D. G., Devane, M. K., Lu, Z. F., Bond, T. C., Sunderland, E. M. and Jacob, D. J.: All-time releases of mercury to the atmosphere from human activities, *Environ. Sci. Technol.*, 45, 10485-10491, 2011.
- Sun, R., Streets, D. G., Horowitz, H. M., Amos, H. M., Liu, G., Perrot, V., Toutain, J.-P., Hintelmann, H., Sunderland, E. M. and Sonke, J. E.: Historical (1850-2010) mercury stable isotope inventory from anthropogenic sources to the atmosphere, *Elementa: Science of the Anthropocene* 4, doi:10.12952/journal.elementa.000091, 2016.
- Sutton, M. A., Milford, C., Nemitz, E., Theobald, M. R., Hill, P. W., Fowler, D., Schjoerring, J. K., Mattsson, M. E., Nielsen, K. H., Husted, S., Erismann, J. W., Otjes, R., Hensen, A., Mosquera, J., Cellier, P., Loubet, B., David, M., Genermont, S., Neftel, A., Blatter, A., Herrmann, B., Jones, S. K., Horvath, L., Fuhrer, E. C., Mantzanas, K., Koukoura, Z., Gallagher, M., Williams, P., Flynn, M. and Riedo, M.: Biosphere-atmosphere interactions of ammonia with grasslands: Experimental strategy and results from a new European initiative, *Plant and Soil*, 228, 131-145, 2001.
- Teutschbein, C., Grabs, T., Karlsen, R. H., Laudon, H. and Bishop, K.: Hydrological response to changing climate conditions: Spatial streamflow variability in the boreal region, *Water Resour. Res.*, 51, 9425-9446, 2015.
- Truong, H.-Y. T., Chen, Y.-W. and Belzile, N.: Effect of sulfide, selenite and mercuric mercury on the growth and methylation capacity of the sulfate reducing bacterium *Desulfovibrio desulfuricans*, *Sci. Total Environ.*, 449, 373-384, 2013.
- Turunen, J., Tomppo, E., Tolonen and K., Reinikainen, A.: Estimating carbon accumulation rates of undrained mires in Finland - application to boreal and subarctic regions, *Holocene* 12, 69-80, 2012.
- UNECE: Hemispheric Transport of air pollution 2010. Part B: Mercury, edited by Pirrone, N. and Keating, T., United Nations Publication, Geneva, Switzerland, 2012.



- United Nations Environment Programme: Summary of supply, trade and demand information on mercury. UNEP's Division of Technology, Industry and Economics (DTIE), UNEP Chemical Branch, Geneva, Switzerland, 2006.
- United Nations Environment Programme: Minamata Convention on Mercury, available at: <http://www.mercuryconvention.org> [last access: 31 March 2016], 62 pp., 2013a.
- United Nations Environment Programme: Global Mercury Assessment 2013: Sources, emissions, releases and environmental transport, UNEP Chemicals Branch, Geneva, Switzerland, 42 pp., 2013b.
- VBBö: Verordnung über Belastung des Bodens vom 1. Juli 1998, available at: <https://www.admin.ch/opc/de/classified-compilation/19981783/index.html> [last access: 31 March 2016]
- Vriens, B., Lenz, M., Charlet, L., Berg, M. and Winkel, L. H. E.: Natural wetland emissions of methylated trace elements, *Nat. Commun.*, 5, doi:10.1038/ncomms4035, 2014.
- Walcek, C., De Santis, S. and Gentile, T.: Preparation of mercury emissions for eastern North America, *Environ. Pollut.*, 123, 375-381, 2003.
- Wallschläger, D., Turner, R. R., London, J., Ebinghaus, R., Kock, H.H., Sommar, J., and Xiao, Z. F.: Factors affecting the measurement of mercury emissions from soils with flux chambers, *J. Geophys. Res.-Atmos.*, 104, 21859-21871, 1999.
- Wang, S., Feng, X., Qiu, G., Wei, Z. and Xiao, T.: Mercury emission to atmosphere from Lanmuchang Hg-Tl mining area, Southwestern Guizhou, China, *Atmos. Environ.*, 39, 7459-7473, 2005.
- Wang, X., Lin, C.-J. and Feng, X.: Sensitivity analysis of an updated bidirectional air-surface exchange model for elemental mercury vapor, *Atmos. Chem. Phys.*, 14, 6273-6287, 2014.
- Watras C. J. and Bloom N. S.: Mercury and methylmercury in individual zooplankton: implication for bioaccumulation, *Limnol. Oceanogr.*, 37, 1313-1318, 1992.
- Wängberg, I., Schmolke, S., Schager, P., Munthe, J., Ebinghaus, R. and Iverfeldt, A.: Estimates of air-sea exchange of mercury in the Baltic Sea, *Atmos. Environ.* 35, 5477-5484, 2001.
- Wängberg, I., Munthe, J., Berg, T., Ebinghaus, R., Kock, H. H., Temme, C., Bieber, E., Spain, T.G. and Stolk, A.: Trends in air concentration and deposition of mercury in the coastal environment of the North Sea Area, *Atmospheric Environment*, 41, 2612-2619, 2007.
- Wesely, M. L., and Hicks, B. B.: A review of the current status of knowledge on dry deposition, *Atmospheric 1660 Environment*, 34, 2261-2282, 2000.
- WHO: WHO air quality guidelines for Europe, chapter 6.9, 2nd edition, WHO Regional Office for Europe, Copenhagen, Denmark, 2000.
- Wiedermann, M. M., Nordin, A., Gunnarsson, U., Nilsson, M. B. and Ericson, L.: Global change shifts vegetation and plant-parasite interactions in a boreal peatland, *Ecology* 88, 454-464, 2007.
- Won, J. H., Park, J. Y. and Lee, T.G.: Mercury emissions from automobiles using gasoline, diesel, and LPG, *Atmos. Environ.*, 41, 7547-7552, 2007.
- Wright, L. P. and Zhang, L.: An approach estimating bidirectional air-surface exchange for gaseous elemental mercury at AMNet sites, *J. Adv. Model. Earth Syst.*, 7, 35-49, 2015.
- Xiao, Z. F., Munthe, J., Schröder, W. H. and Lindqvist, O.: Vertical fluxes of volatile mercury over forest soil and lake surfaces in Sweden, *Tellus B*, 43, 267-279, 1991.
- Xin, M. and Gustin, M. S.: Gaseous elemental mercury exchange with low mercury containing soils: investigation of controlling factors, *Appl. Geochem.*, 22, 1451-1466, 2007.
- Xin, M., Gustin, M. and Johnson, D. Laboratory investigation of the potential for re-emission of atmospherically derived Hg from soils, *Environ. Sci. Technol.*, 41, 4946-4951, 2007.

## References

---

- Yu, R.-Q., Flanders, J. R., Mack, E. E., Turner, R., Mirza, M. B. and Barkay, T.: Contribution of coexisting sulfate and iron reducing bacteria to methylmercury. Production in freshwater river sediments, *Environ. Sci. Technol.*, 46, 2684-2691, 2012.
- Zehner, R. E. and Gustin, M. S.: Estimation of mercury vapor flux from natural substrate in Nevada, *Environ. Sci. Technol.*, 36, 4039-4045, 2002.
- Zhang, H. and Lindberg, S. E.: Sunlight and iron(III)-induced photochemical production of dissolved gaseous mercury in freshwater, *Environ. Sci. Technol.*, 35, 928-935, 2001.
- Zhang, H., Lindberg, S. E., Marsik, F. J. and Keeler, G. J.: Mercury air/surface exchange kinetics of background soils of the Tahquamenon river watershed in the Michigan Upper Peninsula. *Water, Air, Soil Pollut.*, 126, 151-169, 2001.
- Zhang, H., Lindberg, S. E., Barnett, M. O., Vette, A. F. and Gustin, M. S.: Dynamic flux chamber measurement of gaseous mercury emission fluxes over soils. Part 1: simulation of gaseous mercury emissions from soils using a two-resistance exchange interface model, *Atmospheric Environment* 36, 835e846, 2002.
- Zhang, L. M., Wright, L. P. and Blanchard, P.: A review of current knowledge concerning dry deposition of atmospheric mercury, *Atmos. Environ.*, 43, 5853-5864, 2009.
- Zhang, L., Wang, S., Wu, Q., Wang, F., Lin, C.-J., Zhang, L., Hui, M., Yang, M., Su, H. and Hao, J.: Mercury transformation and speciation in flue gases from anthropogenic emission sources: a critical review, *Atmos. Chem. Phys.*, 16, 2417-2433, 2016.
- Zhu, W., Sommar, J., Lin, C.-J., and Feng, X.: Mercury vapor air-surface exchange measured by collocated micrometeorological and enclosure methods – Part I: Data comparability and method characteristics, *Atmos. Chem. Phys.*, 15, 685-702, 2015a.
- Zhu, W., Sommar, J., Lin, C.-J. and Feng, X.: Mercury vapor air-surface exchange measured by collocated micrometeorological and enclosure methods – Part II: Bias and uncertainty analysis, *Atmos. Chem. Phys.*, 15, 5359-5376, 2015b.
- Zhu, W., Lin, C.-J., Wang, X., Sommar, J., Fu, X. W., Feng, X.: Global observations and modeling of atmosphere-surface exchange of elemental mercury – A critical review, *Atmos. Chem. Phys.*, 16, 4451-4480, 2016.

# Appendix

## Supporting Information to Chapter 2

- Table S2.1: To enable reproducibility of the system, the main REA components and their quantity, their manufacturing company, the county of origin and model number is given. The capital letters in the Index column of the table point to the components in Figure 2.1 in the main text.
- Figure S2.1: The manual calibration of the Hg detector was done after each measurement campaign in the laboratory in Basel and in situ at Degerö. Repeated injections of a GEM concentration to both air streams, every 30 min, resulted in 8 and 18 data points for each linear regression fit in Basel and Degerö, respectively.
- Figure S2.2: Limitations in turbulence mixing were defined applying a turbulence characteristic test (Eq. 2.8). 6% of the data in Basel and 4% at Degerö were rejected due to insufficient turbulence. The threshold (green dotted lines) is defined as a deviation of 2 from the model. Measurements beyond that point were rejected.
- Figure S2.3: The systematic bias in “same-air” measurements caused by the sampling line offset was corrected for in the GEM flux calculation. The strict rejection criteria allow a maximum standard deviation of the offset of 0.05 and a maximum difference in gold cartridge response of 10%. At both sites gold cartridge pair 1-3 failed the bias test. In Basel the standard deviation of the offset was too high (Fig S2.3a, blue line) and at Degerö the difference in the gold cartridge response between C1 and C2 was greater than the defined threshold (Fig S2.3a, blue line).
- Figure S2.4: The substandard performance of gold cartridge pair 1-3 was confirmed by plotting the difference between the updraft and downdraft integrated air samples to the updraft air sample. The gold cartridge pair 1-3 data (blue dots) scatter considerably more compared to gold cartridge pair 2-4 (red dots) indicating a malfunction in a piece of equipment (Teflon® PTFE Isolation Valves in energized status).
- Figure S2.5: The polar histograms show how the 30 min averages of wind speed, GEM concentration and wind direction are distributed at both sites during the campaigns. The polar histograms a) and b) describe the situation in Basel and c) and d) at Degerö.
- Figure S2.6: The fast-response valve switching frequency (30 min average) was considerably higher at Degerö (red) compared to Basel (black) indicating the presence of smaller eddies. The switching interval tended to increase with increasing friction velocity.
- Figure S2.7: Turbulence regimes have been investigated at both sides. Integral REA flux damping factors dependent on wind speed and stability conditions were derived. The simulation indicates that considerable flux damping in Basel occurs just during

unstable conditions and low wind velocities (a). At Degerö, the integral damping factor is considerable during stable conditions and high wind velocities (b).

- Figure S2.8: The total REA flux damping factor at average wind speeds at both sites increased with increasing wind speed during stable conditions. In Basel REA flux damping just occurred at very low frequency ranges.

**Table S2.1:** Most important REA components. They are indexed in the text and in the schematic of the REA system hardware (Fig. 2.1) with capital letters.

Index	Quantity	Components	Manufacturer	Country	Model number
A1	1	Sonic anemometer	Metek	GER	USA-1
A2	1	Sonic anemometer	Gill Instruments	UK	Solent1012R2
B	3	Rocker Solenoid Valves	Bürkert Fluid Control Systems	GER	6128 + 2507
C	1	LabVIEW 2011	National Instruments	USA	22.6.2011
D	100 m	PTFE tubing 1/4"	VICI AG International	SUI	JR-T-6810
E	3	0.2 µm PTFE filters	Merck Millipore	GER	SLFG65010
F	6	0.2 µm PTFE filters	Pall Corporation	USA	Acro 50, 4400
G	10	PTFE Isolation Valves	N Research	USA	SH360T041
H	1	Pressure transmitter	WIKA	GER	A-10
I	3	Red-y smart controller GSC	Vögtlin Instruments	SUI	3214101
J	1	Rotary vane pump	Gardner Denver GmbH	GER	G 08
K	3	Uniplast boxes	Swibox	SUI	UCP 540/750
L	1	Dynacalibrator	VICI AG International	SUI	150
M	1	CVAFS Hg Detector	TEKRAN Inc.	CAN	2500
N	1	Swing piston vacuum pump	KNF Neuberger	GER	NPK 09 DC
O	1	Pressure gauge with water trap	Servatechnik	SUI	-
P	1	¼" Hydrocarbon trap	Chromatography R.S, Inc.	USA	300
Q	20 L	Argon gas (purity>99.9997%)	Air Liquide S.A.	FRA	N57
R	1	Hg Vapor Calibration Unit	TEKRAN Inc.	CAN	2505
S	1	Digital gas-tight syringe	Hamilton	USA	1700
T	1	Hg Zero-Air Generator	TEKRAN Inc.	CAN	1100

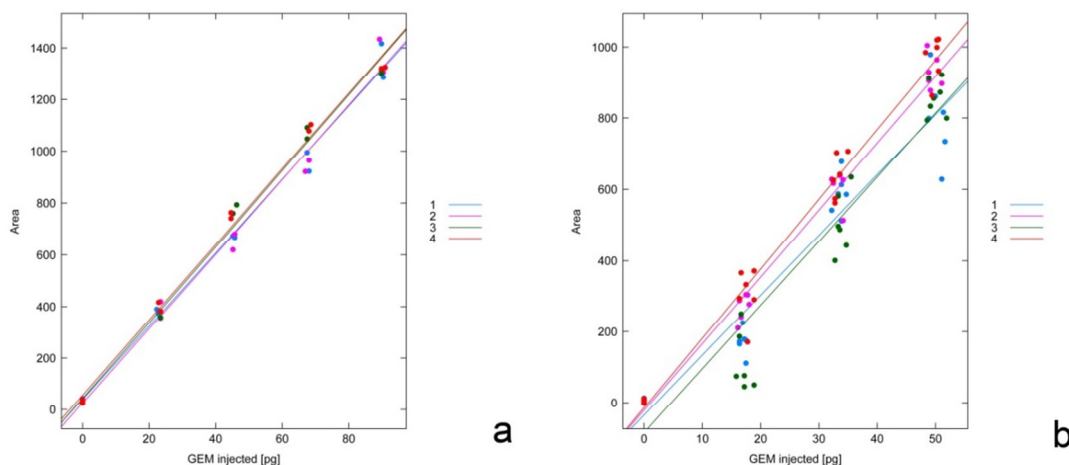


**Figure S2.1:** Linear relationship between detected GEM reference gas concentration on each of the four gold cartridges (Area, 1-4) and manually injected GEM [pg] for Basel (a) and Degerö (b).

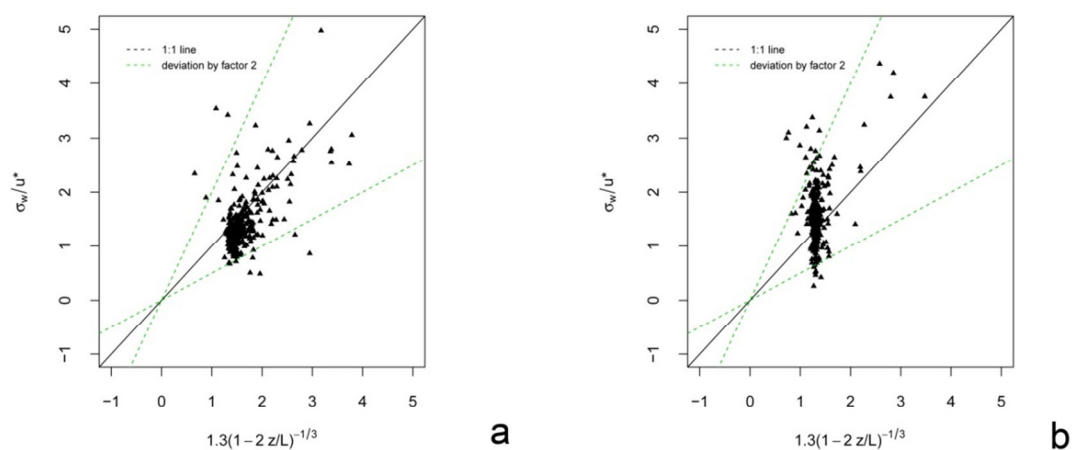


**Figure S2.2:** A deviation by more than a factor of 2 from the model (green dotted line) was used as the threshold to reject data measured in Basel (a) and Degerö (b) during periods of insufficient and larger than expected turbulence.

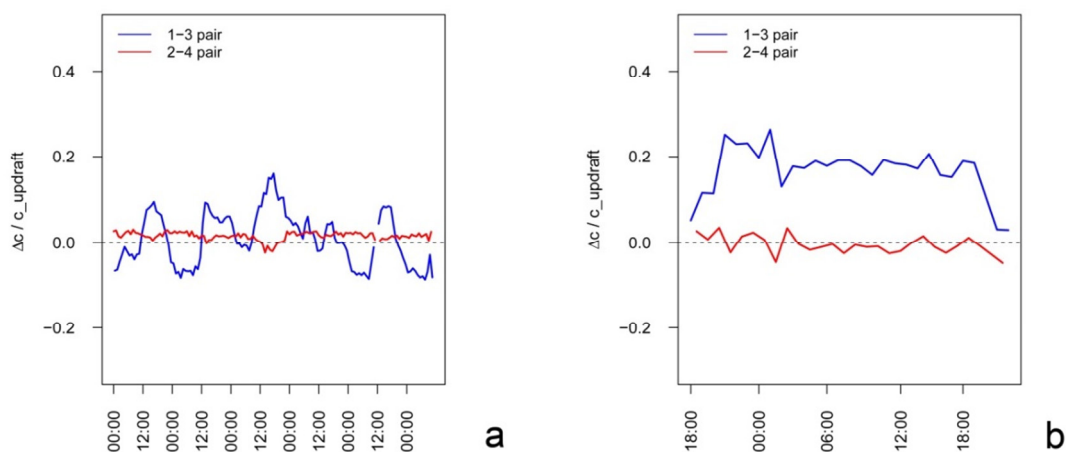


**Figure S2.3:** Precision in concentration difference measurements of the same GEM concentration between gold cartridge pair 1-3 (blue) and 2-4 (red) in Basel (a) and at Degerö (b).

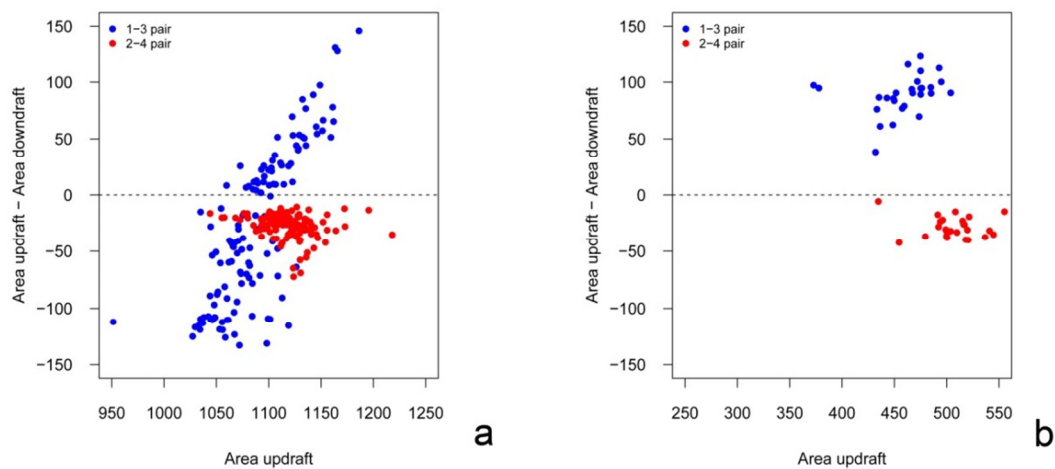


**Figure S2.4:** Ratio of the difference between the updraft and downdraft integrated air sampling to the updraft signal for both gold cartridge pairs during the bias test in Basel (a) and Degerö (b).

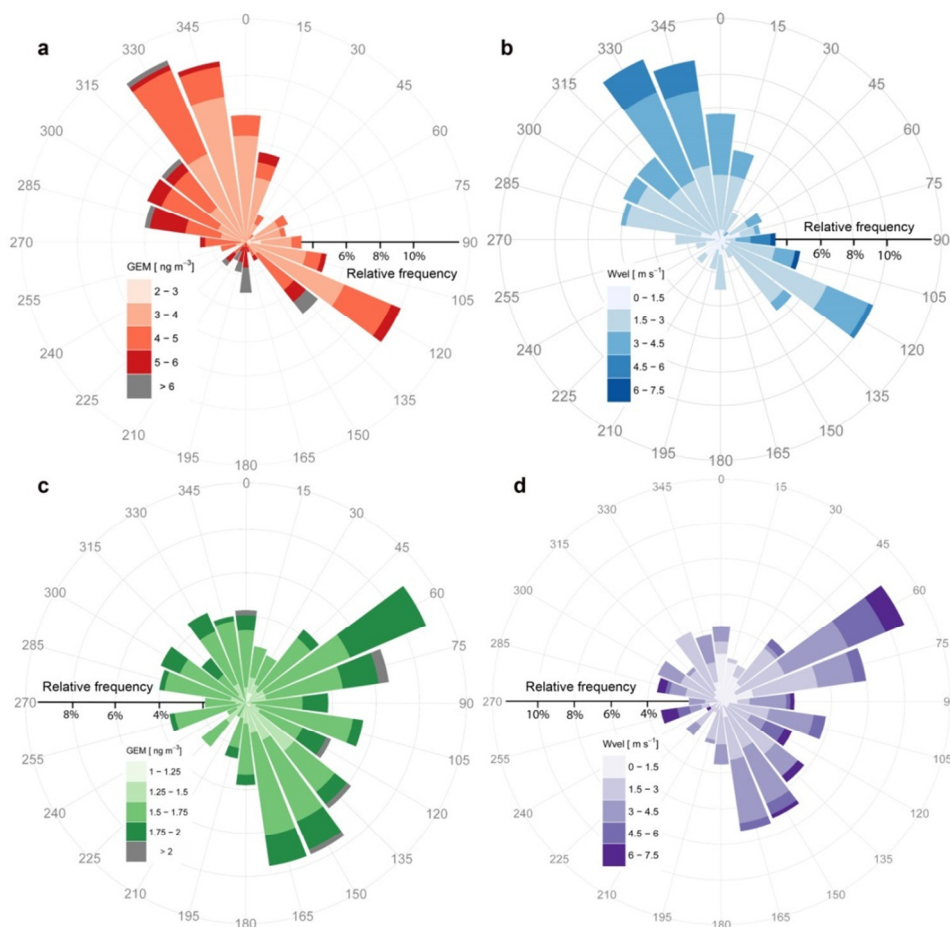


**Figure S2.5:** GEM concentration (a) and wind rose (b) during the Basel campaign and GEM concentration (c) and wind rose (d) during the Degerö campaign. Polar histograms show 30 min averaged GEM concentrations ( $\text{ng m}^{-3}$ ) and wind speed ( $\text{m s}^{-1}$ ).

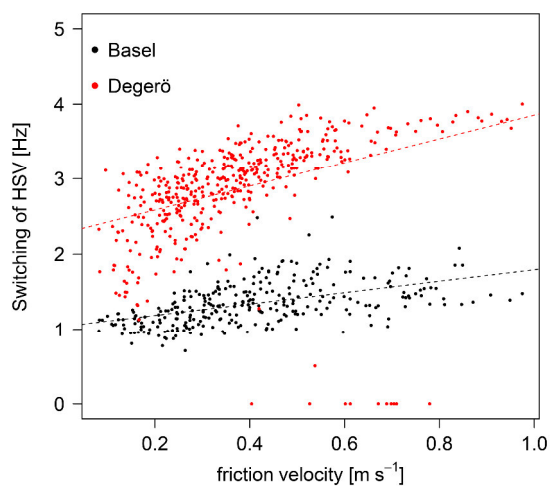


**Figure S2.6:** 30 min averaged switching frequency of fast-response valves (HSV) at Basel (black) and Degerö (red) in relation to friction velocity.

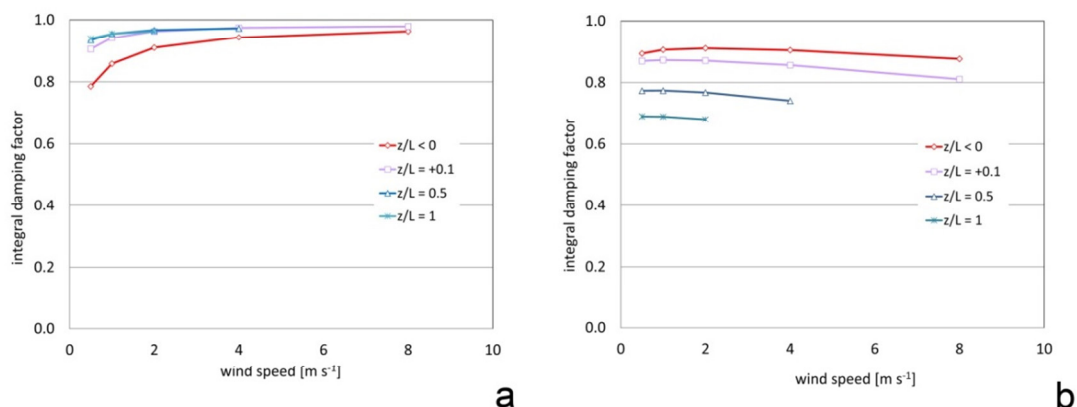


**Figure S2.7:** Simulated integral damping factors for REA fluxes in Basel (a) and Degerö (b) dependent on wind speed (0 - 10  $\text{m s}^{-1}$ ) and stability conditions: Unstable ( $z/L < 0$ ); stable ( $z/L = 0.1$ ,  $z/L = 0.5$ ,  $z/L = 1$ ).

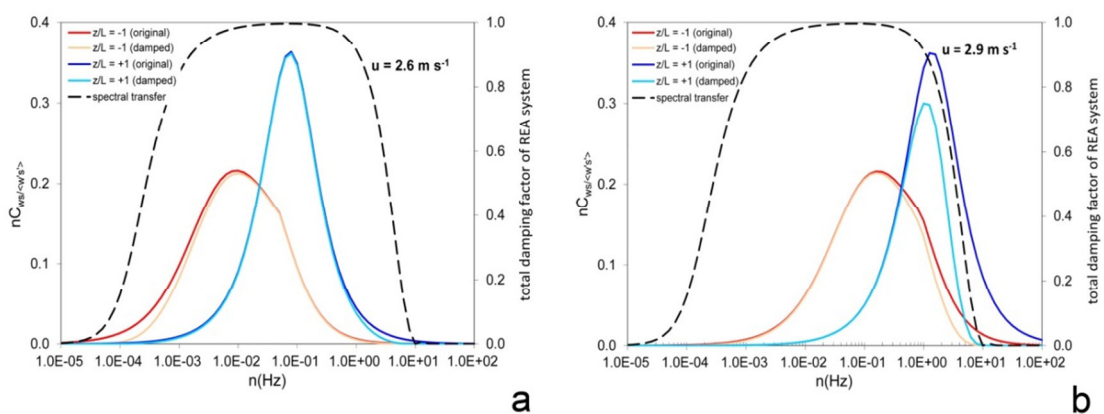


**Figure S2.8:** Modeled original and damped cospectral density and total damping factor (secondary y-axis) of REA system for Basel (a) and Degerö (b) dependent on stable ( $z/L = +1$ ) and unstable ( $z/L = -1$ ) conditions and mean horizontal wind speeds for both sites ( $u = 2.6$  and  $2.9 \text{ m s}^{-1}$ , respectively).





## Supporting Information to Chapter 3

### S3.1 Research site and REA footprint

The Degerö catchment is predominantly drained by the stream Vargstugbäcken northwest of the REA tower (Fig S3.1a). 71% of the 1.9 km<sup>2</sup> catchment consists of peat, 29% of mineral soils (till). The potential contribution of THg from the mineral soils to the calculated fluxes is considered low due to the spatial arrangement of the till and peat relative to the stream (Figs. S3.1, S3.2a). The micro-topography within the source area of the gaseous elemental mercury (GEM) flux is characterized mainly by carpets and lawns, with sparse occurrences of hummocks. The vascular plant community in this area was dominated by *Eriophorum vaginatum* L., *Trichophorum cespitosum* L. Hartm., *Vaccinium oxycoccos* L., *Andromeda polifolia* L., and *Rubus chamaemorus* L. On the bottom of the carpets *Sphagnum majus* C. Jens. is prevalent while *Sphagnum balticum* C. Jens. dominates the lawn. On the hummocks *Sphagnum fuscum* Schimp. Klinggr. and *Sphagnum rubellum* Wils. are the most common mosses (Nilsson et al., 2008; Laine et al., 2012).

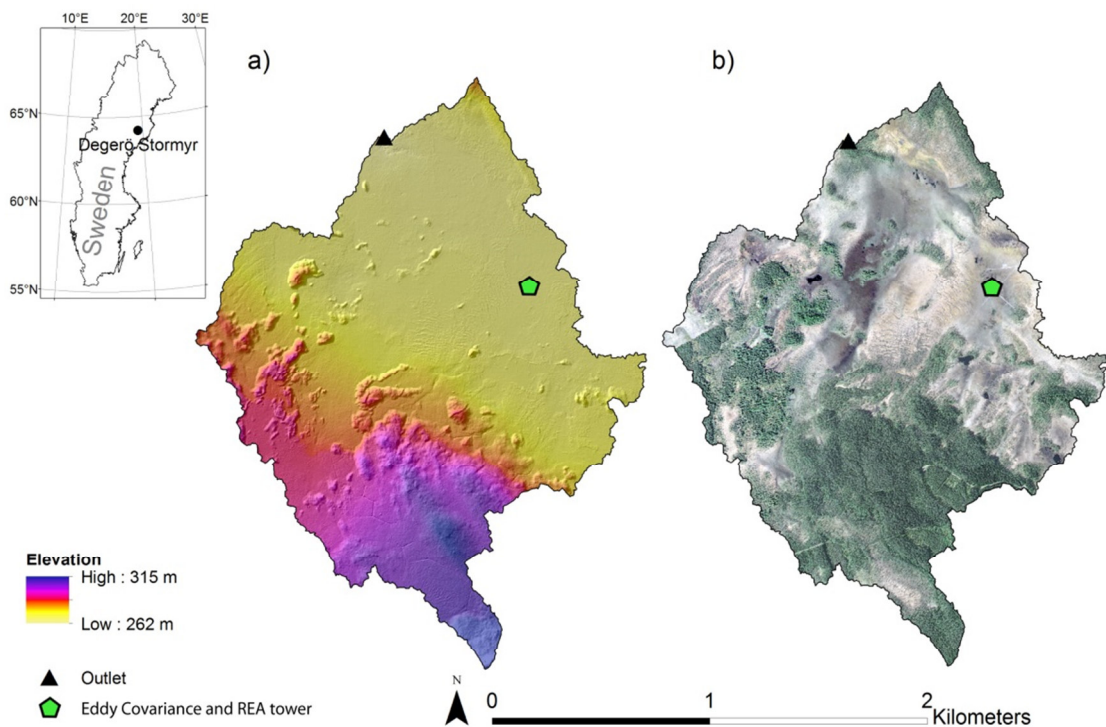


**Figure S3.1:** Map of the Degerö Stormyr catchment, located in northern Sweden (from Leach et al., 2016). Digital elevation model of the catchment derived from LiDAR (a) and aerial photo (b). The location of the eddy covariance and REA tower is indicated by a green pentagon. The black triangle indicates the catchment outlet. GIS data sources are from the Swedish Mapping, Cadastral and Land Registration Authority.

In order to confirm the homogeneity of the footprint, i.e. to assure that forest areas do not considerably influence the GEM source area, the REA footprint (Fig. S3.2b) was calculated using a Lagrangian stochastic forward model (Rannik et al., 2000). Data were based on measurements between March 7 and June 26, 2014. 50%, 80% and 95% of the total GEM flux

source area covered 0.4, 2.5 and 10.1 ha, respectively. The roughness length was set to 0.02 m. The main wind direction during periods when the footprint was calculated was SW (Fig. S3.2c)

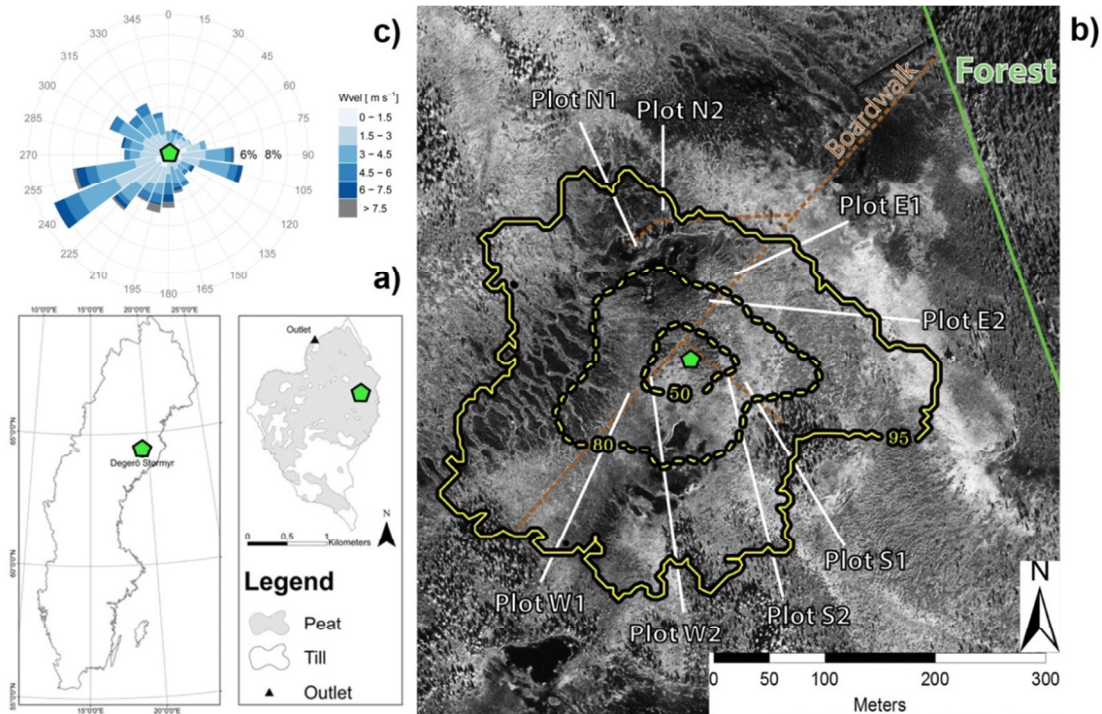


**Figure S3.2:** Location and catchment area of Degerö Stormyr adapted from Figure S3.1 (a). Soil types are indicated by hatched (peat) and blank (till) areas. Aerial photograph with yellow contours containing 50%, 80% and 95% of the REA footprint calculated using 2841 half-hourly flux values between March 7 and June 26, 2014 (b). Eight plots are indicated where the peat cores were taken and DGM was analyzed. The green pentagon indicates the location of the REA tower. Polar histogram of the 30 min averaged wind speed ( $\text{m s}^{-1}$ ) measured at 3.5 m above the surface (c).

### S3.2 Hg in the peat

The pool of total Hg (THg) in the peat was calculated from eight depth profiles of measured THg concentrations and bulk density (Fig. S3.3, Tab. S3.1). The peat dating was derived from mean vertical peat growth rate at Degerö determined by Olid et al. (2014). For the period from 2003 to 2015 a peat growth rate of  $0.8 \text{ cm yr}^{-1}$  was applied. In the older peat layers ( $> 12 \text{ yr}$ ) the vertical growth rate values were  $0.4 \text{ cm yr}^{-1}$ .

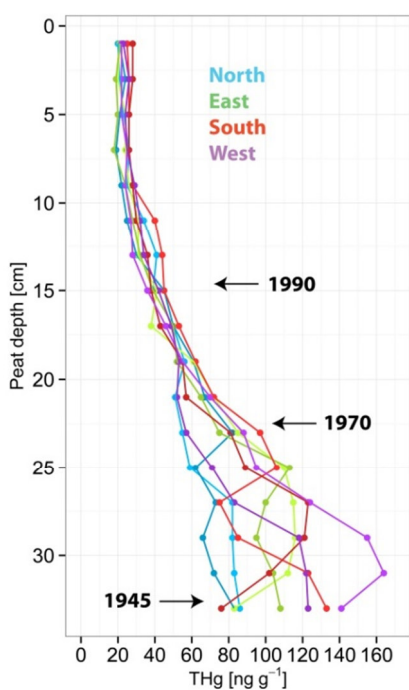


**Table S3.1:** Mean  $\pm$  SE ( $n = 8$ ) concentration profile of Hg (THg<sub>c</sub>) and stored Hg within each depth interval (THg<sub>s</sub>) from eight peat cores. Linear depth, bulk density, estimated peat age (year) and accumulation rate of Hg (HgAR) are also given.

Depth (cm)	THg <sub>c</sub> (ng g <sup>-1</sup> )	THg <sub>s</sub> (μg m <sup>-2</sup> )	Bulk density (g cm <sup>-3</sup> )	year <sup>a</sup>	HgAR (μg m <sup>-2</sup> yr <sup>-1</sup> )
0-2	22.6 ± 0.9	10.0 ± 0.7	0.022	2014	4
2-4	23.3 ± 1.1	8.7 ± 0.9	0.019	2011	3
4-6	23.3 ± 0.8	9.7 ± 0.8	0.021	2009	4
6-8	23.6 ± 1.1	10.4 ± 0.7	0.022	2006	4
8-10	25.8 ± 0.9	13.0 ± 0.9	0.026	2004	5
10-12	30.9 ± 1.7	17.8 ± 1.2	0.029	1999	4
12-14	34.5 ± 2.0	23.6 ± 2.5	0.034	1994	5
14-16	40.6 ± 1.1	30.3 ± 3.3	0.038	1989	6
16-18	47.4 ± 1.7	34.8 ± 3.1	0.037	1984	7
18-20	56.9 ± 1.4	47.9 ± 4.6	0.042	1979	10
20-22	63.3 ± 3.1	57.3 ± 5.8	0.045	1974	11
22-24	77.5 ± 5.2	77.1 ± 9.4	0.048	1969	15
22-26	88.1 ± 7.7	91.4 ± 11.9	0.051	1964	18
26-28	96.9 ± 7.6	99.7 ± 13.3	0.051	1959	20
28-30	104.8 ± 10.0	100.7 ± 12.2	0.049	1954	20
30-32	110.3 ± 9.9	122.6 ± 15.8	0.055	1949	25
32-34	104.1 ± 9.0	127.5 ± 12.3	0.063	1944	26

a) dated after Olid et al. (2014)

**Figure S3.3:** Depth profile of total Hg (THg) concentrations from eight peat cores paired in all cardinal directions.

### S3.3 Hg in wet bulk deposition

Cumulative atmospheric wet bulk deposition of Hg for Degerö was derived from wet bulk deposition data from Bredkålen ( $3.9 \mu\text{g m}^{-2} \text{yr}^{-1}$ ), located ~210 km west of Degerö and from precipitation data at Degerö. Hg wet bulk deposition was within the range of measurements conducted at Råö ( $5.6 \mu\text{g m}^{-2} \text{yr}^{-1}$ ) and Pallas ( $1.5 \mu\text{g m}^{-2} \text{yr}^{-1}$ ), located ~850 km southwest and ~470 km northeast of Degerö, respectively. Continuous Hg wet bulk measurements at Råö ( $57^{\circ}24'N$ ,  $11^{\circ}55'E$ ), Bredkålen ( $63^{\circ}51'N$ ,  $15^{\circ}20'E$ ) and Pallas ( $67^{\circ}58'N$ ,  $24^{\circ}07'E$ ) were conducted by the Swedish Environmental Research Institute (IVL) as part of the European Monitoring and Evaluation Programme (EMEP).

**Table S3.2:** Precipitation (Precip), total mercury concentrations in the precipitation samples ( $\text{Hg}_p$ ) and total mercury in wet bulk deposition ( $\text{Hg}_D$ ) measured at Bredkålen. Wet bulk deposition of Hg for the Degerö catchment ( $\text{Hg}_D$ ) was derived from precipitation measurements 1 km east of Degerö Stormyr.

Timespan		Bredkålen			Degerö	
		Precip (mm)	$\text{Hg}_p$ ( $\text{ng L}^{-1}$ )	$\text{Hg}_D$ ( $\text{ng m}^{-2}$ )	Precip (mm)	$\text{Hg}_D$ ( $\text{ng m}^{-2}$ )
18.06.2013	02.07.2013	80.1	5.9	252.2	60.3	354.4
02.07.2013	30.07.2013	96.9	12.7	1234.9	51.5	656.3
30.07.2013	03.09.2013	88.0	5.5	484.9	91.9	506.4
03.09.2013	01.10.2013	97.2	2.4	229.1	69.1	162.9
01.10.2013	29.10.2013	32.6	2.8	92.1	47.7	134.7
29.10.2013	03.12.2013	24.5	3.1	76.7	47.4	148.5
03.12.2013	31.12.2013	26.0	4.0	103.3	64.9	257.9
31.12.2013	04.02.2014	9.7	11.4	110.6	36.4	415.0
04.02.2014	04.03.2014	24.2	6.7	163.1	62.1	418.5
04.03.2014	01.04.2014	24.9	6.1	152.4	13.9	85.1
01.04.2014	29.04.2014	1.8	42.4	76.3	1.8	76.3
29.04.2014	03.06.2014	80.0	7.1	564.3	50.9	359.0
03.06.2014	17.06.2014	55.2	12.4	332.6	23.1	324.8

### S3.4 Peatland-atmosphere flux of gaseous elemental Hg

Vertical wind velocity ( $w$ ) was measured with a USA-1 sonic anemometer (Metek, Elmshorn, Germany) at 3.5 m height. Its signal determined the switching frequency of the fast-response solenoid valves that isolated GEM in up- and downdrafts. GEM was collected on two pairs of gold cartridges and analyzed every 30 min with a CVAFS Hg detector (Tekran Model 2500, Toronto, Canada). The turbulent GEM flux ( $\text{ng m}^{-2} \text{h}^{-1}$ ) was computed according to Equation 2.1.  $\beta$  was derived from concurrent eddy covariance measurements of sensible heat flux for each averaging period. A fixed zero centered dead band to omitted sampling if  $w_0 \pm 0.2 \text{ ms}^{-1}$  was introduced to enlarge the GEM concentration difference. Bias in vertical wind measurements was removed through the application of a recursive high-pass filter. The air was drawn through 8.5 m long Teflon® PTFE sampling tubes and was conditionally sampled at a flow rate of  $1.5 \text{ L min}^{-1}$ . The system was placed within a dome shaped plexiglass container (Igloo Satellite Cabin, Icewall One, Australia), which also houses the main part of ICOS instrumentation.

The system hardware was improved as suggested in a previous study (Osterwalder et al., 2016): (i) the Hg detector and the Hg reference gas generator were kept at a constant ambient temperature of  $25^\circ\text{C}$ , (ii) a pair of pressure sensors and a second set of fast response valves (V1.2, V2.2, V2.3) were implemented to better control pressure fluctuations and (iii) the up- and downdraft air volumes were now measured with two high precision thermal mass flow meters (Vögtlin Instruments, Aesch, Switzerland) (Fig. S3.4).

The analyzed air samples were corrected for changes in sensitivity of the gold cartridges and the Hg detector. The GEM concentrations were calculated considering results from the manual calibration procedure and air volumes drawn over the gold cartridges (minimum of 3 L per gold cartridge). They were discarded when differing more than 3 times the standard deviation of their moving average (window width of 48 observations). GEM concentrations were corrected for the bias between the two sampling lines by interpolation between reference mode sampling. GEM fluxes were discarded due to poorly developed turbulence (Foken et al., 2006, Osterwalder et al., 2016) and in general during periods of very stable atmospheric conditions ( $z/L > 2$ ). Short gaps in the flux time series smaller than 9 observations were filled using a standard look-up table (LUT) method (Falge et al., 2001). Therefore, a LUT with 6 fixed intervals for solar radiation was used to “look up” GEM flux at similar meteorological conditions. After gap filling (+ 14% of the data), the total number of 30 min observations during growing- and non-growing season and the snow season was 3417, 1563 and 466 respectively.

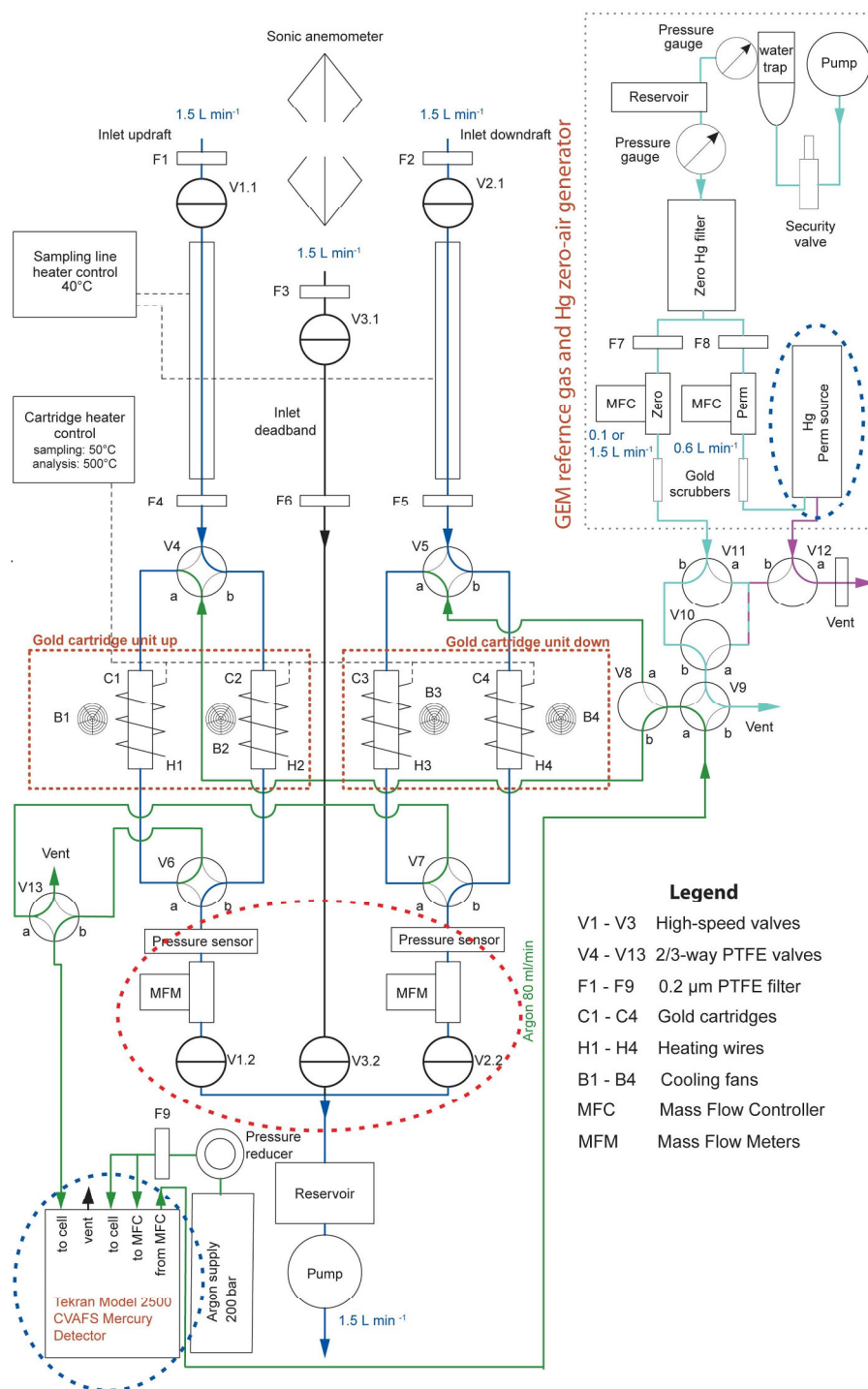


**Figure S3.4:** Schematic of the REA system hardware consisting of a GEM sampling unit, a GEM reference gas and Hg zero-air generator (upper right). The major novelties compared to the system presented in Figure 2.1 are marked with dashed ellipses.



### S3.5 Hg in catchment discharge

Stream discharge at the catchment outlet has been measured continuously at a flume within a heated hut since 2008 (Fig. S3.1). Stream water was sampled in high-density polyethylene bottles on a monthly basis. The THg samples were preserved, within 24 - 48 h after the sampling, by adding 0.7 mL suprapur HNO<sub>3</sub> to the 125 mL samples.

THg analysis was performed by the Stockholm University Department of Applied Environmental Science on unfiltered water samples by using cold vapor atomic fluorescence spectroscopy (CV-AFS) after oxidation by BrCl and reduction to Hg<sup>0</sup> with SnCl<sub>2</sub>. The detection limit was 0.3 ng L<sup>-1</sup> and the analytical precision was ±3% for THg in a concentration range of 5 - 50 ng L<sup>-1</sup>.

The THg concentrations did not correlate with the discharge rate on the day of sampling (data not shown). To calculate the total loss of THg from the Degerö catchment in stream discharge (Tab. S3.3), stream THg concentrations were interpolated linearly between sampling occasions and multiplied by the daily discharge.

Atmospheric wet bulk deposition and GEM uptake by plants are the only new Hg sources to the peatland catchment that can offset either emission to the atmosphere or discharge from the catchment. The diffuse flow of water from mineral soils surrounding the peatland into the peatland itself mostly occurs far from the stream outlet. Due to the strong binding properties of peat for metals, the metals in groundwater from the mineral soil areas are generally held in the organic peat directly adjacent to where the water from the mineral soil enters the peat in the “lag” zone (Lidman et al., 2014).

**Table S3.3:** Monthly total mercury in discharge (THg) and total discharge from the catchment (10<sup>6</sup> L).

Month	THg (ng m <sup>-2</sup> )	Discharge (10 <sup>6</sup> L)
Jul 13	89.9	35.5
Aug 13	70.6	32.4
Sep 13	107.2	77.5
Oct 13	111.2	73
Nov 13	126.6	77.6
Dec 13	53.3	32.8
Jan 14	37.3	22.9
Feb 14	3.8	2.7
Mar 14	39.9	21.6
Apr 14	463.3	245.3
May 14	129.5	95.2
June 13/14	73.6	41.4
Annual total	1307	759

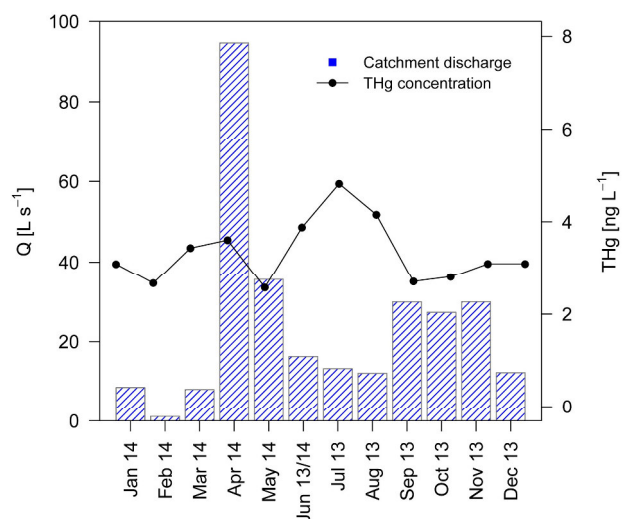


**Figure S3.5:** Monthly averages of catchment discharge (Q) and total Hg (THg) concentration in the discharge.

### S3.6 Dissolved gaseous Hg in the peat pore water

Once a week from June - October 2013 and May - July 2014 four peat pore-water samples were taken from the same areas as the peat cores were extracted (Fig. S3.2). Pore-water was sucked from the water table level down to 10 cm using a Teflon® FEP pole connected to a rotary vane pump and collected in a 1 L Teflon® PFA vessel protected from sunlight to eliminate photolytic reactions (Fig. S3.6). Before sampling the vessel was acid washed, cleaned with ultrapure water (Milli-Q, 18.2 M $\Omega$ -cm, Millipore Corp.) and rinsed with peat pore water. Polyethylene gloves were worn during the sampling and analysis. The vessels were immediately transferred to the onsite field laboratory (< 5 min) and placed in a water bath protected from sunlight with temperatures kept close to the temperature of the peat pore water. The samples were then analyzed using a Tekran Automated Purging System after Lindberg et al. (2000).

For purging, the inlet line to the Hg analyzer (Tekran Model 2537A, Toronto, Canada) was connected to the vessel outlet at the beginning of a measurement sequence. The outlet airstream was mixed with a stream of Hg-free air (0.2 L min<sup>-1</sup>). The Hg analyzer was set to a flow rate of 1.2 L min<sup>-1</sup> and purged the vessel at a rate of 1 L min<sup>-1</sup> (Fig. S3.6). Twelve, 5 min purge samples were collected for a total of 60 min (40 min sample, 20 min whole-blank). At the vessel inlet an activated carbon trap supplied Hg-free air. The flow rates were continuously controlled using digital mass flow controllers (Red-y compact series, Vögtlin, Aesch, Switzerland) to identify potential leaks during the measurement. The blanks were tested prior to every sampling by purging the vessel filled with ultrapure water. The measurements declined immediately to values below the detection limit (~0.5 pg). The diurnal pattern of the DGM concentrations showed a slight increase of the median from noon to 3 PM (Fig. S3.7).

The DGM concentration was calculated from the difference between the sample that was purged free of DGM and the whole-blank purge. This difference was then expressed on a water volume basis. The average whole-blank signal was 2.5% and was always below 9%. The DGM concentrations showed a distinct seasonal pattern and ranged from 2 pg L<sup>-1</sup> (May 2014) to 82 pg L<sup>-1</sup> (July 2014). In 86% of the measurements the peatland pore water was supersaturated with DGM. The degree of saturation is calculated by the ratio of Henry's law constant times DGM concentration divided by the atmospheric GEM concentration (Eqs. in Gårdfeldt et al., 2001).



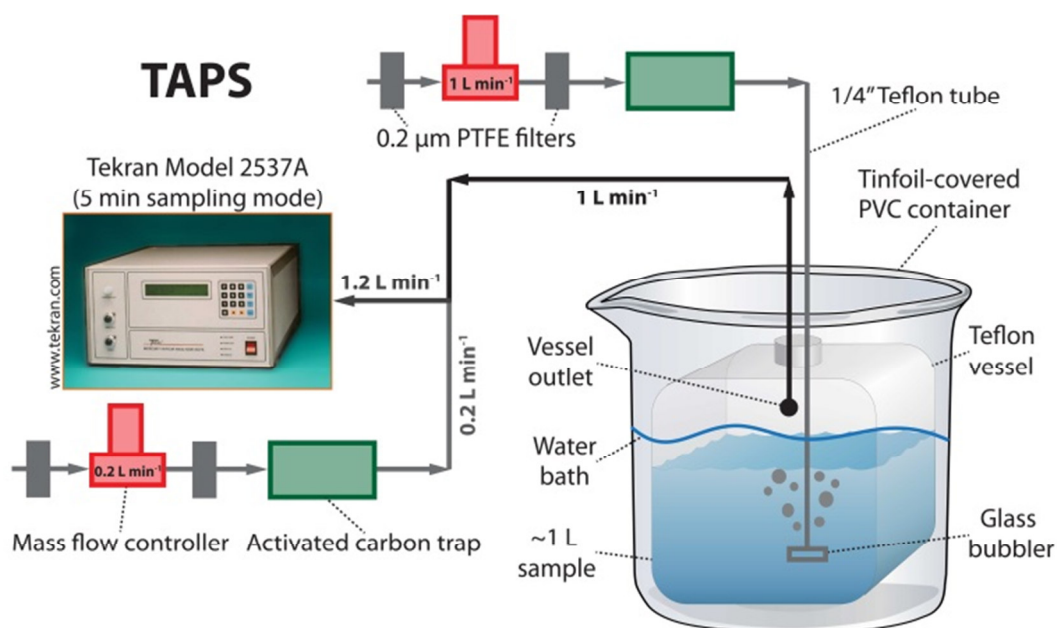
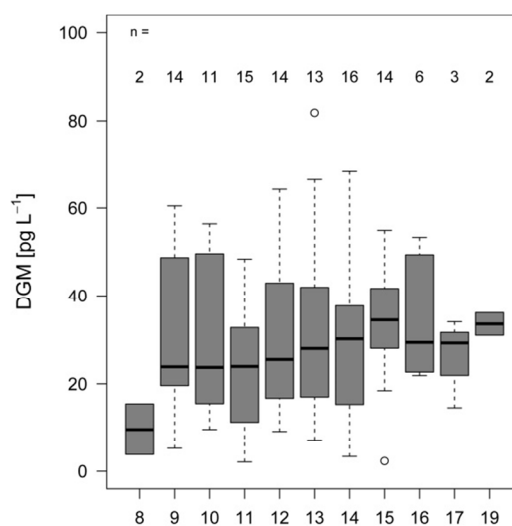


**Figure S3.6:** Schematic of dissolved gaseous Hg (DGM) measurement setup adapted from the Tekran Automated Purge System (TAPS) described in Lindberg et al. (2000).



Time of day (18.06. – 09.10.2013 and 02.05. – 17.07.2014)

**Figure S3.7:** Diurnal pattern of dissolved gaseous mercury (DGM) measurements performed in every cardinal direction on one day per week from 18.06 - 09.10.2013 and 02.05 - 17.07.2014. The bold line in the box represents the median DGM concentration. The horizontal border lines indicate the 25<sup>th</sup> (Q1) and 75<sup>th</sup> (Q3) percentiles, from bottom to top. The lower whisker marks Q1 minus 1.5 times the interquartile range (IQR). The upper whisker marks Q3 plus 1.5 IQR.



## Supporting Information to Chapter 4

**Table S4.1:** Average of Teflon® PFA and new type dynamic flux chamber (TDFC and NDFC, respectively) measurements and plot parameters such as total Hg (THg) down to 34 cm depth, vascular plant cover (VP), water table level (WTL) and dissolved gaseous Hg (DGM) for each cardinal direction (N, E, S, W).

	N	E	S	W
THg [ng g <sup>-1</sup> ]	48.7	58.0	60.4	62.0
VP coverage [%]	32	38	38	52
WTL [cm]	4.5	14.1	12.6	13.9
DGM [pg L <sup>-1</sup> ]	28.0	50.9	46.2	36.0
TDFC [ng m <sup>-2</sup> h <sup>-1</sup> ]	1.0	0.7	0.3	0.6
NDFC [ng m <sup>-2</sup> h <sup>-1</sup> ]	1.9	3.2	1.3	1.4

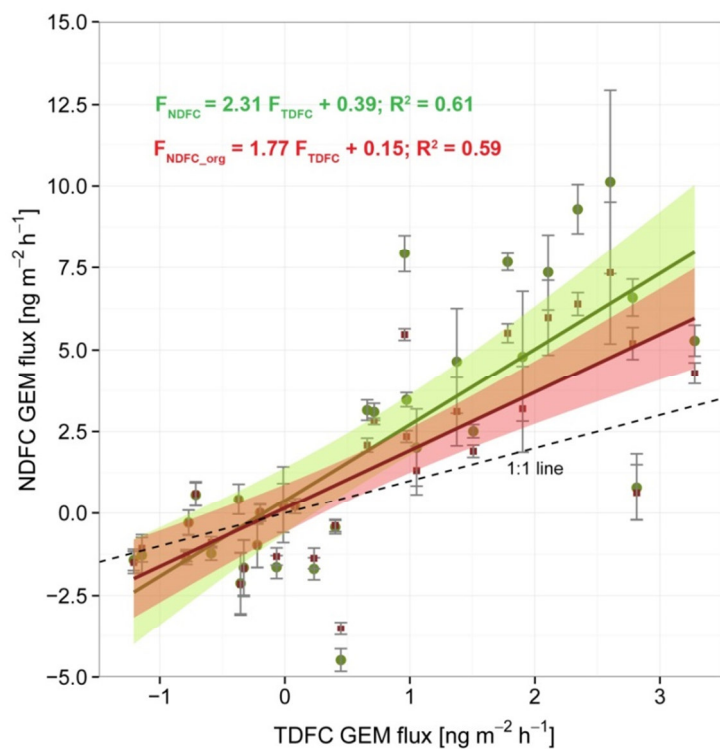


**Figure S4.1:** Scatterplot of GEM flux (mean  $\pm$  SE) obtained from shear corrected new type DFC (NDFC) measurements (Eq. 4.4) (green circles), and the NDFC calculated using Equation 4.3 (red squares) versus Teflon® PFA DFC (TDFC) flux.

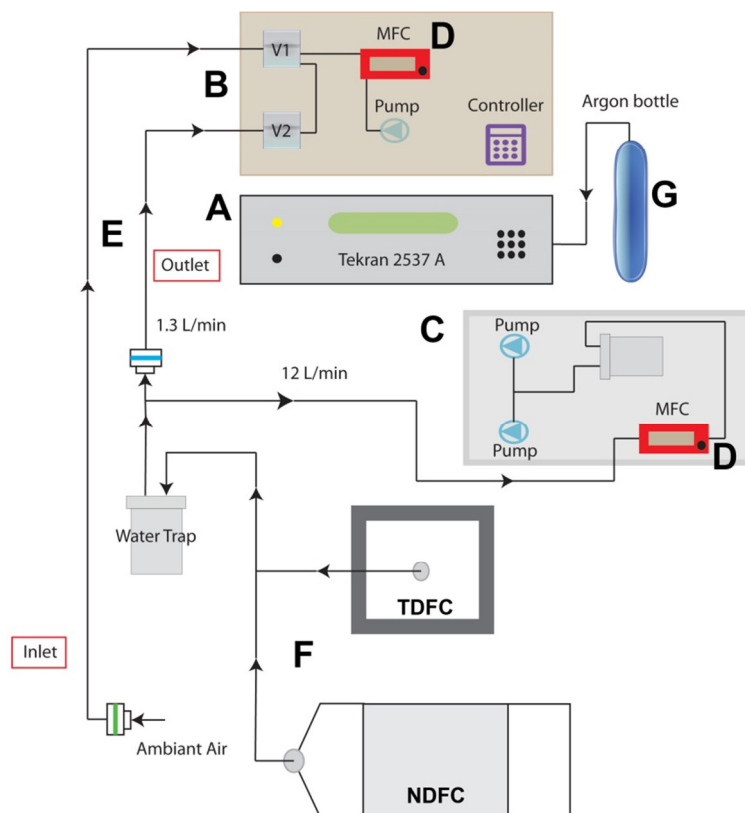


**Figure S4.2:** Setup for continuous GEM flux measurements with the Teflon® PFA DFC (TDFC) and new type dynamic flux chambers (NDFC) (F). The flushing unit (C) is placed close to the DFCs and connected to the detection valve unit (B) with 30 m of Teflon® PFA tubing (E). Pumps generate a continuous airflow ( $12 \text{ L min}^{-1}$ ) regulated by a mass flow controller (D) through the DFC (F).  $1.3 \text{ L air min}^{-1}$  is analyzed for GEM concentrations using a Hg detector (Tekran Model 2537A) (A). High-purity Ar is the carrier gas (G). Alternately, GEM concentrations inside and outside the DFC are determined and used to calculate the GEM flux (Eqs. 4.3 and 4.4).

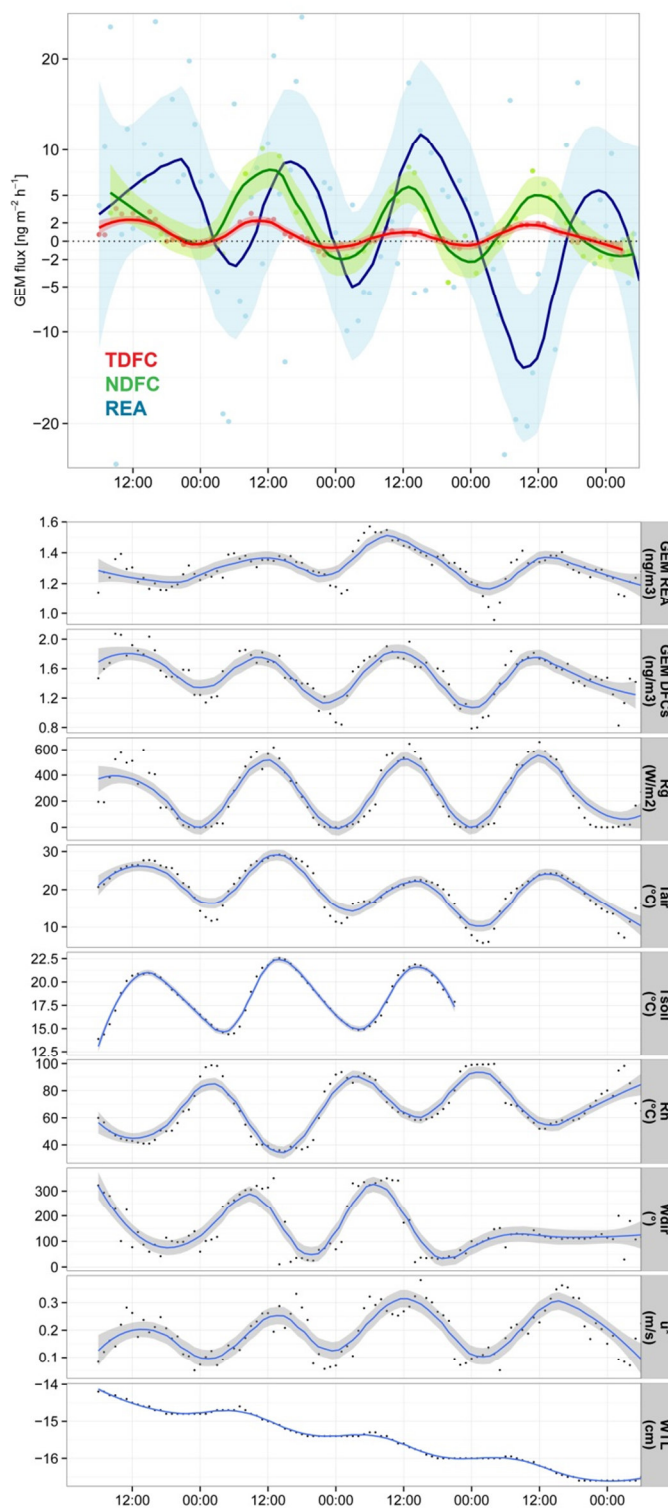


**Figure S4.3:** Time series of GEM fluxes measured with Teflon<sup>®</sup> PFA DFC (TDFC), new type DFC (NDFC) and the relaxed eddy accumulation (REA) system. Atmospheric GEM concentrations derived from both methods (REA and DFCs), global radiation ( $R_g$ ), air temperature ( $T_{\text{air}}$ ), soil temperature ( $T_{\text{soil}}$ ), relative humidity ( $R_h$ ), wind direction ( $^{\circ}$ ), friction velocity ( $u^*$ ) and water table level (WTL) during the campaign are illustrated. Black dots are hourly averages. Locally weighted scatterplot smoothing (blue line) was applied (R v3.1.2, loess {stats}, span = 0.3) with a confidence interval level of 0.95 (grey band).



## Supporting Information to Chapter 6

**Table S6.1:** Summary of plot averaged atmospheric gaseous elemental Hg (GEM) concentrations and GEM fluxes as well as the soil parameters total Hg concentration (THg), pH, temperature (Tsoil) and moisture (Moist) and meteorological parameters such as air temperature (Tair) and wind velocity (Wvel).

Site	ID	GEM (ng m <sup>-3</sup> )	F <sub>GEM</sub> (ng m <sup>-2</sup> h <sup>-1</sup> )	THg (mg kg <sup>-1</sup> )	pH	Tsoil (°C)	Moist (%)	Tair (°C)	Wvel (m s <sup>-1</sup> )
VS015	91	2.2	71.3	0.2	5.7	19.2	6.8	22.6	0.35
	92	2.2	50.8	0.2	6.3	19.3	9.5	22.8	0.40
	93	2.1	16.6	0.7	6.7	19.6	7.9	23.7	0.38
HW108	11	2.8	37.2	0.4	7.3	20.2	38.4	17.6	1.47
	12	2.5	28.0	0.4	7.2	20.3	38.3	17.3	1.45
	13	2.5	49.1	2.1	7.3	20.3	33.7	17.5	1.58
HK081b	31	3.2	119.8	2.7	7.6	17.1	27.0	15.7	0.23
	32	3.5	108.3	3.0	7.5	17.0	23.8	15.9	0.19
	33	3.8	109.4	2.5	7.7	17.1	31.0	16.1	0.28
TT9	51	3.5	31.9	2.6	7.6	19.7	44.0	19.2	0.87
	52	3.6	64.8	1.1	7.2	19.8	47.1	19.9	0.92
	53	3.7	187.3	4.4	7.7	19.7	47.3	19.3	1.04
HK045	21	2.8	176.2	1.4	7.3	20.4	28.3	16.8	0.68
	22	3.8	260.8	3.5	6.3	20.4	30.0	16.5	0.58
	23	3.3	269.4	3.5	6.8	20.4	33.0	16.5	0.71
XX32	41	3.5	179.9	8.8	7.4	20.6	38.7	20.3	1.40
	42	3.2	194.0	3.7	7.5	20.7	43.4	19.5	1.49
	43	3.2	247.6	10.2	7.2	20.5	39.0	19.6	1.32
T35	61	4.7	627.0	46.3	8.4	17.0	38.3	15.9	1.03
	62	4.8	610.4	38.8	8.1	17.3	39.6	16.0	1.00
	63	6.2	787.1	29.1	8.1	17.1	39.5	15.7	0.99
X2	71	4.0	129.5	12.8	7.2	17.6	28.9	19.3	0.71
	72	4.2	223.3	26.0	7.0	17.5	25.5	19.5	0.66
	73	4.2	169.2	12.0	7.8	17.5	32.4	19.3	0.61
VS009	81	6.8	1370.3	230.0	7.4	18.2	11.1	21.7	0.33
	82	7.4	1138.0	310.0	7.0	18.2	9.2	21.8	0.32
	83	7.8	1265.1	390.0	7.4	18.2	8.3	21.7	0.30

**Table S6.2:** Total Hg emission per sector, their trend from 1990 to 2010, 2005 to 2013 and their contribution to total emissions in 2012. LULUCF stands for Land-Use, Land-Use Change and Forestry. Source: BAFU (2015)

Hg emissions	1990	2005	2010	2013	1990-2010	2005-2013	share in 2013
	t	t	t	t	t	t	
1 Energy	4.17	0.42	0.39	0.35	-3.78	-0.07	40.4%
1A Fuel combustion	4.17	0.42	0.39	0.35	-3.78	-0.07	40.4%
1A1 Energy industries	3.91	0.33	0.29	0.24	-3.62	-0.09	27.5%
1A2 Manufacturing industries	0.24	0.06	0.07	0.08	-0.16	0.02	9.1%
1A3 Transport	0.00	0.00	0.00	0.00	0.00	0.00	0.0%
1A4 Other sectors	0.02	0.03	0.03	0.03	0.01	0.00	3.8%
1A5 Other (Military)	NA	NA	NA	NA	-	-	-
1B Fugitive emissions from fuels	NA	NA	NA	NA	-	-	-
2 Industrial processes	1.50	0.37	0.39	0.39	-1.11	0.02	45.5%
3 Agriculture	NA	NA	NA	NA	-	-	-
4 LULUCF	NR	NR	NR	NR	-	-	-
5 Waste	0.82	0.07	0.05	0.04	-0.77	-0.03	4.9%
6 Other	0.08	0.08	0.08	0.08	0.00	0.00	9.3%
National total	6.57	0.94	0.91	0.86	-5.66	-0.08	100.0%

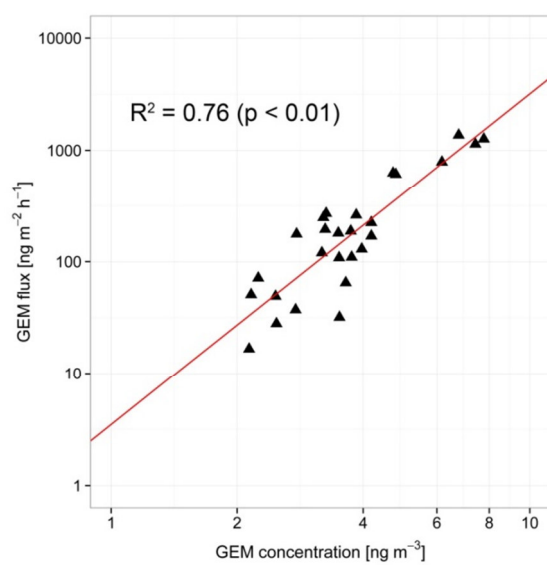


**Figure S6.1:** Log-log-relationship (trendline in red) between daily averaged gaseous elemental Hg (GEM) fluxes over each plot and atmospheric GEM concentrations measured simultaneously (filled triangles black,  $n = 27$ ). The equation is given in the main text (Eq. 6.2).



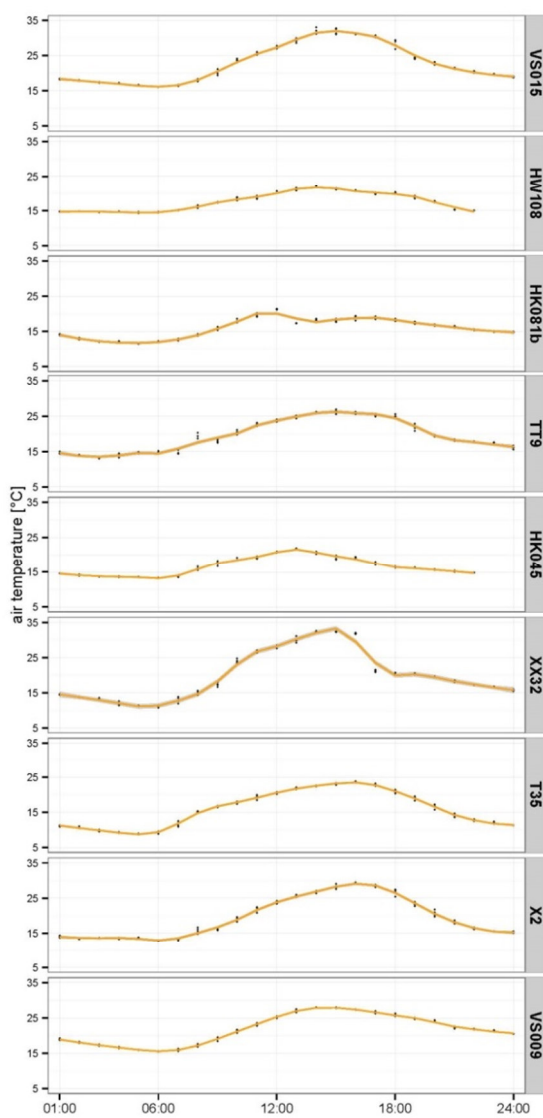


**Figure S6.2:** Diel patterns of air temperatures measured in 2 m above the surface during the gaseous elemental Hg flux measurements. The smoothing curve shows local polynomial regression fitting (R v3.1.2, loess {stats}, span = 0.3) with a confidence interval of 95% (grey).

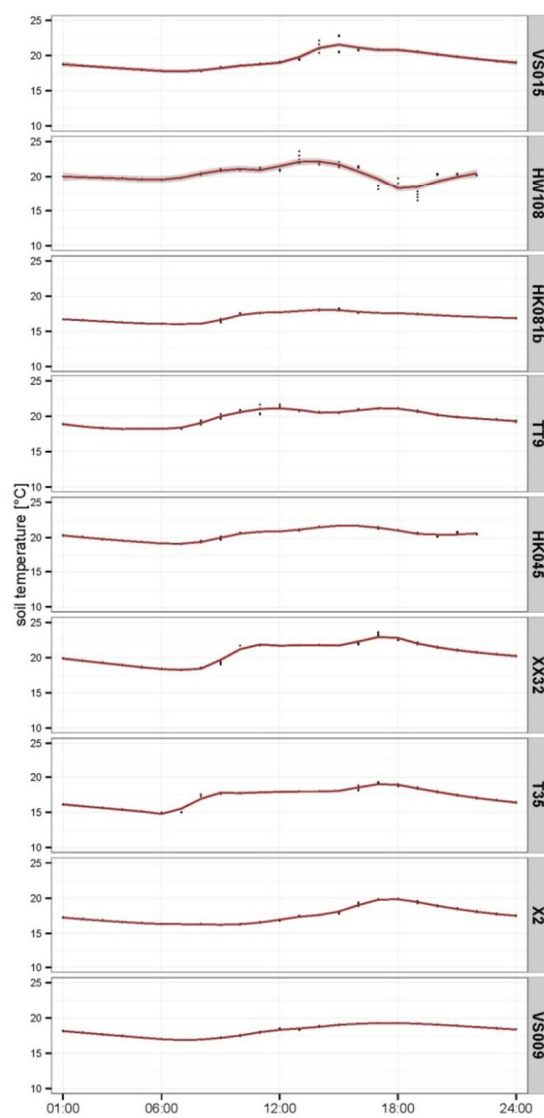


**Figure S6.3:** Diel patterns of the soil temperatures measured at 2 cm depth. Plot description in Figure S6.2.

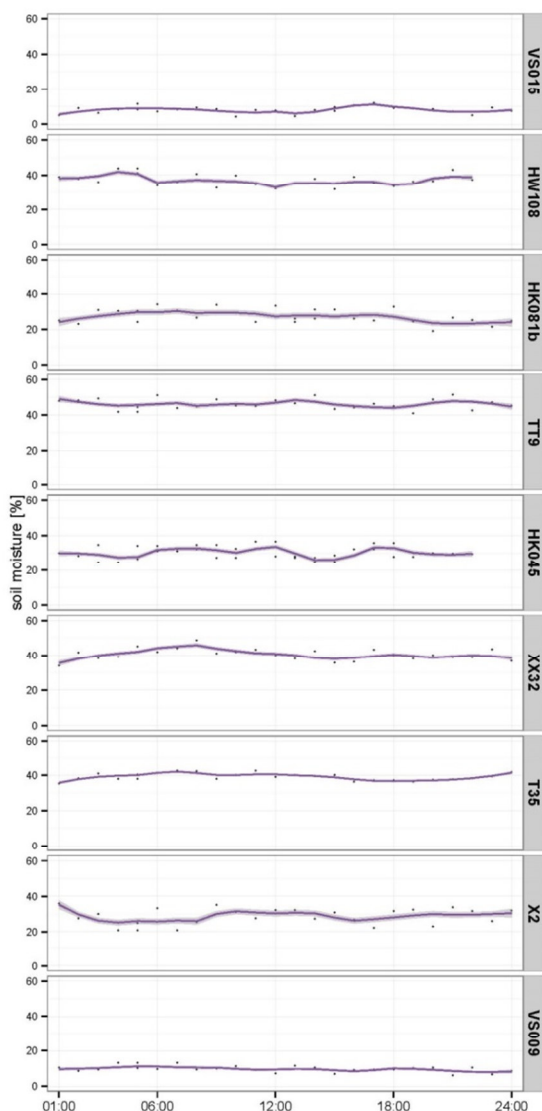


**Figure S6.4:** Diel patterns of the soil moisture content measured at 10 cm depth. Plot description in Figure S6.2.

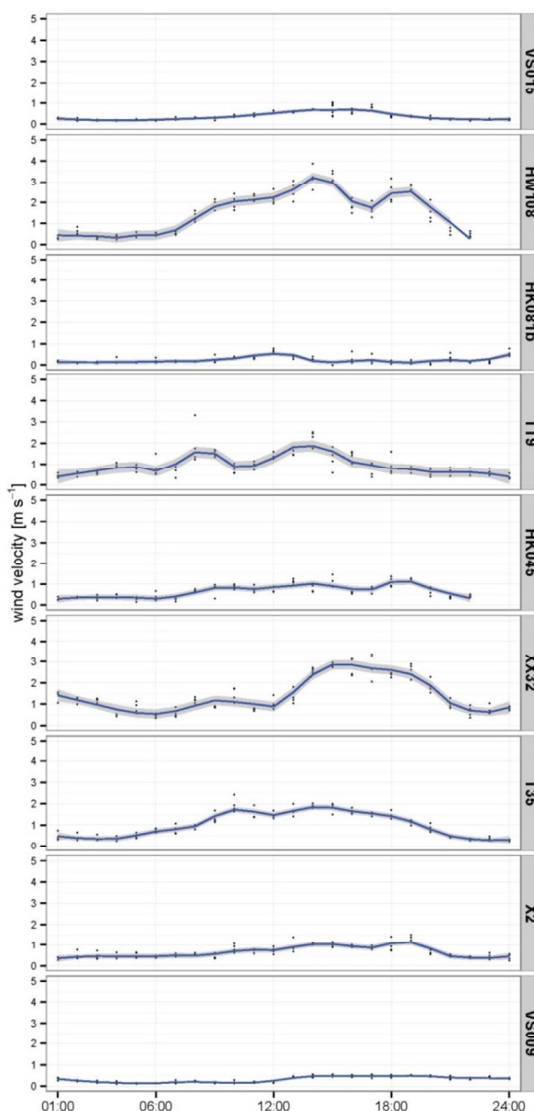


**Figure S6.5:** Diel patterns of wind velocity measured in 2 m above the surface. Plot description in Figure S6.2.

Photo documentation of sampling sites:



Visp South; Site **VS015**; View in west direction



Trutig North; Site **HW108**; View in south direction



Visp Kleegarten; Site **HK081b**; View in south direction



Turtig East; Site **TT9**; View in east direction



Visp Kleegarten; Site **HK045**; View in northeast direction



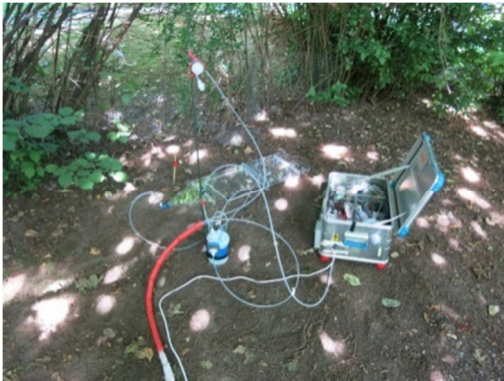
Turtig West; Site **XX32**; View in north direction



Turtig East; Site **T35**; View in north direction



Turtig East; Site **X2**; View in north direction



Visp South; Site **VS009**; View in west direction



# Acknowledgements

I would like to express my sincere gratitude to Prof. Christine Alewell for all her support over the years. She always took the time to answer questions I had and has created a friendly working environment. In addition she gave me the opportunity to attend three international conferences on the subject of mercury as a global pollutant and this has facilitated stimulating collaborations with many mercury researchers around the world.

I especially want to thank Prof. Kevin Bishop and Prof. Mats B. Nilsson for the opportunity to perform the major part of my research in northern Sweden. I have very much benefited from a 15 month stay at SLU in Umeå, the host institution during my SNF Doc.Mobility fellowship. I appreciate all the scientific inputs and helpful discussions we had at Uppsala University, at SLU in Umeå, in Vindeln and Granö and of course out in the moor. I'm looking forward to a continued cooperation within the Sino-Swedish Mercury Management Research Framework.

I share the credit of my work with Dr. Johannes Fritsche who introduced me to the world of mercury and gave me the first insight into measurement techniques and programming. He was never short of advice and it was a great pleasure to work with him in the field.

The field work in Sweden would not have been possible without the technical and maintenance support provided by the crew of the Field-based Forest Research Unit in Vindeln. I especially want to thank Dr. Jörgen Sagerfors and Dr. Mikael Ottosson Löfvenius for providing data from Degerö Stormyr and for their support regarding the micrometeorological measurements.

I would also like to thank Dr. William Larsson and the late Lars Lundmark from Umeå University for technical assistance and engineering. Thanks to Raymond Strittmatter from the Center for Molecular Life Sciences here in Basel for manufacturing various components needed for the system setups.

It gives me great pleasure to acknowledge the help of Dr. Staffan Åkerblom both in the lab and out in the field. I also greatly appreciate the support provided by several very dedicated interns: Lazaro J. Perez, Jeremy Watkins, Christian Hecht, Sylvain Gény and Fanny Giraud. I very much enjoyed performing field work together with Prof. Jonas Sommar who is an expert in the area of mercury flux measurements.

I would like to thank Roland Vogt from the University of Basel's MCR lab for the use of their eddy covariance system, for providing meteorological data and for the loan of their mobile weather station during the campaign in the Upper Valais.

In the context of that study I would like to acknowledge Jacqueline Riedi for her excellent work during system preparation and in the field, Prof. Daniel Obrist and Dr. Stéphane Westermann

from the Dienststelle für Umweltschutz of the Canton Valais for administrative and scientific support and Dr. David Trudel from Arcadis Schweiz AG for providing maps of Hg soil contamination.

Further, many thanks also go to all the other scientists who were involved in this project: Dr. Christof Ammann from Agroscope, Dr. Markus Meili from Stockholm University, Dr. Matthias Peichl from SLU Umeå and Dr. Jen-How Huang from our group. The whole UGW-team is kindly acknowledged not only for their very valuable scientific inputs but also for the lively discussions in the “mensa” and during coffee breaks, support at conferences and the “challenging” ping-pong games.

During my stay in Umeå I was extremely fortunate to meet and get to know great people who introduced me to the Swedish lifestyle and made me feel at home. I’m deeply grateful to Jonas, Josefin, Roger and Elin for their warm hospitality. Many thanks also to Anders, Ida, Johan, Mari, Eskil and Jenny for the great times we shared together both indoors and outdoors in the Swedish nature.

Last but by no means least I would like to thank Annika Bangerter for all of her creative inputs, patience and cheer ups during the last four years. Many thanks must also go to my parents, Bernadette and Rudolf, and my brother Marco who have always been a great source of motivation and support.

# Curriculum Vitae

## **Stefan Osterwalder**

Born on 29 January 1985 in Muri AG, Switzerland

Address: Margarethenstrasse 52, 4053 Basel

Mobil: +41 76 4773589

---

2012 - 2016	<b>Doctoral Student</b> <i>Environmental Geosciences at the Department of Environmental Sciences, University of Basel, Switzerland</i> <i>Department of Forest Ecology and Management, Swedish University of Agricultural Sciences, Umeå, Sweden (SNF Doc.Mobility fellowship).</i> <b>Doctoral Thesis:</b> Land-atmosphere exchange of elemental mercury: New insights using a novel relaxed eddy accumulation system and enclosure techniques
2009 - 2012	<b>MASTER OF SCIENCE IN ENVIRONMENTAL GEOSCIENCES</b> <i>University of Basel, Switzerland</i> Major in Environmental Sciences Minor in Meteorology
2005 - 2008	<b>BACHELOR OF SCIENCE IN GEOSCIENCES</b> <i>University of Basel, Switzerland</i> Major in Environmental Sciences
2000 - 2004	<b>MATURA</b> <i>Kantonsschule Wohlen, Switzerland</i>

---